

UNIVERSIDAD DE CONCEPCIÓN
DIRECCIÓN DE POSTGRADO
CONCEPCIÓN-CHILE



CONTRIBUCIÓN AL ANÁLISIS MATEMÁTICO Y
NUMÉRICO DE ALGUNOS PROBLEMAS DE
ELECTROMAGNETISMO

*Tesis para optar al grado de
Doctor en Ciencias Aplicadas con mención en Ingeniería Matemática*

PABLO ANTONIO VENEGAS TAPIA

JUNIO 2013
FACULTAD DE CIENCIAS FÍSICAS Y MATEMÁTICAS
DEPARTAMENTO DE INGENIERÍA MATEMÁTICA

**CONTRIBUCIÓN AL ANÁLISIS MATEMÁTICO Y NUMÉRICO DE
ALGUNOS PROBLEMAS DE ELECTROMAGNETISMO**

Pablo Venegas Tapia

Directores de Tesis: Rodolfo Rodríguez, Universidad de Concepción, Chile.
Alfredo Bermúdez, Universidad de Santiago de Compostela, España.
Dolores Gómez, Universidad de Santiago de Compostela, España.

Director de Programa: Prof. Raimund Bürger, Universidad de Concepción, Chile

COMISIÓN EVALUADORA

Prof. Michela Eleuteri, Università degli Studi di Milano, Italia.
Prof. Enrique Fernández, Universidad de Sevilla, España.
Prof. Ricardo Nochetto, Universidad, E.E.U.U.

COMISIÓN EXAMINADORA

Firma: _____
Prof. Rodolfo Araya.
Universidad de Concepción, Chile.

Firma: _____
Prof. Rodolfo Rodríguez.
Universidad de Concepción, Chile.

Firma: _____
Prof. Alberto Valli.
Università degli Studi di Trento, Italia.

Fecha Examen de Grado: _____

Calificación: _____

Concepción–Junio de 2013

Resumen

El objetivo principal de esta tesis doctoral es el análisis matemático y numérico de dos problemas importantes en electromagnetismo; el primero de ellos está relacionado con diversas aplicaciones de la magnetohidrodinámica, mientras que el segundo tiene que ver con el estudio de corrientes inducidas.

En lo que se refiere al primer problema, el estudio se centra en la aproximación numérica de los autovalores del operador rotacional, cuyas soluciones se denominan campos de Beltrami y que surgen en diversas áreas de la física.

Para llevar a cabo este estudio, primero se analiza matemáticamente el problema espectral, para lo cual se propone una formulación variacional mixta mediante la que se obtiene una caracterización completa de las soluciones del problema de autovalores. Además, se considera una formulación primal la cual resulta ser “equivalente”, bajo ciertas hipótesis, a dicho problema. Para la aproximación numérica del problema de autovalores se consideran esquemas de elementos finitos asociados a cada una de estas formulaciones. En ambos casos se obtienen aproximaciones espectrales con orden de convergencia óptimo, las cuales se corroboran mediante ejemplos numéricos.

En la segunda parte de la tesis se aborda el análisis matemático y numérico de diversos problemas de corrientes inducidas en régimen transitorio, suponiendo dominios axisimétricos. Los materiales considerados son no lineales y pueden presentar o no histéresis magnética.

Para ello, y motivados por las aplicaciones físicas, se consideran dos tipos de datos: el primero de ellos se corresponde con una condición de Dirichlet no homogénea en la frontera del dominio (usualmente la intensidad de corriente), mientras que el segundo consiste en suponer conocido el flujo magnético que atraviesa una sección meridional del dominio. En ambos casos, se propone una formulación en términos del campo magnético, y se considera que la relación entre este campo y la inducción magnética está dada bien mediante una función no lineal, o bien mediante un operador de histéresis.

Inicialmente se estudia el problema no lineal de corrientes inducidas considerando el flujo magnético como dato. Se demuestra la existencia y unicidad de solución de la formulación variacional correspondiente mediante un resultado abstracto. Para la aproximación numérica se propone una discretización espacial mediante elementos finitos para la cual se demuestran existencia de solución y una estimación de error. El esquema anterior se combina con un esquema de Euler implícito para la discretización temporal y se demuestran estimaciones óptimas de error.

A continuación, se analiza el problema de corrientes inducidas con condición de Dirich-

let no homogénea. En este caso, la existencia y unicidad de solución se basan en técnicas de discretización temporal, estimaciones a priori y paso al límite mediante compacidad. La aproximación numérica de este problema se estudia considerando un esquema de Euler implícito para la discretización temporal, que posteriormente se combina con un método de elementos finitos en espacio. Al igual que en el problema anterior, se demuestran estimaciones óptimas de error en las normas apropiadas, tanto para la semi-discretización temporal como para el problema completamente discreto.

Para ambos problemas se muestran test de convergencia que confirman los resultados teóricos obtenidos.

Finalmente, se estudia el problema axisimétrico de corrientes inducidas en el caso en que la relación entre el campo magnético y la inducción magnética viene dada mediante un operador de histéresis. Se demuestra la existencia de solución del problema considerando un operador de histéresis general y las distintas condiciones de contorno. Al igual que en el problema sin histéresis, el estudio de la existencia de solución se basa en una discretización implícita del tiempo; este procedimiento de aproximación es utilizado con frecuencia en el análisis de ecuaciones que incluyen operadores con memoria. Para la aproximación numérica, se considera un esquema completamente discreto mediante elementos finitos y Euler implícito, con una elección particular del operador de histéresis dada por el operador de Preisach clásico. Al contrario que en los problemas sin histéresis, el análisis de convergencia del esquema utilizado se realiza únicamente mediante ejemplos numéricos.

Contents

1	Introducción	1
1.1	Electromagnetismo y ecuaciones de Maxwell	1
1.2	Aproximación numérica de campos de Beltrami	4
1.3	Problemas de corrientes inducidas en materiales no lineales	7
2	Numerical approximation of the spectrum of the curl operator	17
2.1	Introduction	17
2.2	Preliminaries	19
2.3	Spectral problem for the curl operator	20
2.4	Finite element approximation	26
2.5	Implementation issues	32
2.6	Numerical experiments	34
2.6.1	Validation	34
2.6.2	Eigenvalues of the curl on a rectangular box	36
3	Numerical solution of a transient nonlinear axisymmetric eddy current model	43
3.1	Introduction	43
3.2	The transient nonlinear eddy current model	45
3.2.1	Axisymmetric eddy current model with enforced magnetic flux	45
3.3	Mathematical analysis	48
3.3.1	Functional spaces and preliminary results	48
3.3.2	Weak formulation	48
3.3.3	Existence of solution	49
3.4	Numerical analysis	52
3.4.1	Space discretization	54
3.4.2	Full discretization	58
3.5	Numerical results	63
4	Mathematical and numerical analysis of a transient non-linear axisymmetric eddy current model	67
4.1	Introduction	67
4.2	The transient eddy current model	69

4.2.1	Axisymmetric case	69
4.3	Mathematical analysis	71
4.3.1	Functional spaces and preliminary results	71
4.3.2	Weak formulation	72
4.3.3	Existence and uniqueness	72
4.4	Numerical analysis. Time semi-discrete problem	81
4.4.1	Error estimates for the time discretization	82
4.5	Numerical analysis. Fully discrete problem	85
4.5.1	Finite element approximation properties	87
4.5.2	Error estimates for the full discretization	93
4.6	Numerical experiments	99
5	Numerical solution of transient non-linear axisymmetric eddy current models with hysteresis	103
5.1	Introduction	103
5.2	Hysteresis operators	106
5.2.1	Space and time dependence	108
5.2.2	Magnetic hysteresis	110
5.3	The transient eddy current model with hysteresis	111
5.3.1	Axisymmetric eddy current model	112
5.4	Mathematical analysis	115
5.4.1	Functional spaces and preliminary results	115
5.4.2	Weak formulation	116
5.4.3	Existence of solution. Magnetic flux problem	118
5.4.4	Existence of solution. Dirichlet problem	126
5.5	Numerical implementation	131
5.5.1	The Preisach model	134
5.6	Numerical example	155
5.6.1	The eddy current model in a toroidal laminated core	155
5.6.2	Numerical solution	157
6	Conclusiones y trabajo futuro	165
6.1	Conclusiones	165
6.2	Trabajo futuro	166

Chapter 1

Introducción

«I happen to have discovered a direct relation between magnetism and light, also electricity and light, and the field it opens is so large and I think rich.»

Michael Faraday, The Letters of Faraday and Schoenbein

1.1 Electromagnetismo y ecuaciones de Maxwell

El electromagnetismo es la rama de la Física que se ocupa del estudio conjunto de los fenómenos eléctricos y magnéticos causados por cargas eléctricas en reposo o en movimiento.

Durante mucho tiempo los científicos han tratado de comprender estos fenómenos y si bien algunos efectos eléctricos y magnéticos se conocen desde la antigüedad, no fue sino hasta el siglo XIX cuando la relación entre la electricidad y el magnetismo quedó patente. Hoy sabemos que tanto electricidad como magnetismo son dos manifestaciones distintas de un mismo campo: el electromagnético.

La vinculación de ambos fenómenos mediante la teoría electromagnética fue uno de los principales logros de la física matemática del siglo XIX y su importancia hoy en día es incuestionable para entender la mayoría de los fenómenos físicos que nos rodean. Así, la fuerza electromagnética contribuye a que los electrones se mantengan cerca del núcleo formando los átomos y, a su vez, a que los núcleos se enlacen entre sí mediante el intercambio de energía electromagnética constituyendo moléculas y cuerpos. Pero también es el origen de las fuerzas de contacto como el rozamiento, la presión, la viscosidad,..., de la energía que las plantas absorben a través de la luz para poder realizar la fotosíntesis,... Es el fundamento de gran parte de la tecnología actual basada en la producción, transporte y utilización de corriente eléctrica.

Los estudios del electromagnetismo se remontan a la segunda mitad del siglo XVII cuando empiezan a establecerse las bases de lo que hoy denominamos electromagnetismo clásico. En 1820, Oersted estableció la primera relación experimental entre electricidad y magnetismo, al observar que una aguja imantada (una brújula) podía ser desviada por una corriente eléctrica. Este descubrimiento fue desarrollado por Ampère al estudiar las fuerzas entre cables por los que circulan corrientes eléctricas, y por Arago, que magnetizó un pedazo de hierro colocándolo cerca de un cable recorrido por una corriente. Estos experimentos fueron completados y explicados por

Faraday quien, en 1831, realizó el descubrimiento inverso al hallado por Oersted al comprobar que el movimiento de un imán en las proximidades de un cable induce en éste una corriente eléctrica transitoria.

Pero fue el escocés James Clerk Maxwell quien fundó la teoría moderna del electromagnetismo con la publicación de su obra *A Treatise on Electricity and Magnetism*, en el año 1873. Para construir un conjunto de ecuaciones matemáticamente consistente, que unificara los resultados de electricidad y magnetismo conocidos hasta el momento, Maxwell tuvo que postular la existencia de un nuevo efecto electromagnético, el cual era desconocido experimentalmente y conocido en la literatura como corriente de desplazamiento. Pocos años después de que Maxwell propusiese la inclusión de este término, Hertz comprobó experimentalmente su acierto con los primeros experimentos de telecomunicación mediante ondas electromagnéticas.

Considerando este nuevo campo y recopilando las leyes experimentales obtenidas por Gauss, Coulomb, Ampère y Faraday entre otros, Maxwell describió los efectos de la electricidad y el magnetismo con un conjunto de ecuaciones en derivadas parciales de primer orden que se aplicaban a todos los fenómenos electromagnéticos macroscópicos. Dichas ecuaciones muestran que la electricidad y el magnetismo, junto con los fenómenos de la óptica, obedecen un conjunto único de leyes. A partir de este momento, todos estos fenómenos se engloban bajo el término electromagnetismo

En medios continuos, y utilizando su forma diferencial, las ecuaciones de Maxwell se escriben del modo siguiente:

$$\begin{aligned} \frac{\partial \mathbf{D}}{\partial t} - \mathbf{curl} \mathbf{H} &= -\mathbf{J} && \text{(ley de Ampère-Maxwell),} \\ \frac{\partial \mathbf{B}}{\partial t} + \mathbf{curl} \mathbf{E} &= \mathbf{0} && \text{(ley de Faraday),} \\ \mathbf{div} \mathbf{B} &= 0 && \text{(ley de Gauss del magnetismo),} \\ \mathbf{div} \mathbf{D} &= \rho && \text{(ley de Gauss),} \end{aligned}$$

donde la notación utilizada es la usual en electromagnetismo, es decir,

- \mathbf{D} es el desplazamiento eléctrico (C/m^2),
- \mathbf{H} es el campo magnético (A/m),
- \mathbf{J} es la densidad de corriente (A/m^2),
- \mathbf{E} es la intensidad de campo eléctrico (V/m o N/C),
- \mathbf{B} es la inducción magnética (Wb/m^2 o T) y
- ρ es la densidad de carga eléctrica (C/m^3).

Entre paréntesis se indican las unidades de cada una de estas magnitudes en el sistema internacional.

Estas ecuaciones relacionan la divergencia y el rotacional de los campos eléctrico y magnético, que son los operadores que definen unívocamente cualquier campo vectorial, con sus fuentes o causas, que son las cargas eléctricas y las corrientes. La ley de Ampère-Maxwell coincide con la ley de Ampère salvo por el término adicional $\partial \mathbf{D} / \partial t$ introducido por Maxwell y que se corresponde con las corrientes de desplazamiento. Además, todos los campos que aparecen son funciones vectoriales que dependen de la variable espacial $\mathbf{x} = (x_1, x_2, x_3) \in \mathbb{R}^3$ y del tiempo $t > 0$.

El sistema anterior debe completarse con las denominadas *leyes de comportamiento o relaciones constitutivas* ya que sin ellas el sistema es indeterminado. Dichas relaciones expresan las propiedades del medio en que se propagarán los campos y su forma precisa depende de los materiales que lo constituyen.

Las propiedades electromagnéticas de los materiales pueden definirse por medio de su permitividad eléctrica ϵ , su permeabilidad magnética μ , y su conductividad eléctrica σ .

La *permitividad eléctrica* de un material describe cómo un campo eléctrico afecta y es afectado por un medio. El campo eléctrico tiende a polarizar las moléculas del interior del material, constituyéndose un campo eléctrico neto que se opone al campo eléctrico aplicado. Como resultado, el campo eléctrico total es menor de lo que sería en el vacío.

La *permeabilidad magnética* está relacionada con la capacidad del material para atraer y hacer pasar a través de él campos magnéticos y viene dada por la relación entre la inducción magnética existente y la intensidad de campo magnético que aparece en el interior de dicho material. Dicho de otro modo, esta magnitud refleja el grado de magnetización que el material adquiere bajo la acción de un campo magnético. A fin de comparar entre sí los diversos materiales se define la permeabilidad magnética relativa μ_r como el cociente entre la permeabilidad magnética de un material y la del vacío, denotada por μ_0 . Así

$$\mu = \mu_r \mu_0.$$

En el sistema internacional, $\mu_0 = 4\pi \times 10^{-7}$ H/m.

Por último, la *conductividad eléctrica* es una medida de la capacidad de un material para conducir corriente eléctrica y normalmente depende de la temperatura y de la frecuencia.

Un material donde los parámetros μ , ϵ y σ son independientes de la posición se denomina *homogéneo*; en caso contrario hablaremos de material *no homogéneo*.

Por otro lado, un material *isótropo* es aquel cuyas propiedades son independientes de la dirección espacial en que son examinadas. En caso contrario, el material se denomina *anisótropo*. En medios isótropos, los parámetros μ , ϵ y σ toman valores escalares mientras que en medios anisótropos se representan mediante tensores.

Finalmente, un material se dice no lineal si alguno de los parámetros μ , ϵ o σ depende de la intensidad de los campos aplicados.

En esta tesis consideraremos materiales isótropos, lineales desde el punto de vista eléctrico y no lineales desde el punto de vista magnético. Por tanto, las leyes constitutivas que relacionan

los campos \mathbf{B} , \mathbf{D} , \mathbf{E} y \mathbf{H} se escriben

$$\mathbf{D} = \varepsilon \mathbf{E} \quad (1.1)$$

$$\mathbf{B}(\mathbf{x}) = \mathcal{B}(\mathbf{x}, \mathbf{H}(\mathbf{x})), \quad (1.2)$$

donde, en general, \mathcal{B} es un operador no lineal. En el caso lineal e isótropo se tiene que

$$\mathbf{B} = \mu \mathbf{H},$$

con μ constante.

En esta tesis se distinguen dos partes bien definidas y diferentes entre sí, ambas relacionadas con aplicaciones del electromagnetismo:

- La aproximación numérica de campos de Beltrami, la cual guarda relación con algunos problemas de magnetohidrodinámica.
- El estudio de problemas de corrientes inducidas en materiales no lineales.

El objetivo es hacer una contribución al análisis matemático y numérico de cada uno de estos problemas. En los siguientes apartados resumiremos en qué consisten y cuáles serán las aportaciones fundamentales de nuestro estudio.

1.2 Aproximación numérica de campos de Beltrami

Los campos vectoriales \mathbf{u} con divergencia nula que satisfacen $\mathbf{curl} \mathbf{u} \times \mathbf{u} = \mathbf{0}$ en una región $\Omega \subset \mathbb{R}^3$ se denominan *campos de Beltrami*. Esta igualdad significa que $\mathbf{curl} \mathbf{u}$ es paralelo a \mathbf{u} en Ω y se suele escribir como

$$\mathbf{curl} \mathbf{u} = \lambda \mathbf{u}, \quad (1.3)$$

donde λ es una función escalar desconocida. En el contexto del electromagnetismo, los campos de Beltrami se llaman también *campos libres de fuerza* (force-free fields). La razón es que dichos campos conllevan fuerzas de Lorentz nulas. En efecto, si en la ecuación (1.3) \mathbf{u} denota el campo magnético, de dicha ecuación se deduce que \mathbf{H} y $\mathbf{curl} \mathbf{H}$ tienen la misma dirección. Si ahora suponemos que el término de desplazamiento en la ley de Ampère es despreciable, resulta que \mathbf{J} y \mathbf{H} son paralelos. Si además el medio es lineal, $\mathbf{H} = \mu \mathbf{B}$, donde μ es una constante y por tanto \mathbf{J} y \mathbf{B} serán, también, paralelos. Como consecuencia, y en ausencia de densidades de carga, la fuerza de Lorentz, $\mathbf{F} = \mathbf{J} \times \mathbf{B}$, será nula.

El estudio de los campos de Beltrami tiene gran interés para la comprensión de multitud de fenómenos físicos. En particular, en los problemas de magnetohidrodinámica (MHD), disciplina que estudia la dinámica de los fluidos que son buenos conductores de la electricidad y, específicamente, los efectos que aparecen por la interacción entre el movimiento del fluido y un campo magnético cualquiera que pueda estar presente. Para ello es preciso combinar las ecuaciones de Maxwell con las de Navier-Stokes de la dinámica de fluidos. Es un campo que abarca

un gran abanico de problemas y, en particular, aquellos relacionados con fenómenos solares, que se pueden aproximar por una solución en régimen estacionario de las ecuaciones magnetohidrodinámicas. Así, es posible estudiar el campo magnético en la corona solar, el cual está relacionado con las erupciones solares y la eyección de masa coronal (ver Figura 1.1). En efecto, en la mayoría de las áreas de la corona solar las fuerzas magnéticas son dominantes, por lo que las demás fuerzas como el gradiente de presiones y la gravedad pueden despreciarse. Asumiendo además que el cociente entre la presión del plasma y la presión magnética es pequeño comparado con la unidad (la denominada aproximación *low- β*) podemos suponer que la fuerza de Lorentz es nula y, por lo tanto, los campos resultantes serán libres de fuerza. En efecto, si $\mathbf{J} \times \mathbf{B} = \mathbf{0}$, suponiendo que el medio es lineal podemos escribir

$$\mathbf{J} \times (\mu_0 \mathbf{H}) = \mathbf{0}. \quad (1.4)$$

Teniendo en cuenta la Ley de Ampère despreciando el término de desplazamiento y la ley de Gauss obtenemos

$$\mathbf{curl} \mathbf{H} = \mathbf{J}, \quad (1.5)$$

$$\mathbf{div} \mathbf{H} = 0, \quad (1.6)$$

y, por tanto, de (1.4)-(1.6) deducimos que \mathbf{H} es un campo libre de fuerza.

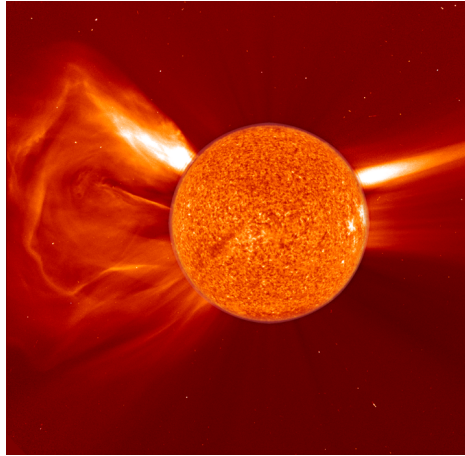


Figure 1.1: Eyección de masa coronal, 24 de enero de 2007. Imágenes obtenidas de SOHO/LASCO <http://sohowww.nascom.nasa.gov/>.

El estudio de los campos libres de fuerza en el ámbito de la dinámica de fluidos se remonta a Beltrami [7], razón por la que estos campos llevan su nombre. Lakhtakia [59], en una breve reseña histórica sobre este tema, señala que en ocasiones se les designa como campos *Trkalianos* en honor a las contribuciones realizadas por el físico y matemático checo Viktor Trkal [87]. En la física de fluidos, los campos de Beltrami son soluciones particulares de la ecuación de Euler

$$\nabla \mathbf{v} \mathbf{v} + \nabla p = \mathbf{0}$$

con $p = -|\mathbf{v}|^2/2$. En efecto, teniendo en cuenta la relación

$$\mathbf{curl} \mathbf{v} \times \mathbf{v} = \nabla \mathbf{v} \mathbf{v} - \nabla |\mathbf{v}|^2/2,$$

se deduce que el campo de velocidades correspondiente es un campo de Beltrami.

Los campos de Beltrami aparecen también relacionados con el estudio del equilibrio estático de cristales líquidos, así como en problemas de superconductividad, o en estudios de turbulencia en física de plasma, por citar algunos ejemplos; incluso el movimiento de partículas en tornados y trombas marinas puede aproximarse por campos de Beltrami (ver, por ejemplo, [23] y las referencias allí mencionadas).

Dependiendo de la elección del parámetro λ en la ecuación (1.3) consideraremos diferentes tipos de campos. Así, los campos *no lineales* corresponden al caso en que λ es una función escalar mientras que los campos *lineales* son aquellos para los que λ es constante. Distinguimos el caso en que $\lambda = 0$, cuyos campos asociados se denominan *campos potenciales* (en ese caso, $\mathbf{curl} \mathbf{u} = \mathbf{0}$ y $\mathbf{u} = \text{grad} \varphi$ si el dominio es simplemente conexo).

Nosotros estamos interesados en el problema lineal. Obsérvese que, en este caso, la determinación de λ y los campos asociados está directamente relacionada con el cálculo de los valores propios del operador rotacional, para lo cual es necesario considerar restricciones sobre el dominio de cálculo y condiciones de contorno adecuadas. Consideraremos $\mathbf{u} \cdot \mathbf{n} = 0$ como condición de contorno, la cual corresponde a un campo confinado en el interior de un dominio acotado. Así, el problema a resolver se escribe

$$\mathbf{curl} \mathbf{u} = \lambda \mathbf{u} \quad \text{en } \Omega, \tag{1.7}$$

$$\text{div} \mathbf{u} = 0 \quad \text{en } \Omega, \tag{1.8}$$

$$\mathbf{u} \cdot \mathbf{n} = 0 \quad \text{en } \partial\Omega. \tag{1.9}$$

Nótese que la ecuación (1.8) se obtiene inmediatamente de (1.7), salvo si $\lambda = 0$.

Únicamente en dominios con ciertas simetrías pueden calcularse soluciones analíticas para este problema. Por ejemplo, en el modelado de la corona solar considerando simetrías esféricas, cabe mencionar los trabajos de Chandrasekhar y Kendall [27, 28]. Recientemente, Morse [69] estudió el problema considerando simetrías cilíndricas en dominio acotados.

En dominios generales, Boulmezaud, Maday y Amari [23] estudiaron diferentes problemas de contorno cuyas soluciones son campos de Beltrami y demostraron existencia, unicidad y regularidad de solución. Basándose en estos resultados se han propuesto y analizado diferentes aproximaciones utilizando el método elementos finitos para resolver tanto el problema lineal ([21]) como el no lineal ([22]) de campos de Beltrami.

En lo que respecta al análisis matemático del problema de autovalores asociado a (1.7)–(1.9) podemos mencionar a Yoshida y Giga [98], quienes estudiaron las propiedades espectrales del operador rotacional en diferentes espacios funcionales. En particular, demostraron que si

el dominio Ω es múltiplemente conexo, el problema (1.7)–(1.9) tiene solución para cualquier número complejo λ . Es decir, el problema de autovalores asociado tiene espectro continuo.

En el Capítulo 2 de esta tesis se aborda el análisis matemático y numérico del problema espectral (1.7)–(1.9), en el caso en que el dominio Ω es simplemente-conexo. En primer lugar, y con el fin de caracterizar el espectro del problema de autovalores, se introduce una formulación mixta, que se demuestra es equivalente a la anterior.

Se demuestra también que dicha formulación mixta es equivalente al problema espectral de un operador autoadjunto compacto, lo cual nos permite caracterizar las soluciones del problema (1.7)–(1.9). Además, se considera una formulación primal y se demuestra que, bajo ciertas condiciones, es equivalente al problema de autovalores.

Se estudia la aproximación numérica del problema espectral considerando una discretización mediante elementos finitos de Nédélec [72], de las formulaciones mixta y primal. La aproximación numérica del esquema mixto conduce a un problema degenerado de valores propios generalizado que implica trabajar con dos matrices no invertibles, mientras que el esquema asociado al problema primal involucra una matriz Hermitiana definida positiva.

Por último, se demuestran ordenes de convergencia óptimos para ambos esquemas utilizando resultados clásicos ([66, 33, 34]) y se presentan ejemplos numéricos que corroboran los resultados teóricos obtenidos.

Los resultados contenidos en este capítulo se recogen en el artículo:

- R. RODRÍGUEZ AND P. VENEGAS: *Numerical approximation of the spectrum of the curl operator*, Mathematics of Computation, to appear.

1.3 Problemas de corrientes inducidas en materiales no lineales

Uno de los problemas más importantes a tener en cuenta en el análisis y diseño de máquinas eléctricas es el cálculo de las pérdidas de energía. Estas pérdidas determinan en gran medida la eficiencia del dispositivo e influyen en el coste operacional del mismo.

Por su importancia en ingeniería eléctrica, este problema ha atraído la atención de numerosos investigadores desde el siglo XIX; a partir de los fundamentos teóricos del electromagnetismo y de experimentos en el laboratorio, se han propuesto diversas fórmulas analíticas que tratan de dar una respuesta al problema, y las cuales son válidas bajo supuestos que frecuentemente no se cumplen en la práctica.

Las dificultades fundamentales del problema son dos: una de carácter físico, el comportamiento fuertemente no lineal de los materiales que incluye histéresis magnética, y otra de carácter geométrico y matemático, dado que los materiales que componen el núcleo suelen ser laminados para disminuir las pérdidas, y el pequeño espesor de las láminas frente a otras dimensiones características del problema hace muy complicada la simulación numérica tridimensional.

Estas dificultades son la causa de que el problema no se encuentre a día de hoy satisfactoriamente resuelto y el origen de que todavía se publiquen un gran número de artículos en los

que se intenta mejorar las fórmulas para calcular las pérdidas, con una metodología que generalmente no pasa por un análisis teórico de los modelos sino por conseguir un “mejor” ajuste a los resultados experimentales.

En efecto, esta metodología olvida frecuentemente las bases teóricas del electromagnetismo, por una parte, y, por otra, una herramienta reciente pero ya muy bien establecida: la simulación numérica, es decir, la posibilidad de resolver las ecuaciones de Maxwell y obtener a posteriori las pérdidas a partir de sus expresiones teóricas exactas.

Inicialmente, desde mediados del siglo XIX, se distinguían tan sólo dos tipos de pérdidas: por histéresis y por corrientes de Foucault, las cuales aparecen claramente en el balance de energía que se obtiene a partir de las ecuaciones de Maxwell. La necesidad de ajustar adecuadamente los resultados experimentales llevó, en la década de los 80 del siglo pasado, a introducir un tercer tipo de pérdidas, las llamadas por exceso y a dar una justificación física de su presencia.

El primer paso en el cálculo de las pérdidas es la solución numérica del problema de electromagnetismo asociado. Esto requiere resolver el modelo de Maxwell cuasi-estático, también denominado modelo de *corrientes inducidas*, que surge al despreciar el término del desplazamiento eléctrico en la ley de Ampère, obteniéndose así el siguiente sistema de ecuaciones:

$$\mathbf{curl} \mathbf{H} = \mathbf{J}, \quad (1.10)$$

$$\frac{\partial \mathbf{B}}{\partial t} + \mathbf{curl} \mathbf{E} = \mathbf{0}, \quad (1.11)$$

$$\mathbf{div} \mathbf{B} = 0, \quad (1.12)$$

el cual debe resolverse teniendo en cuenta las leyes constitutivas de los materiales.

Dado que estas ecuaciones están definidas en \mathbb{R}^3 , para resolver el problema mediante un método de elementos finitos es necesario restringirlas a un dominio acotado e imponer condiciones de contorno adecuadas de tal forma que el problema tenga una única solución, así como también una condición inicial.

Pérdidas por corrientes inducidas

Las corrientes inducidas o *eddy currents*, son corrientes generadas en materiales conductores que se producen cuando el material está expuesto a un campo magnético variable con el tiempo. Este fenómeno, y el correspondiente calentamiento de los conductores, fue observado y estudiado por L. Foucault y es por ello que las corrientes generadas se conocen también como *corrientes de Foucault*.

El calor generado por la corriente en el conductor viene dado por la Ley de Joule y es proporcional al cuadrado de la corriente I que circula por el conductor, al tiempo t durante el que está circulando y a la resistencia R del mismo, es decir,

$$Q = I^2 R t \quad (\text{J}).$$

Recordemos que la resistencia de un conductor varía inversamente con el área de su sección transversal. Es por ello que, para disminuir las pérdidas por corrientes inducidas, los núcleos

de las máquinas eléctricas están constituidos por láminas apiladas con espesor muy pequeño y aisladas unas de otras por una fina capa de barniz (ver Figura 1.2).



Figure 1.2: Núcleo magnético y bobinado (izquierda) y detalle del laminado (derecha).

Por otro lado, considerando la forma diferencial de la Ley de Joule, podemos calcular la densidad de potencia (potencia por unidad de volumen) en un punto \mathbf{x} y en un instante t como

$$\mathbf{J}(\mathbf{x}, t) \cdot \mathbf{E}(\mathbf{x}, t) = \frac{1}{\sigma} |\mathbf{J}(\mathbf{x}, t)|^2 = \sigma |\mathbf{E}(\mathbf{x}, t)|^2 \quad (\text{W/m}^3),$$

donde se ha tenido en cuenta la ley de Ohm.

Por tanto, la determinación de las pérdidas requiere el cálculo previo del campo densidad de corriente $\mathbf{J}(\mathbf{x}, t)$ a lo largo del tiempo. Para ello, es necesario resolver numéricamente las ecuaciones (1.10)-(1.12). Sin embargo, en el caso de un material laminado se presentan dificultades prácticas severas debido a que el espesor de las láminas es demasiado pequeño (inferior a 1 mm) frente a otras dimensiones del dispositivo, como para permitir un mallado del dominio de cálculo que “respete” la estructura en láminas del medio (ver Figura 1.2). En efecto, para conseguir precisión en el cálculo sería necesario introducir varias capas de elementos finitos tridimensionales en cada lámina, lo que conduciría a mallas con gran cantidad de elementos, con el consiguiente coste computacional.

Materiales magnéticos. Histéresis

Los materiales magnéticos son aquellos que presentan polarización magnética o magnetización cuando se someten a un campo magnético externo. El fenómeno de la magnetización se produce por el alineamiento de los dipolos magnéticos del material al aplicar un campo magnético. Un material magnético posee gran número de dipolos magnéticos que en ausencia de un campo magnético se orientan de manera aleatoria por lo que, a escala macroscópica, el vector suma de los momentos magnéticos correspondientes es nulo. Cuando el material se somete a un campo magnético externo, representado por una densidad de flujo \mathbf{B} , los dipolos tenderán a alinearse en la dirección de \mathbf{B} . De este modo el campo magnético resultante en cada punto del material será superior al valor que existiría en el mismo punto en ausencia de dicho campo.

La densidad macroscópica de dipolos se representa por un campo vectorial \mathbf{M} llamado densidad de magnetización o simplemente magnetización. Sus unidades son $\text{Am}^2/\text{m}^3 = \text{A/m}$. La relación entre \mathbf{M} , \mathbf{B} y la intensidad del campo magnético \mathbf{H} es

$$\mathbf{H} = \frac{\mathbf{B}}{\mu_0} - \mathbf{M} \quad (\text{A/m}). \quad (1.13)$$

En el caso de materiales magnéticamente isótropos, es decir,

$$\mathbf{B}(\mathbf{x}, t) = B(\mathbf{x}, t)\mathbf{u}(\mathbf{x}), \quad \mathbf{H}(\mathbf{x}, t) = H(\mathbf{x}, t)\mathbf{u}(\mathbf{x}) \quad (1.14)$$

para algún vector unitario \mathbf{u} . Asumiendo además que son magnéticamente lineales, se tiene que \mathbf{M} es proporcional a \mathbf{H}

$$\mathbf{M} = \chi_m \mathbf{H},$$

donde el parámetro adimensional χ_m se llama susceptibilidad magnética del material. Considerando esta ecuación en (1.13), obtenemos

$$\mathbf{H} = \frac{\mathbf{B}}{\mu_0} - \chi_m \mathbf{H},$$

de donde

$$\mathbf{B} = (1 + \chi_m)\mu_0 \mathbf{H}.$$

Se tiene además que

$$\mu_r = 1 + \chi_m.$$

En función de su respuesta a los campos magnéticos externos aplicados, los materiales pueden clasificarse en *diamagnéticos*, *paramagnéticos* y *ferromagnéticos*.

El diamagnetismo se caracteriza por una susceptibilidad magnética pequeña y negativa. Esto significa que los materiales diamagnéticos se magnetizan débilmente en dirección opuesta a la del campo magnético aplicado.

Los materiales paramagnéticos tienen susceptibilidades pequeñas pero positivas, así que también se magnetizan débilmente pero en la misma dirección del campo aplicado.

Los materiales ferromagnéticos se caracterizan por su fuerte magnetización remanente, es decir, la magnetización que subsiste en ausencia de un campo magnético. En la mayoría de los casos estos materiales presentan histéresis, lo que significa que el valor de la inducción magnética \mathbf{B} es una función, que no sólo depende del valor presente del campo magnético, sino también de la historia magnética pasada de \mathbf{H} . Por lo tanto los materiales ferromagnéticos no pueden ser caracterizados por una relación constitutiva univaluada simple. En consecuencia, la simulación numérica del comportamiento de dispositivos que poseen materiales ferromagnéticos es todavía un desafío.

Para ilustrar la relación B-H mediante un ejemplo, consideramos un material magnético isótropo desmagnetizado que se somete a un campo magnético creciente comenzando por el valor cero. Entonces en cada punto \mathbf{x} los pares $(H(\mathbf{x}, t), B(\mathbf{x}, t))$ describen la curva número 1

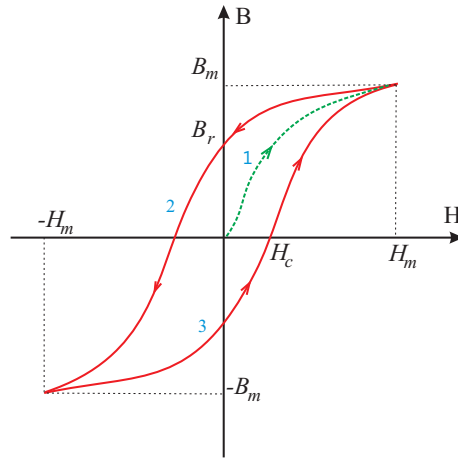


Figure 1.3: Ciclo mayor de histéresis.

de la Figura 1.3. De este modo, la inducción magnética también crece hasta un valor máximo B_m en el que se alcanza la saturación. Esta curva se llama curva de magnetización inicial. A continuación se hace decrecer monótonamente la intensidad del campo magnético desde el valor de saturación H_m hasta el valor opuesto $-H_m$. Entonces los puntos $(H(\mathbf{x}, t), B(\mathbf{x}, t))$ no recorren hacia atrás la curva inicial sino la señalada con el número 2 en la Figura 1.3, hasta que el campo magnético alcanza el valor $-H_m$. Si incrementamos de nuevo el campo magnético los puntos $(H(\mathbf{x}, t), B(\mathbf{x}, t))$ describen la curva número 3. Con más generalidad, si el campo magnético oscila monótonamente entre dos valores extremos opuestos H_m and $-H_m$ (es decir, $H(\mathbf{x}, t)$ no tiene extremos locales aparte de los globales), entonces los pares $(H(\mathbf{x}, t), B(\mathbf{x}, t))$ siguen alternativamente las curvas 2 y 3 en el sentido indicado en la Figura 1.3, es decir, recorren el llamado *bucle mayor* de histéresis.

Hay dos magnitudes importantes relacionadas con los materiales ferromagnéticos: la *remanencia* y el *campo coercitivo*. La remanencia representa la magnetización que persiste después de aplicar un campo magnético “grande” y suprimirlo a continuación. Corresponde a la inducción magnética remanente denotada por B_r en la Figura 1.3. A su vez, el campo coercitivo es la intensidad del campo magnético necesaria para llevar la magnetización desde el valor remanente al valor cero, es decir, corresponde al valor denominado H_c en la Figura 1.3.

En relación al área encerrada por el ciclo mayor de histéresis, los materiales ferromagnéticos se clasifican en *blandos* (soft materials) y *duros* (hard materials). Los materiales ferromagnéticos blandos son aquellos fáciles de magnetizar y sus bucles de histéresis son delgados. Por el contrario, el área encerrada por el ciclo mayor de histéresis de los materiales magnéticos duros es mayor (ver Figura 1.4).

Pérdidas por histéresis

En los materiales ferromagnéticos no lineales, la presencia de la histéresis implica que (para soluciones periódicas de las ecuaciones de Maxwell) la energía electromagnética disipada en forma de calor durante un ciclo $[t_1, t_2]$ no sólo depende de las pérdidas por efecto Joule generado



Figure 1.4: Ejemplos de ciclos de histéresis en un material blando (izquierda) y duro (derecha).

por las corrientes inducidas, sino también de las denominadas pérdidas por histéresis. Haciendo un balance de energía electromagnética puede deducirse que dichas pérdidas vienen dadas por

$$\int_{\Omega} \left(\int_{t_1}^{t_2} \frac{\partial \mathbf{B}}{\partial t}(\mathbf{x}, t) \cdot \mathbf{H}(\mathbf{x}, t) dt \right) d\mathbf{x}$$

la cual, en general, es no nula.

El campo escalar

$$\int_{t_1}^{t_2} \frac{\partial B}{\partial t}(\mathbf{x}, t) \cdot \mathbf{H}(\mathbf{x}, t) dt$$

proporciona la llamada densidad de pérdidas por histéresis en el punto \mathbf{x} durante un ciclo. En el caso de histéresis isotrópica, es decir, cuando \mathbf{H} y \mathbf{B} tienen la misma dirección (ver (1.14)), los puntos $(B(\mathbf{x}, t), H(\mathbf{x}, t))$ describen curvas en el plano B-H. Además podemos reescribir la ecuación anterior de la siguiente forma

$$\int_{t_1}^{t_2} \frac{\partial B}{\partial t}(\mathbf{x}, t) \cdot \mathbf{H}(\mathbf{x}, t) dt = \int_{t_1}^{t_2} \frac{\partial B}{\partial t}(\mathbf{x}, t) H(\mathbf{x}, t) dt. \quad (1.15)$$

En el caso periódico estas curvas son cerradas y están contenidas en el llamado bucle mayor de histéresis. Además, en el caso periódico puede deducirse que la integral (1.15) corresponde al área neta encerrada por la curva,

$$t \in [t_1, t_2] \rightarrow (H(\mathbf{x}, t), B(\mathbf{x}, t)) \quad (1.16)$$

la cual coincide con la densidad de pérdidas por histéresis en el punto \mathbf{x} a lo largo de un ciclo.

Como hemos señalado anteriormente, un caso particular más sencillo se presenta cuando el campo $H(\mathbf{x}, t)$ oscila periódica y monótonamente en el tiempo (es decir, sin extremos locales) entre dos valores opuestos $H_e(x)$ y $-H_e(x)$. Entonces la correspondiente inducción magnética también varía entre dos valores opuestos $B_e(x)$ y $-B_e(x)$ y la curva (1.16) no se corta a sí misma, es decir, es una curva cerrada simple (bucle), en general un bucle interior al bucle mayor de histéresis, denominado *bucle menor* (ver Figura 1.5). Bajo estas circunstancias, la densidad de pérdidas por histéresis en cada punto \mathbf{x} a lo largo de un ciclo coincide con el área de dicho bucle, que se puede medir en el laboratorio para cada material ferromagnético particular. Concretamente,

$$\mathcal{W}_h(\mathbf{x}) = \mathcal{A}(B_e(\mathbf{x})) \quad (\text{J/m}^3),$$

donde $\mathcal{A}(B_e(\mathbf{x}))$ es el área encerrada en el ciclo debido a la oscilación entre $H_e(x)$ y $-H_e(x)$. A modo de ejemplo, en la Tabla 1.1 se recogen los valores de estas pérdidas en tres materiales

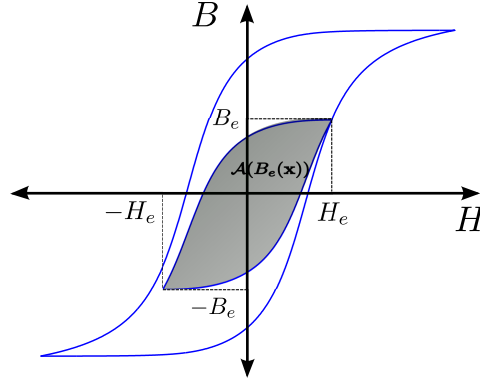


Figure 1.5: Ciclo mayor y ciclo interior.

distintos.

Tabla 1.1: Pérdidas por histéresis en distintos materiales en función de B_r y H_c .

Material	B_r (T)	H_c (A/m)	\mathcal{W}_h (J/m ³)
Fe comercial (99.8% pureza)	2.2	80	250
Fe (99.95% pureza)	2.2	4	30
Supermalloy (aleación compuesta de Ni, Mo y Fe)	0.8	0.3	2

De este modo, la densidad de potencia de las pérdidas por histéresis, promediada en el ciclo y en el punto \mathbf{x} es

$$\mathcal{P}_h(\mathbf{x}) = f \mathcal{A}(B_e(\mathbf{x})) \quad (\text{W/m}^3),$$

siendo $f = 1/(t_2 - t_1)$ la frecuencia. Por tanto, la potencia de las pérdidas por histéresis en una región Ω , promediada en un ciclo, viene dada por

$$f \int_{\Omega} \mathcal{A}(B_e(\mathbf{x})) d\mathbf{x} \quad (\text{W}).$$

Nótese que la potencia de las pérdidas por histéresis depende linealmente de la frecuencia.

Por otra parte, de acuerdo con las fórmulas anteriores, para determinar la densidad de pérdidas en el caso periódico, es necesario conocer previamente el ciclo (H, B) en cada punto \mathbf{x} . Con este fin deben resolverse las ecuaciones de Maxwell (más en concreto, el modelo de corrientes inducidas) lo que conduce, en principio, a la necesidad de disponer de un modelo matemático de la histéresis. La complejidad de los modelos de histéresis que existen en la bibliografía, junto con la dificultad de medir en el laboratorio los parámetros que involucran, explicarían el hecho de que los paquetes comerciales de simulación electromagnética más utilizados no posean actualmente ningún módulo para calcular el campo electromagnético que incluya modelos de histéresis. La

alternativa, válida para materiales ferromagnéticos blandos, consiste en despreciar la histéresis estableciendo que la relación entre el campo magnético y la inducción magnética es unívoca y dada por la curva de magnetización inicial o anisterética del material, que es, en general, no lineal. De este modo, uno puede calcular el campo electromagnético resolviendo numéricamente un modelo de corrientes inducidas transitorio y no lineal.

De lo expuesto en esta sección se deduce que el estudio de las corrientes inducidas es de suma importancia en el cálculo de pérdidas de energía, en el caso de materiales no lineales, sin o con presencia de histéresis. Es por esto que en la tesis se abordan ambos problemas bajo la hipótesis de simetría axial. Así, los capítulos de la última parte de la tesis se organizan de la siguiente forma.

En el Capítulo 3, se estudia un problema axisimétrico de corrientes inducidas no lineal, en donde la relación B-H (ver (1.2)) está dada mediante una función no lineal fuertemente monótona. Se estudia una formulación propuesta por Van Keer *et al.* en [89, 90] la cual está motivada por el cálculo de pérdidas de energía en materiales laminados. Esta formulación consiste en el cálculo del campo electromagnético en una sección transversal del dominio tridimensional, ortogonal a la dirección del flujo. Esto involucra un término no local, que, junto con el hecho de que no existe flujo de corriente a través de la frontera, da lugar a un problema parabólico no lineal con una condición de contorno no clásica. Esta condición trae algunas complicaciones técnicas, por ejemplo, requiere tratar con una forma bilineal que, en lugar de ser elíptica, satisface una desigualdad de Gårding. Se prueba la existencia de solución de una formulación débil de este problema en términos del campo magnético mediante la aplicación de un resultado abstracto [52].

Para la resolución numérica del problema, se supone, además, que la relación no lineal B-H es Lipschitz continua. En primer lugar se considera una discretización por elementos finitos mediante funciones lineales a trozos en mallas triangulares, para la cual se demuestra existencia de solución. Después, se combina el esquema anterior con una discretización temporal utilizando el método de Euler implícito. Bajo las hipótesis adecuadas, se deducen estimaciones de error de orden óptimo tanto para el esquema semi-discreto espacial, como para el esquema completamente discreto. Estas demostraciones se basan en argumentos de [82] y también se adaptan a nuestro caso argumentos de la teoría clásica de problemas parabólicos lineales (ver, por ejemplo, [86]). Finalmente, se presentan resultados numéricos que confirman las estimaciones de error obtenidas teóricamente.

Los resultados obtenidos en este capítulo se recogen en el artículo:

- ▶ A. BERMÚDEZ, D. GÓMEZ, P. SALGADO, R. RODRÍGUEZ AND P. VENEGAS: *Numerical solution of a transient nonlinear axisymmetric eddy current model with non local boundary conditions*, Mathematical Models and Methods in Applied Sciences, to appear.

En el Capítulo 4 se estudia el problema axisimétrico de corrientes inducidas considerando que la relación B-H está dada mediante una función de Carathéodory no lineal monótona. Como dato fuente se considera el campo magnético en la frontera, es decir, una condición de Dirichlet

no homogénea. Esta condición es físicamente realista en el sentido de que hay aplicaciones industriales en las que se puede obtener fácilmente este dato a partir de cantidades medibles. Este es el caso, por ejemplo, de la simulación numérica de corrientes de Foucault en electrodos metalúrgicos [8, 9, 54], sistemas de calentamiento por inducción [29] o pérdidas de corriente en un núcleo laminado toroidal [62, 70]. En todas estas aplicaciones la condición Dirichlet puede obtenerse a partir de la intensidad de corriente.

Para este problema, se demuestra la existencia de solución de una formulación débil en términos del campo magnético. La técnica utilizada para este propósito (comúnmente conocido como método de Rothe [77]) consiste en introducir una discretización implícita del tiempo, obtener estimaciones a priori y a continuación, pasar al límite cuando el paso temporal tiende a cero.

Para la solución numérica, primero se discretiza temporalmente el problema mediante un esquema de Euler implícito para el cual se demuestra existencia y unicidad de solución. A continuación se considera una discretización espacial mediante elementos finitos lineales a trozos. Bajos los supuestos adecuados, se analizan ambos esquemas numéricos. En el primer caso nuestro análisis se basa en [82], mientras que el análisis del esquema completamente discreto se adapta la teoría clásica de ecuaciones parabólicas lineales y para hacer frente a la condición de Dirichlet no homogénea se recurre a argumentos de [5]. De esta forma para el problema totalmente discreto se obtiene una estimación tipo- L^2 sin asumir regularidad adicional de la solución. Por otra parte, bajo hipótesis de regularidad adecuadas, también se obtiene una estimación de error con orden óptimo. Por último, se presentan resultados numéricos que confirman las estimaciones demostradas.

Los resultados obtenidos en este capítulo se recogen en el artículo:

- A. BERMÚDEZ, D. GÓMEZ, R. RODRÍGUEZ AND P. VENEGAS: *Mathematical and numerical analysis of a transient non-linear axisymmetric eddy current model*, submitted to *Numerische Mathematik*.

Finalmente, en el Capítulo 5 se estudia el problema de corrientes inducidas con histéresis, es decir, la curva de B-H está dada por un operador de histéresis general. Como en los capítulos anteriores, se consideran dos tipos de término fuente: bien el campo magnético en la frontera (condición de Dirichlet), bien el flujo magnético a través de una sección transversal del dominio (condiciones de flujo magnético). Se demuestra existencia de solución para las formulaciones variacionales obtenidas considerando los distintos términos fuente. Para ello, se introduce una discretización implícita en tiempo, se obtienen estimaciones a priori y a continuación, se hace un paso al límite cuando el paso temporal tiende a cero (ver [77]). Este procedimiento de aproximación se utiliza a menudo en el análisis de las ecuaciones que incluyen un operador de la memoria (ver, por ejemplo, [42, 95]), ya que, en cada paso de tiempo se resuelve un problema en el cual el operador de memoria se reduce a una función no lineal. En particular, en la demostración se recurre a argumentos de [95] donde se aborda un problema parabólico con histéresis, considerando una condición de Dirichlet homogénea.

Para la modelización de la histéresis y su posterior implementación en el esquema numérico se considera el operador de Preisach clásico [76], el cual se describe brevemente basándonos en los trabajos de Visintin [95] y Mayergoyz [63].

Para la resolución numérica del problema se considera una discretización espacial mediante elementos finitos lineales a trozos, y un esquema de Euler implícito para la discretización temporal. También se propone un algoritmo iterativo para resolver el problema no lineal. Este algoritmo introducido por Bermúdez y Moreno [12] se basa en algunas propiedades de la regularizada Yosida de operadores maximales monótonos. En este caso no se ha estudiado analíticamente la convergencia del esquema propuesto, pero se presenta un ejemplo con el fin de evaluar numéricamente el orden de convergencia del mismo.

Con algunos de los resultados obtenidos en este capítulo se encuentra en preparación el artículo:

- A. BERMÚDEZ, D. GÓMEZ, R. RODRÍGUEZ AND P. VENEGAS: *Numerical solution of a transient non-linear axisymmetric eddy current model with hysteresis.*

Chapter 2

Numerical approximation of the spectrum of the curl operator

2.1 Introduction

The aim of this chapter is to study the numerical approximation of the spectrum of the curl operator. More precisely, we focus on the following eigenvalue problem: find $\lambda \in \mathbb{C}$ and $\mathbf{u} \neq \mathbf{0}$ such that

$$\mathbf{curl} \mathbf{u} = \lambda \mathbf{u} \quad \text{in } \Omega, \tag{2.1}$$

$$\operatorname{div} \mathbf{u} = 0 \quad \text{in } \Omega, \tag{2.2}$$

$$\mathbf{u} \cdot \mathbf{n} = 0 \quad \text{on } \Gamma, \tag{2.3}$$

where Ω is a bounded domain with boundary Γ and outer unit normal vector \mathbf{n} . To analyze this problem, Yoshida and Giga studied in [98] the spectral properties of the curl in various functions spaces. In particular, they show that if Ω is multiply-connected, then the problem above has a nontrivial solution for any complex λ . Because of this, we restrict our analysis to simply-connected domains.

The spectral problem for the curl operator has a longstanding tradition in mathematical physics. A large measure of the credit goes to Beltrami [7], who seems to be the first who considered this problem in the context of fluid dynamics. This is the reason why the corresponding eigenfunctions are called *Beltrami fields* (also *Trkalian fields* [87]; we refer to [59] for a brief survey on the history of this subject). Such fields are useful in solar physics for testing theories on flares and coronal heating, in fluid mechanics for the study of the static equilibrium of smectic liquid crystals, and in superconducting materials, just to name a few; even particle movement in tornadoes and waterspouts can be approximated by Beltrami fields.

On the other hand, the eigenfunctions of this spectral problem are particular cases of the so-called *force-free fields*. These are vector fields which satisfy the first equation of the eigenvalue problem above, with λ not necessarily a constant but a scalar function. The name arises from magnetohydrodynamics, since a magnetic field \mathbf{H} satisfying such an equation, induces a vanishing Lorentz force: $\mathbf{F} := \mathbf{J} \times \mathbf{B} = \mathbf{curl} \mathbf{H} \times (\mu \mathbf{H}) = \mathbf{0}$. In [97], Woltjer showed that the

lowest state of magnetic energy density within a closed system is attained when λ is spatially constant. In such a case \mathbf{H} is called a *linear force-free field* and its determination is naturally related with the spectral problem for the curl operator. The eigenfunctions of this problem are also known as *free-decay fields* or *Taylor fields* and play an important role, for instance, in the study of turbulence in plasma physics [85].

The boundary condition $\mathbf{u} \cdot \mathbf{n} = 0$ is the most natural one for a bounded domain and corresponds to a field confined within it. Analytical solutions of this problem are only known under particular symmetry assumptions. The first one was obtained by Chandrasekhar and Kendall for spherical domains in the context of astrophysical plasmas arising in modeling of the solar crown [27] (see also [28, 97, 96]). More recently, Morse [69] studied the problem on cylindrical bounded domains.

On general domains, Boulmezaud, Maday, and Amari studied in [23] different boundary value problems whose solutions are linear force-free fields and they prove existence, uniqueness, and regularity of the solution. Based on the analysis of that paper, Boulmezaud and Amari proposed and analyzed finite element discretizations for numerically solving various linear [21] and non-linear [22] force-free field problems.

In this chapter, we focus on the spectral problem (2.1)–(2.3). First we give a mixed weak formulation and prove that it is equivalent to the spectral problem for a self-adjoint compact operator. This allows us to give a thorough characterization of the solutions of (2.1)–(2.3). The finite element discretization of this mixed formulation leads to a degenerate generalized eigenvalue problem involving two non-definite matrices. Although the resulting eigenvalue problem is proved to be well-posed, its degeneracy prevents us from using standard eigensolvers for its computer solution. We postpone to an appendix the analysis of such discretization, which relies on using the spectral approximation theory for mixed methods derived in [66].

As an alternative, we derive another weak formulation more amenable for numerical purposes, since it leads to a generalized eigenvalue problem involving two Hermitian matrices, that on the right-hand side being positive definite. Therefore, standard software can be used to solve this problem. We propose a discretization based on Nédélec finite elements of arbitrary order [72]. By using the spectral theory for non-compact operators from [33, 34], we prove spectral convergence and establish optimal-order error estimates. We also prove that the method is free of spurious modes.

The eigenvalues of this alternative formulation are the squares of the eigenvalues λ of (2.1)–(2.3). The eigenfunctions associated to simple eigenvalues λ^2 are Beltrami fields satisfying (2.1)–(2.3). However, if λ and $-\lambda$ are both eigenvalues of (2.1)–(2.3), then λ^2 is a multiple eigenvalue of this alternative formulation and the corresponding eigenspace is the direct sum of the eigenspaces of λ and $-\lambda$ in (2.1)–(2.3). When this happens, the numerical solution of this alternative formulation in general does not lead to an actual Beltrami field, but to a linear combination of Beltrami fields associated to λ and $-\lambda$. In such a case, one can resort to the solution of the degenerate generalized eigenvalue problem analyzed in the appendix.

The outline of the chapter is as follows. In Section 2.2, we introduce some function spaces that will be used in the sequel. In Section 2.3, first we give a mixed weak formulation and use it to obtain a spectral characterization of the solutions of the eigenproblem. Then, we propose an

alternative weak formulation more amenable for numerical purposes. In Section 2.4, we introduce a finite element discretization of the latter. We prove optimal-order spectral convergence and absence of spurious modes. We describe how to efficiently implement this methods in Section 2.5. In Section 2.6, we report the results of a couple of numerical tests, which allow us to check the theoretical results and to assess the performance of the method. Finally, in an appendix, we introduce and analyze a finite element discretization of the mixed weak form derived in Section 2.3.

2.2 Preliminaries

Let $\Omega \in \mathbb{R}^3$ be a bounded simply-connected domain with a Lipschitz continuous boundary Γ . We assume that Ω is bounded and either Γ is smooth or Ω is a polyhedron. Let $\Gamma_0, \dots, \Gamma_I$ be the connected components of Γ , with Γ_0 being the boundary of the only unbounded connected component of $\mathbb{R}^3/\bar{\Omega}$. The remaining connected components, $\Gamma_1 \dots, \Gamma_I$, are in its turn the boundaries of the bounded connected components of $\mathbb{R}^3/\bar{\Omega}$ and, hence, closed surfaces.

We consider the space $L^2(\Omega)$ with its corresponding norm $\|\cdot\|_{0,\Omega}$; for convenience, we denote $\|\cdot\|_{0,\Omega}$ the norm of $L^2(\Omega)^3$, too. As usual, for all $s > 0$, we consider the Hilbertian Sobolev space $H^s(\Omega)$ with norm $\|\cdot\|_{s,\Omega}$; we also denote by $\|\cdot\|_{s,\Omega}$ the norm of the space $H^s(\Omega)^3$.

Let $\mathcal{D}(\Omega)$ be the space of infinitely differentiable functions with compact support in Ω and $\mathcal{D}(\bar{\Omega}) := \{\phi|_{\Omega} : \phi \in \mathcal{D}(\mathbb{R}^3)\}$.

Let $H^{1/2}(\Gamma)$ be the space of traces on Γ of functions in $H^1(\Omega)$, with dual space $H^{-1/2}(\Gamma)$ and dual pairing $\langle \cdot, \cdot \rangle_{\Gamma}$.

Throughout the chapter, we will use the Hilbert spaces

$$\begin{aligned} \mathbf{H}(\mathbf{curl}; \Omega) &:= \{\mathbf{v} \in L^2(\Omega)^3 : \mathbf{curl} \mathbf{v} \in L^2(\Omega)^3\}, \\ \mathbf{H}(\mathbf{div}; \Omega) &:= \{\mathbf{v} \in L^2(\Omega)^3 : \mathbf{div} \mathbf{v} \in L^2(\Omega)\}, \end{aligned}$$

with their respective norms defined by $\|\mathbf{v}\|_{\mathbf{curl},\Omega}^2 := \|\mathbf{v}\|_{0,\Omega}^2 + \|\mathbf{curl} \mathbf{v}\|_{0,\Omega}^2$ and $\|\mathbf{v}\|_{\mathbf{div},\Omega}^2 := \|\mathbf{v}\|_{0,\Omega}^2 + \|\mathbf{div} \mathbf{v}\|_{0,\Omega}^2$, and the followings closed subspaces:

$$\begin{aligned} \mathbf{H}_0(\mathbf{div}; \Omega) &:= \{\mathbf{v} \in \mathbf{H}(\mathbf{div}; \Omega) : \mathbf{v} \cdot \mathbf{n} = 0 \text{ on } \Gamma\}, \\ \mathbf{H}_0(\mathbf{curl}; \Omega) &:= \{\mathbf{v} \in \mathbf{H}(\mathbf{curl}; \Omega) : \mathbf{v} \times \mathbf{n} = \mathbf{0} \text{ on } \Gamma\}, \\ \mathbf{H}(\mathbf{div}^0; \Omega) &:= \{\mathbf{v} \in \mathbf{H}(\mathbf{div}; \Omega) : \mathbf{div} \mathbf{v} = 0 \text{ in } \Omega\}, \\ \mathbf{H}(\mathbf{curl}^0; \Omega) &:= \{\mathbf{v} \in \mathbf{H}(\mathbf{curl}; \Omega) : \mathbf{curl} \mathbf{v} = \mathbf{0} \text{ in } \Omega\}, \\ \mathbf{H}_0(\mathbf{div}^0; \Omega) &:= \mathbf{H}_0(\mathbf{div}; \Omega) \cap \mathbf{H}(\mathbf{div}^0; \Omega), \\ \mathbf{H}_0(\mathbf{curl}^0; \Omega) &:= \mathbf{H}_0(\mathbf{curl}; \Omega) \cap \mathbf{H}(\mathbf{curl}^0; \Omega). \end{aligned}$$

Notice that the conditions $\mathbf{v} \cdot \mathbf{n} = 0$ and $\mathbf{v} \times \mathbf{n} = \mathbf{0}$ on Γ , must be understood in the sense of $H^{-1/2}(\Gamma)$.

The spaces $\mathbf{H}(\mathbf{curl}^0; \Omega) \cap \mathbf{H}_0(\mathbf{div}^0; \Omega)$ and $\mathbf{H}_0(\mathbf{curl}^0; \Omega) \cap \mathbf{H}(\mathbf{div}^0; \Omega)$ will also appear often in the sequel. Under the assumption of Ω being simply-connected the former is trivial (see, for

instance, [45, Remark I.2.2]):

$$\mathbf{H}(\mathbf{curl}^0; \Omega) \cap \mathbf{H}_0(\operatorname{div}^0; \Omega) = \{\mathbf{0}\}.$$

This is not the case for the latter. The following characterization can be found in [2, Proposition 3.18].

Lemma 2.2.1 *The dimension of $\mathbf{H}_0(\mathbf{curl}^0; \Omega) \cap \mathbf{H}(\operatorname{div}^0; \Omega)$ is equal to I . It is spanned by the functions ∇q_i , $1 \leq i \leq I$, where each $q_i \in \mathbf{H}^1(\Omega)$ is the unique solution of the problem*

$$\begin{cases} -\Delta q_i = 0 & \text{in } \Omega, \\ q_i|_{\Gamma_0} = 0 & \text{and } q_i|_{\Gamma_k} = \text{constant}, \quad 1 \leq k \leq I, \\ \langle \partial_n q_i, 1 \rangle_{\Gamma_0} = -1 & \text{and } \langle \partial_n q_i, 1 \rangle_{\Gamma_k} = \delta_{ik}, \quad 1 \leq k \leq I. \end{cases}$$

Finally, we will also use the space

$$\mathbf{H}^s(\mathbf{curl}; \Omega) := \{\mathbf{v} \in \mathbf{H}^s(\Omega)^3 : \mathbf{curl} \mathbf{v} \in \mathbf{H}^s(\Omega)^3\}, \quad s > 0.$$

Let us recall that there exists $s > 1/2$, only depending on the domain Ω , such that the inclusions

$$\mathbf{H}_0(\mathbf{curl}; \Omega) \cap \mathbf{H}(\operatorname{div}; \Omega) \hookrightarrow \mathbf{H}^s(\Omega)^3, \quad \mathbf{H}(\mathbf{curl}; \Omega) \cap \mathbf{H}_0(\operatorname{div}; \Omega) \hookrightarrow \mathbf{H}^s(\Omega)^3 \quad (2.4)$$

are continuous (see, for instance, [2], Proposition 3.7, if Ω is a polyhedron, and Theorems 2.9 and 2.12, if Γ is smooth).

Throughout the chapter, C will denote a generic constant, not necessarily the same at each occurrence.

2.3 Spectral problem for the curl operator

We consider the following problem:

Problem 2.3.1 *Find $\lambda \in \mathbb{C}$ and $\mathbf{u} \in \mathbf{H}(\mathbf{curl}; \Omega)$, $\mathbf{u} \neq \mathbf{0}$, such that*

$$\begin{aligned} \mathbf{curl} \mathbf{u} &= \lambda \mathbf{u} && \text{in } \Omega, \\ \operatorname{div} \mathbf{u} &= 0 && \text{in } \Omega, \\ \mathbf{u} \cdot \mathbf{n} &= 0 && \text{on } \Gamma. \end{aligned}$$

Notice that, for any solution of this problem, $\lambda \neq 0$. In fact, $\lambda = 0$ would imply $\mathbf{u} \in \mathbf{H}(\mathbf{curl}^0; \Omega) \cap \mathbf{H}_0(\operatorname{div}^0; \Omega)$ and this space is trivial in our case.

The following is a mixed formulation of this problem.

Problem 2.3.2 *Find $\lambda \in \mathbb{C}$ and $(\mathbf{u}, \varphi) \in \mathbf{H}(\mathbf{curl}; \Omega) \times \mathbf{H}^1(\Omega)/\mathbb{C}$, $(\mathbf{u}, \varphi) \neq \mathbf{0}$, such that*

$$\begin{aligned} \int_{\Omega} \mathbf{curl} \mathbf{u} \cdot \mathbf{curl} \bar{\mathbf{v}} + \int_{\Omega} \nabla \varphi \cdot \bar{\mathbf{v}} &= \lambda \int_{\Omega} \mathbf{u} \cdot \mathbf{curl} \bar{\mathbf{v}} && \forall \mathbf{v} \in \mathbf{H}(\mathbf{curl}; \Omega), \\ \int_{\Omega} \mathbf{u} \cdot \nabla \bar{\psi} &= 0 && \forall \psi \in \mathbf{H}^1(\Omega)/\mathbb{C}. \end{aligned}$$

In order to establish the equivalence of these two problems, first note that the last two equations of the former are equivalent to the last equation of the latter. Hence, it is clear that if (λ, \mathbf{u}) is a solution of Problem 2.3.1, then, $(\lambda, \mathbf{u}, 0)$ solves Problem 2.3.2. Conversely, if $(\lambda, \mathbf{u}, \varphi)$ is a solution of Problem 2.3.2, by taking $\mathbf{v} = \nabla\varphi$ in its first equation, we conclude that $\varphi = 0$. Therefore, we only need to prove that $\mathbf{curl} \mathbf{u} = \lambda \mathbf{u}$ in Ω .

With this end, we test the first equation of Problem 2.3.2 with $\mathbf{v} \in \mathcal{D}(\Omega)^3$ and integrate by parts to conclude that

$$\mathbf{curl}(\mathbf{curl} \mathbf{u} - \lambda \mathbf{u}) = \mathbf{0} \quad \text{in } \Omega.$$

Then, taking $\mathbf{v} \in H^1(\Omega)^3$, by integration by parts it follows that

$$(\mathbf{curl} \mathbf{u} - \lambda \mathbf{u}) \times \mathbf{n} = \mathbf{0} \quad \text{on } \Gamma.$$

Thus, we have that $\mathbf{curl} \mathbf{u} - \lambda \mathbf{u} \in H_0(\mathbf{curl}^0; \Omega) \cap H(\text{div}^0; \Omega)$. Therefore, from Lemma 2.2.1, it follows that there exists $q \in H^1(\Omega)$, with $q|_{\Gamma_0} = 0$ and $q|_{\Gamma_k} = C_k$ (constant), $1 \leq k \leq I$, such that $\mathbf{curl} \mathbf{u} - \lambda \mathbf{u} = \nabla q$. Then, integrating by parts we have

$$\begin{aligned} \|\nabla q\|_{0,\Omega}^2 &= \int_{\Omega} (\mathbf{curl} \mathbf{u} - \lambda \mathbf{u}) \cdot \nabla \bar{q} = \int_{\Omega} \mathbf{curl} \mathbf{u} \cdot \nabla \bar{q} \\ &= \langle \mathbf{curl} \mathbf{u} \cdot \mathbf{n}, q \rangle_{\Gamma} = \sum_{k=1}^I C_k \langle \mathbf{curl} \mathbf{u} \cdot \mathbf{n}, 1 \rangle_{\Gamma_k} = 0, \end{aligned}$$

where the last equality follows from Stokes theorem, density arguments, and the fact that Γ_k are closed surfaces. Whence, $\nabla q = 0$ and consequently $\mathbf{curl} \mathbf{u} = \lambda \mathbf{u}$ in Ω . Thus we conclude the following equivalence result.

Proposition 2.3.1 *If (λ, \mathbf{u}) is a solution of Problem 2.3.1, then $(\lambda, \mathbf{u}, 0)$ is a solution of Problem 2.3.2. Conversely, if $(\lambda, \mathbf{u}, \varphi)$ is a solution of Problem 2.3.2, then $\varphi = 0$ and (λ, \mathbf{u}) is a solution of Problem 2.3.1.*

For the analysis of Problem 2.3.2, we consider the following solution operator:

$$\begin{aligned} S : H_0(\text{div}^0; \Omega) &\longrightarrow H_0(\text{div}^0; \Omega), \\ \mathbf{f} &\longmapsto S\mathbf{f} := \mathbf{w}, \end{aligned}$$

with $\mathbf{w} \in H(\mathbf{curl}; \Omega)$ such that there exists $\xi \in H^1(\Omega)/\mathbb{C}$ satisfying

$$\int_{\Omega} \mathbf{curl} \mathbf{w} \cdot \mathbf{curl} \bar{\mathbf{v}} + \int_{\Omega} \nabla \xi \cdot \bar{\mathbf{v}} = \int_{\Omega} \mathbf{f} \cdot \mathbf{curl} \bar{\mathbf{v}} \quad \forall \mathbf{v} \in H(\mathbf{curl}; \Omega), \quad (2.5)$$

$$\int_{\Omega} \mathbf{w} \cdot \nabla \bar{\psi} = 0 \quad \forall \psi \in H^1(\Omega)/\mathbb{C}. \quad (2.6)$$

The Babuška-Brezzi conditions for this mixed problem are easy to check. In particular, the ellipticity in the kernel follows from the fact that, since Ω is simply-connected, $\|\mathbf{v}\|_{\mathbf{curl}, \Omega} \leq C \|\mathbf{curl} \mathbf{v}\|_{0,\Omega}$ for all $\mathbf{v} \in H(\mathbf{curl}; \Omega) \cap H_0(\text{div}^0; \Omega)$; see [2, Corollary 3.16]). Consequently, (2.5)–(2.6) has a unique solution (\mathbf{w}, ξ) , which satisfies $\xi = 0$ and $\|\mathbf{w}\|_{\mathbf{curl}, \Omega} \leq C \|f\|_{0,\Omega}$. Moreover, (2.6) shows that $\mathbf{w} \in H_0(\text{div}^0; \Omega)$. Hence, the operator S is well-defined and continuous.

Clearly, $S\mathbf{u} = \mu\mathbf{u}$, with $\mu \neq 0$, if and only if $(\lambda, \mathbf{u}, 0)$ is a solution of Problem 2.3.2, with $\lambda = \frac{1}{\mu}$. Thus, we focus on characterizing the spectrum of S .

We note that $S(\mathbf{H}_0(\operatorname{div}^0; \Omega)) \subset \mathbf{H}(\mathbf{curl}; \Omega) \cap \mathbf{H}_0(\operatorname{div}^0; \Omega)$. Since, according to (2.4), there exists $s > 1/2$ such that

$$\mathbf{H}(\mathbf{curl}; \Omega) \cap \mathbf{H}_0(\operatorname{div}^0; \Omega) \hookrightarrow \mathbf{H}^s(\Omega)^3 \cap \mathbf{H}_0(\operatorname{div}^0; \Omega) \hookrightarrow \mathbf{H}_0(\operatorname{div}^0; \Omega),$$

the first inclusion being continuous and the second one compact (cf. [45, Theorem I.1.3]), we conclude that S is compact.

Moreover, from (2.5), by proceeding as for Problem 2.3.2 we obtain

$$\mathbf{curl}(\mathbf{curl} \mathbf{w} - \mathbf{f}) = \mathbf{0} \quad \text{in } \Omega \quad \text{and} \quad (\mathbf{curl} \mathbf{w} - \mathbf{f}) \times \mathbf{n} = \mathbf{0} \quad \text{on } \Gamma.$$

Hence, using Lemma 2.2.1 again, it is straightforward to show that $\mathbf{curl} \mathbf{w} = \mathbf{f}$ in Ω . Thus \mathbf{w} belongs to the space

$$\mathcal{Z} := \{\mathbf{v} \in \mathbf{H}(\mathbf{curl}; \Omega) : \mathbf{curl} \mathbf{v} \cdot \mathbf{n} = 0 \text{ on } \Gamma\}.$$

We summarize these results in the following lemma.

Lemma 2.3.1 *Operator S is compact. Moreover, $S(\mathbf{H}_0(\operatorname{div}^0; \Omega)) \subset \mathcal{Z}$ and, for all $\mathbf{f} \in \mathbf{H}_0(\operatorname{div}^0; \Omega)$, if $\mathbf{w} = S\mathbf{f}$, then $\mathbf{curl} \mathbf{w} = \mathbf{f}$ in Ω .*

Next step is to establish some properties of the space \mathcal{Z} that will be used in the sequel. The first one is the following result, which has been proved in [98, Theorem 1] in a more general setting (see also [65, Proposition 2.3]). We include here an elementary proof, for completeness.

Proposition 2.3.2 *For all $\mathbf{y}, \mathbf{z} \in \mathcal{Z}$*

$$\int_{\Omega} (\mathbf{curl} \mathbf{y} \cdot \bar{\mathbf{z}} - \mathbf{y} \cdot \mathbf{curl} \bar{\mathbf{z}}) = 0.$$

Proof. Let $\mathbf{y} \in \mathcal{Z}$. Then $\mathbf{curl} \mathbf{y} \in \mathbf{H}_0(\operatorname{div}^0; \Omega)$. Since Ω is simply-connected, we know (cf. [45, Theorem I.3.6]) that there exists a unique $\Phi \in \mathbf{H}_0(\mathbf{curl}; \Omega) \cap \mathbf{H}(\operatorname{div}^0; \Omega)$, such that

$$\mathbf{curl} \mathbf{y} = \mathbf{curl} \Phi \quad \text{in } \Omega$$

and, consequently, there exists a unique $\psi \in \mathbf{H}^1(\Omega)/\mathbb{C}$, such that

$$\mathbf{y} = \nabla \psi + \Phi \quad \text{in } \Omega.$$

Then, for $\mathbf{z} \in \mathcal{Z}$, we have

$$\int_{\Omega} (\mathbf{curl} \mathbf{y} \cdot \bar{\mathbf{z}} - \mathbf{y} \cdot \mathbf{curl} \bar{\mathbf{z}}) = \int_{\Omega} (\mathbf{curl} \Phi \cdot \bar{\mathbf{z}} - \Phi \cdot \mathbf{curl} \bar{\mathbf{z}}) - \int_{\Omega} \nabla \psi \cdot \mathbf{curl} \bar{\mathbf{z}}.$$

Now, since for all $\mathbf{v} \in \mathbf{H}^1(\Omega)^3$

$$\int_{\Omega} (\mathbf{curl} \Phi \cdot \bar{\mathbf{v}} - \Phi \cdot \mathbf{curl} \bar{\mathbf{v}}) = \langle \Phi \times \mathbf{n}, \mathbf{v} \rangle_{\Gamma} = 0$$

and $H^1(\Omega)^3 \hookrightarrow H(\mathbf{curl}; \Omega)$ densely, we obtain

$$\int_{\Omega} (\mathbf{curl} \Phi \cdot \bar{z} - \Phi \cdot \mathbf{curl} \bar{z}) = 0.$$

On the other hand, using integration by parts we have that

$$\int_{\Omega} \nabla \psi \cdot \mathbf{curl} \bar{z} = \langle \mathbf{curl} z \cdot \mathbf{n}, \psi \rangle_{\Gamma} = 0.$$

Thus, we conclude the proof. \square

A first consequence of the above proposition is the following density result for the smooth functions of \mathcal{Z} .

Proposition 2.3.3 *Subspace $\mathcal{D}(\bar{\Omega})^3 \cap \mathcal{Z}$ is dense in \mathcal{Z} .*

Proof. The proof is based on a classical property (see, for instance, [45, Section I, (2.14)]), which in our case reads as follows: $\mathcal{D}(\bar{\Omega})^3 \cap \mathcal{Z}$ is dense in \mathcal{Z} if and only if every element of \mathcal{Z}' that vanish on $\mathcal{D}(\bar{\Omega})^3 \cap \mathcal{Z}$ also vanishes on \mathcal{Z} .

Let $L \in \mathcal{Z}'$. Since \mathcal{Z} is a Hilbert space, there exists $l \in \mathcal{Z}$ such that

$$\langle L, v \rangle = \int_{\Omega} (l \cdot \bar{v} + \tilde{l} \cdot \mathbf{curl} \bar{v}) \quad \forall v \in \mathcal{Z},$$

where $\langle \cdot, \cdot \rangle$ denote the duality pairing between \mathcal{Z}' and \mathcal{Z} and $\tilde{l} := \mathbf{curl} l$. Now, assume that L vanishes on $\mathcal{D}(\bar{\Omega})^3 \cap \mathcal{Z}$, namely,

$$\langle L, v \rangle = \int_{\Omega} (l \cdot \bar{v} + \tilde{l} \cdot \mathbf{curl} \bar{v}) = 0 \quad \forall v \in \mathcal{D}(\bar{\Omega})^3 \cap \mathcal{Z}.$$

We need to prove that L vanishes on \mathcal{Z} , too. With this end, note that since $\mathcal{D}(\Omega)^3 \subset \mathcal{D}(\bar{\Omega})^3 \cap \mathcal{Z}$, it follows that

$$\int_{\Omega} l \cdot \bar{v} + \int_{\Omega} \tilde{l} \cdot \mathbf{curl} \bar{v} = 0 \quad \forall v \in \mathcal{D}(\Omega)^3$$

and, hence, $l = -\mathbf{curl} \tilde{l}$. On the other hand, given that $\nabla(\mathcal{D}(\bar{\Omega})) \subset \mathcal{D}(\bar{\Omega})^3 \cap \mathcal{Z}$ too, we have

$$\int_{\Omega} l \cdot \nabla \bar{\psi} = 0 \quad \forall \psi \in \mathcal{D}(\bar{\Omega}).$$

Then, $\mathbf{curl} \tilde{l} = -l \in H_0(\text{div}^0; \Omega)$, so that $\tilde{l} \in \mathcal{Z}$. Therefore, using Proposition 2.3.2 we obtain

$$\langle L, v \rangle = \int_{\Omega} (l \cdot \bar{v} + \tilde{l} \cdot \mathbf{curl} \bar{v}) = \int_{\Omega} (-\mathbf{curl} \tilde{l} \cdot \bar{v} + \tilde{l} \cdot \mathbf{curl} \bar{v}) = 0 \quad \forall v \in \mathcal{Z}.$$

This proves the claimed density. \square

Another consequence of Proposition 2.3.2 is the self-adjointness of the operator S which, together with its compactness, will allow us to obtain a thorough characterization of its spectrum.

Proposition 2.3.4 *S is self-adjoint.*

Proof. Given $\mathbf{f}, \mathbf{g} \in \mathbf{H}_0(\operatorname{div}^0; \Omega)$, let $\mathbf{w} := S\mathbf{f}$ and $\mathbf{v} := S\mathbf{g}$. From Lemma 2.3.1, $\operatorname{curl} \mathbf{w} = \mathbf{f}$ and $\operatorname{curl} \mathbf{v} = \mathbf{g}$ in Ω . Hence, by using Proposition 2.3.2, we have that

$$\int_{\Omega} (S\mathbf{f}) \cdot \bar{\mathbf{g}} = \int_{\Omega} \mathbf{w} \cdot \bar{\mathbf{g}} = \int_{\Omega} \mathbf{w} \cdot \operatorname{curl} \bar{\mathbf{v}} = \int_{\Omega} \operatorname{curl} \mathbf{w} \cdot \bar{\mathbf{v}} = \int_{\Omega} \mathbf{f} \cdot \bar{\mathbf{v}} = \int_{\Omega} \mathbf{f} \cdot (\overline{S\mathbf{g}})$$

and we conclude the proof. \square

Now, we are in a position to establish a spectral characterization of S .

Lemma 2.3.2 *The spectrum of S is given by $\sigma(S) = \{\mu_n\}_{n \in \mathbb{N}} \cup \{0\}$, with $\{\mu_n\}$ being a sequence of non-vanishing finite-multiplicity eigenvalues which converge to zero. Moreover, $\mu = 0$ is not an eigenvalue of S and there exists a Hilbertian basis $\{\mathbf{u}_n\}_{n \in \mathbb{N}}$ of $\mathbf{H}_0(\operatorname{div}^0; \Omega)$ of eigenfunctions of S ; i.e., such that $S\mathbf{u}_n = \mu_n \mathbf{u}_n$, $n \in \mathbb{N}$.*

Proof. The result is a consequence of the classical spectral characterization of compact self-adjoint operators. There only remains to prove that $\mu_n \neq 0 \forall n \in \mathbb{N}$. We proceed by contradiction. Assume $\mu_n = 0$. Hence, $\int_{\Omega} \mathbf{u}_n \cdot \operatorname{curl} \mathbf{v} = 0 \forall \mathbf{v} \in \mathbf{H}(\operatorname{curl}; \Omega)$. Then, $\mathbf{u}_n \in \mathbf{H}_0(\operatorname{curl}^0; \Omega) \cap \mathbf{H}_0(\operatorname{div}^0; \Omega) = \{\mathbf{0}\}$. \square

The above lemma and the relation between the spectrum of S and Problem 2.3.2, yields a thorough characterization for the solutions of the latter and, consequently, for the solutions of Problem 2.3.1.

Theorem 2.3.1 *Problem 2.3.1 has a denumerable set of solutions $(\lambda_n, \mathbf{u}_n)$, $n \in \mathbb{N}$, and $\{\mathbf{u}_n\}_{n \in \mathbb{N}}$ is a Hilbertian basis of $\mathbf{H}_0(\operatorname{div}^0; \Omega)$.*

One way to approximate the solutions of Problem 2.3.1 is to consider an appropriate discretization of the variational form given in Problem 2.3.2. For the sake of clarity, we postpone this approach to the appendix, where we propose and analyze a finite element method applied to a convenient variant of this problem (cf. Problem 2.7.1). This leads to a generalized eigenvalue problem involving two non-definite matrices. In spite of this fact, we prove in the appendix that this degenerate matrix eigenvalue problem is well posed. However, because of this degenerate character, standard eigensolvers cannot be used, which makes its computer solution significantly more complicated.

In what follows we introduce an alternative formulation which overcomes this drawback. This formulation will lead, after discretization, to a generalized eigenvalue problem involving two Hermitian matrices, that on the right-hand side being positive definite. Thus, standard software can be used for its numerical solution.

To derive this alternative formulation, notice that, for $\lambda \neq 0$, Problem 2.3.1 is equivalent to the following one: find $\lambda \in \mathbb{C}$ and $\mathbf{u} \in \mathbf{H}(\operatorname{curl}; \Omega)$, $\mathbf{u} \neq \mathbf{0}$, such that

$$\begin{aligned} \operatorname{curl} \mathbf{u} &= \lambda \mathbf{u} \quad \text{in } \Omega, \\ \operatorname{curl} \mathbf{u} \cdot \mathbf{n} &= 0 \quad \text{on } \Gamma. \end{aligned}$$

Clearly, the solution \mathbf{u} of the above problem belongs to \mathcal{Z} and satisfies

$$\int_{\Omega} \operatorname{curl} \mathbf{u} \cdot \operatorname{curl} \bar{\mathbf{v}} = \lambda \int_{\Omega} \mathbf{u} \cdot \operatorname{curl} \bar{\mathbf{v}} = \lambda \int_{\Omega} \operatorname{curl} \mathbf{u} \cdot \bar{\mathbf{v}} = \lambda^2 \int_{\Omega} \mathbf{u} \cdot \bar{\mathbf{v}} \quad \forall \mathbf{v} \in \mathcal{Z},$$

where we have also used Proposition 2.3.2. Therefore, we are led to consider the following problem:

Problem 2.3.3 Find $\lambda \in \mathbb{C}$ and $\mathbf{u} \in \mathcal{Z}$, $\mathbf{u} \neq \mathbf{0}$, such that

$$\int_{\Omega} \mathbf{curl} \mathbf{u} \cdot \mathbf{curl} \bar{\mathbf{v}} = \lambda^2 \int_{\Omega} \mathbf{u} \cdot \bar{\mathbf{v}} \quad \forall \mathbf{v} \in \mathcal{Z}.$$

We have just proved the following result.

Lemma 2.3.3 If (λ, \mathbf{u}) is a solution of Problem 2.3.1, then it is a solution of Problem 2.3.3.

The converse is partially true. To prove it, we consider the solution operator:

$$\begin{aligned} T : L^2(\Omega)^3 &\longrightarrow L^2(\Omega)^3, \\ \mathbf{f} &\longmapsto T\mathbf{f} := \mathbf{w}, \end{aligned}$$

with $\mathbf{w} \in \mathcal{Z}$ such that

$$\int_{\Omega} \mathbf{curl} \mathbf{w} \cdot \mathbf{curl} \bar{\mathbf{v}} + \int_{\Omega} \mathbf{w} \cdot \bar{\mathbf{v}} = \int_{\Omega} \mathbf{f} \cdot \bar{\mathbf{v}} \quad \forall \mathbf{v} \in \mathcal{Z}. \quad (2.7)$$

The well-posedness of problem (2.7) is a direct consequence of Lax Milgram lemma, whence T is well-defined and continuous. Note that $T\mathbf{u} = \mu\mathbf{u}$, with $\mu \neq 0$, if and only if (λ, \mathbf{u}) is a solution of Problem 2.3.3, with $\lambda^2 + 1 = \frac{1}{\mu}$.

Clearly $\mu = 1$ is an eigenvalue of T (correspondingly, $\lambda = 0$ is an eigenvalue of Problem 2.3.3) with associated eigenspace

$$\mathcal{K} := \{\mathbf{v} \in \mathcal{Z} : \mathbf{curl} \mathbf{v} = \mathbf{0} \text{ in } \Omega\} = \nabla(\mathbf{H}^1(\Omega)). \quad (2.8)$$

Since T is clearly self-adjoint (cf. (2.7)), the orthogonal complement of \mathcal{K} ,

$$\mathcal{K}^{\perp_{L^2(\Omega)^3}} = \mathbf{H}_0(\mathbf{div}^0; \Omega)$$

is an invariant subspace for T . Therefore,

$$\widehat{T} := T|_{\mathbf{H}_0(\mathbf{div}^0; \Omega)} : \mathbf{H}_0(\mathbf{div}^0; \Omega) \longrightarrow \mathbf{H}_0(\mathbf{div}^0; \Omega)$$

is a well-defined bounded operator and $\sigma(T) = \sigma(\widehat{T}) \cup \{1\}$. Moreover, since T takes values in the space $\mathcal{Z} \subset \mathbf{H}(\mathbf{curl}; \Omega)$ and, by virtue of (2.4) $\mathbf{H}(\mathbf{curl}; \Omega) \cap \mathbf{H}_0(\mathbf{div}^0; \Omega) \hookrightarrow \mathbf{H}_0(\mathbf{div}^0; \Omega)$ compactly, we derive the compactness of \widehat{T} .

The following theorem shows how the eigenpairs of T , with $\mu \neq 1$, are related with the solution of Problem 2.3.1.

Theorem 2.3.2 The following properties hold true:

a) The spectrum of T decomposes as follows:

$$\sigma(T) = \{1\} \cup \{\mu_n\}_{n \in \mathbb{N}} \cup \{0\}.$$

Moreover:

- $\mu = 1$ is an eigenvalue of T with infinite-dimensional eigenspace \mathcal{K} ;
 - $\{\mu_n\}_{n \in \mathbb{N}}$ is a sequence of finite-multiplicity eigenvalues $\mu_n \in (0, 1)$, $n \in \mathbb{N}$, which converge to 0;
 - $\mu = 0$ is not an eigenvalue of T .
- b) If λ is an eigenvalue of Problem 2.3.1 with eigenspace \mathcal{E} , then $\mu = \frac{1}{1+\lambda^2}$ is an eigenvalue of T and \mathcal{E} is an invariant subspace of T .
- c) If $\mu \neq 1$ is an eigenvalue of T with eigenspace \mathcal{E} , then there exists an eigenvalue λ of Problem 2.3.1 such that $\mu = \frac{1}{1+\lambda^2}$ and \mathcal{E} is an invariant subspace of Problem 2.3.1.

Proof. We have already proved that $\mu = 1$ is an eigenvalue of T with corresponding eigenspace \mathcal{K} and that $\sigma(T) = \sigma(\widehat{T}) \cup \{1\}$. Thus, the spectral characterization of T is a consequence of the compactness of \widehat{T} . On the other hand, $\mu = 0$ is not an eigenvalue of T ; in fact, if $T\mathbf{f} = \mathbf{0}$, then it follows from (2.7) that $\mathbf{f} \perp \mathcal{Z} \supset \mathcal{D}(\Omega)^3$ dense in $L^2(\Omega)^3$, so that $\mathbf{f} = \mathbf{0}$. Moreover, for all the eigenvalues $\mu_n \neq 1$, it is also easy to show from (2.7) that $\mu_n \in (0, 1)$. Thus, we conclude (a).

In its turn, Lemma 2.3.3 and the arguments above lead to (b).

It remains to prove that all the eigenvalues of \widehat{T} are of the form $\mu = \frac{1}{1+\lambda^2}$, with λ being an eigenvalue of Problem 2.3.1. In fact, according to Theorem 2.3.1, the sequence of eigenfunctions of Problem 2.3.1 is a Hilbertian basis of $H_0(\operatorname{div}^0; \Omega)$. Since we have already proved in (b) that all of them are eigenfunctions of \widehat{T} , this operator cannot have an additional eigenpair; otherwise, since T is self adjoint, the additional eigenfunction would have to be orthogonal to the whole Hilbertian basis, which cannot happen. Thus, we conclude (c). \square

As a consequence of this theorem and the relation between the eigenpairs of Problem 2.3.3 and those of the operator T , we obtain the following result.

Corollary 2.3.1 *Let $\nu \neq 0$ be an eigenvalue of Problem 2.3.3 and \mathcal{E} the corresponding eigenspace. Then, there exists an eigenvalue λ of Problem 2.3.1 such that $\nu = \lambda^2$ and \mathcal{E} is an invariant subspace of Problem 2.3.1.*

Remark 2.3.1 *Notice that the eigenfunctions of Problem 2.3.3 are not necessarily eigenfunctions of Problem 2.3.1. In fact, if λ and $-\lambda$ were both eigenvalues of Problem 2.3.1, then λ^2 would be an eigenvalue of Problem 2.3.3, with multiplicity equal to the sum of those of λ and $-\lambda$. Moreover, an eigenfunction of Problem 2.3.3 corresponding to λ^2 would be a linear combination of the eigenfunctions of Problem 2.3.1 associated to λ and $-\lambda$, but not necessarily an eigenfunction itself. In other words, in such a case, in general the eigenfunctions of Problem 2.3.3 are not Beltrami fields satisfying $\operatorname{curl} \mathbf{u} = \pm \lambda \mathbf{u}$. At first glance one might think it would be very unusual for λ and $-\lambda$ to be both eigenvalues of Problem 2.3.1. However, as will be shown in Section 2.6.1, this is something that always happens when the domain Ω is symmetric.*

2.4 Finite element approximation

In this section, we introduce a Galerkin approximation of Problem 2.3.3 and prove some convergence results. From now on, we assume that Ω is a polyhedral domain and $\{\mathcal{T}_h\}_{h>0}$ is

a regular family of partitions of $\bar{\Omega}$ in tetrahedra T , so that $\bar{\Omega} = \bigcup_{T \in \mathcal{T}_h} T$; parameter h stands for the mesh-size and we assume that any generic constant denoted by C is independent of h . We denote by \mathcal{T}_h^Γ the corresponding triangulation induced on the boundary of Ω , namely, $\mathcal{T}_h^\Gamma := \{F \text{ face of } T \in \mathcal{T}_h : F \subset \Gamma\}$.

For any $T \in \mathcal{T}_h$, let $\mathcal{N}^k(T) := \mathbb{P}_{k-1}(T)^3 \oplus \{\mathbf{p} \in \bar{\mathbb{P}}_k(T)^3 : \mathbf{p}(\mathbf{x}) \cdot \mathbf{x} = 0\}$, where \mathbb{P}_k is the set of polynomials of degree not greater than k and $\bar{\mathbb{P}}_k$ the subset of homogeneous polynomials of degree k .

The corresponding global space to approximate $\mathbf{H}(\mathbf{curl}; \Omega)$ is the space of functions that are locally in $\mathcal{N}^k(T)$ and have continuous tangential components across the faces of the triangulation \mathcal{T}_h . This is the well-known Nédélec space:

$$\mathcal{N}_h := \left\{ \mathbf{v}_h \in \mathbf{H}(\mathbf{curl}; \Omega) : \mathbf{v}_h|_T \in \mathcal{N}^k(T) \quad \forall T \in \mathcal{T}_h \right\}$$

(for further details see, for instance, [68, Section 5.5]). Whence, the natural approximation space for \mathcal{Z} is

$$\mathcal{Z}_h := \mathcal{N}_h \cap \mathcal{Z} = \{ \mathbf{v}_h \in \mathcal{N}_h : \mathbf{curl} \mathbf{v}_h \cdot \mathbf{n} = 0 \text{ on } \Gamma \}.$$

The Galerkin approximation of Problem 2.3.3 reads as follows:

Problem 2.4.1 Find $\lambda_h \in \mathbb{C}$ and $\mathbf{u}_h \in \mathcal{Z}_h$, $\mathbf{u}_h \neq \mathbf{0}$, such that

$$\int_{\Omega} \mathbf{curl} \mathbf{u}_h \cdot \mathbf{curl} \bar{\mathbf{v}}_h = \lambda_h^2 \int_{\Omega} \mathbf{u}_h \cdot \bar{\mathbf{v}}_h \quad \forall \mathbf{v}_h \in \mathcal{Z}_h.$$

Notice that Problem 2.4.1 leads to a well-posed generalized matrix eigenvalue problem, because the sesquilinear form on the right hand side is Hermitian positive definite. To solve this problem, it is necessary to impose somehow the constraint $\mathbf{curl} \mathbf{u}_h \cdot \mathbf{n} = 0$ in the definition of \mathcal{Z}_h ; we will address this point in Section 2.5.

Consider the corresponding discrete solution operator:

$$\begin{aligned} T_h : L^2(\Omega)^3 &\longrightarrow L^2(\Omega)^3, \\ \mathbf{f} &\longmapsto T_h \mathbf{f} := \mathbf{w}_h, \end{aligned}$$

with $\mathbf{w}_h \in \mathcal{Z}_h$ such that

$$\int_{\Omega} \mathbf{curl} \mathbf{w}_h \cdot \mathbf{curl} \bar{\mathbf{v}}_h + \int_{\Omega} \mathbf{w}_h \cdot \bar{\mathbf{v}}_h = \int_{\Omega} \mathbf{f} \cdot \bar{\mathbf{v}}_h \quad \forall \mathbf{v}_h \in \mathcal{Z}_h.$$

As a consequence of Lax Milgram lemma, T_h is a well-defined bounded linear operator. Clearly λ_h is an eigenvalue of Problem 2.4.1 if and only if $\frac{1}{1+\lambda_h^2} \in \sigma(T_h)$.

To prove convergence and error estimates for the proposed Galerkin scheme, we will use the results on spectral approximation for non-compact operators from [33, 34]. With this aim, we consider the restrictions of the operators T and T_h to the respective invariant subspaces \mathcal{Z} and \mathcal{Z}_h . To avoid overburdening the notation, from now on T and T_h will denote $T|_{\mathcal{Z}}$ and $T_h|_{\mathcal{Z}_h}$, respectively. Note that the spectral characterization of T given in Theorem 2.3.2 remains the same without the need of any modification.

In order to use the theory from [33, 34] we need to prove the following properties:

$$\text{P1: } \lim_{h \rightarrow 0} \|(T - T_h)|_{\mathcal{Z}_h}\| = 0,$$

$$\text{P2: } \forall \mathbf{v} \in \mathcal{Z} \lim_{h \rightarrow 0} \inf_{\mathbf{v}_h \in \mathcal{Z}_h} \|\mathbf{v} - \mathbf{v}_h\|_{\mathbf{curl}, \Omega} = 0.$$

Property P2 follows immediately from Proposition 2.3.3 and standard interpolation error estimates for Nédélec finite elements. In order to prove property P1, we establish some preliminary results.

Let us define

$$r_k := \min \{s, k\}, \quad (2.9)$$

where $k \geq 1$ is the degree of the Nédélec finite elements and $s > 1/2$ is a Sobolev exponent such that (2.4) holds true.

Let us recall that $\mathcal{K} \subset \mathcal{Z}$ is the eigenspace of T associated with the eigenvalue $\mu = 1$ and let $\mathcal{V} := \mathcal{K}^{\perp \mathcal{Z}}$. It is immediate to show from (2.8) that $\mathcal{V} = \mathbf{H}_0(\text{div}^0; \Omega) \cap \mathcal{Z}$. Operator T restricted to \mathcal{K} is the identity; instead, restricted to its orthogonal complement is a regularizing operator, as shown in the following lemma.

Lemma 2.4.1 *Let $\mathbf{f} \in \mathcal{V}$ and $\mathbf{w} := T\mathbf{f}$. Then, $\mathbf{w} \in \mathbf{H}^s(\mathbf{curl}; \Omega)$ and*

$$\|\mathbf{w}\|_{s, \Omega} + \|\mathbf{curl} \mathbf{w}\|_{s, \Omega} \leq C \|\mathbf{f}\|_{0, \Omega}.$$

Proof. From the definition of T , \mathbf{w} and \mathbf{f} are related by (2.7). Taking $\mathbf{v} = \mathbf{w}$ in this equation, we have

$$\|\mathbf{w}\|_{\mathbf{curl}, \Omega} \leq \|\mathbf{f}\|_{0, \Omega}. \quad (2.10)$$

Moreover, since $\nabla(\mathbf{H}^1(\Omega)) \subset \mathcal{Z}$, taking in (2.7) $\mathbf{v} = \nabla\psi$, $\psi \in \mathbf{H}^1(\Omega)$, it follows that

$$\int_{\Omega} \mathbf{w} \cdot \nabla \bar{\psi} = \int_{\Omega} \mathbf{f} \cdot \nabla \bar{\psi} = 0 \quad \forall \psi \in \mathbf{H}^1(\Omega).$$

Hence, for $\mathbf{f} \in \mathcal{V} \subset \mathbf{H}_0(\text{div}^0; \Omega)$, we have that $\mathbf{w} \in \mathbf{H}_0(\text{div}^0; \Omega)$, too. Consequently, $\mathbf{w} \in \mathbf{H}(\mathbf{curl}; \Omega) \cap \mathbf{H}_0(\text{div}^0; \Omega) \hookrightarrow \mathbf{H}^s(\Omega)^3$ (cf. (2.4)) and, using (2.10), it follows that

$$\|\mathbf{w}\|_{s, \Omega} \leq C \|\mathbf{w}\|_{\mathbf{curl}, \Omega} \leq C \|\mathbf{f}\|_{0, \Omega}.$$

On the other hand, taking $\mathbf{v} \in \mathcal{D}(\Omega)^3 \subset \mathcal{Z}$ in (2.7), we obtain

$$\mathbf{curl}(\mathbf{curl} \mathbf{w}) + \mathbf{w} = \mathbf{f} \quad \text{in } \Omega. \quad (2.11)$$

Hence, $\mathbf{curl} \mathbf{w} \in \mathbf{H}(\mathbf{curl}; \Omega)$ and, since $\mathbf{w} \in \mathcal{Z}$, $\mathbf{curl} \mathbf{w} \in \mathbf{H}_0(\text{div}^0; \Omega)$, too. Then, the same arguments as above allow us to conclude that $\mathbf{curl} \mathbf{w} \in \mathbf{H}^s(\Omega)^3$ and

$$\|\mathbf{curl} \mathbf{w}\|_{s, \Omega} \leq C \|\mathbf{curl} \mathbf{w}\|_{\mathbf{curl}, \Omega} \leq C \|\mathbf{f}\|_{0, \Omega},$$

the last inequality because of (2.11) and (2.10). Thus, we conclude the proof. \square

Clearly $\mu_h = 1$ is an eigenvalue of T_h with associated eigenspace

$$\mathcal{K}_h := \{\mathbf{v}_h \in \mathcal{Z}_h : \mathbf{curl} \mathbf{v}_h = \mathbf{0}\} \subset \mathcal{K},$$

so that T_h restricted to \mathcal{K}_h is the identity, too. Let $\mathcal{V}_h := \mathcal{K}_h^{\perp \mathcal{Z}_h}$. Notice that $\mathcal{V}_h \not\subset \mathcal{V}$. However, the following lemma shows that the curl-free terms in the Helmholtz decomposition of \mathcal{V}_h are asymptotically negligible.

Lemma 2.4.2 For $\mathbf{f}_h \in \mathcal{V}_h$, there exist $\boldsymbol{\chi} \in \mathcal{V}$ and $\boldsymbol{\eta} \in \mathcal{K}$ such that $\mathbf{f}_h = \boldsymbol{\chi} + \boldsymbol{\eta}$ and there hold:

- a) $\boldsymbol{\chi} \in \mathbf{H}^s(\Omega)^3$ with $\|\boldsymbol{\chi}\|_{s,\Omega} \leq C \|\mathbf{curl} \mathbf{f}_h\|_{0,\Omega}$,
- b) $\|\boldsymbol{\eta}\|_{0,\Omega} \leq Ch^{r_1} \|\mathbf{curl} \mathbf{f}_h\|_{0,\Omega}$, with r_1 as defined in (2.9).

Proof. Since $\mathbf{f}_h \in \mathcal{V}_h \subset \mathcal{Z}$, the decomposition $\mathbf{f}_h = \boldsymbol{\chi} + \boldsymbol{\eta}$ follows from the fact that $\mathcal{V} = \mathcal{K}^{\perp \mathcal{Z}}$. Now, since $\mathcal{V} \subset \mathbf{H}(\mathbf{curl}; \Omega) \cap \mathbf{H}_0(\text{div}^0; \Omega)$, we have that $\boldsymbol{\chi} \in \mathbf{H}^s(\Omega)^3$ (cf. (2.4), again). Moreover, because of the definition of \mathcal{K} , $\mathbf{curl} \boldsymbol{\chi} = \mathbf{curl} \mathbf{f}_h$. Hence,

$$\|\boldsymbol{\chi}\|_{s,\Omega} \leq C \|\boldsymbol{\chi}\|_{\mathbf{curl},\Omega} \leq C \|\mathbf{curl} \boldsymbol{\chi}\|_{0,\Omega} = C \|\mathbf{curl} \mathbf{f}_h\|_{0,\Omega},$$

the last inequality because, for Ω simply-connected, $\|\boldsymbol{\chi}\|_{0,\Omega} \leq C \|\mathbf{curl} \boldsymbol{\chi}\|_{0,\Omega}$ for all $\boldsymbol{\chi} \in \mathbf{H}(\mathbf{curl}; \Omega) \cap \mathbf{H}_0(\text{div}^0; \Omega)$ (cf. [2, Corollary 3.16]). Thus we conclude (a).

To prove (b), we will use the Nédélec interpolant I_h^N . According to [68, Theorem 5.41(2)], since $\mathbf{curl} \boldsymbol{\chi} = \mathbf{curl} \mathbf{f}_h$, we have that

$$\|\boldsymbol{\chi} - I_h^N \boldsymbol{\chi}\|_{0,\Omega} \leq C \left(h^{r_1} \|\boldsymbol{\chi}\|_{s,\Omega} + h \|\mathbf{curl} \mathbf{f}_h\|_{0,\Omega} \right) \leq Ch^{r_1} \|\mathbf{curl} \mathbf{f}_h\|_{0,\Omega}. \quad (2.12)$$

On the other hand, let I_h^R be the divergence-conforming Raviart-Thomas interpolant (see [68, Section 5.4]). Since $\mathbf{curl} \boldsymbol{\chi} = \mathbf{curl} \mathbf{f}_h \in \mathbf{H}^\varepsilon(\Omega)^3$ for all $\varepsilon \in (0, \frac{1}{2})$, according to Remark 5.16 and Lemma 5.40 from [68], it follows that

$$\mathbf{curl} (I_h^N \boldsymbol{\chi}) = I_h^R (\mathbf{curl} \boldsymbol{\chi}) = I_h^R (\mathbf{curl} \mathbf{f}_h) = \mathbf{curl} \mathbf{f}_h. \quad (2.13)$$

Now, we write

$$\|\boldsymbol{\eta}\|_{0,\Omega}^2 = \int_{\Omega} \boldsymbol{\eta} \cdot (\mathbf{f}_h - \boldsymbol{\chi}) = \int_{\Omega} \boldsymbol{\eta} \cdot (\mathbf{f}_h - I_h^N \boldsymbol{\chi}) + \int_{\Omega} \boldsymbol{\eta} \cdot (I_h^N \boldsymbol{\chi} - \boldsymbol{\chi}). \quad (2.14)$$

By virtue of (2.13) we have that $\mathbf{f}_h - I_h^N \boldsymbol{\chi} \in \mathcal{K}_h \subset \mathcal{K}$, so that $\boldsymbol{\chi} \perp (\mathbf{f}_h - I_h^N \boldsymbol{\chi})$ in $L^2(\Omega)^3$ and, since $\mathbf{f}_h \in \mathcal{V}_h = \mathcal{K}_h^{\perp \mathcal{Z}_h}$, it follows that

$$\int_{\Omega} \boldsymbol{\eta} \cdot (\mathbf{f}_h - I_h^N \boldsymbol{\chi}) = \int_{\Omega} \mathbf{f}_h \cdot (\mathbf{f}_h - I_h^N \boldsymbol{\chi}) - \int_{\Omega} \boldsymbol{\chi} \cdot (\mathbf{f}_h - I_h^N \boldsymbol{\chi}) = 0.$$

Hence, from (2.14) and (2.12), we conclude that

$$\|\boldsymbol{\eta}\|_{0,\Omega} \leq \|I_h^N \boldsymbol{\chi} - \boldsymbol{\chi}\|_{0,\Omega} \leq Ch^{r_1} \|\mathbf{curl} \mathbf{f}_h\|_{0,\Omega}.$$

Thus, we end the proof. \square

Now we are ready to prove the following result, from which we will derive property P1.

Lemma 2.4.3 There exists $C > 0$ such that, for all $\mathbf{f}_h \in \mathcal{V}_h$,

$$\|(T - T_h) \mathbf{f}_h\|_{\mathbf{curl},\Omega} \leq Ch^{r_1} \|\mathbf{f}_h\|_{\mathbf{curl},\Omega},$$

with r_1 as defined in (2.9).

Proof. Given $\mathbf{f}_h \in \mathcal{V}_h$, let $\boldsymbol{\chi} \in \mathcal{V}$ and $\boldsymbol{\eta} \in \mathcal{K}$ be as in Lemma 2.4.2. Let $\mathbf{z} := T\boldsymbol{\chi}$ and $\mathbf{z}_h := T_h\boldsymbol{\chi}$. The following Cea estimate follows immediately from the definitions of T and T_h :

$$\|\mathbf{z} - \mathbf{z}_h\|_{\mathbf{curl},\Omega} \leq C \inf_{\mathbf{v}_h \in \mathcal{Z}_h} \|\mathbf{z} - \mathbf{v}_h\|_{\mathbf{curl},\Omega}.$$

Then, using the Nédélec interpolant and standard error estimates (cf. [68, Theorem 5.41(1)]), it follows that

$$\|\mathbf{z} - \mathbf{z}_h\|_{\mathbf{curl},\Omega} \leq C \|\mathbf{z} - I_h^N \mathbf{z}\|_{\mathbf{curl},\Omega} \leq Ch^{r_k} \left(\|\mathbf{z}\|_{s,\Omega} + \|\mathbf{curl} \mathbf{z}\|_{s,\Omega} \right).$$

Thus, from Lemma 2.4.1, and the fact that $\mathcal{K} \perp \mathcal{V}$ in $L^2(\Omega)$, we have

$$\|(T - T_h)\boldsymbol{\chi}\|_{\mathbf{curl},\Omega} = \|\mathbf{z} - \mathbf{z}_h\|_{\mathbf{curl},\Omega} \leq Ch^{r_k} \|\boldsymbol{\chi}\|_{0,\Omega} \leq Ch^{r_k} \|\mathbf{f}_h\|_{0,\Omega}.$$

On the other hand, for $\boldsymbol{\eta} \in \mathcal{K}$, since $T\boldsymbol{\eta} = \boldsymbol{\eta}$ and $T_h\boldsymbol{\eta}$ is the Galerkin projection of $\boldsymbol{\eta}$ onto \mathcal{Z}_h , using Lemma 2.4.2(b) we can write

$$\|(T - T_h)\boldsymbol{\eta}\|_{\mathbf{curl},\Omega} \leq \|\boldsymbol{\eta}\|_{\mathbf{curl},\Omega} = \|\boldsymbol{\eta}\|_{0,\Omega} \leq Ch^{r_1} \|\mathbf{f}_h\|_{\mathbf{curl},\Omega}.$$

Therefore,

$$\|(T - T_h)\mathbf{f}_h\|_{\mathbf{curl},\Omega} \leq \|(T - T_h)\boldsymbol{\chi}\|_{\mathbf{curl},\Omega} + \|(T - T_h)\boldsymbol{\eta}\|_{\mathbf{curl},\Omega} \leq Ch^{r_1} \|\mathbf{f}_h\|_{\mathbf{curl},\Omega}$$

and we conclude the proof. \square

Property P1 clearly follows from the above lemma and the fact that T and T_h coincide on \mathcal{K}_h . As a first consequence, we have the next result, which was proved to follow from property P1 in [33, Theorem 1].

Theorem 2.4.1 *Let $J \subset \mathbb{R}$ be an open set containing $\sigma(T)$. Then, there exists $h_0 > 0$ such that $\sigma(T_h) \subset J \ \forall h < h_0$.*

As a consequence of the above theorem, we know that the proposed numerical method does not introduce spurious modes (which would be the case, for instance, if Lagrangian finite elements were used; see [18]).

Now, we are in a position to write the main result of this chapter related to the convergence of the proposed scheme.

Theorem 2.4.2 *Let $\mu \in \sigma(T)$ be an eigenvalue of finite-multiplicity m . Let \mathcal{E} be the corresponding eigenspace. There exists $h_0 > 0$ such that, for all $h < h_0$, $\sigma(T_h)$ contains m eigenvalues $\mu_h^{(1)}, \dots, \mu_h^{(m)}$ (repeated accordingly to their respective multiplicities) such that*

$$\mu_h^{(i)} \xrightarrow{h \rightarrow 0} \mu, \quad i = 1, \dots, m.$$

Let \mathcal{E}_h be the direct sum of the corresponding eigenspaces. Then,

$$\widehat{\delta}(\mathcal{E}, \mathcal{E}_h) \leq C\gamma_h,$$

and

$$\max_{1 \leq i \leq m} \left| \mu - \mu_h^{(i)} \right| \leq C\gamma_h^2,$$

where

$$\gamma_h := \delta(\mathcal{E}, \mathcal{Z}_h) := \sup_{\mathbf{v} \in \mathcal{E}} \inf_{\substack{\mathbf{v}_h \in \mathcal{Z}_h \\ \|\mathbf{v}\|_{\mathbf{curl}, \Omega} = 1}} \|\mathbf{v} - \mathbf{v}_h\|_{\mathbf{curl}, \Omega}$$

and

$$\widehat{\delta}(\mathcal{E}, \mathcal{E}_h) := \max \{ \delta(\mathcal{E}, \mathcal{E}_h), \delta(\mathcal{E}_h, \mathcal{E}) \}.$$

Proof. Since we have already proved that properties P1 and P2 hold true, the results are direct consequences of [33, Section 2] and Theorems 1 and 3 from [34]. \square

To conclude spectral convergence with an optimal order of approximation from the previous theorem, we only need an appropriate estimate for the term γ_h .

Theorem 2.4.3 *Let γ_h be as in Theorem 2.4.2. Then, there exists $C > 0$ such that*

$$\gamma_h \leq Ch^{r_k},$$

with r_k as defined in (2.9).

Proof. Let $\mathbf{v} \in \mathcal{E}$ be such that $\|\mathbf{v}\|_{\mathbf{curl}, \Omega} = 1$. Since $T\mathbf{v} = \mu\mathbf{v}$, from Lemma 2.4.1 it follows that $\mathbf{v} \in H^s(\mathbf{curl}; \Omega)$ and

$$\|\mathbf{v}\|_{s, \Omega} + \|\mathbf{curl} \mathbf{v}\|_{s, \Omega} \leq \frac{C}{\mu} \|\mathbf{v}\|_{0, \Omega} \leq \frac{C}{\mu}.$$

Let $I_h^N \mathbf{v} \in \mathcal{N}_h$ be the Nédélec interpolant of \mathbf{v} ; in what follows, we show that $I_h^N \mathbf{v} \in \mathcal{Z}_h$ (this has been proved in [65, Proposition 4.3] and [13, Lemma 2.2], but only for lowest-order Nédélec elements and under different topological assumptions). Let I_h^R be the divergence-conforming Raviart-Thomas interpolant. Since $\mathbf{v} \in \mathcal{E} \subset \mathcal{Z}$, we have that $\mathbf{curl} \mathbf{v} \cdot \mathbf{n} = 0$ on Γ . Hence, $\mathbf{curl}(I_h^N \mathbf{v}) \cdot \mathbf{n} = (I_h^R \mathbf{curl} \mathbf{v}) \cdot \mathbf{n} = 0$ on Γ , too, the first equality because of [68, Lemma 5.40] and the second one because of the well known property that the Raviart-Thomas interpolant preserves vanishing normal components on the boundary. Thus, $I_h^N \mathbf{v} \in \mathcal{Z} \cap \mathcal{N}_h = \mathcal{Z}_h$.

Therefore, using again the standard error estimate for the Nédélec interpolant (cf. [68, Theorem 5.41(1)]), we obtain

$$\delta(\mathcal{E}, \mathcal{Z}_h) \leq \sup_{\substack{\mathbf{v} \in \mathcal{E} \\ \|\mathbf{v}\|_{\mathbf{curl}, \Omega} = 1}} \|\mathbf{v} - I_h^N \mathbf{v}\|_{\mathbf{curl}, \Omega} \leq Ch^{r_k} \left(\|\mathbf{v}\|_{s, \Omega} + \|\mathbf{curl} \mathbf{v}\|_{s, \Omega} \right) \leq \frac{C}{\mu} h^{r_k}.$$

Thus, we end the proof. \square

As a consequence of the two previous theorems we conclude that the eigenvalues and eigenfunctions of Problem 2.4.1 converge with optimal order to those of Problem 2.3.3.

2.5 Implementation issues

For the implementation of Problem 2.4.1, it is necessary to impose the condition $\mathbf{curl} \mathbf{u}_h \cdot \mathbf{n} = 0$ on Γ . To do this, we follow a similar approach to that used in [65] and [13] for lowest-order Nédélec elements.

Since we have assumed that the domain Ω is simply-connected, each connected component of its boundary is simply-connected, too. In such a case, $\mathbf{curl} \mathbf{u}_h \cdot \mathbf{n} = 0$ on Γ if and only if the tangential component of \mathbf{u}_h satisfies

$$\mathbf{n} \times \mathbf{u}_h \times \mathbf{n} = \nabla_{\Gamma} \varphi_h \quad \text{on } \Gamma, \quad (2.15)$$

where $\varphi_h \in \mathcal{L}_h^{\Gamma} := \{\psi_h \in \mathcal{C}(\Gamma) : \psi_h|_F \in \mathbb{P}_k(F) \quad \forall F \in \mathcal{T}_h^{\Gamma}\}$ and ∇_{Γ} denotes the surface gradient (i.e., the two-dimensional gradient on each plane face of Γ ; see [25] for its proper definition). In fact, it is shown in [25, Section 4] that $\mathbf{curl} \mathbf{u}_h \cdot \mathbf{n} = \text{curl}_{\Gamma}(\mathbf{n} \times \mathbf{u}_h \times \mathbf{n})$ on Γ , where curl_{Γ} denotes the scalar surface curl. Hence, from [25, Theorem 5.1], we know that there exists $\varphi_h \in \mathbb{H}^1(\Gamma)$ such that $\mathbf{n} \times \mathbf{u}_h \times \mathbf{n} = \nabla_{\Gamma} \varphi_h$ on Γ . Moreover, by using [68, Remark 5.29], it is easy to show that $\varphi_h \in \mathcal{L}_h^{\Gamma}$.

Let

$$\mathcal{L}_h := \{\psi_h \in \mathcal{C}(\Omega) : \psi_h|_T \in \mathbb{P}_k(T) \quad \forall T \in \mathcal{T}_h\}.$$

Let $\{\varphi_j\}_{j=1}^K$ be the nodal basis of \mathcal{L}_h . Without loss of generality we order these basis functions so that the first J of them correspond to all the nodal values on the boundary Γ . Therefore $\{\varphi_j|_{\Gamma}\}_{j=1}^J$ is a basis of \mathcal{L}_h^{Γ} . Moreover, $\langle \{\nabla_{\Gamma} \varphi_j\}_{j=1}^J \rangle = \nabla_{\Gamma}(\mathcal{L}_h^{\Gamma})$. However, these functions are not linearly independent. To obtain a basis of $\nabla_{\Gamma}(\mathcal{L}_h^{\Gamma})$, we must choose one vertex on each connected component $\Gamma_0, \dots, \Gamma_I$ of Γ and drop out the basis function corresponding to these vertices. Let us assume for simplicity that these basis function are the last ones. Then, it is straightforward to show that $\{\nabla_{\Gamma} \varphi_j\}_{j=1}^L$ ($L := J - I - 1$) is a basis of $\nabla_{\Gamma}(\mathcal{L}_h^{\Gamma})$.

Let $\{\phi_m\}_{m=1}^M$ be the nodal basis of \mathcal{N}_h ; without loss of generality we also assume that the last ones, $\{\phi_m\}_{m=N+1}^M$, are those corresponding to the degrees of freedom related to the faces or edges on Γ . Notice that all the other basis functions lie in \mathcal{Z}_h . Thus, we have the following proposition that characterizes a basis of this space.

Proposition 2.5.1 *The set $\{\phi_m\}_{m=1}^N \cup \{\nabla \varphi_j\}_{j=1}^L$ is a basis of \mathcal{Z}_h .*

Proof. It is essentially identical to that of Proposition 4.2 from [65], where a similar result is proved in the case that Γ is connected for lowest-order Nédélec elements. We include it for completeness.

First we prove that $\{\phi_m\}_{m=1}^N \cup \{\nabla \varphi_j\}_{j=1}^L$, which is clearly a subset of \mathcal{Z}_h , spans this space. Let $\phi_h \in \mathcal{Z}_h$. Because of (2.15), $\mathbf{n} \times \phi_h|_{\Gamma} \times \mathbf{n} \in \nabla_{\Gamma}(\mathcal{L}_h^{\Gamma})$ and, hence, there exist β_j , $j = 1, \dots, L$, such that

$$\mathbf{n} \times \phi_h|_{\Gamma} \times \mathbf{n} = \sum_{j=1}^L \beta_j \nabla_{\Gamma} \varphi_j.$$

Then, the degrees of freedom of $\phi_h - \sum_{j=1}^L \beta_j \nabla \varphi_j \in \mathcal{N}_h$ corresponding to edges or faces lying on the boundary vanish. Therefore,

$$\phi_h - \sum_{j=1}^L \beta_j \nabla \varphi_j \in \langle \phi_1, \dots, \phi_N \rangle.$$

It only remains to prove that $\{\phi_m\}_{m=1}^N \cup \{\nabla \varphi_j\}_{j=1}^L$ is a linearly independent set. Let us assume that

$$\sum_{m=1}^N \alpha_m \phi_m + \sum_{j=1}^L \beta_j \nabla \varphi_j = 0.$$

Since $\mathbf{n} \times \phi_m|_{\Gamma} \times \mathbf{n}$ vanish for all $m = 1, \dots, N$ and $\mathbf{n} \times \nabla \varphi_j|_{\Gamma} \times \mathbf{n} = \nabla_{\Gamma} \varphi_j$ is a basis of $\nabla_{\Gamma}(\mathcal{L}_h^{\Gamma})$, we have that $\beta_1 = \dots = \beta_L = 0$. Thus the result follows from the linear independence of $\{\phi_m\}_{m=1}^N$. \square

Actually, the constraint $\mathbf{curl} \mathbf{u}_h \cdot \mathbf{n} = 0$ on Γ in the definition of \mathcal{Z}_h can be imposed without the need of using the basis functions $\{\nabla \varphi_j\}_{j=1}^L$. We illustrate this in the case of lowest-order Nédélec elements, which are the ones that we have implemented in the code used for the numerical tests reported in the next section.

Let $\{e_1, \dots, e_M\}$ be the set of all edges in \mathcal{T}_h and $\{\phi_m\}_{m=1}^M$ be the associated nodal basis of \mathcal{N}_h . Then, for any $\mathbf{u}_h \in \mathcal{N}_h$,

$$\mathbf{u}_h = \sum_{m=1}^M \alpha_m \phi_m,$$

where $\alpha_m := \int_{e_m} \mathbf{u}_h \cdot \mathbf{t}_m$, with \mathbf{t}_m a unit tangent to e_m , $m = 1, \dots, M$. We assume as above that the edges lying on Γ are the last ones: e_{N+1}, \dots, e_M .

Let $\{P_j\}_{j=1}^J$ be the set of vertices of \mathcal{T}_h lying on Γ . Also as above, each one of the last $I + 1$ vertices has been chosen on a different connected component of Γ . Let $\{\varphi_j\}_{j=1}^J$ be the corresponding nodal basis of \mathcal{L}_h^{Γ} . In such a case, according to the Proposition 2.5.1, for $\mathbf{u}_h \in \mathcal{Z}_h$, there exist complex numbers $\alpha'_1, \dots, \alpha'_N$ and β_1, \dots, β_J such that

$$\mathbf{u}_h = \sum_{m=1}^N \alpha'_m \phi_m + \sum_{j=1}^J \beta_j \nabla \varphi_j,$$

where $\beta_{L+1} = \dots = \beta_J = 0$. Then, from the definition of α_m and the above relation, we obtain:

$$\alpha_m = \begin{cases} \alpha'_m, & \text{if } e_m \cap \Gamma = \emptyset, \\ \alpha'_m \pm \beta_j, & \text{if } e_m \cap \Gamma = \{P_j\}, \\ \alpha'_m \pm (\beta_j - \beta_k), & \text{if } e_m \cap \Gamma = \{P_j, P_k\} \ (e_m \not\subset \Gamma), \\ \pm (\beta_j - \beta_k), & \text{if } e_m \subset \Gamma, \text{ with end points } P_j, P_k, \end{cases}$$

the signs above depend on the chosen orientation of the tangent vector \mathbf{t}_m .

These relations allow us to define a matrix $\mathbf{C} \in \mathbb{R}^{M \times (N+L)}$ such that $\boldsymbol{\alpha} = \mathbf{C} \hat{\boldsymbol{\alpha}}$, where $\boldsymbol{\alpha} := (\alpha_1, \dots, \alpha_M)^t$ and $\hat{\boldsymbol{\alpha}} := (\alpha'_1, \dots, \alpha'_N, \beta_1, \dots, \beta_L)^t$. Notice that most of the entries of this matrix vanish and the others are ± 1 .

Let $\mathbf{A} := (A_{ij})$ and $\mathbf{B} := (B_{ij})$ be the $M \times M$ matrices defined by

$$A_{ij} := \int_{\Omega} \mathbf{curl} \phi_j \cdot \mathbf{curl} \bar{\phi}_i \quad \text{and} \quad B_{ij} := \int_{\Omega} \phi_j \cdot \bar{\phi}_i, \quad i, j = 1, \dots, M.$$

Then, using the basis of \mathcal{Z}_h from Proposition 2.5.1, the matrix form of Problem 2.4.1 reads as follows:

$$\widehat{\mathbf{A}}\widehat{\boldsymbol{\alpha}} = \lambda_h^2 \widehat{\mathbf{B}}\widehat{\boldsymbol{\alpha}},$$

with Hermitian matrices $\widehat{\mathbf{A}} := \mathbf{C}^t \mathbf{B} \mathbf{C}$ and $\widehat{\mathbf{B}} := \mathbf{C}^t \mathbf{A} \mathbf{C}$, which are positive semi-definite and positive definite, respectively. Thus, this is a well-posed generalized matrix eigenvalue problem.

2.6 Numerical experiments

We have developed a MATLAB code based on lowest-order Nédélec elements ($k = 1$) to solve Problem 2.4.1. We report in this section some numerical experiments which confirm the theoretical results proved in the previous sections.

2.6.1 Validation

As a first numerical test, we have solved a particular problem with a known analytical solution, which allowed us to validate the computer code and to check the performance and convergence properties of the scheme. When the domain Ω is the unit sphere, the least positive eigenvalue is the smallest positive solution of the equation $\lambda = \tan \lambda$, namely, $\lambda = 4.493409\dots$. Moreover, λ is an eigenvalue of multiplicity three (for further details see [26, Theorem A]).

Because of the symmetry of the domain, it is easy to check that $(\lambda, \mathbf{u}(\mathbf{x}))$ is a solution of Problem 2.3.1 if and only if $(-\lambda, \mathbf{u}(-\mathbf{x}))$ is a solution, too. Therefore, λ^2 is an eigenvalue of Problem 2.3.3 with multiplicity six. Whence, by virtue of Theorem 2.4.2, we know that, for h small enough, there exist six eigenvalues $\lambda_{h,1}^2, \dots, \lambda_{h,6}^2$ of Problem 2.4.1 (repeated accordingly to their respective multiplicities) such that

$$\lambda_{h,i}^2 \xrightarrow{h \rightarrow 0} \lambda^2, \quad i = 1, \dots, 6.$$

The code has been used on several meshes \mathcal{T}_h with different levels of refinement; we identify each mesh by its respective number of tetrahedra N_h . We have compared the average $\widehat{\lambda}_h := (\lambda_{h,1} + \dots + \lambda_{h,6})/6$ with the analytical eigenvalue λ . Table 2.1 shows the obtained results. The table also includes an estimate of the order of convergence, the so-called *experimental rate of convergence*:

$$\text{erc} := -3 \frac{\log \left(|\lambda - \widehat{\lambda}_h| / |\lambda - \widehat{\lambda}_{h'}| \right)}{\log (N_h / N_{h'})}.$$

Since the domain is smooth, the theoretical order of convergence for the eigenvalues is in this case $\mathcal{O}(h^{2r_1})$, with $r_1 := \min \{s, 1\} = 1$. It can be seen from Table 2.1 that the obtained results show an estimated order of convergence close to the theoretical one. Figure 2.1 shows a

Table 2.1: Unit sphere. Computed and exact eigenvalues, errors, and experimental rates of convergence.

N_h	$\widehat{\lambda}_h$	λ	$ \lambda - \widehat{\lambda}_h $	erc
53506	4.495885	4.493409	0.002475	—
91286	4.495117	4.493409	0.001708	2.08
157765	4.494620	4.493409	0.001210	1.89
259404	4.494283	4.493409	0.000874	1.96

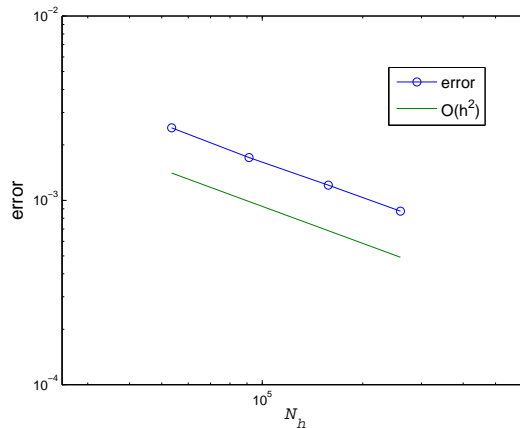


Figure 2.1: Unit sphere. Error $|\lambda - \widehat{\lambda}_h|$ versus number of tetrahedra N_h (log-log scale).

log-log plot of the errors versus the number of tetrahedra N_h . The slope of the line shows a clear quadratic dependence on the mesh-size.

According to the theoretical results, the invariant subspace spanned by the six eigenfunctions of Problem 2.4.1 corresponding to $\lambda_{h,1}, \dots, \lambda_{h,6}$ yields an approximation of the eigenspace of λ^2 in Problem 2.3.3. However, the latter is the direct sum of two three-dimensional eigenspaces of Problem 2.3.1, those corresponding to λ and $-\lambda$. Therefore, the eigenfunctions of Problem 2.4.1 are not in general eigenfunctions of Problem 2.3.1 (and hence Beltrami fields), but linear combination of eigenfunctions corresponding to both eigenvalues, λ and $-\lambda$.

We have also solved this problem by using the finite element discretization of Problem 2.3.2 given in Problem 2.7.2. More details about this numerical method, including the corresponding convergence analysis, are reported in the appendix. Figure 2.2 shows the vector field and some integral curves for one of the eigenfunctions computed in this way. This minimum-eigenvalue field is the well-known *spheromak* introduced in [27] and reported in [26] (see also [28, 97, 96]).

Moreover, we have applied our method to a problem in which the boundary of the domain is not connected: a spherical shell $\{\mathbf{x} \in \mathbb{R}^3 : a \leq |\mathbf{x}| \leq b\}$. In this case, two basis functions of \mathcal{L}_h^Γ has to be eliminated for the implementation, each of them corresponding to a vertex on each connected component.

We have compared the obtained results with the analytical ones reported in [26] for the spherical shell $\{\mathbf{x} \in \mathbb{R}^3 : 0.540183 \leq |\mathbf{x}| \leq 1.05\}$. Table 2.2 shows results similar to those re-

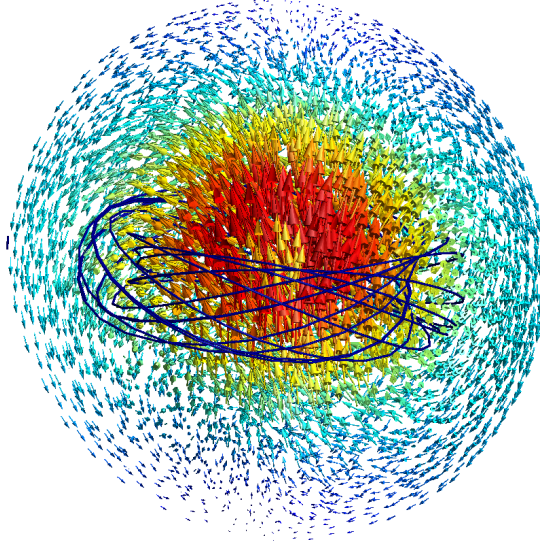


Figure 2.2: The spheromak.

ported in Table 2.1 for the eigenvalue of least absolute value of this problem. Once more, the estimated rates of convergence are close to $\mathcal{O}(h^2)$, as predicted by the theory.

Table 2.2: Spherical shell. Computed and exact eigenvalues, errors, and experimental rates of convergence.

N_h	$\widehat{\lambda}_h$	λ	$ \lambda - \widehat{\lambda}_h $	erc
11875	6.369146	6.423856	0.054711	—
31969	6.394034	6.423856	0.029823	1.84
63693	6.404705	6.423856	0.019151	1.92
131470	6.412565	6.423856	0.011291	2.19

2.6.2 Eigenvalues of the curl on a rectangular box

For the last test, we have chosen as domain a rectangular box. In particular, we have considered the hexahedron $\Omega := (-0.5, 0.5) \times (-0.4, 0.4) \times (-0.6, 0.6)$. Notice that as in the previous tests, because of the symmetry of the domain, λ is an eigenvalue of Problem 2.3.1 is and only if $-\lambda$ is another eigenvalue of the same problem. Therefore each eigenvalue λ^2 of Problem 2.3.3 has multiplicity at least two.

We have used several regular meshes as those shown in Figure 2.3.

On each mesh we have computed the six smallest eigenvalues $\lambda_{h,1}^2 \leq \dots \leq \lambda_{h,6}^2$. In this case, $\lambda_{h,2k-1}^2$ and $\lambda_{h,2k}^2$ converge to a same limit λ_k^2 , $k = 1, 2, 3$, which is a double eigenvalue of Problem 2.3.3.

In this case, we have estimated the order of convergence by means of a least-squares fitting

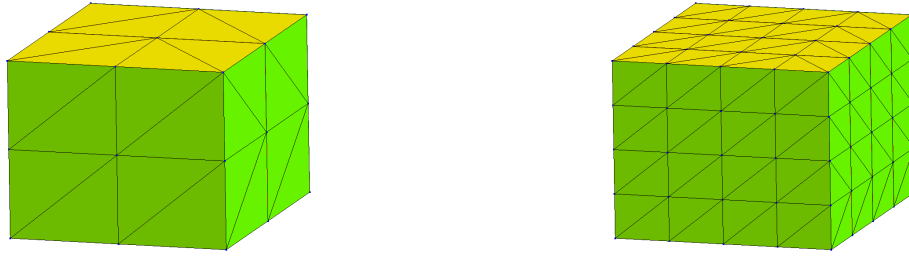


Figure 2.3: Meshes on the rectangular box.

of the model

$$\widehat{\lambda}_{h,k} \approx \lambda_{\text{ex}} + Ch^t,$$

where $\widehat{\lambda}_{h,k} := (\lambda_{h,2k-1} + \lambda_{h,2k})/2$.

Table 2.3 shows the three smallest eigenvalues computed on several meshes. As in the previous examples, N_h denotes the corresponding number of tetrahedra. For each eigenvalue, the table also includes the extrapolated more accurate approximation λ_{ex} and the estimated order of convergence t obtained with this fitting. The obtained orders of convergence are again close to $\mathcal{O}(h^2)$, as predicted by the theory.

Table 2.3: Rectangular box. Computed and extrapolated eigenvalues and computed orders of convergence.

	$N_h = 10368$	$N_h = 34992$	$N_h = 82944$	$N_h = 162000$	λ_{ex}	order
$\widehat{\lambda}_{h,1}$	7.4360	7.4337	7.4329	7.4325	7.4319	2.02
$\widehat{\lambda}_{h,2}$	7.7666	7.7724	7.7741	7.7751	7.7763	2.19
$\widehat{\lambda}_{h,3}$	8.0530	8.0726	8.0802	8.0836	8.0909	1.81

Figure 2.4 shows the eigenfunction corresponding to the third smallest positive eigenvalue computed by solving Problem 2.7.2 as in the previous test. Those corresponding to the first and the second one are essentially similar to rotations of this. Finally, the eigenfunctions corresponding to the negative eigenvalues are obtained from those of the positive ones by means of a symmetry.

Appendix

In this appendix, we consider a finite element approximation of Problem 2.3.2. The simplest minded approach would consist of using the finite element spaces $\mathcal{N}_h \subset \mathbf{H}(\mathbf{curl}; \Omega)$ and $\mathcal{L}_h \subset \mathbf{H}^1(\Omega)$ for a direct discretization of this problem. However, such a procedure leads to a spectral problem for an operator which is not compact and a property analogous to P1 (typical for the spectral approximation of non-compact operators) does not seem to hold, either. To circumvent this drawback, we consider the following problem, which only differs from Problem 2.3.2 in that the space $\mathbf{H}(\mathbf{curl}; \Omega)$ has been substituted by \mathcal{Z} .

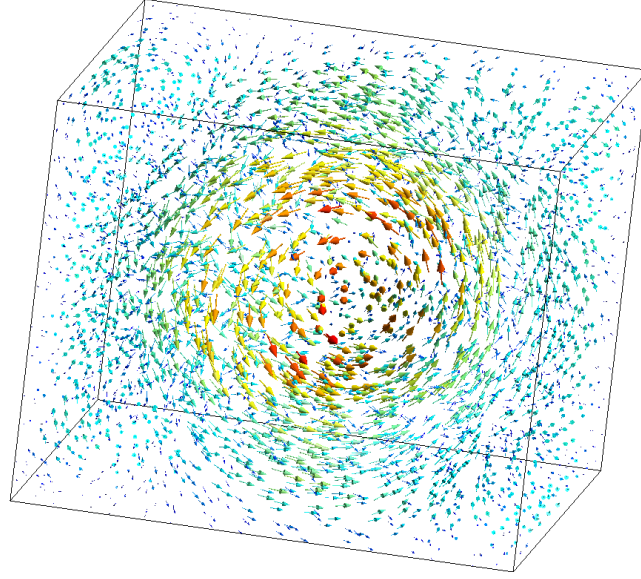


Figure 2.4: Eigenfunction of the curl on a rectangular box.

Problem 2.7.1 Find $\lambda \in \mathbb{C}$ and $(\mathbf{u}, \varphi) \in \mathcal{Z} \times \mathbf{H}^1(\Omega)/\mathbb{C}$, $(\mathbf{u}, \varphi) \neq \mathbf{0}$, such that

$$\begin{aligned} \int_{\Omega} \mathbf{curl} \mathbf{u} \cdot \mathbf{curl} \bar{\mathbf{v}} + \int_{\Omega} \nabla \varphi \cdot \bar{\mathbf{v}} &= \lambda \int_{\Omega} \mathbf{u} \cdot \mathbf{curl} \bar{\mathbf{v}} \quad \forall \mathbf{v} \in \mathcal{Z}, \\ \int_{\Omega} \mathbf{u} \cdot \nabla \bar{\psi} &= 0 \quad \forall \psi \in \mathbf{H}^1(\Omega)/\mathbb{C}. \end{aligned}$$

The following result shows that this is actually equivalent to Problem 2.3.2.

Proposition 2.7.1 Problems 2.3.2 and 2.7.1 have the same set of solutions.

Proof. Let $(\lambda, \mathbf{u}, \varphi)$ be a solution of Problem 2.3.2. By virtue of Proposition 2.3.1, $\mathbf{curl} \mathbf{u} \cdot \mathbf{n} = \lambda \mathbf{u} \cdot \mathbf{n} = 0$ on Γ , so that $\mathbf{u} \in \mathcal{Z}$. Hence, $(\lambda, \mathbf{u}, \varphi)$ solves Problem 2.7.1.

Conversely, let $(\lambda, \mathbf{u}, \varphi)$ be a solution of Problem 2.7.1. Proceeding as done to prove Proposition 2.3.1, we obtain $\varphi = 0$, $\mathbf{u} \in \mathbf{H}_0(\text{div}^0; \Omega)$, and $\mathbf{curl}(\mathbf{curl} \mathbf{u} - \lambda \mathbf{u}) = \mathbf{0}$ in Ω . Hence, for $\mathbf{u} \in \mathcal{Z}$, we have that $\mathbf{curl} \mathbf{u} - \lambda \mathbf{u} \in \mathbf{H}(\mathbf{curl}^0; \Omega) \cap \mathbf{H}_0(\text{div}^0; \Omega) = \{\mathbf{0}\}$. Consequently, $\mathbf{curl} \mathbf{u} = \lambda \mathbf{u}$, and, whence, $(\lambda, \mathbf{u}, \varphi)$ solves Problem 2.3.2. \square

Let $\mathcal{Z}_h \subset \mathcal{Z}$ and $\mathcal{L}_h \subset \mathbf{H}^1(\Omega)$ be the finite element spaces defined in Sections 2.4 and 2.5, respectively. We consider the following discretization of Problem 2.7.1:

Problem 2.7.2 Find $\lambda_h \in \mathbb{C}$ and $(\mathbf{u}_h, \varphi_h) \in \mathcal{Z}_h \times \mathcal{L}_h/\mathbb{C}$, $(\mathbf{u}_h, \varphi_h) \neq \mathbf{0}$, such that

$$\begin{aligned} \int_{\Omega} \mathbf{curl} \mathbf{u}_h \cdot \mathbf{curl} \bar{\mathbf{v}}_h + \int_{\Omega} \nabla \varphi_h \cdot \bar{\mathbf{v}}_h &= \lambda_h \int_{\Omega} \mathbf{u}_h \cdot \mathbf{curl} \bar{\mathbf{v}}_h \quad \forall \mathbf{v}_h \in \mathcal{Z}_h, \\ \int_{\Omega} \mathbf{u}_h \cdot \nabla \bar{\psi}_h &= 0 \quad \forall \psi_h \in \mathcal{L}_h/\mathbb{C}. \end{aligned}$$

Our aim is to prove that the eigenvalues and eigenfunction of Problem 2.7.1 are well approximated by those of Problem 2.7.2. With this end, we will apply the classical theory for mixed eigenvalue problems of the so-called type Q1 reported in [66, Section 3]. The first step is to show that all the following properties, which correspond to assumptions (3.12)–(3.16) from this reference, are fulfilled in our case:

- there exists $\alpha_1 > 0$ such that

$$\int_{\Omega} |\mathbf{curl} \mathbf{v}|^2 \geq \alpha_1 \|\mathbf{v}\|_{\mathbf{curl}, \Omega}^2 \quad \forall \mathbf{v} \in \mathbf{V}, \quad (2.16)$$

where, we recall, $\mathbf{V} = \{\mathbf{v} \in \mathbf{Z} : \int_{\Omega} \mathbf{v} \cdot \nabla \bar{\psi} = 0 \quad \forall \psi \in H^1(\Omega)/\mathbb{C}\}$;

- there exists $\beta_1 > 0$ such that

$$\sup_{\mathbf{v} \in \mathbf{Z}} \frac{|\int_{\Omega} \mathbf{v} \cdot \nabla \bar{\psi}|}{\|\mathbf{v}\|_{\mathbf{curl}, \Omega}} \geq \beta_1 |\psi|_{1, \Omega} \quad \forall \psi \in H^1(\Omega)/\mathbb{C}; \quad (2.17)$$

- there exists $\alpha_2 > 0$, independent of h , such that

$$\int_{\Omega} |\mathbf{curl} \mathbf{v}_h|^2 \geq \alpha_2 \|\mathbf{v}_h\|_{\mathbf{curl}, \Omega}^2 \quad \forall \mathbf{v}_h \in \mathbf{V}_h, \quad (2.18)$$

where, we recall, $\mathbf{V}_h = \{\mathbf{v}_h \in \mathbf{Z}_h : \int_{\Omega} \mathbf{v}_h \cdot \nabla \bar{\psi}_h = 0 \quad \forall \psi_h \in \mathcal{L}_h/\mathbb{C}\}$;

- there exists $\beta_2 > 0$, independent of h , such that

$$\sup_{\mathbf{v}_h \in \mathbf{Z}_h} \frac{|\int_{\Omega} \mathbf{v}_h \cdot \nabla \bar{\psi}_h|}{\|\mathbf{v}_h\|_{\mathbf{curl}, \Omega}} \geq \beta_2 |\psi_h|_{1, \Omega} \quad \forall \psi_h \in \mathcal{L}_h/\mathbb{C}; \quad (2.19)$$

- for each $(\mathbf{v}, \psi) \in \mathbf{Z} \times H^1(\Omega)/\mathbb{C}$,

$$\lim_{h \rightarrow 0} \inf_{(\mathbf{v}_h, \psi_h) \in \mathbf{Z}_h \times \mathcal{L}_h/\mathbb{C}} \left(\|\mathbf{v} - \mathbf{v}_h\|_{\mathbf{curl}, \Omega} + |\psi - \psi_h|_{1, \Omega} \right) = 0. \quad (2.20)$$

The ellipticity in the kernels (2.16) and (2.18) follow from [2, Corollary 3.16] and [2, Proposition 4.6], respectively. The inf-sup conditions (2.17) and (2.19) are easily checked by taking $\mathbf{v} = \nabla \psi$ and $\mathbf{v}_h = \nabla \psi_h$, respectively. Finally, the density result (2.20) follows immediately from Proposition 2.3.3, the fact that for a smooth $\mathbf{v} \in \mathbf{Z}$ its Nédélec interpolant satisfies $I_h^N \mathbf{v} \in \mathbf{Z}_h$ (cf. the proof of Theorem 2.4.3), and standard approximation properties of the Nédélec and the Lagrange interpolants.

The solution operator for Problem 2.7.1 is defined as follows:

$$\begin{aligned} G : \mathbf{Z} \times H^1(\Omega)/\mathbb{C} &\longrightarrow \mathbf{Z} \times H^1(\Omega)/\mathbb{C}, \\ (\mathbf{f}, g) &\longmapsto G(\mathbf{f}, g) := (\mathbf{w}, \xi), \end{aligned}$$

with $(\mathbf{w}, \xi) \in \mathcal{Z} \times \mathbf{H}^1(\Omega)/\mathbb{C}$ such that

$$\begin{aligned} \int_{\Omega} \mathbf{curl} \mathbf{w} \cdot \mathbf{curl} \bar{\mathbf{v}} + \int_{\Omega} \nabla \xi \cdot \bar{\mathbf{v}} &= \int_{\Omega} \mathbf{f} \cdot \mathbf{curl} \bar{\mathbf{v}} \quad \forall \mathbf{v} \in \mathcal{Z}, \\ \int_{\Omega} \mathbf{w} \cdot \nabla \bar{\psi} &= 0 \quad \forall \psi \in \mathbf{H}^1(\Omega)/\mathbb{C}. \end{aligned}$$

Once more, λ is an eigenvalue of Problem 2.7.1 if and only if $\mu = \frac{1}{\lambda}$ is a non-zero eigenvalue of G , with the same eigenfunctions. An additional assumption needed to apply the approximation results for mixed eigenvalue problems of type Q1 from [66, Section 3] is that G has to be compact. This and other properties of this operator are established in the following lemma.

Lemma 2.7.1 *For all $(\mathbf{f}, g) \in \mathcal{Z} \times \mathbf{H}^1(\Omega)/\mathbb{C}$, $G(\mathbf{f}, g) = (\mathbf{w}, 0)$, with $\mathbf{w} \in \mathbf{H}_0(\operatorname{div}^0; \Omega)$. Moreover, $\mathbf{w} \in \mathbf{H}^s(\mathbf{curl}; \Omega)$ and G is compact.*

Proof. Let $(\mathbf{f}, g) \in \mathcal{Z} \times \mathbf{H}^1(\Omega)/\mathbb{C}$. Proceeding again as done to prove Proposition 2.3.1, we obtain $G(\mathbf{f}, g) = (\mathbf{w}, 0)$, with $\mathbf{w} \in \mathbf{H}_0(\operatorname{div}^0; \Omega)$ and $\mathbf{curl}(\mathbf{curl} \mathbf{w}) = \mathbf{curl} \mathbf{f}$ in Ω . Therefore, $\mathbf{w}, \mathbf{curl} \mathbf{w} \in \mathbf{H}(\mathbf{curl}; \Omega) \cap \mathbf{H}_0(\operatorname{div}^0; \Omega) \hookrightarrow \mathbf{H}^s(\Omega)^3$. Hence, $\mathbf{w} \in \mathbf{H}^s(\mathbf{curl}; \Omega)$, which is compactly included in $\mathbf{H}(\mathbf{curl}; \Omega)$, and we end the proof. \square

The spectral approximation theory for mixed problems of type Q1 from [66, Section 3] also involves a formal adjoint operator G_* . In the present case, this operator is defined for $(\mathbf{f}, g) \in \mathcal{Z} \times \mathbf{H}^1(\Omega)/\mathbb{C}$ by $G_*(\mathbf{f}, g) := (\mathbf{w}_*, \xi_*)$, with $(\mathbf{w}_*, \xi_*) \in \mathcal{Z} \times \mathbf{H}^1(\Omega)/\mathbb{C}$ being the solution of the adjoint problem:

$$\begin{aligned} \int_{\Omega} \mathbf{curl} \mathbf{v} \cdot \mathbf{curl} \bar{\mathbf{w}}_* + \int_{\Omega} \mathbf{v} \cdot \nabla \bar{\xi}_* &= \int_{\Omega} \mathbf{v} \cdot \mathbf{curl} \bar{\mathbf{f}} \quad \forall \mathbf{v} \in \mathcal{Z}, \\ \int_{\Omega} \nabla \psi \cdot \bar{\mathbf{w}}_* &= 0 \quad \forall \psi \in \mathbf{H}^1(\Omega)/\mathbb{C}. \end{aligned}$$

In general, for each eigenvalue μ of G , $\bar{\mu}$ is an eigenvalue of G_* with the same ascent α and with invariant subspace $\mathcal{E}^* := \operatorname{Ker}((\bar{\mu}I - G_*)^\alpha)$. In our case, $\mu \in \mathbb{R}$ and, as an immediate consequence of Proposition 2.3.2, we have that $G_* = G$. However, since G_* is just a formal adjoint, we cannot claim that G is self-adjoint. Nevertheless, we prove in the following lemma that its eigenvalues are non-defective.

Lemma 2.7.2 *The ascent of any non-zero eigenvalue of G is one.*

Proof. By contradiction. Let $(\mu, (\mathbf{u}, \varphi))$ be an eigenpair of G , $\mu \neq 0$, and let us assume that G has a corresponding generalized eigenfunction; namely, $G(\mathbf{u}, \varphi) = \mu(\mathbf{u}, \varphi)$, $(\mathbf{u}, \varphi) \neq \mathbf{0}$, and there exists $(\tilde{\mathbf{u}}, \tilde{\varphi})$ such that $G(\tilde{\mathbf{u}}, \tilde{\varphi}) = \mu(\tilde{\mathbf{u}}, \tilde{\varphi}) + (\mathbf{u}, \varphi)$. Hence, $\varphi = \tilde{\varphi} = 0$ and, by using the definition of G for $\mathbf{f} = \mathbf{u}$ with test function $\mathbf{v} = \tilde{\mathbf{u}}$ and for $\mathbf{f} = \tilde{\mathbf{u}}$ with test function $\mathbf{v} = \mathbf{u}$, we respectively obtain

$$\begin{aligned} \mu \int_{\Omega} \mathbf{curl} \mathbf{u} \cdot \mathbf{curl} \tilde{\mathbf{u}} &= \int_{\Omega} \mathbf{u} \cdot \mathbf{curl} \tilde{\mathbf{u}}, \\ \mu \int_{\Omega} \mathbf{curl} \tilde{\mathbf{u}} \cdot \mathbf{curl} \bar{\mathbf{u}} + \int_{\Omega} \mathbf{curl} \mathbf{u} \cdot \mathbf{curl} \bar{\mathbf{u}} &= \int_{\Omega} \tilde{\mathbf{u}} \cdot \mathbf{curl} \bar{\mathbf{u}}. \end{aligned}$$

Subtracting the conjugate of the first equation from the second one and using that $\mu \in \mathbb{R}$, we have that

$$\mu \int_{\Omega} |\mathbf{curl} \mathbf{u}|^2 = \int_{\Omega} (\tilde{\mathbf{u}} \cdot \mathbf{curl} \bar{\mathbf{u}} - \bar{\mathbf{u}} \cdot \mathbf{curl} \tilde{\mathbf{u}}) = 0,$$

the last equality because of Proposition 2.3.2. Therefore, for $\mu \neq 0$, by virtue of (2.16), $\mathbf{u} = \mathbf{0}$. Since $\varphi = 0$, too, this leads to a contradiction and we end the proof. \square

Now, we are in a position to write the following convergence result, which is a direct consequence of [66, Theorem 3.1].

Theorem 2.7.1 *Let λ be an eigenvalue of Problem 2.7.1 of finite-multiplicity m . Let $\mathcal{E} \subset \mathcal{Z} \times \mathbf{H}^1(\Omega)/\mathbb{C}$ be the corresponding eigenspace. Then, there exist exactly m eigenvalues $\lambda_h^{(1)}, \dots, \lambda_h^{(m)}$ of Problem 2.7.2 (repeated accordingly to their respective multiplicities) which converge to λ as h goes to zero.*

Let \mathcal{E}_h be the direct sum of the eigenspaces corresponding to $\lambda_h^{(1)}, \dots, \lambda_h^{(m)}$ and $\hat{\gamma}_h := \delta(\mathcal{E}, \mathcal{Z}_h \times \mathcal{L}_h/\mathbb{C})$. Then,

$$\hat{\delta}(\mathcal{E}, \mathcal{E}_h) \leq C \hat{\gamma}_h$$

and

$$|\lambda - \lambda_h^{(i)}| \leq C \hat{\gamma}_h^2, \quad i = 1, \dots, m.$$

Lemma 2.7.1 and the same arguments used in the proof of Theorem 2.4.3 allow us to show that there exists $C > 0$ such that $\hat{\gamma}_h \leq Ch^{r_k}$, with r_k as defined in (2.9). This, together with Theorem 2.7.1, imply that the eigenvalues and eigenfunctions of Problem 2.7.2 converge to those of Problem 2.7.1 with an optimal order.

The matrix form of Problem 2.7.2 is a generalized eigenvalue problem which involves two non-definite matrices. However, in spite of this, it is well-posed. In fact, it is easy to check that $(\lambda_h, \mathbf{u}_h, \varphi_h)$ is a solution of Problem 2.7.2 if and only if $\varphi_h = 0$ and $(\lambda_h, \mathbf{u}_h)$ is a solution of the following one: find $\lambda_h \in \mathbb{C}$ and $\mathbf{u}_h \in \mathcal{V}_h$, $\mathbf{u}_h \neq \mathbf{0}$, such that

$$\int_{\Omega} \mathbf{curl} \mathbf{u}_h \cdot \mathbf{curl} \bar{\mathbf{v}}_h = \lambda_h \int_{\Omega} \mathbf{u}_h \cdot \mathbf{curl} \bar{\mathbf{v}}_h \quad \forall \mathbf{v}_h \in \mathcal{V}_h. \quad (2.21)$$

The matrix form of the above problem involves two Hermitian matrices, that of the right hand side being so because of Proposition 2.3.2. Moreover, the matrix on the left hand side is positive definite because of (2.18). Therefore, the eigenvalues of this discrete problem are real and non-defective.

Problem 2.7.2 is equivalent to the well-posed generalized eigenvalue problem (2.21). However, since there is no basis available for \mathcal{V}_h , its computer implementation requires dealing with Problem 2.7.2, in spite of its degeneracy, rather than with (2.21).

Chapter 3

Numerical solution of a transient nonlinear axisymmetric eddy current model

3.1 Introduction

An important challenge to bear in mind in the analysis and design of electrical machines is the accurate computation of the power losses in the ferromagnetic components of the core. These losses determine the efficiency of the device and have a significant influence on its operating cost.

At the macroscopic level, two main types of losses can be distinguished: hysteresis losses, which are related to the intrinsic nature of magnetic materials, and eddy current losses, due to the Joule effect [15].

There are numerous publications devoted to obtain analytical simplified expressions to approximate the different losses, which are only valid under assumptions that often do not hold in practice (see, for instance, [15] and [19]). Numerical modeling is an interesting alternative to overcome these limitations and, thus, we can find several works focused on the computation of hysteresis and eddy current losses (see [37, 75, 90] and references therein).

A first step in the computation of this kind of losses is the numerical solution of the underlying electromagnetic problem. This requires solving the quasi-static Maxwell's partial differential equations, a well established subject, even in the three-dimensional (3D) case, where edge finite elements are very useful (see [1, 20, 50] and references therein). This issue was studied in [80] and [82] in terms of the magnetic field and in the absence of hysteresis effects. In these references the 3D problem is posed on a bounded conducting domain and homogeneous Dirichlet boundary conditions are assumed. Current sources are not taken into account, the only source term being the initial condition. A time semi-discretization scheme is proposed and analyzed to approximate this problem.

However, major difficulties arise from the fact that cores are laminated to reduce the eddy current losses. Thus, to account for the detailed geometry, extremely fine meshes should be needed, which becomes unaffordable. To overcome this difficulty, one can find different strategies

based on the use of the so-called equivalent conductivity [11, 47, 53, 75] or on homogenization techniques [36]. In this chapter, we are interested in an alternative approach proposed by Van Keer *et al.* [89, 90], which consists in computing the electromagnetic field in a cross-section of the laminated device, orthogonal to the direction of the enforced flux. This leads to a nonlocal source term, which together with the fact that there is no current flux through the boundary yield a nonlinear parabolic problem with a non-classical boundary condition. Such a condition brings some technical complications; for instance, it involves dealing with a bilinear form which, instead of being elliptic, satisfies a Gårding inequality.

The aims of this chapter are to analyze the resulting problem, to propose a numerical method for its approximate solution and to prove its convergence. We will address these issues in the axisymmetric case without including hysteresis effects. The behavior of the material is defined by a general pointwise continuous and strongly monotone nonlinear relation on the H-B curve, which, unlike Refs. [80] and [82], allows us to deal with heterogeneous materials. Moreover, we can also consider a time and space-dependent conductivity. This is important in practical applications, because the conductivity is a function of temperature which, in its turn, is a time-dependent field. We prove the existence of a solution of a weak formulation of this problem in terms of the magnetic field by applying an abstract result [52]. We also prove uniqueness of solution in the case of a time-independent conductivity.

For the numerical solution of the problem, we further assume that the nonlinear relation on the H-B curve is Lipschitz continuous. First we consider a finite element discretization by using piecewise linear functions on triangular meshes. By means of a suitable change of variables, we reduce the semi discrete problem to a classical nonlinear ODE system and prove its well-posedness. Then, we combine it with a backward Euler time-discretization. Under appropriate assumptions, we prove optimal order error estimates for both, fully and semi-discretized schemes. The proofs are based on arguments from [82] and adapting to our problem the classical theory of linear parabolic problems (see, for instance, [86]). However, special care must be taken to deal with the nonlocal boundary condition.

To the best of the authors' knowledge, the numerical analysis of the fully and semi-discrete in space schemes had not been previously performed. There are not many references for nonlinear problems of this kind, even with more classical (homogeneous Dirichlet or Neumann) boundary conditions. Some of them [55, 73] deal with the Stefan problem, so that the application of their arguments to our framework would in principle even allow for a multivalued nonlinear H-B curve (although this is not the kind of curve that appears in our problem). Other references [80, 82] deal with a similar three dimensional eddy current problem as that of the present chapter, but provide only error estimates for the semi-discrete in time scheme. None of all these references considers neither the nonlocal boundary conditions of the present problem nor a pointwise defined H-B curve.

The chapter is organized as follows. In Section 3.2, we describe the transient axisymmetric eddy current model and introduce the nonlinear parabolic partial differential equation to be solved. Next, in Section 3.3, we obtain a weak formulation of the problem. The existence of solution is proved by applying results for abstract nonlinear parabolic equations. Section 3.4 is devoted to numerical methods. A space semi-discretization by finite elements is introduced

and, then, a backward Euler scheme is applied for time discretization. Error estimates for both schemes are obtained. Finally, numerical results that confirm the theoretical estimates are shown in Section 3.5.

3.2 The transient nonlinear eddy current model

The eddy current model is an approximation of the full Maxwell system of equations obtained by neglecting the displacement currents in Ampère's law. This simplified model is suitable for most electrical engineering applications (the so-called low-frequency regime), for instance, in the numerical simulation of electrical machines working at power frequencies. The eddy current model reads

$$\mathbf{curl} \mathbf{H} = \mathbf{J}, \quad (3.1)$$

$$\frac{\partial \mathbf{B}}{\partial t} + \mathbf{curl} \mathbf{E} = \mathbf{0}, \quad (3.2)$$

$$\mathbf{div} \mathbf{B} = 0, \quad (3.3)$$

where we have used standard notation in electromagnetism: \mathbf{H} is the magnetic field, \mathbf{J} the current density, \mathbf{B} the magnetic induction and \mathbf{E} the electric field. In order to obtain a closed system we need to add constitutive laws. Assuming that the materials are electrically linear but magnetically nonlinear, we have

$$\mathbf{J} = \sigma \mathbf{E}, \quad (3.4)$$

$$\mathbf{B} = \mathcal{B}(\mathbf{H}). \quad (3.5)$$

Equation (3.4) is Ohm's law, where σ denotes the electrical conductivity of the medium. In the magnetic constitutive relation (3.5), \mathcal{B} is in general a nonlinear mapping. Two extreme cases are the following: linear isotropic materials, for which this mapping reduces to $\mathcal{B}(\mathbf{H}) = \mu \mathbf{H}$ with μ being the constant magnetic permeability, and ferromagnetic materials where hysteresis phenomena may occur, in which case the H-B relation exhibits a history-dependent behavior. Our analysis allows for a nonlinear magnetic material, that will be represented through an anhysteretic H-B curve, which could have a very steep slope. This choice is a simplification frequently used for soft magnetic materials by electrical engineers (see, for instance, [88]).

Equations (3.1), (3.2) and (3.4), lead to the following vector partial differential equation in conductors:

$$\frac{\partial \mathbf{B}}{\partial t} + \mathbf{curl} \left(\frac{1}{\sigma} \mathbf{curl} \mathbf{H} \right) = \mathbf{0}. \quad (3.6)$$

Our aim is to solve this together with the nonlinear constitutive equation (3.5).

3.2.1 Axisymmetric eddy current model with enforced magnetic flux

Let us consider a cylindrical coordinate system (r, θ, z) and denote by \mathbf{e}_r , \mathbf{e}_θ and \mathbf{e}_z the corresponding unit vectors of the local orthonormal basis as sketched in Figure 3.1 (left). We

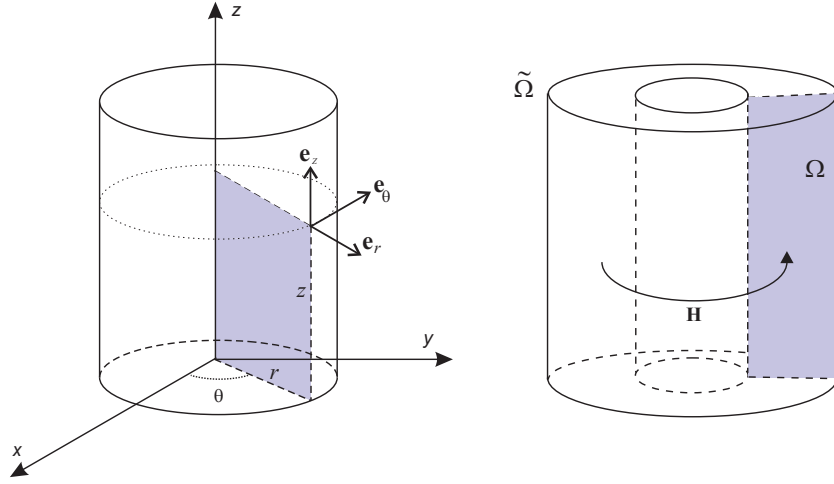


Figure 3.1: Cylindrical coordinate system (left) and sketch of the domain (right).

suppose that the computational domain $\tilde{\Omega}$ has cylindrical symmetry and that the current sources are independent of the azimuth θ and do not have azimuthal component, so that on each meridian section these currents lie on this section. We denote by Ω one such section, which we assume is an open connected domain with a Lipschitz boundary. In such a case, none of the electromagnetic fields depend on θ and, furthermore, from Faraday's law (3.2), \mathbf{B} has to be of the form,

$$\mathbf{B}(r, z, t) = B(r, z, t)\mathbf{e}_\theta. \quad (3.7)$$

Since we are assuming that the material is isotropic, the magnetic field \mathbf{H} must be of the same form as \mathbf{B} , namely,

$$\mathbf{H}(r, z, t) = H(r, z, t)\mathbf{e}_\theta, \quad (3.8)$$

and the H-B relation reads

$$B(r, z, t) = \mathcal{B}(r, z, H(r, z, t)), \quad (3.9)$$

with $\mathcal{B}(r, z, \cdot)$ being a nonlinear mapping in \mathbb{R} for each (r, z) . Dependence of \mathcal{B} in coordinates (r, z) is permitted to allow for computational domains including different materials. We notice that any field of the form (3.7) is divergence-free, so that (3.3) is automatically satisfied. Moreover, since

$$\mathbf{curl} \mathbf{H}(r, z, t) = -\frac{\partial H}{\partial z}(r, z, t)\mathbf{e}_r + \frac{1}{r}\frac{\partial}{\partial r}(rH)(r, z, t)\mathbf{e}_z, \quad (3.10)$$

equation (3.6) leads to

$$\frac{\partial B}{\partial t} - \frac{\partial}{\partial r}\left(\frac{1}{\sigma r}\frac{\partial(rH)}{\partial r}\right) - \frac{\partial}{\partial z}\left(\frac{1}{\sigma}\frac{\partial H}{\partial z}\right) = 0. \quad (3.11)$$

This equation holds in any meridian section Ω of the domain $\tilde{\Omega}$ for all time $t \in [0, T]$ ($T > 0$ fixed). To have a well-posed nonlinear parabolic problem we must add to equations (3.11) and

(3.9) an initial condition

$$B(r, z, 0) = B_0(r, z) \quad \text{in } \Omega, \quad (3.12)$$

and suitable boundary conditions on the boundary $\Gamma := \partial\Omega$.

The application that has motivated this chapter is the computation of eddy current losses in laminated media. Thus, following the work of Van Keer *et al.* [89], we will impose the magnetic flux $b(t)$ flowing through the meridian section Ω of the domain (see Figure 3.1, (right)). This leads to the nonlocal source condition

$$\int_{\Omega} B(r, z, t) \, drdz = b(t). \quad (3.13)$$

Moreover, we have also to impose that there is no current flux through the boundary of Ω ; namely, $\mathbf{curl} \mathbf{H} \cdot \mathbf{n} = \mathbf{J} \cdot \mathbf{n} = 0$ on Γ , where \mathbf{n} is the unit normal to Γ . Hence, from (3.10), it is straightforward to obtain that the tangential derivative of (rH) has to vanish on Γ . Therefore, provided Γ is connected, for each $t \in [0, T]$ $(rH(t))$ has to be a constant (which depends on t) on the whole Γ . Consequently, there exists an (unknown) function $\psi(t)$ which varies in time but is space-independent on Γ such that

$$rH(r, z, t) = \psi(t) \quad \text{on } \Gamma. \quad (3.14)$$

All together, the resulting axisymmetric problem reads:

Problem 3.2.1 Find $H(r, z, t)$ and $B(r, z, t)$ such that

$$\frac{\partial B}{\partial t} - \frac{\partial}{\partial r} \left(\frac{1}{\sigma r} \frac{\partial(rH)}{\partial r} \right) - \frac{\partial}{\partial z} \left(\frac{1}{\sigma} \frac{\partial H}{\partial z} \right) = f \quad \text{in } \Omega \times (0, T), \quad (3.15)$$

$$B(r, z, t) = \mathcal{B}(r, z, H(r, z, t)) \quad \text{in } \Omega \times (0, T), \quad (3.16)$$

$$rH(r, z, t) = \psi(t) \quad \text{on } \Gamma \times (0, T), \quad (3.17)$$

$$\int_{\Omega} B(r, z, t) \, drdz = b(t) \quad \text{in } (0, T), \quad (3.18)$$

$$B(r, z, 0) = B_0(r, z) \quad \text{in } \Omega, \quad (3.19)$$

where $\sigma(r, z, t)$, $f(r, z, t)$, $b(t)$ and $B_0(r, z)$ are given data and $\psi(t)$ is unknown.

Remark 3.2.1 We include in (3.15) a right-hand side f to consider a more general parabolic problem, although in the case of the eddy current model f is zero. Moreover, we consider a space- and time-dependent electrical conductivity σ because in practical applications it is a function of temperature which, in its turn, is a time-dependent field.

Problem 3.2.1 has been proposed and numerically solved in [89] in a more general setting including hysteresis. The goal of the present chapter is to study the well-posedness and the numerical approximation of this problem.

3.3 Mathematical analysis

In this section, we derive a weak formulation for Problem 3.2.1 and prove that it is well-posed.

3.3.1 Functional spaces and preliminary results

We recall some weighted Sobolev spaces typical in axisymmetric problems. We refer to [67] and [14] for more details. For the sake of simplicity, partial derivatives will be also denoted by ∂_r , ∂_z and so on.

Let $\Omega \subset \{(r, z) \in \mathbb{R}^2 : r > 0\}$ be a Lipschitz bounded simply connected open set. Let $L_r^p(\Omega)$ denote the weighted Lebesgue space of all measurable functions u defined in Ω for which

$$\|u\|_{L_r^p(\Omega)}^p := \int_{\Omega} |u|^p r \, dr dz < \infty \quad 1 \leq p < \infty.$$

The weighted Sobolev space $H_r^k(\Omega)$ consists of all functions in $L_r^2(\Omega)$ whose derivatives up to order k are also in $L_r^2(\Omega)$. We define the norms and semi-norms in the standard way; for instance,

$$\|u\|_{H_r^1(\Omega)}^2 := \int_{\Omega} \left(|\partial_r u|^2 + |\partial_z u|^2 \right) r \, dr dz.$$

Let $L_{1/r}^2(\Omega)$ denote the set of all measurable functions u defined in Ω for which

$$\|u\|_{L_{1/r}^2(\Omega)}^2 := \int_{\Omega} \frac{|u|^2}{r} \, dr dz < \infty.$$

We also define $H_{1/r}^k(\Omega)$ as before.

Finally, we introduce the function space $\widehat{H}_r^1(\Omega)$ defined by

$$\widehat{H}_r^1(\Omega) = \{u \in L_r^2(\Omega) : \partial_r(ru) \in L_{1/r}^2(\Omega), \partial_z u \in L_r^2(\Omega)\},$$

which is a Hilbert space with the norm

$$\|u\|_{\widehat{H}_r^1(\Omega)} := \left(\|u\|_{L_r^2(\Omega)}^2 + \|\partial_r(ru)\|_{L_{1/r}^2(\Omega)}^2 + \|\partial_z u\|_{L_r^2(\Omega)}^2 \right)^{1/2}.$$

Remark 3.3.1 For Ω being the meridian section of a 3D axisymmetric domain $\widetilde{\Omega}$, the space $\widehat{H}_r^1(\Omega)$ can be considered as an axisymmetric version of the 3D space $\mathbf{H}(\mathbf{curl}, \widetilde{\Omega})$. More precisely, from the expression of the **curl** operator in cylindrical coordinates it is immediate to see that $G(r, z) \in \widehat{H}_r^1(\Omega)$ if and only if $\mathbf{G}(r, z, \theta) = G(r, z) \mathbf{e}_{\theta}(\theta) \in \mathbf{H}(\mathbf{curl}, \widetilde{\Omega})$.

3.3.2 Weak formulation

Before stating a weak formulation of Problem 3.2.1, we notice that if the boundary of Ω intersect the symmetry axis ($r = 0$), then $\psi(t)$ should be identically zero because r vanishes there. In such a case, (3.17) would become a homogeneous Dirichlet boundary condition. However, this does not happen in the application that motivates this problem in which the domain is well

separated from the symmetry axis (see [89]). This is the reason why, from now on, we will assume that $\inf\{r > 0 : (r, z) \in \Omega\} > 0$ and, hence, $L_r^2(\Omega)$ and $L_{1/r}^2(\Omega)$ are both identical to $L^2(\Omega)$. Similarly, $\widehat{H}_r^1(\Omega)$ is identical to $H^1(\Omega)$.

Let us introduce the following closed subspace of $\widehat{H}_r^1(\Omega)$:

$$\mathcal{W} := \{G \in \widehat{H}_r^1(\Omega) : (rG)|_\Gamma \text{ is constant}\}. \quad (3.20)$$

Since $\widehat{H}_r^1(\Omega)$ is densely and compactly included in $L_r^2(\Omega)$, the same is true for \mathcal{W} (the density because $\mathcal{W} \supset \mathcal{D}(\Omega)$). Thus, if we identify $L_r^2(\Omega)$ with its topological dual, we have that $\mathcal{W} \subset L_r^2(\Omega) \subset \mathcal{W}'$. We denote by $\langle \cdot, \cdot \rangle_{\mathcal{W}, \mathcal{W}'}$ the corresponding duality paring.

In order to obtain a weak formulation, first we integrate (3.15) in Ω and use Gauss theorem to write

$$\frac{d}{dt} \int_{\Omega} B(r, z, t) \, drdz - \int_{\Gamma} \frac{1}{\sigma r} \left(\frac{\partial(rH)}{\partial r} n_r + \frac{\partial(rH)}{\partial z} n_z \right) d\Gamma = \int_{\Omega} f \, drdz,$$

where $\mathbf{n} = n_r \mathbf{e}_r + n_z \mathbf{e}_z$ is the outward unit normal vector to Γ . Hence, by using (3.18) we deduce that

$$\int_{\Gamma} \frac{1}{\sigma r} \left(\frac{\partial(rH)}{\partial r} n_r + \frac{\partial(rH)}{\partial z} n_z \right) d\Gamma = b'(t) - \int_{\Omega} f \, drdz. \quad (3.21)$$

Next, we multiply (3.15) by (rG) , G being any test function in \mathcal{W} , integrate in Ω and use a Green's formula. From the resulting expression and (3.21), we easily obtain the following weak formulation for Problem 3.2.1:

Problem 3.3.1 *Given $b \in H^1(0, T)$, $f \in L^2(0, T; \mathcal{W}')$ and $B_0 \in L_r^2(\Omega)$, find $H \in L^2(0, T; \mathcal{W})$ and $B \in H^1(0, T; \mathcal{W}')$ such that*

$$\begin{aligned} & \left\langle \frac{\partial B}{\partial t}, G \right\rangle_{\mathcal{W}, \mathcal{W}'} + \int_{\Omega} \frac{1}{\sigma r} \left(\frac{\partial(rH)}{\partial r} \frac{\partial(rG)}{\partial r} + \frac{\partial(rH)}{\partial z} \frac{\partial(rG)}{\partial z} \right) \, drdz \\ & = \langle f, G \rangle_{\mathcal{W}, \mathcal{W}'} + (b'(t) - \langle f, r^{-1} \rangle_{\mathcal{W}, \mathcal{W}'}) (rG)|_\Gamma \quad \forall G \in \mathcal{W}, \text{ a.e. } t \in (0, T), \\ & B(r, z, t) = \mathcal{B}(r, z, H(r, z, t)) \quad \text{a.e. in } \Omega \times (0, T), \\ & B(r, z, 0) = B_0(r, z) \quad \text{a.e. in } \Omega. \end{aligned}$$

Notice that $\langle f, r^{-1} \rangle_{\mathcal{W}, \mathcal{W}'}$ is well defined because $r^{-1} \in \mathcal{W}$.

3.3.3 Existence of solution

We introduce the following hypotheses and notations that will be used to prove the existence of a solution to the above problem.

H.1: $\mathcal{B}(r, z, u)$ is the derivative with respect to u of a (differentiable) normal convex integrand α defined in $\Omega \times \mathbb{R}$ (see, for instance, [4]); i.e.,

$$\mathcal{B}(r, z, u) := \partial_u \alpha(r, z, u) \quad \forall u \in \mathbb{R}, \forall (r, z) \in \Omega. \quad (3.22)$$

Moreover, we assume that α satisfies the following conditions:

- there exist $\beta_1 \in L_r^2(\Omega)$ and $\beta_2 \in L_r^1(\Omega)$ such that

$$\alpha(r, z, u) \geq \beta_1(r, z)u + \beta_2(r, z) \quad \forall u \in \mathbb{R}, \forall (r, z) \in \Omega;$$

- for each $w \in L_r^2(\Omega)$, $\alpha(\cdot, \cdot, w(\cdot, \cdot)) \in L_r^1(\Omega)$.

H.2: There exist two positive constants N_1 and N_2 such that

$$|\mathcal{B}(r, z, u)| \leq N_1|u| + N_2 \quad \forall u \in \mathbb{R}, \forall (r, z) \in \Omega.$$

H.3: $\mathcal{B}(r, z, u)$ is strongly monotone with respect to u uniformly in Ω ; i.e., there exists a strictly positive constant ω such that

$$(\mathcal{B}(r, z, u) - \mathcal{B}(r, z, v))(u - v) \geq \omega|u - v|^2 \quad \forall u, v \in \mathbb{R}, \forall (r, z) \in \Omega.$$

H.4: $\sigma : (0, T) \rightarrow L^\infty(\Omega)$ is measurable and there exist constants σ_* and σ^* such that

$$0 < \sigma_* \leq \sigma(r, z, t) \leq \sigma^* \quad \forall (r, z) \in \Omega, \text{ a.e. } t \in (0, T).$$

H.5: There exists $H_0 \in \mathcal{W}$ such that $B_0(r, z) = \mathcal{B}(r, z, H_0(r, z))$ a.e. in Ω .

Note that, as a consequence of H.5 and H.2, $B_0 \in L_r^2(\Omega)$.

Let us introduce the function $\varphi : L_r^2(\Omega) \rightarrow \mathbb{R}$ defined by

$$\varphi(H) := \int_{\Omega} \alpha(r, z, H(r, z)) r \, dr dz, \quad H \in L_r^2(\Omega), \quad (3.23)$$

which is well defined because of the last property in H.1. Then, from the assumptions on α , φ is a differentiable convex function in $L_r^2(\Omega)$ (see [3, Proposition 2.7]) and its differential, which we denote $\partial\varphi$, satisfies

$$\partial\varphi(H)(r, z) = \partial_u \alpha(r, z, H(r, z)) = \mathcal{B}(r, z, H(r, z)) \quad (r, z) \in \Omega, \forall H \in L_r^2(\Omega), \quad (3.24)$$

the last equality because of (3.22).

On the other hand, for each $t \in [0, T]$, let us denote by $a_t(\cdot, \cdot)$ the bilinear form defined by

$$a_t(H, G) := \int_{\Omega} \frac{1}{\sigma(\cdot, t)} \left(\frac{1}{r} \frac{\partial(rH)}{\partial r} \frac{1}{r} \frac{\partial(rG)}{\partial r} + \frac{\partial H}{\partial z} \frac{\partial G}{\partial z} \right) r \, dr dz \quad H, G \in \widehat{\mathbf{H}}_r^1(\Omega). \quad (3.25)$$

From H.4, we have the following result whose proof is straightforward.

Lemma 3.3.1 *The bilinear forms $a_t : \widehat{\mathbf{H}}_r^1(\Omega) \times \widehat{\mathbf{H}}_r^1(\Omega) \rightarrow \mathbb{R}$, $t \in [0, T]$, are continuous uniformly in t . Moreover, they satisfy the Gårding's inequality*

$$a_t(G, G) + \lambda \|G\|_{L_r^2(\Omega)}^2 \geq \gamma \|G\|_{\widehat{\mathbf{H}}_r^1(\Omega)}^2 \quad \forall G \in \widehat{\mathbf{H}}_r^1(\Omega), \quad (3.26)$$

with $\lambda = \gamma = 1/\sigma^*$.

Let us introduce $R \in L^2(0, T; \mathcal{W}')$ defined by

$$\langle R(t), G \rangle_{\mathcal{W}, \mathcal{W}'} := \langle f(t), G \rangle_{\mathcal{W}, \mathcal{W}'} + (b'(t) - \langle f(t), r^{-1} \rangle_{\mathcal{W}, \mathcal{W}'}) (rG)|_{\Gamma},$$

for all $G \in \mathcal{W}$, a.e. $t \in (0, T)$.

Now we are in position to prove that Problem 3.3.1 has a solution.

Theorem 3.3.1 *Let us assume hypotheses H.1 to H.5. Then, Problem 3.3.1 has a solution.*

Proof. We will derive this result as a consequence of Theorem 2 from [52]. With this aim, first we rewrite Problem 3.3.1 as follows:

Find $H \in L^2(0, T; \mathcal{W})$ and $B \in H^1(0, T; \mathcal{W}')$ such that

$$\frac{\partial B}{\partial t}(t) + A(t)H(t) = R(t), \quad \text{a.e. } t \in (0, T), \quad (3.27)$$

$$B(t) = \partial\varphi(H(t)), \quad \text{a.e. } t \in (0, T), \quad (3.28)$$

$$B(0) = B_0, \quad (3.29)$$

where, for a.e. $t \in (0, T)$, $A(t) : \mathcal{W} \rightarrow \mathcal{W}'$ is the linear operator induced by $a_t(\cdot, \cdot)$; namely,

$$\langle A(t)H, G \rangle_{\mathcal{W}', \mathcal{W}} := a_t(H, G) \quad \forall H, G \in \mathcal{W}.$$

Notice that from H.5 and (3.24) we have $B_0 = \partial\varphi(H_0)$. In order to apply Theorem 2 from [52] to Problem (3.27)–(3.29), we must check all the hypotheses of this theorem. Some of them are void (C.1 to C.4), or automatically satisfied (A.2, A.6) or consequence of the other hypotheses in our case (A.3, A.4), mainly because φ is time-independent (cf. Remark 1 from [52]). In what follows we check the remaining ones:

A.1: As stated above, in our case φ is differentiable and convex.

A.5: From H.3 and (3.24), $\partial\varphi$ is strongly monotone; namely,

$$(\partial\varphi(H_1) - \partial\varphi(H_2), H_1 - H_2)_{L_r^2(\Omega)} \geq \omega \|H_1 - H_2\|_{L_r^2(\Omega)}^2 \quad \forall H_1, H_2 \in L_r^2(\Omega).$$

A.7: From H.2 and (3.24),

$$\|\partial\varphi(H)\|_{L_r^2(\Omega)} \leq N_1 \|H\|_{L_r^2(\Omega)} + N_2 \quad \forall H \in L_r^2(\Omega).$$

B.1: $A(t)$ is maximal monotone in \mathcal{W} , because it is a linear bounded operator and $a_t(G, G) \geq 0$ for all $G \in \mathcal{W}$ (see, for instance, [3, Theorem 2.4]). Moreover, we also have from the definition of $A(t)$ that

$$\|A(t)H\|_{\mathcal{W}'} \leq \frac{1}{\sigma_*} \|H\|_{\hat{H}_r^1(\Omega)} \quad \forall H \in \mathcal{W}, \quad \text{a.e. } t \in (0, T).$$

B.2: It follows from the assumption that $\sigma : (0, T) \rightarrow L^\infty(\Omega)$ is measurable (cf. H.4) and the fact that $A(t)$ is a linear bounded operator.

B.3: It is a consequence of Gårding's inequality from Lemma 3.3.1.

Thus, all the hypothesis of Theorem 2 from [52] are fulfilled and we are allowed to apply it to Problem (3.27)–(3.29) to conclude the proof. \square

Remark 3.3.2 *As a consequence of H.2, the solution of Problem 3.3.1 also satisfies $B \in L^2(0, T; L_r^2(\Omega))$.*

Remark 3.3.3 *The above existence result is independent of the slope of the H-B curve; even an infinite slope is allowed.*

Remark 3.3.4 *The previous theorem yields the existence of solution to Problem 3.3.1. If the electrical conductivity σ does not depend on time, we can also conclude the uniqueness. Indeed, let H_1 and H_2 be two solutions to Problem 3.3.1; then, for a.e. $t \in (0, T)$,*

$$\left\langle \frac{\partial \mathcal{B}(H_1(t))}{\partial t} - \frac{\partial \mathcal{B}(H_2(t))}{\partial t}, G \right\rangle_{\mathcal{W}, \mathcal{W}'} + a(H_1(t) - H_2(t), G) = 0 \quad \forall G \in \mathcal{W},$$

where $a(\cdot, \cdot)$ denotes the bilinear form defined in (3.25) for σ independent of t . By integrating this equation with respect to time, choosing $G = H_1(t) - H_2(t)$ as test function and using the monotonicity of \mathcal{B} , we obtain

$$\omega \|H_1(t) - H_2(t)\|_{L_r^2(\Omega)}^2 + a\left(\int_0^t (H_1 - H_2)(s) ds, H_1(t) - H_2(t)\right) \leq 0.$$

Thus, by integrating in $(0, T)$, using the equality

$$\begin{aligned} & 2 \int_0^T a\left(\int_0^t (H_1 - H_2)(s) ds, H_1(t) - H_2(t)\right) dt \\ &= a\left(\int_0^T (H_1 - H_2)(t) dt, \int_0^T (H_1 - H_2)(t) dt\right) \end{aligned} \quad (3.30)$$

and taking into account that $a(\cdot, \cdot)$ is positive semi-definite, we conclude that $H_1 = H_2$.

3.4 Numerical analysis

In this section we propose a numerical method to approximate the solution to Problem 3.3.1. In order to obtain error estimates for this numerical method, from now on we consider the following additional assumptions:

H.6 σ is time-independent and satisfies $\sigma \in W^{1, \infty}(\Omega)$.

H.7 $\mathcal{B}(r, z, u)$ is uniformly Lipschitz continuous with respect to u , namely: there exists a positive constant L such that

$$|\mathcal{B}(r, z, u) - \mathcal{B}(r, z, v)| \leq L|u - v| \quad \forall u, v \in \mathbb{R}, \forall (r, z) \in \Omega.$$

Notice that H.2 immediately follows from H.7.

To impose the constraint of (rH) being constant on Γ (cf. (3.14)) we proceed as in [89]: we make a change of unknown and write the equations in terms of $\tilde{H} := rH$ and $\tilde{B} := rB$.

With this end, we introduce some additional notation. First notice that $G \in \hat{H}_r^1(\Omega)$ if and only if $\tilde{G} := rG \in H_{1/r}^1(\Omega)$. Hence, $G \in \mathcal{W}$ if and only if \tilde{G} belongs to the following space:

$$\mathcal{Y} := \left\{ Y \in H_{1/r}^1(\Omega) : Y|_{\Gamma} \text{ is constant} \right\},$$

which we endow with the $H_{1/r}^1(\Omega)$ -norm. Since, $H_{1/r}^1(\Omega)$ is densely included in $L_{1/r}^2(\Omega)$, if we identify $L_{1/r}^2(\Omega)$ with its dual space, we have

$$\mathcal{Y} \subset L_{1/r}^2(\Omega) \subset \mathcal{Y}'.$$

We denote by $\langle \cdot, \cdot \rangle$ the duality pairing between \mathcal{Y}' and \mathcal{Y} .

From now on, we fix the data of Problem 3.3.1: $b \in H^1(0, T)$, $f \in L^2(0, T; \mathcal{W}')$ and $B_0 \in L_r^2(\Omega)$, and define $\tilde{R} \in L^2(0, T; \mathcal{Y}')$ and $\tilde{B}_0 \in L_{1/r}^2(\Omega)$ by

$$\langle \tilde{R}(t), \tilde{G} \rangle := \langle f(t), r^{-1}\tilde{G} \rangle_{\mathcal{W}, \mathcal{W}'} + (b'(t) - \langle f(t), r^{-1} \rangle_{\mathcal{W}, \mathcal{W}'}) (\tilde{G}|_{\Gamma}) \quad \tilde{G} \in \mathcal{Y}, \text{ a.e. } t \in [0, T],$$

and

$$\tilde{B}_0(r, z) := rB_0(r, z) \quad (r, z) \in \Omega.$$

Moreover, let

$$\tilde{\mathcal{B}}(r, z, u) := r\mathcal{B}(r, z, r^{-1}u) \quad (r, z) \in \Omega, u \in \mathbb{R}.$$

It is easy to check that $\tilde{\mathcal{B}}$ is also strongly monotone and Lipschitz continuous, namely: there exists positive constants ω and L (the same as in H.3 and H.7) such that

$$(\tilde{\mathcal{B}}(r, z, u) - \tilde{\mathcal{B}}(r, z, v))(u - v) \geq \omega|u - v|^2 \quad \forall u, v \in \mathbb{R}, \forall (r, z) \in \Omega \quad (3.31)$$

and

$$|\tilde{\mathcal{B}}(r, z, u) - \tilde{\mathcal{B}}(r, z, v)| \leq L|u - v| \quad \forall u, v \in \mathbb{R}, \forall (r, z) \in \Omega. \quad (3.32)$$

Finally, let us introduce the bilinear form $\tilde{a}(\cdot, \cdot) : H_{1/r}^1(\Omega) \times H_{1/r}^1(\Omega) \rightarrow \mathbb{R}$ defined by

$$\tilde{a}(\tilde{G}_1, \tilde{G}_2) := a_t(r^{-1}\tilde{G}_1, r^{-1}\tilde{G}_2) = \int_{\Omega} \frac{1}{\sigma r} \left(\frac{\partial \tilde{G}_1}{\partial r} \frac{\partial \tilde{G}_2}{\partial r} + \frac{\partial \tilde{G}_1}{\partial z} \frac{\partial \tilde{G}_2}{\partial r} \right) dr dz$$

for $\tilde{G}_1, \tilde{G}_2 \in H_{1/r}^1(\Omega)$. Notice that now, because of H.6, a_t actually does not depend on t . As a consequence of Lemma 3.3.1 we have the following result.

Lemma 3.4.1 *The bilinear form \tilde{a} is continuous and satisfies the Gårding's inequality*

$$\tilde{a}(\tilde{G}, \tilde{G}) + \lambda \|\tilde{G}\|_{L_{1/r}^2(\Omega)}^2 \geq \gamma \|\tilde{G}\|_{H_{1/r}^1(\Omega)}^2 \quad \forall \tilde{G} \in H_{1/r}^1(\Omega),$$

with $\lambda = \gamma = 1/\sigma^*$.

Under assumptions H.1 to H.5 we have shown that Problem 3.3.1 has a solution. Moreover, under the same assumptions and H.6, it is easy to prove that (H, B) is the unique solution to Problem 3.3.1 if and only if (\tilde{H}, \tilde{B}) is a solution to the following:

Problem 3.4.1 Find $\tilde{H} \in L^2(0, T; \mathcal{Y})$ and $\tilde{B} \in H^1(0, T; \mathcal{Y}')$ such that

$$\begin{aligned} \left\langle \frac{\partial \tilde{B}}{\partial t}, \tilde{G} \right\rangle + \tilde{a}(\tilde{H}, \tilde{G}) &= \langle \tilde{R}, \tilde{G} \rangle \quad \forall \tilde{G} \in \mathcal{Y}, \text{ a.e. } t \in (0, T), \\ \tilde{B}(r, z, t) &= \tilde{\mathcal{B}}(r, z, \tilde{H}(r, z, t)) \quad \text{a.e. in } \Omega \times (0, T), \\ \tilde{B}(r, z, 0) &= \tilde{B}_0(r, z) \quad \text{a.e. in } \Omega. \end{aligned}$$

3.4.1 Space discretization

We introduce in this section a space semi-discretization of Problem 3.4.1 and obtain an optimal order error estimate in the $L^2(0, T, L^2_{1/r}(\Omega))$ -norm. The following analysis is inspired in [82] and on the classical numerical analysis of linear parabolic equations (see, for instance, [86]).

To begin with, from now on we assume Ω is a convex polygon. We associate a family of partitions $\{\mathcal{T}_h\}_{h>0}$ of Ω into triangles, where h denotes the mesh size (i.e., the maximal length of the sides of the triangulation). Let $\mathcal{Y}_h := \mathcal{V}_h \cap \mathcal{Y}$, where \mathcal{V}_h denotes the space of continuous piecewise linear finite elements. By using this finite element space, we are led to the following discretization of Problem 3.4.1.

Problem 3.4.2 Find $\tilde{H}_h \in L^2(0, T; \mathcal{Y}_h)$ and $\tilde{B}_h \in H^1(0, T; \mathcal{Y}')$, satisfying

$$\begin{aligned} \left\langle \frac{\partial \tilde{B}_h}{\partial t}, \tilde{G}_h \right\rangle + \tilde{a}(\tilde{H}_h, \tilde{G}_h) &= \langle \tilde{R}, \tilde{G}_h \rangle \quad \forall \tilde{G}_h \in \mathcal{Y}_h, \text{ a.e. } t \in (0, T), \\ \tilde{B}_h(r, z, t) &= \tilde{\mathcal{B}}(r, z, \tilde{H}_h(r, z, t)) \quad \text{a.e. in } \Omega \times (0, T), \\ \tilde{B}_h(r, z, 0) &= \tilde{B}_{0h}(r, z) \quad \text{a.e. in } \Omega, \end{aligned}$$

where we assume that there exists $\tilde{H}_{0h} \in \mathcal{Y}_h$ such that

$$\tilde{B}_{0h}(r, z) = \tilde{\mathcal{B}}(r, z, \tilde{H}_{0h}(r, z)) \quad \text{a.e. in } \Omega. \quad (3.33)$$

A convenient \tilde{H}_{0h} has to be used for the solution of Problem 3.4.2 to approximate that of Problem 3.4.1. A possible (theoretical) choice is the Scott-Zhang interpolant of $\tilde{H}_0 := rH_0$ (see [79]) which preserves its constant values on Γ .

The existence of solution to the above problem is given by the following lemma:

Lemma 3.4.2 There exists a unique solution to Problem 3.4.2

Proof. Let $\{\tilde{\varphi}_i\}_{i=1}^K$ be a basis of \mathcal{Y}_h , then for all $t \in [0, T]$, a solution \tilde{H}_h to Problem 3.4.2, can be written as follows:

$$\tilde{H}_h(r, z, t) = \sum_{i=1}^K \alpha_i(t) \tilde{\varphi}_i(r, z) \quad (r, z) \in \Omega. \quad (3.34)$$

Similarly, we write

$$\tilde{H}_{0h}(r, z) = \sum_{i=1}^K \alpha_i^0 \tilde{\varphi}_i(r, z) \quad (r, z) \in \Omega.$$

We set $\boldsymbol{\alpha}(t) := (\alpha_i(t))_{1 \leq i \leq K}$, $t \in [0, T]$, and $\boldsymbol{\alpha}_0 := (\alpha_i^0)_{1 \leq i \leq K}$. By choosing $\tilde{G}_h = \tilde{\varphi}_j$, $j = 1, \dots, K$, in Problem 3.4.2, we obtain the following nonlinear system of differential equations:

$$\frac{d}{dt} \mathbf{C}(\boldsymbol{\alpha}(t)) + \mathbf{D}\boldsymbol{\alpha}(t) = \mathbf{R}(t) \quad \text{a.e. } t \in [0, T], \quad (3.35)$$

$$\boldsymbol{\alpha}(0) = \boldsymbol{\alpha}_0, \quad (3.36)$$

where the nonlinear function $\mathbf{C} : \mathbb{R}^K \rightarrow \mathbb{R}^K$, the matrix $\mathbf{D} := (D_{i,j})_{1 \leq i, j \leq K}$ and the vector $\mathbf{R}(t) := (R_i(t))_{1 \leq i \leq K}$ are defined by

$$\mathbf{C}(\boldsymbol{\alpha})_i := \int_{\Omega} \frac{1}{r} \tilde{\mathbf{B}} \left(r, z, \sum_{j=1}^K \tilde{\varphi}_j(r, z) \alpha_j \right) \tilde{\varphi}_i(r, z) \, dr dz,$$

$$D_{i,j} := \tilde{a}(\tilde{\varphi}_i, \tilde{\varphi}_j) \quad \text{and} \quad R_i(t) := \langle \tilde{R}(t), \tilde{\varphi}_i \rangle.$$

In order to prove the existence of solution to (3.35)-(3.36), we make a change of variable: we define $\psi_i(t) := \int_0^t \alpha_i(s) \, ds$, so that $\alpha_i = d\psi_i/dt$. Then, integrating in time (3.35), we obtain

$$\mathbf{C} \left(\frac{d\boldsymbol{\psi}}{dt}(t) \right) + \mathbf{D}\boldsymbol{\psi}(t) = \int_0^t \mathbf{R}(s) \, ds - \mathbf{C}(\boldsymbol{\alpha}_0) \quad \text{a.e. } t \in [0, T],$$

$$\boldsymbol{\psi}(0) = \mathbf{0},$$

where $\boldsymbol{\psi} := (\psi_i)_{1 \leq i \leq K}$.

Since $\tilde{\mathbf{B}}$ is strongly monotone and Lipschitz continuous (cf. (3.31) and (3.32)), it is straightforward to show that \mathbf{C} is strongly monotone and Lipschitz continuous, too. Therefore, \mathbf{C} is invertible and \mathbf{C}^{-1} is also Lipschitz continuous. Hence, the system above has a unique solution $\boldsymbol{\psi} \in C^1(0, T; \mathbb{R}^K)$ (see, for instance, [30]), $\boldsymbol{\alpha} = d\boldsymbol{\psi}/dt$ is the unique solution to (3.35)-(3.36) and \tilde{H}_h given by (3.34) that to Problem 3.4.2. \square

In what follows we will prove error estimates for this semi-discrete problem. With this aim, let us introduce the so-called elliptic projector $P_h : \mathcal{Y} \cap \mathbf{H}_0^1(\Omega) \rightarrow \mathcal{Y}_h \cap \mathbf{H}_0^1(\Omega)$, defined for $u \in \mathbf{H}_0^1(\Omega)$ by

$$\tilde{a}(P_h u, w_h) = \tilde{a}(u, w_h) \quad \forall w_h \in \mathcal{Y}_h \cap \mathbf{H}_0^1(\Omega).$$

The following lemma yields an error estimate for $P_h u$. Its proof, based on Galerkin orthogonality and a duality argument, is standard. From now on, we suppose that C is a strictly positive constant independent of h and Δt (the time step that will be introduced below).

Lemma 3.4.3 *There exists $C > 0$ such that, for all $u \in \mathbf{H}_{1/r}^2(\Omega) \cap \mathbf{H}_0^1(\Omega)$,*

$$\|P_h u - u\|_{L_{1/r}^2(\Omega)} + h \|P_h u - u\|_{\mathbf{H}_{1/r}^1(\Omega)} \leq Ch^2 \|u\|_{\mathbf{H}_{1/r}^2(\Omega)}.$$

Next, we define the operator $\tilde{P}_h : \mathcal{Y} \rightarrow \mathcal{Y}_h$ by

$$\tilde{P}_h v := P_h(v - (v|_\Gamma)) + (v|_\Gamma) \quad \forall v \in \mathcal{Y}.$$

It is easy to show that

$$\tilde{a}(\tilde{P}_h v, v_h) = \tilde{a}(v, v_h) \quad \forall v_h \in \mathcal{Y}_h. \quad (3.37)$$

Moreover, from Lemma 3.4.3 we have the following result.

Lemma 3.4.4 *There exists $C > 0$ such that, for all $u \in \mathbf{H}_{1/r}^2(\Omega) \cap \mathcal{Y}$,*

$$\|\tilde{P}_h u - u\|_{\mathbf{L}_{1/r}^2(\Omega)} + h\|\tilde{P}_h u - u\|_{\mathbf{H}_{1/r}^1(\Omega)} \leq C h^2 \|u\|_{\mathbf{H}_{1/r}^2(\Omega)}.$$

Now we are in position to obtain an error estimate for the above semi-discrete problem.

Theorem 3.4.1 *Let \tilde{H} and \tilde{H}_h be the solutions to Problems 3.4.1 and 3.4.2, respectively. If $\tilde{H} \in \mathbf{L}^2(0, T; \mathbf{H}_{1/r}^2(\Omega))$, then there exists $C > 0$ such that*

$$\|\tilde{H}_h - \tilde{H}\|_{\mathbf{L}^2(0, T; \mathbf{L}_{1/r}^2(\Omega))} \leq C \left\{ h^2 \|\tilde{H}\|_{\mathbf{L}^2(0, T; \mathbf{H}_{1/r}^2(\Omega))} + \|\tilde{H}_0 - \tilde{H}_{0h}\|_{\mathbf{L}_{1/r}^2(\Omega)} \right\}. \quad (3.38)$$

Proof. We proceed by means of a classical technique for parabolic equations. Let us write

$$\tilde{H}(t) - \tilde{H}_h(t) = \left(\tilde{H}(t) - \tilde{P}_h \tilde{H}(t) \right) + \left(\tilde{P}_h \tilde{H}(t) - \tilde{H}_h(t) \right). \quad (3.39)$$

Notice that the term $\tilde{H}(t) - \tilde{P}_h \tilde{H}(t)$ can be bounded as in Lemma 3.4.4. To estimate the other one, we test Problem 3.4.1 with $\tilde{G}_h \in \mathcal{Y}_h$, subtract from Problem 3.4.2 and integrate in time. Thus we obtain, for $t \in (0, T]$

$$\int_{\Omega} \frac{1}{r} (\tilde{B} - \tilde{B}_h)(t) \tilde{G}_h \, dr dz + \tilde{a} \left(\int_0^t (\tilde{H} - \tilde{H}_h)(s) \, ds, \tilde{G}_h \right) = \int_{\Omega} \frac{1}{r} (\tilde{B}_0 - \tilde{B}_{0h}) \tilde{G}_h \, dr dz.$$

Hence, from (3.37) we arrive at

$$\begin{aligned} & \int_{\Omega} \frac{1}{r} (\tilde{B}(\tilde{P}_h \tilde{H}(t)) - \tilde{B}(\tilde{H}_h(t))) \tilde{G}_h \, dr dz + \tilde{a} \left(\int_0^t (\tilde{P}_h \tilde{H} - \tilde{H}_h)(s) \, ds, \tilde{G}_h \right) \\ &= \int_{\Omega} \frac{1}{r} (\tilde{B}_0 - \tilde{B}_{0h}) \tilde{G}_h \, dr dz + \int_{\Omega} \frac{1}{r} (\tilde{B}(\tilde{P}_h \tilde{H}(t)) - \tilde{B}(\tilde{H}_h(t))) \tilde{G}_h \, dr dz. \end{aligned}$$

Now we take $\tilde{G}_h := \tilde{P}_h \tilde{H}(t) - \tilde{H}_h(t)$. Integrating in time, using the strong monotonicity and Lipschitz continuity of \tilde{B} (cf. (3.31) and (3.32)) and Cauchy-Schwartz and Young inequalities, we obtain

$$\begin{aligned} & \frac{\omega}{2} \int_0^T \|\tilde{P}_h \tilde{H}(t) - \tilde{H}_h(t)\|_{\mathbf{L}_{1/r}^2(\Omega)}^2 \, dt \\ &+ \int_0^T \tilde{a} \left(\int_0^t (\tilde{P}_h \tilde{H} - \tilde{H}_h)(s) \, ds, \tilde{P}_h \tilde{H}(t) - \tilde{H}_h(t) \right) \, dt \\ &\leq \frac{TL^2}{\omega} \|\tilde{H}_0 - \tilde{H}_{0h}\|_{\mathbf{L}_{1/r}^2(\Omega)}^2 + \frac{L^2}{\omega} \int_0^T \|\tilde{P}_h \tilde{H}(t) - \tilde{H}(t)\|_{\mathbf{L}_{1/r}^2(\Omega)}^2 \, dt. \end{aligned} \quad (3.40)$$

To estimate the right-hand side above we use Lemma 3.4.4, whereas, for the left-hand side we use the following equality (analogous to (3.30))

$$\begin{aligned} & \int_0^T \tilde{a} \left(\int_0^t (\tilde{P}_h \tilde{H} - \tilde{H}_h)(s) ds, \tilde{P}_h \tilde{H}(t) - \tilde{H}_h(t) \right) dt \\ &= \frac{1}{2} \tilde{a} \left(\int_0^T (\tilde{P}_h \tilde{H} - \tilde{H}_h)(t) dt, \int_0^T (\tilde{P}_h \tilde{H} - \tilde{H}_h)(t) dt \right) \end{aligned} \quad (3.41)$$

and the fact that

$$\begin{aligned} & \frac{\omega}{4} \int_0^T \|\tilde{P}_h \tilde{H}(t) - \tilde{H}_h(t)\|_{L^2_{1/r}(\Omega)}^2 dt + \beta \left\| \int_0^T (\tilde{P}_h \tilde{H} - \tilde{H}_h)(t) dt \right\|_{H^1_{1/r}(\Omega)}^2 \\ & \leq \frac{\omega}{2} \int_0^T \|\tilde{P}_h \tilde{H}(t) - \tilde{H}_h(t)\|_{L^2_{1/r}(\Omega)}^2 dt \\ & \quad + \frac{1}{2} \tilde{a} \left(\int_0^T (\tilde{P}_h \tilde{H} - \tilde{H}_h)(t) dt, \int_0^T (\tilde{P}_h \tilde{H} - \tilde{H}_h)(t) dt \right), \end{aligned} \quad (3.42)$$

for some positive constant β , which follows from (3.41) and Lemma 3.4.1. Thus, from (3.40) and (3.42) we obtain

$$\begin{aligned} & \|\tilde{P}_h \tilde{H} - \tilde{H}_h\|_{L^2(0,T;L^2_{1/r}(\Omega))} + \left\| \int_0^T (\tilde{P}_h \tilde{H} - \tilde{H}_h)(t) dt \right\|_{H^1_{1/r}(\Omega)} \\ & \leq C \left\{ h^2 \|\tilde{H}\|_{L^2(0,T;H^2_{1/r}(\Omega))} + \|\tilde{H}_0 - \tilde{H}_{0h}\|_{L^2_{1/r}(\Omega)} \right\}. \end{aligned} \quad (3.43)$$

Therefore, (3.38) follows from (3.39), (3.43) and Lemma 3.4.4, and we conclude the proof. \square

Remark 3.4.1 *If $\tilde{H}_0 \in H^2_{1/r}(\Omega)$, then we can use the Lagrange interpolant of \tilde{H}_0 as \tilde{H}_{0h} , and in such a case, we have*

$$\|\tilde{H}_h - \tilde{H}\|_{L^2(0,T;L^2_{1/r}(\Omega))} \leq Ch^2 \left\{ \|\tilde{H}\|_{L^2(0,T;H^2_{1/r}(\Omega))} + \|\tilde{H}_0\|_{H^2_{1/r}(\Omega)} \right\}.$$

Remark 3.4.2 *It is straightforward to obtain from (3.39), Lemma 3.4.4 and (3.43) the following error estimate:*

$$\sup_{t \in [0,T]} \left\| \int_0^t (\tilde{H}_h - \tilde{H})(s) ds \right\|_{L^2(0,T;H^1_{1/r}(\Omega))} \leq C \left\{ \|\tilde{H}_0 - \tilde{H}_{0h}\|_{L^2_{1/r}(\Omega)} + h \|\tilde{H}\|_{L^2(0,T;H^2_{1/r}(\Omega))} \right\}.$$

Remark 3.4.3 *The assumption on the convexity of the domain has been used to obtain an $\mathcal{O}(h^2)$ estimate in (3.38). For a non-convex domain, a reduced-order error estimate can be proved, too. In fact, the $\mathcal{O}(h^2)$ in (3.38) follows from Lemma 3.4.4 and this from Lemma 3.4.3, which holds true for any non-convex polygonal domain, but with a fractional power of h .*

3.4.2 Full discretization

In this section we introduce a time discretization of Problem 3.4.2 by means of a backward Euler scheme and prove its convergence. We consider a uniform partition $\{t^i := i\Delta t, i = 0, \dots, M\}$ of $[0, T]$, with time step $\Delta t := T/M$, $M \in \mathbb{N}$. The notation $\bar{\partial}z^{i+1}$ refers to the difference quotient

$$\bar{\partial}z^{i+1} := \frac{z^{i+1} - z^i}{\Delta t}.$$

We consider the following further assumption on the data of the problem:

$$\text{H.8 } f \in H^1(0, T; \mathcal{W}').$$

A full discretization of Problem 3.4.1 stands as follows:

Problem 3.4.3 For $i = 0, \dots, M-1$, find $\tilde{H}_h^{i+1} \in \mathcal{Y}_h$ and $\tilde{B}_h^{i+1} \in L^2_{1/r}(\Omega)$ satisfying

$$\int_{\Omega} \frac{1}{r} \bar{\partial} \tilde{B}_h^{i+1} \tilde{G}_h \, dr dz + \tilde{a}(\tilde{H}_h^{i+1}, \tilde{G}_h) = \langle \tilde{R}^{i+1}, \tilde{G}_h \rangle \quad \forall \tilde{G}_h \in \mathcal{Y}_h, \quad (3.44)$$

$$\tilde{B}_h^{i+1}(r, z) = \tilde{\mathcal{B}}(r, z, \tilde{H}_h^{i+1}(r, z)) \quad \text{a.e. in } \Omega, \quad (3.45)$$

$$\tilde{B}_h^0(r, z) = \tilde{B}_{0h}(r, z) \quad \text{a.e. in } \Omega, \quad (3.46)$$

where \tilde{B}_{0h} is as in (3.33). In the problem above, we have used $\tilde{R}^{i+1} \in \mathcal{Y}'$, defined by

$$\langle \tilde{R}^{i+1}, \tilde{G} \rangle := \langle f(t^{i+1}), r^{-1} \tilde{G} \rangle_{\mathcal{W}, \mathcal{W}'} + (\bar{\partial} b(t^{i+1}) - \langle f(t^{i+1}), r^{-1} \rangle_{\mathcal{W}, \mathcal{W}'}) (\tilde{G}|_{\Gamma}) \quad G \in \mathcal{Y},$$

to approximate $\tilde{R}(t^{i+1})$, $i = 0, \dots, M-1$.

The existence of solution at each time step is guaranteed by the following lemma.

Lemma 3.4.5 There exists a unique solution to Problem 3.4.3.

Proof. For each $i = 0, \dots, M-1$, we rewrite (3.44) as follows:

$$\mathcal{Z}(\tilde{H}_h^{i+1}) = \tilde{R}^{i+1}|_{\mathcal{Y}_h} + \tilde{F}^{i+1} \quad \text{in } \mathcal{Y}'_h, \quad (3.47)$$

with $\mathcal{Z} : \mathcal{Y}_h \rightarrow \mathcal{Y}'_h$ defined by

$$\langle \mathcal{Z}(\tilde{H}_h^{i+1}), \tilde{G}_h \rangle_{\mathcal{Y}_h, \mathcal{Y}'_h} := \int_{\Omega} \frac{1}{r} \tilde{\mathcal{B}}(r, z, \tilde{H}_h^{i+1}(r, z)) \tilde{G}_h \, dr dz + \Delta t \tilde{a}(\tilde{H}_h^{i+1}, \tilde{G}_h) \quad \tilde{G}_h \in \mathcal{Y}_h$$

and $\tilde{F}^{i+1} \in \mathcal{Y}'_h$ by

$$\langle \tilde{F}^{i+1}, \tilde{G}_h \rangle_{\mathcal{Y}_h, \mathcal{Y}'_h} := \int_{\Omega} \frac{1}{r} \tilde{\mathcal{B}}(r, z, \tilde{H}_h^i(r, z)) \tilde{G}_h \, dr dz \quad \forall \tilde{G}_h \in \mathcal{Y}_h.$$

Since $\tilde{\mathcal{B}}$ is strongly monotone and Lipschitz continuous (cf. (3.31) and (3.32)) and

$$\tilde{a}(\tilde{G}_h, \tilde{G}_h) \geq \frac{1}{\sigma^*} |\tilde{G}_h|_{H^1_{1/r}(\Omega)}^2 \quad \forall \tilde{G}_h \in \mathcal{Y}_h,$$

we have that $\mathcal{Z} : \mathcal{Y}_h \rightarrow \mathcal{Y}'_h$ is a strongly monotone, Lipschitz continuous operator. Thus, applying the Banach fixed-point technique, it can be shown that the equation (3.47) ($i = 0, \dots, M-1$) has a unique solution (see, for instance, [78, Proposition 2.22]). \square

The following theorem provides an error estimate for the fully-discrete problem.

Theorem 3.4.2 *Let \tilde{H} and \tilde{H}_h^{i+1} be the solutions to Problems 3.4.1 and 3.4.3, respectively. If $\tilde{H} \in \mathbf{H}^1(0, T; \mathbf{H}_{1/r}^2(\Omega))$, then there exists $C > 0$ such that*

$$\begin{aligned} & \left(\sum_{i=0}^{M-1} \Delta t \|\tilde{H}(t^{i+1}) - \tilde{H}_h^{i+1}\|_{\mathbf{L}_{1/r}^2(\Omega)}^2 \right)^{1/2} \\ & \leq C \left\{ (\Delta t + h^2) \|\tilde{H}\|_{\mathbf{H}^1(0, T; \mathbf{H}_{1/r}^2(\Omega))} + \|\tilde{H}_0 - \tilde{H}_{0h}\|_{\mathbf{L}_{1/r}^2(\Omega)} + \Delta t \|f\|_{\mathbf{H}^1(0, T; \mathcal{W}')} \right\}. \end{aligned}$$

Proof. We write as in the proof of Theorem 3.4.1

$$\tilde{H}(t^{i+1}) - \tilde{H}_h^{i+1} = \left(\tilde{H}(t^{i+1}) - \tilde{P}_h \tilde{H}(t^{i+1}) \right) + \left(\tilde{P}_h \tilde{H}(t^{i+1}) - \tilde{H}_h^{i+1} \right) \quad (3.48)$$

and focus on estimating the second term. First, by taking $\tilde{G} = \tilde{G}_h$ in Problem 3.4.1, integrating from 0 to $t^{l+1} \in (0, T]$ and using (3.37), we obtain

$$\begin{aligned} & \int_{\Omega} \frac{1}{r} \tilde{\mathcal{B}}(\tilde{H}(t^{l+1})) \tilde{G}_h \, dr dz + \Delta t \tilde{a} \left(\sum_{i=0}^l \tilde{P}_h \tilde{H}(t^{i+1}), \tilde{G}_h \right) \\ & = \tilde{a} \left(\int_0^{t^{l+1}} (\tilde{H}_{\Delta t} - \tilde{H})(t) \, dt, \tilde{G}_h \right) + \left\langle \int_0^{t^{l+1}} \tilde{R}(t) \, dt, \tilde{G}_h \right\rangle \\ & \quad + \int_{\Omega} \frac{1}{r} \tilde{B}_0 \tilde{G}_h \, dr dz \quad \forall \tilde{G}_h \in \mathcal{Y}_h, \end{aligned} \quad (3.49)$$

with $\tilde{H}_{\Delta t}$ being the piecewise constant interpolant of \tilde{H} (i.e., $\tilde{H}_{\Delta t}(t^0) := \tilde{H}(t^0)$ and $\tilde{H}_{\Delta t}(t) := \tilde{H}(t^i)$, $t \in (t^{i-1}, t^i]$). Then, by summing up (3.44) for $i = 0, \dots, l$, with $l \in \{0, \dots, M-1\}$, and subtracting from (3.49), we have

$$\begin{aligned} & \int_{\Omega} \frac{1}{r} (\tilde{\mathcal{B}}(\tilde{P}_h \tilde{H}(t^{l+1})) - \tilde{\mathcal{B}}(\tilde{H}_h^{l+1})) \tilde{G}_h \, dr dz + \Delta t \tilde{a} \left(\sum_{i=0}^l (\tilde{P}_h \tilde{H}(t^{i+1}) - \tilde{H}_h^{i+1}), \tilde{G}_h \right) \\ & = \int_{\Omega} \frac{1}{r} (\tilde{B}_0 - \tilde{B}_{0h}) \tilde{G}_h \, dr dz + \int_{\Omega} \frac{1}{r} (\tilde{\mathcal{B}}(\tilde{P}_h \tilde{H}(t^{l+1})) - \tilde{\mathcal{B}}(\tilde{H}(t^{l+1}))) \tilde{G}_h \, dr dz \\ & \quad + \tilde{a} \left(\int_0^{t^{l+1}} (\tilde{H}_{\Delta t} - \tilde{H})(t) \, dt, \tilde{G}_h \right) + \left\langle \int_0^{t^{l+1}} \tilde{R}(t) \, dt - \Delta t \sum_{i=0}^l \tilde{R}^{i+1}, \tilde{G}_h \right\rangle. \end{aligned} \quad (3.50)$$

The last term above can be written as follows: for all $\tilde{G}_h \in \mathcal{Y}_h$

$$\left\langle \int_0^{t^{l+1}} \tilde{R}(t) \, dt - \Delta t \sum_{i=0}^l \tilde{R}^{i+1}, \tilde{G}_h \right\rangle = \int_0^{t^{l+1}} \langle E_f(t), \tilde{G} \rangle \, dt,$$

where $E_f \in \mathbf{L}^2(0, T, \mathcal{Y}')$ is defined, a.e. $t \in (0, T)$, by

$$\begin{aligned} \langle E_f(t), \tilde{G} \rangle & := \left\langle (f - f_{\Delta t})(t), r^{-1} \tilde{G} \right\rangle_{\mathcal{W}, \mathcal{W}'} \\ & \quad - \left\langle (f - f_{\Delta t})(t), r^{-1} \right\rangle_{\mathcal{W}, \mathcal{W}'} (\tilde{G}|_{\Gamma}) \end{aligned}$$

for $\tilde{G} \in \mathcal{Y}$, with $f_{\Delta t}$ being the piecewise constant interpolant of f defined as above. Notice that, clearly,

$$\|E_f\|_{L^2(0,T;\mathcal{Y}')} \leq C \|f - f_{\Delta t}\|_{L^2(0,T;\mathcal{W}')}. \quad (3.51)$$

Now, by choosing $\tilde{G}_h = \tilde{P}_h \tilde{H}(t^{l+1}) - \tilde{H}_h^{l+1}$ in (3.50) and using the monotonicity and Lipschitz continuity of $\tilde{\mathcal{B}}$ (cf. (3.31) and (3.32)) and Cauchy-Schwartz and Young inequalities, we obtain

$$\begin{aligned} & \frac{\omega}{2} \|\tilde{P}_h \tilde{H}(t^{l+1}) - \tilde{H}_h^{l+1}\|_{L^2_{1/r}(\Omega)}^2 + \Delta t \tilde{a} \left(\sum_{i=0}^l (\tilde{P}_h \tilde{H}(t^{i+1}) - \tilde{H}_h^{i+1}), \tilde{P}_h \tilde{H}(t^{l+1}) - \tilde{H}_h^{l+1} \right) \\ & \leq \frac{L^2}{\omega} \|\tilde{H}_0 - \tilde{H}_{0h}\|_{L^2_{1/r}(\Omega)}^2 + \frac{L^2}{\omega} \|\tilde{P}_h \tilde{H}(t^{l+1}) - \tilde{H}(t^{l+1})\|_{L^2_{1/r}(\Omega)}^2 \\ & \quad + \tilde{a} \left(\int_0^{t^{l+1}} (\tilde{H}_{\Delta t} - \tilde{H})(t) dt, \tilde{P}_h \tilde{H}(t^{l+1}) - \tilde{H}_h^{l+1} \right) \\ & \quad + \left\langle \int_0^{t^{l+1}} E_f(t) dt, \tilde{P}_h \tilde{H}(t^{l+1}) - \tilde{H}_h^{l+1} \right\rangle. \end{aligned}$$

Summing up the above equation for $l = 0, \dots, M-1$, we obtain

$$\begin{aligned} & \frac{\omega}{2} \sum_{l=0}^{M-1} \Delta t \|\tilde{P}_h \tilde{H}(t^{l+1}) - \tilde{H}_h^{l+1}\|_{L^2_{1/r}(\Omega)}^2 \\ & \quad + \Delta t^2 \sum_{l=0}^{M-1} \tilde{a} \left(\sum_{i=0}^l (\tilde{P}_h \tilde{H}(t^{i+1}) - \tilde{H}_h^{i+1}), \tilde{P}_h \tilde{H}(t^{l+1}) - \tilde{H}_h^{l+1} \right) \\ & \leq \frac{L^2 T}{\omega} \|\tilde{H}_0 - \tilde{H}_{0h}\|_{L^2_{1/r}(\Omega)}^2 + \frac{L^2 \Delta t}{\omega} \sum_{l=0}^{M-1} \|\tilde{P}_h \tilde{H}(t^{l+1}) - \tilde{H}(t^{l+1})\|_{L^2_{1/r}(\Omega)}^2 \\ & \quad + \Delta t \sum_{l=0}^{M-1} \tilde{a} \left(\int_0^{t^{l+1}} (\tilde{H}_{\Delta t} - \tilde{H})(t) dt, \tilde{P}_h \tilde{H}(t^{l+1}) - \tilde{H}_h^{l+1} \right) \\ & \quad + \Delta t \sum_{l=0}^{M-1} \left\langle \int_0^{t^{l+1}} E_f(t) dt, \tilde{P}_h \tilde{H}(t^{l+1}) - \tilde{H}_h^{l+1} \right\rangle. \quad (3.52) \end{aligned}$$

First, we will deal with the left-hand side above. We rewrite its second term by using the following identity, for $l \geq 1$:

$$\tilde{P}_h \tilde{H}(t^{l+1}) - \tilde{H}_h^{l+1} = \sum_{i=0}^l (\tilde{P}_h \tilde{H}(t^{i+1}) - \tilde{H}_h^{i+1}) - \sum_{i=0}^{l-1} (\tilde{P}_h \tilde{H}(t^{i+1}) - \tilde{H}_h^{i+1}). \quad (3.53)$$

Thus we obtain a discrete version of (3.41), namely,

$$\begin{aligned} & \Delta t^2 \sum_{l=0}^{M-1} \tilde{a} \left(\sum_{i=0}^l (\tilde{P}_h \tilde{H}(t^{i+1}) - \tilde{H}_h^{i+1}), \tilde{P}_h \tilde{H}(t^{l+1}) - \tilde{H}_h^{l+1} \right) \\ & = \frac{1}{2} \tilde{a} \left(\Delta t \sum_{l=0}^{M-1} (\tilde{P}_h \tilde{H}(t^{l+1}) - \tilde{H}_h^{l+1}), \Delta t \sum_{l=0}^{M-1} (\tilde{P}_h \tilde{H}(t^{l+1}) - \tilde{H}_h^{l+1}) \right). \end{aligned}$$

Using this and Lemma 3.4.1, we obtain the following estimates for the left-hand side of (3.52): there exists $\beta > 0$ (which depends on ω, T and σ^*) such that

$$\begin{aligned}
& \frac{\omega}{2} \sum_{l=0}^{M-1} \Delta t \|\tilde{P}_h \tilde{H}(t^{l+1}) - \tilde{H}_h^{l+1}\|_{L^2_{1/r}(\Omega)}^2 \\
& \quad + \frac{1}{2} \tilde{a} \left(\Delta t \sum_{l=0}^{M-1} (\tilde{P}_h \tilde{H}(t^{l+1}) - \tilde{H}_h^{l+1}), \Delta t \sum_{l=0}^{M-1} (\tilde{P}_h \tilde{H}(t^{l+1}) - \tilde{H}_h^{l+1}) \right) \\
& \geq \frac{\omega}{4} \sum_{l=0}^{M-1} \Delta t \|\tilde{P}_h \tilde{H}(t^{l+1}) - \tilde{H}_h^{l+1}\|_{L^2_{1/r}(\Omega)}^2 \\
& \quad + \beta \left\| \Delta t \sum_{l=0}^{M-1} (\tilde{P}_h \tilde{H}(t^{l+1}) - \tilde{H}_h^{l+1}) \right\|_{\mathbf{H}^1_{1/r}(\Omega)}^2. \tag{3.54}
\end{aligned}$$

Next, we estimate the right-hand side of (3.52). The second term will be easily bounded by means of Lemma 3.4.4. For the third term we use (3.53) and summation by parts to obtain

$$\begin{aligned}
& \Delta t \sum_{l=0}^{M-1} \tilde{a} \left(\int_0^{t^{l+1}} (\tilde{H}_{\Delta t} - \tilde{H})(t) dt, \tilde{P}_h \tilde{H}(t^{l+1}) - \tilde{H}_h^{l+1} \right) \\
& = \tilde{a} \left(\int_0^T (\tilde{H}_{\Delta t} - \tilde{H})(t) dt, \Delta t \sum_{l=0}^{M-1} (\tilde{P}_h \tilde{H}(t^{l+1}) - \tilde{H}_h^{l+1}) \right) \\
& \quad - \sum_{l=0}^{M-2} \tilde{a} \left(\int_{t^{l+1}}^{t^{l+2}} (\tilde{H}_{\Delta t} - \tilde{H})(t) dt, \Delta t \sum_{i=0}^l (\tilde{P}_h \tilde{H}(t^{i+1}) - \tilde{H}_h^{i+1}) \right).
\end{aligned}$$

Hence, using the continuity of \tilde{a} and Young's inequality, we obtain that for all $\alpha > 0$, there exists $C_\alpha > 0$ such that

$$\begin{aligned}
& \left| \Delta t \sum_{l=0}^{M-1} \tilde{a} \left(\int_0^{t^{l+1}} (\tilde{H}_{\Delta t} - \tilde{H})(t) dt, \tilde{P}_h \tilde{H}(t^{l+1}) - \tilde{H}_h^{l+1} \right) \right| \\
& \leq C_\alpha \|\tilde{H}_{\Delta t} - \tilde{H}\|_{L^2(0,T;\mathbf{H}^1_{1/r}(\Omega))}^2 + \frac{\alpha}{2} \left\| \Delta t \sum_{l=0}^{M-1} (\tilde{P}_h \tilde{H}(t^{l+1}) - \tilde{H}_h^{l+1}) \right\|_{\mathbf{H}^1_{1/r}(\Omega)}^2 \\
& \quad + \frac{1}{2} \sum_{l=0}^{M-2} \left\| \Delta t \sum_{i=0}^l (\tilde{P}_h \tilde{H}(t^{i+1}) - \tilde{H}_h^{i+1}) \right\|_{\mathbf{H}^1_{1/r}(\Omega)}^2. \tag{3.55}
\end{aligned}$$

For the last term of (3.52), we proceed analogously to obtain

$$\begin{aligned}
& \left| \Delta t \sum_{l=0}^{M-1} \left\langle \int_0^{t^{l+1}} E_f(t) dt, \tilde{P}_h \tilde{H}(t^{l+1}) - \tilde{H}_h^{l+1} \right\rangle \right| \\
& \leq C_\alpha \|E_f\|_{L^2(0,T;\mathcal{Y}')}^2 + \frac{\alpha}{2} \left\| \Delta t \sum_{l=0}^{M-1} (\tilde{P}_h \tilde{H}(t^{l+1}) - \tilde{H}_h^{l+1}) \right\|_{\mathbf{H}_{1/r}^1(\Omega)}^2 \\
& \quad + \frac{1}{2} \sum_{l=0}^{M-2} \left\| \Delta t \sum_{i=0}^l (\tilde{P}_h \tilde{H}(t^{i+1}) - \tilde{H}_h^{i+1}) \right\|_{\mathbf{H}_{1/r}^1(\Omega)}^2. \tag{3.56}
\end{aligned}$$

By taking $\alpha := \beta/2$, replacing (3.54)-(3.56) in (3.52) and using (3.51) and the discrete Gronwall's inequality, we arrive at

$$\begin{aligned}
& \sum_{l=0}^{M-1} \Delta t \|\tilde{P}_h \tilde{H}(t^{l+1}) - \tilde{H}_h^{l+1}\|_{L_{1/r}^2(\Omega)}^2 + \left\| \Delta t \sum_{l=0}^{M-1} (\tilde{P}_h \tilde{H}(t^{l+1}) - \tilde{H}_h^{l+1}) \right\|_{\mathbf{H}_{1/r}^1(\Omega)}^2 \\
& \leq C \left\{ \|\tilde{H}_{\Delta t} - \tilde{H}\|_{L^2(0,T;\mathbf{H}_{1/r}^1(\Omega))}^2 + \|f - f_{\Delta t}\|_{L^2(0,T;\mathcal{W}')}^2 \right. \\
& \quad \left. + \|\tilde{H}_0 - \tilde{H}_{0h}\|_{L_{1/r}^2(\Omega)}^2 + \Delta t \sum_{l=0}^{M-1} \|\tilde{P}_h \tilde{H}(t^{l+1}) - \tilde{H}(t^{l+1})\|_{L_{1/r}^2(\Omega)}^2 \right\}. \tag{3.57}
\end{aligned}$$

Thus, the result follows from (3.48), Lemma 3.4.4 and classical approximation results for the piecewise constant interpolant. \square

Remark 3.4.4 *As noted in Remark 3.4.1, if $\tilde{H}_0 \in \mathbf{H}_{1/r}^2(\Omega)$, then the Lagrange interpolant of \tilde{H}_0 can be used as \tilde{H}_{0h} and, in such a case, we conclude that*

$$\begin{aligned}
& \left(\sum_{i=0}^{M-1} \Delta t \|\tilde{H}(t^{i+1}) - \tilde{H}_h^{i+1}\|_{L_{1/r}^2(\Omega)}^2 \right)^{1/2} \\
& \leq C \left\{ (\Delta t + h^2) \|\tilde{H}\|_{\mathbf{H}^1(0,T;\mathbf{H}_{1/r}^2(\Omega))} + h^2 \|\tilde{H}_0\|_{\mathbf{H}_{1/r}^2(\Omega)} + \Delta t \|f\|_{\mathbf{H}^1(0,T;\mathcal{W}')} \right\}.
\end{aligned}$$

Remark 3.4.5 *A result analogous to that of Remark 3.4.2 also holds true. In fact, from (3.48), Lemma 3.4.4 and (3.57) it is straightforward to prove that*

$$\begin{aligned}
& \max_{l \in \{1, \dots, M\}} \left\| \sum_{i=0}^{l-1} \Delta t (\tilde{H}(t^{i+1}) - \tilde{H}_h^{i+1}) \right\|_{\mathbf{H}_{1/r}^1(\Omega)} \\
& \leq C \left\{ (\Delta t + h) \|\tilde{H}\|_{\mathbf{H}^1(0,T;\mathbf{H}_{1/r}^2(\Omega))} + \|\tilde{H}_0 - \tilde{H}_{0h}\|_{L_{1/r}^2(\Omega)} + \Delta t \|f\|_{\mathbf{H}^1(0,T;\mathcal{W}')} \right\}.
\end{aligned}$$

Remark 3.4.6 *The same arguments used in Remark 3.4.3, allow us to show that a reduced-order form of Theorem 3.4.2 holds true for a non-convex polygonal domain.*

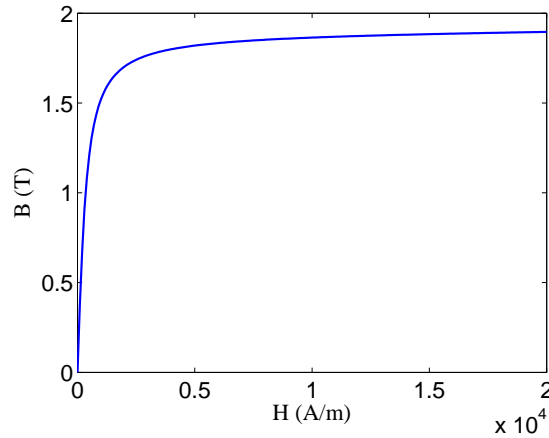


Figure 3.2: Positive part of the H-B curve.

3.5 Numerical results

In this section we report some numerical results obtained with a Fortran code which implements the numerical method described above. In order to analyze the convergence properties of the numerical scheme, we apply it to a test problem with a known analytical solution. The main purpose of this test is to check that the orders of convergence are consistent with the theoretical results. With this end, we have solved a problem which corresponds to a laminated electromagnetic core, where the magnetic flux flowing through it is known [89]. The geometry corresponds to the meridian section of such a device, whereas the physical parameters used in the simulation are similar to those of nonlinear steels frequently used in its manufacture (see, for instance, [88]).

We consider the eddy current Problem 3.2.1 defined in the meridian section $\Omega := (0.06, 0.18) \times (0, 0.06)$, where the dimensions are given in meters. The right-hand side f is chosen so that

$$H = \frac{150 \exp(t)}{r} \sin\left(\frac{\pi r}{0.06}\right) \sin\left(\frac{\pi z}{0.06}\right)$$

is the solution to the problem. Notice that $\tilde{H} = rH$ is constant (actually it vanishes) on the boundary of the domain.

We consider a nonlinear material whose magnetization is given by its anhysteretic H-B curve defined by

$$\mathcal{B}(H) := \mu_0 H + \frac{2J_s}{\pi} \arctan\left(\frac{\pi(\mu_r - 1)\mu_0 H}{2J_s}\right), \quad (3.58)$$

where $\mu_0 = 4\pi \times 10^{-7} \text{ Hm}^{-1}$, $\mu_r = 3000$ and $J_s = 1.89 \text{ T}$. This curve, whose positive part is shown in Figure 3.2, is very similar to the first magnetization curve of laminated steels (cf. [88]). The value of the electrical conductivity is $\sigma = 4 \times 10^6 \text{ (Ohm m)}^{-1}$.

The problem has been solved in the time interval $[0, 2]$ so that the values of the solution H vary approximately between -12×10^3 and $12 \times 10^3 \text{ A/m}$. Hence, the nonlinear part of the curve is clearly attained (see Figure 3.2).

The numerical method has been applied with several successively refined meshes and time-steps. The nonlinear system arising at each time step has been solved with a Newton's iteration. A sufficiently small tolerance has been chosen (10^{-4}), so that the error of this iteration be negligible. The computed approximate solutions have been compared with the analytical one by calculating the percentual relative error for \tilde{H} and $\mathbf{grad} \tilde{H}$ in the $L^2(0, T; L^2_{1/r}(\Omega))$ -norm by means of

$$\mathcal{E}_h^{\Delta t}(\tilde{H}) := 100 \frac{\left(\sum_{k=1}^M \Delta t \|\tilde{H}(t^k) - \tilde{H}_h^k\|_{L^2_{1/r}(\Omega)}^2 \right)^{1/2}}{\left(\sum_{k=1}^M \Delta t \|\tilde{H}(t^k)\|_{L^2_{1/r}(\Omega)}^2 \right)^{1/2}},$$

$$\mathcal{E}_h^{\Delta t}(\mathbf{grad} \tilde{H}) := 100 \frac{\left(\sum_{k=1}^M \Delta t \|\mathbf{grad} \tilde{H}(t^k) - \mathbf{grad} \tilde{H}_h^k\|_{L^2_{1/r}(\Omega)}^2 \right)^{1/2}}{\left(\sum_{k=1}^M \Delta t \|\mathbf{grad} \tilde{H}(t^k)\|_{L^2_{1/r}(\Omega)}^2 \right)^{1/2}}.$$

Table 3.1 shows the relative errors for \tilde{H} at different levels of discretization. We notice that by taking a small enough time-step Δt one can observe the behavior of the error with respect to the space discretization (see the row corresponding to $\Delta t/128$). On the other hand, by considering a small enough mesh-size h , one can inspect the order of convergence with respect to Δt (see the column corresponding to $h/16$). In this example, we observe an order of convergence $\mathcal{O}(h^2 + \Delta t)$ for \tilde{H} , which is the one expected from the theoretical analysis (cf. Remark 3.4.4).

In Table 3.2 we show the percentual relative errors for $\mathbf{grad} \tilde{H}$ in the $L^2(0, T; L^2_{1/r}(\Omega))$ -norm. In this case, the space discretization error dominates the time discretization one, even for the finest mesh. In fact, an order $\mathcal{O}(h)$ can be observed for both time steps. Let us remark that we have not proved theoretically this experimental result (note that the estimates in Remark 3.4.5 are in a different norm).

Table 3.1: Relative error (%) for \tilde{H} : $\mathcal{E}_h^{\Delta t}(\tilde{H})$.

	h	$h/2$	$h/4$	$h/8$	$h/16$
Δt	13.85	2.91	0.63	0.65	0.75
$\Delta t/2$	14.04	3.14	0.61	0.30	0.38
$\Delta t/4$	14.14	3.25	0.70	0.15	0.18
$\Delta t/8$	14.19	3.32	0.77	0.15	0.08
$\Delta t/16$	14.21	3.36	0.80	0.17	0.04
$\Delta t/32$	14.22	3.37	0.82	0.19	0.04
$\Delta t/64$	14.21	3.38	0.83	0.20	0.04
$\Delta t/128$	14.20	3.38	0.83	0.20	0.04

Once the order of convergence is checked, we report in one single figure the simultaneous dependence on h and Δt for \tilde{H} in $L^2(0, T; L^2_{1/r}(\Omega))$ -norm by proceeding in the following way:

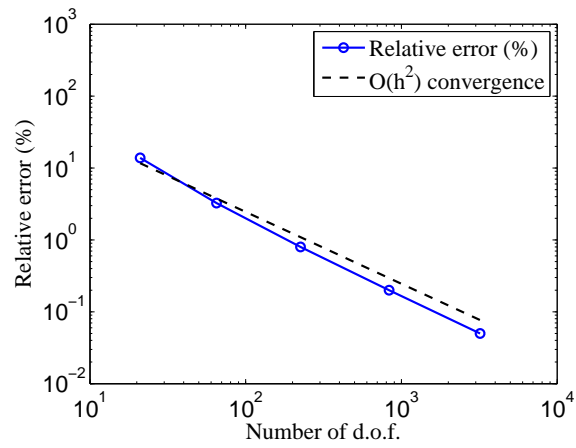


Figure 3.3: $\mathcal{E}_h^{\Delta t}(\tilde{H})$ versus number of d.o.f. (log-log scale), $\Delta t = Ch^2$.

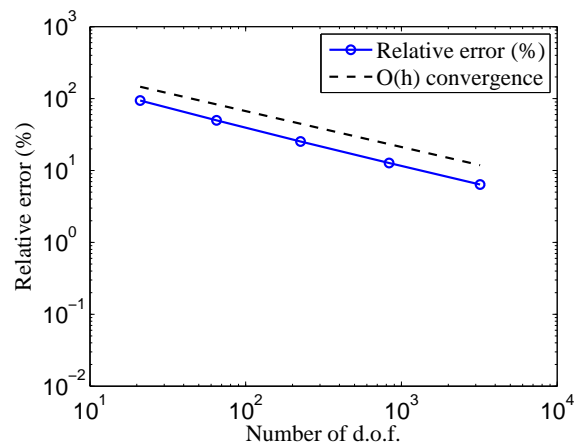


Figure 3.4: $\mathcal{E}_h^{\Delta t}(\mathbf{grad} \tilde{H})$ versus number of d.o.f. (log-log scale), $\Delta t = Ch$.

Table 3.2: Relative error (%) for $\mathbf{grad} \tilde{H}$: $\mathcal{E}_h^{\Delta t}(\mathbf{grad} \tilde{H})$.

	h	$h/2$	$h/4$	$h/8$	$h/16$
Δt	94.04	49.88	25.33	12.73	6.41
$\Delta t/2$	94.13	49.95	25.36	12.73	6.38

we choose initial coarse values of h and Δt and, for each successively refined mesh, we take a value of Δt proportional to h^2 (see the values within boxes in Table 3.1). Figure 3.3 shows a log-log plot of the corresponding relative errors for \tilde{H} in the $L^2(0, T; L^2_{1/r}(\Omega))$ -norm versus the number of degrees of freedom (d.o.f.). The slope of the curve shows an order of convergence $\mathcal{O}(h^2) = \mathcal{O}(h^2 + \Delta t)$. In a similar way, Figure 3.4 shows an order $\mathcal{O}(h + \Delta t)$ for $\mathbf{grad} \tilde{H}$ in the $L^2(0, T; L^2_{1/r}(\Omega))$ -norm.

Chapter 4

Mathematical and numerical analysis of a transient non-linear axisymmetric eddy current model

4.1 Introduction

An important challenge in the analysis and design of electrical machines is the accurate computation of power losses in the ferromagnetic components of the core due to hysteresis and eddy-current effects. These losses determine the efficiency of the device and have a significant influence on its operating cost. There are numerous publications devoted to obtain analytical simplified expressions to approximate their different components, which are only valid under certain assumptions that do not hold in many practical situations. Numerical modeling is an interesting alternative to overcome these limitations (see [37, 90, 75]).

We focus on the eddy current losses. Their numerical computation requires solving the Maxwell quasi-static partial differential equations, which is the aim of this chapter. For linear magnetic materials this is a well established subject, even for three-dimensional (3D) models where edge finite elements are very useful (see, for instance, [1, 20, 50]). The non-linear case was studied in [80, 82] in terms of the magnetic field, where a transient eddy current model is considered on a 3D bounded conducting domain under homogeneous Dirichlet boundary conditions. A time semi-discretization scheme to approximate this problem is proposed and analyzed in these references; however, current sources are not taken into account, the only non vanishing data being the initial condition.

More recently, a non-linear axisymmetric transient eddy current model was analyzed in [10] under rather general assumptions on the non-linear constitutive relation between the magnetic field H and the magnetic induction B (i.e., the so called H-B curve). In this case, the source term enters in the model by setting the magnetic flux across a meridian section of the device. Existence of solution was obtained by applying an abstract result which needs, in particular, the strong monotonicity of the H-B curve. A full discretization to approximate this problem was also proposed in this reference and error estimates were obtained.

In the present chapter we also focus on the axisymmetric eddy current model defined in a non-linear magnetic device. However, we consider the case in which the source term enters in the model by setting the magnetic field on the boundary, which results in a non-homogeneous Dirichlet boundary condition. This is shown to be a mathematically suitable condition for the problem to be well posed and, at the same time, it is physically realistic in the sense that there are industrial applications where it can be readily obtained from easily measurable quantities. This is the case, for instance, of the numerical simulation of eddy currents in metallurgical electrodes [8, 9, 54], induction heating systems [29] or current losses in a toroidal laminated core [62, 70]. In all these applications the Dirichlet boundary data for the magnetic field can be obtained from the current intensity. We notice that the non-homogeneous character of the boundary condition brings some technical complications in both the mathematical and the numerical analysis with respect to previous works on the subject [10, 80, 82].

In our case, the behavior of the material is defined by means of a general continuous and monotone non-linear H-B curve which (unlike in references [80] and [82]) may also depend on the position, what allows us to deal with heterogeneous media. Moreover, we also consider a time and space dependent electrical conductivity. This is important in practical applications, because this quantity is typically a function of temperature, which in its turn is a time dependent field.

By using classical weighted two-dimensional Sobolev spaces for axisymmetric problems, we prove the existence of a solution to a weak formulation in terms of the magnetic field. The technique used for this purpose (commonly known as the Rothe's method, see [77]) consists of introducing an implicit time discretization, obtaining a priori estimates and then passing to the limit as the time-step goes to zero. Let us remark that, to the best of the authors' knowledge, this problem does not fit in other existing results because of the time dependence of the coefficients as well as the non-homogeneous character of the boundary condition.

Under further assumptions, we also prove the uniqueness of solution and perform the numerical analysis of the problem. For the numerical solution, first the problem is discretized in time with a backward Euler scheme, which is proved to be well posed. Then, a full discrete approximation is introduced by using continuous piecewise linear functions on triangular meshes. Under appropriate assumptions, we analyze both, the semi- and the fully discrete schemes. For the former our analysis is based on [82]. For the latter we adapt the classical theory of linear parabolic equations (see, for instance, [86]), whereas to deal with the non-homogeneous Dirichlet boundary condition we resort to some arguments from [5]. Therefore, for the fully discrete problem, we obtain an L^2 -like estimate without assuming any additional regularity of the solution. Moreover, under appropriate smoothness assumptions, we also obtain an optimal-order error estimate.

The chapter is organized as follows. First, in Section 4.2, we describe the transient axisymmetric eddy current model and introduce the non-linear parabolic partial differential equation to be solved. In Section 4.3, we recall some functional spaces, establish a weak formulation of the problem and study its well posedness. Section 4.4 is devoted to the numerical analysis of the semi-discrete problem arising from a backward Euler time-discretization. In Section 4.5, we combine it with a finite element method for space discretization and prove stability and error estimates of the resulting full discretization. Finally, in Section 4.6, we report a numerical test

which confirms the theoretical results.

4.2 The transient eddy current model

Eddy currents are usually modeled by the so called low-frequency Maxwell's equations (see, for instance, [1]):

$$\begin{aligned}\mathbf{curl} \mathbf{H} &= \mathbf{J}, \\ \frac{\partial \mathbf{B}}{\partial t} + \mathbf{curl} \mathbf{E} &= \mathbf{0}, \\ \operatorname{div} \mathbf{B} &= 0.\end{aligned}$$

We have used above standard notations in electromagnetism: \mathbf{E} is the electric field, \mathbf{B} the magnetic induction, \mathbf{H} the magnetic field and \mathbf{J} the current density. To obtain a closed system we need to add constitutive laws. On one hand, assuming that the materials are electrically linear, Ohm's law in conductors reads

$$\mathbf{J} = \sigma \mathbf{E},$$

where σ is the electrical conductivity, which is supposed to be bounded above and below away from zero. On the other hand, assuming that the magnetic materials are soft and hysteresis effects can be neglected, we may consider that \mathbf{B} and \mathbf{H} are related as follows:

$$\mathbf{B} = \mathcal{B}(\mathbf{H}), \quad (4.1)$$

where \mathcal{B} is a non-linear mapping.

The above equations lead to the partial differential equation in conductors

$$\frac{\partial \mathbf{B}}{\partial t} + \mathbf{curl} \left(\frac{1}{\sigma} \mathbf{curl} \mathbf{H} \right) = \mathbf{0}, \quad (4.2)$$

which has to be solved together with the non-linear equation (4.1) and appropriate boundary and initial conditions.

4.2.1 Axisymmetric case

We restrict our attention to the case where a 3D conducting domain $\tilde{\Omega}$ has cylindrical symmetry and all fields are independent of the angular variable θ . Then, in order to reduce the dimension and thereby the computational effort, it is convenient to consider a cylindrical coordinate system (r, θ, z) . Let us denote by \mathbf{e}_r , \mathbf{e}_θ and \mathbf{e}_z the corresponding unit vectors of the local orthonormal basis.

We assume that the magnetic field is of the form

$$\mathbf{H}(r, z, t) = H(r, z, t) \mathbf{e}_\theta.$$

Then, assuming an isotropic behavior of the material, the magnetic induction \mathbf{B} will be of the same form,

$$\mathbf{B}(r, z, t) = B(r, z, t) \mathbf{e}_\theta,$$

and hence automatically divergence-free. Therefore, a scalar non-linear model

$$B(r, z, t) = \mathcal{B}(r, z, H(r, z, t)),$$

with $\mathcal{B}(r, z, \cdot)$ a non-linear mapping in \mathbb{R} , may be used to describe the H-B relation.

Taking into account that

$$\mathbf{curl} \mathbf{H}(r, z, t) = -\frac{\partial H}{\partial z}(r, z, t)\mathbf{e}_r + \frac{1}{r}\frac{\partial}{\partial r}(rH)(r, z, t)\mathbf{e}_z, \quad (4.3)$$

it is straightforward to check that (4.2) is equivalent to the scalar partial differential equation

$$\frac{\partial B}{\partial t} - \frac{\partial}{\partial r} \left(\frac{1}{\sigma r} \frac{\partial(rH)}{\partial r} \right) - \frac{\partial}{\partial z} \left(\frac{1}{\sigma} \frac{\partial H}{\partial z} \right) = 0,$$

which holds in any meridian section Ω of $\tilde{\Omega}$ and for all time $t \in [0, T]$. In order to have a well-posed problem, we add an initial condition

$$B(r, z, 0) = B_0(r, z) \quad \text{in } \Omega,$$

and suitable boundary condition on the boundary $\Gamma := \partial\Omega$. In view of applications, we consider a non-homogeneous Dirichlet boundary condition

$$H(r, z, t) = g(r, z, t) \quad \text{on } \Gamma \times [0, T],$$

where g is a given function. For applications of this model, we refer for instance to [8, 29, 54], where this kind of problem arises in the simulation of metallurgical heating processes. We also refer to [62, 70], where it is shown how g can be obtained from the current intensity along the coil of a toroidal solenoid.

Altogether, the resulting axisymmetric problem consists of finding scalar fields $H(r, z, t)$ and $B(r, z, t)$ such that,

$$\frac{\partial B}{\partial t} - \frac{\partial}{\partial r} \left(\frac{1}{\sigma r} \frac{\partial(rH)}{\partial r} \right) - \frac{\partial}{\partial z} \left(\frac{1}{\sigma} \frac{\partial H}{\partial z} \right) = f \quad \text{in } \Omega \times (0, T), \quad (4.4)$$

$$B = \mathcal{B}(H) \quad \text{in } \Omega \times (0, T), \quad (4.5)$$

$$H = g \quad \text{in } \Gamma \times (0, T), \quad (4.6)$$

$$B|_{t=0} = B_0 \quad \text{in } \Omega, \quad (4.7)$$

where $\sigma(r, z, t)$, $f(r, z, t)$, $g(r, z, t)$ and $B_0(r, z)$ are given data. Notice that although most of the variables and coefficients are function of the space variables (r, z) and the time t , when there is no possibility of confusion we will not write explicitly this dependence, as in the equations above.

Remark 4.2.1 *We have allowed a general right-hand side f in (4.4) in order to consider a more general parabolic problem, although in the eddy current model f is null.*

4.3 Mathematical analysis

In this section, we make a precise statement of the problem to be solved by means of a weak formulation suitable for its mathematical analysis. Then, we prove the existence and, under additional assumptions, the uniqueness of a solution. First, we introduce some preliminary results which will be used along the chapter.

4.3.1 Functional spaces and preliminary results

We define weighted Sobolev spaces appropriate for the mathematical analysis of the problem and recall some of their properties. For compactness of notation, from now on, the partial derivatives will be denoted by ∂_r , ∂_z and ∂_t .

Let $\Omega \subset \{(r, z) \in \mathbb{R}^2 : r > 0\}$ be a bounded domain with a Lipschitz boundary Γ . We denote by $\mathbf{n} = n_r \mathbf{e}_r + n_z \mathbf{e}_z$ and $\mathbf{t} = t_r \mathbf{e}_r + t_z \mathbf{e}_z$ (with $t_r := -n_z$ and $t_z := n_r$) the outer normal and tangent vectors to Ω . Let $L_r^2(\Omega)$ denote the weighted Lebesgue space of all measurable functions u defined in Ω for which

$$\|u\|_{L_r^2(\Omega)}^2 := \int_{\Omega} |u|^2 r \, dr dz < \infty.$$

Given $k \in \mathbb{N}$, the weighted Sobolev space $H_r^k(\Omega)$ consists of all functions in $L_r^2(\Omega)$ whose derivatives up to order k are also in $L_r^2(\Omega)$. We define the norms and semi-norms of these spaces in the standard way; for instance,

$$\|u\|_{H_r^1(\Omega)}^2 := \int_{\Omega} (|\partial_r u|^2 + |\partial_z u|^2) r \, dr dz.$$

Let

$$\tilde{H}_r^1(\Omega) := H_r^1(\Omega) \cap L_{1/r}^2(\Omega),$$

where $L_{1/r}^2(\Omega)$ denotes the set of all measurable functions u defined in Ω for which

$$\|u\|_{L_{1/r}^2(\Omega)}^2 := \int_{\Omega} \frac{|u|^2}{r} \, dr dz < \infty.$$

$\tilde{H}_r^1(\Omega)$ is a Hilbert space with the norm

$$\|u\|_{\tilde{H}_r^1(\Omega)}^2 := \|u\|_{H_r^1(\Omega)}^2 + \|u\|_{L_{1/r}^2(\Omega)}^2.$$

Let $\tilde{H}_r^2(\Omega) := \left\{ u \in \tilde{H}_r^1(\Omega) : \|u\|_{\tilde{H}_r^2(\Omega)} < \infty \right\}$, where

$$\|u\|_{\tilde{H}_r^2(\Omega)}^2 := \|u\|_{\tilde{H}_r^1(\Omega)}^2 + \left\| \frac{1}{r} \partial_r(ru) \right\|_{H_r^1(\Omega)}^2 + \|\partial_z u\|_{\tilde{H}_r^1(\Omega)}^2.$$

Finally we recall from [46, Section 3] that functions in $\tilde{H}_r^1(\Omega)$ have traces on Γ . We denote

$$\tilde{H}_r^{1/2}(\Gamma) := \left\{ v|_{\Gamma} : v \in \tilde{H}_r^1(\Omega) \right\},$$

endowed with the norm

$$\|g\|_{\tilde{H}_r^{1/2}(\Gamma)} := \inf \left\{ \|v\|_{\tilde{H}_r^1(\Omega)} : v \in \tilde{H}_r^1(\Omega) \text{ with } v|_{\Gamma} = g \right\},$$

which makes the trace operator $v \rightarrow v|_{\Gamma}$ continuous from $\tilde{H}_r^1(\Omega)$ onto $\tilde{H}_r^{1/2}(\Gamma)$.

4.3.2 Weak formulation

In order to establish a weak formulation of the above problem, we consider the following subspace of $\tilde{\mathbf{H}}_r^1(\Omega)$:

$$\mathcal{U} := \left\{ G \in \tilde{\mathbf{H}}_r^1(\Omega) : G|_{\Gamma} = 0 \right\}.$$

We multiply equation (4.4) by rG , with G being a test function in \mathcal{U} , integrate in Ω and use a Green's formula, to obtain the following weak formulation of (4.4)–(4.7):

Problem 4.3.1 *Given $g \in L^\infty(0, T; \tilde{\mathbf{H}}_r^{1/2}(\Gamma))$, $f \in L^\infty(0, T; \mathcal{U}')$ and $B_0 \in L_r^2(\Omega)$, find $H \in L^\infty(0, T; \tilde{\mathbf{H}}_r^1(\Omega))$ and $B \in L^\infty(0, T; L_r^2(\Omega))$ with $\partial_t B \in L^\infty(0, T; \mathcal{U}')$, such that*

$$\begin{aligned} \langle \partial_t B, G \rangle + a_t(H, G) &= \langle f, G \rangle & \forall G \in \mathcal{U}, \quad \text{a.e. in } [0, T], \\ B &= \mathcal{B}(H) & \text{in } \Omega \times (0, T), \\ H &= g & \text{in } \Gamma \times (0, T), \\ B|_{t=0} &= B_0 & \text{in } \Omega. \end{aligned}$$

In the first equation above, $a_t : \tilde{\mathbf{H}}_r^1(\Omega) \times \tilde{\mathbf{H}}_r^1(\Omega) \rightarrow \mathbb{R}$ denotes the bilinear form defined by

$$a_t(G_1, G_2) := \int_{\Omega} \frac{1}{\sigma(\cdot, t)r} \left(\partial_r(rG_1) \partial_r(rG_2) + \partial_z(rG_1) \partial_z(rG_2) \right) dr dz$$

and $\langle \cdot, \cdot \rangle$ denotes the pairing between \mathcal{U} and its dual space \mathcal{U}' .

4.3.3 Existence and uniqueness

We introduce the following hypotheses that will be used to prove the existence of a solution to the above problem:

H.1: The mapping $\mathcal{B} : \Omega \times \mathbb{R} \rightarrow \mathbb{R}$ is a Carathéodory function, namely,

- $\mathcal{B}(\cdot, u) : \Omega \rightarrow \mathbb{R}$ is measurable for each $u \in \mathbb{R}$,
- $\mathcal{B}(r, z, \cdot) : \mathbb{R} \rightarrow \mathbb{R}$ is continuous for each $(r, z) \in \Omega$.

H.2: $\mathcal{B}(r, z, u)$ is monotone with respect to u , namely,

$$(\mathcal{B}(r, z, u) - \mathcal{B}(r, z, v))(u - v) \geq 0 \quad \forall u, v \in \mathbb{R}, \quad \text{a.e. } (r, z) \in \Omega.$$

H.3: There exist $a_0 \in L_r^2(\Omega)$ and $b_0 \geq 0$ such that

$$|\mathcal{B}(\cdot, v)| \leq a_0(\cdot) + b_0 |v| \quad \forall v \in \mathbb{R}.$$

H.4: The electrical conductivity $\sigma : \Omega \times (0, T) \rightarrow \mathbb{R}$ belongs to $W^{1,\infty}(0, T; L^\infty(\Omega))$ and there exist strictly positive constants σ_* and σ^* such that

$$\sigma_* \leq \sigma(r, z, t) \leq \sigma^* \quad \text{a.e. } (r, z, t) \in \Omega \times (0, T).$$

H.5: There exists $H_0 \in \widetilde{\mathbf{H}}_r^1(\Omega)$ such that

$$B_0(r, z) = \mathcal{B}(r, z, H_0(r, z)) \quad \text{a.e. } (r, z) \in \Omega.$$

H.6: There holds $g \in \mathbf{H}^2(0, T; \widetilde{\mathbf{H}}_r^{1/2}(\Gamma))$ and $f \in \mathbf{H}^1(0, T; \mathcal{U}')$.

From the boundedness assumption on σ , we derive the following result.

Lemma 4.3.1 *The bilinear forms a_t are continuous uniformly in $t \in [0, T]$. Moreover, they are elliptic also uniformly in $t \in [0, T]$; namely,*

$$a_t(G, G) \geq \gamma \|G\|_{\widetilde{\mathbf{H}}_r^1(\Omega)}^2 \quad \forall G \in \mathcal{U},$$

where γ is a positive constant depending only on σ^* and Ω .

Proof. For the continuity, it is immediate to check that, for all $G_1, G_2 \in \widetilde{\mathbf{H}}_r^1(\Omega)$, $a_t(G_1, G_2) \leq \frac{2}{\sigma^*} \|G_1\|_{\widetilde{\mathbf{H}}_r^1(\Omega)} \|G_2\|_{\widetilde{\mathbf{H}}_r^1(\Omega)}$. The ellipticity follows from the fact that

$$a_t(G, G) \geq \frac{1}{\sigma^*} \left(|G|_{\widetilde{\mathbf{H}}_r^1(\Omega)}^2 + \|G\|_{L_{1/r}^2(\Omega)}^2 + 2 \int_{\Omega} G (\partial_r G) \, dr dz \right)$$

and

$$2 \int_{\Omega} G (\partial_r G) \, dr dz = \int_{\Omega} \partial_r (G^2) \, dr dz = \int_{\Gamma} G^2 n_r \, dS = 0 \quad \forall G \in \mathcal{U}.$$

□

Now, for each $t \in [0, T]$, let $H_g(t) \in \widetilde{\mathbf{H}}_r^1(\Omega)$ be the unique solution of the Dirichlet problem

$$\begin{aligned} (H_g(t), w)_{\widetilde{\mathbf{H}}_r^1(\Omega)} &= 0 & \forall w \in \mathcal{U}, \\ H_g(t) &= g(t) & \text{on } \Gamma, \end{aligned}$$

where $(\cdot, \cdot)_{\widetilde{\mathbf{H}}_r^1(\Omega)}$ denotes the Hilbert product in $\widetilde{\mathbf{H}}_r^1(\Omega)$. It is easy to check that $\|H_g(t)\|_{\widetilde{\mathbf{H}}_r^1(\Omega)} = \|g(t)\|_{\widetilde{\mathbf{H}}_r^{1/2}(\Gamma)}$ for all $t \in [0, T]$ and, by virtue of H.6, $H_g \in \mathbf{H}^2(0, T; \widetilde{\mathbf{H}}_r^1(\Omega))$ with

$$\|H_g\|_{\mathbf{H}^k(0, T; \widetilde{\mathbf{H}}_r^1(\Omega))} = \|g\|_{\mathbf{H}^k(0, T; \widetilde{\mathbf{H}}_r^{1/2}(\Gamma))}, \quad k = 0, 1, 2. \quad (4.8)$$

In order to prove that Problem 4.3.1 has a solution, we write $H = H_u + H_g$, with H_g as defined above. Clearly $H_u \in \mathcal{U}$ for all $t \in [0, T]$. Then, Problem 4.3.1 is equivalent to finding $H_u \in L^\infty(0, T; \mathcal{U})$ and $B \in L^\infty(0, T; L_r^2(\Omega))$ with $\partial_t B \in L^\infty(0, T; \mathcal{U}')$ such that

$$\langle \partial_t B, G \rangle + a_t(H_u, G) = \langle F(t), G \rangle \quad \forall G \in \mathcal{U}, \quad \text{a.e. in } [0, T], \quad (4.9)$$

$$B = \widetilde{\mathcal{B}}(H_u, t) \quad \text{in } \Omega \times (0, T), \quad (4.10)$$

$$H_u|_{t=0} = H_0 - H_g(0) \quad \text{in } \Omega, \quad (4.11)$$

where $\widetilde{\mathcal{B}} : \Omega \times \mathbb{R} \times [0, T] \rightarrow \mathbb{R}$ is defined by

$$\widetilde{\mathcal{B}}(r, z, v, t) := \mathcal{B}(r, z, v + H_g(r, z, t)), \quad (r, z) \in \Omega, \quad t \in [0, T], \quad v \in \mathbb{R},$$

and $F : [0, T] \rightarrow \mathcal{U}'$ by

$$\langle F(t), G \rangle := \langle f(t), G \rangle - a_t(H_g(t), G) \quad \forall G \in \mathcal{U}, \quad t \in [0, T].$$

It is easy to check that $\tilde{\mathcal{B}}$ satisfies a monotonicity property similar to H.2, namely,

$$(\tilde{\mathcal{B}}(r, z, v, t) - \tilde{\mathcal{B}}(r, z, w, t))(v - w) \geq 0 \quad \forall v, w \in \mathbb{R} \quad \forall (r, z, t) \in \Omega \times [0, T]. \quad (4.12)$$

Moreover, from the regularity of H_g , we have that $\tilde{\mathcal{B}}(\cdot, t)$ is a Carathéodory function for all $t \in [0, T]$ (cf. Hypothesis H.1) and that there exist $b_0 \geq 0$ (the same as in H.3) and

$$\tilde{a}_0(\cdot, t) := a_0(\cdot) + b_0 |H_g(\cdot, t)| \in L_r^2(\Omega), \quad t \in [0, T],$$

such that

$$\left| \tilde{\mathcal{B}}(\cdot, v, t) \right| \leq \tilde{a}_0(\cdot, t) + b_0 |v| \quad \forall (v, t) \in \mathbb{R} \times [0, T]. \quad (4.13)$$

To prove the existence of solution, we proceed by classical arguments of time discretization, a priori estimates and passing to the limit. First, we introduce the linear operators $A(t) : \tilde{\mathbb{H}}_r^1(\Omega) \rightarrow \tilde{\mathbb{H}}_r^1(\Omega)'$ induced by $a_t(\cdot, \cdot)$ (i.e., $A(t)G := a_t(G, \cdot)$, $G \in \tilde{\mathbb{H}}_r^1(\Omega)$), which by virtue of Lemma 4.3.1 are bounded uniformly in $t \in [0, T]$.

Time discretization

Let us fix $m \in \mathbb{N}$ and set $\Delta t := T/m$. For $i = 0, \dots, m$, we define $t^i := i\Delta t$, $H_g^i(r, z) := H_g(r, z, t^i)$, $f^i(r, z) := f(r, z, t^i)$, $\sigma^i(r, z) := \sigma(r, z, t^i)$, $A^i := A(t^i)$ and $F^i := F(t^i)$. Notice that all these terms are well defined because σ , f and g are continuous in time, as a consequence of H.4 and H.6. Moreover, there holds

$$\langle F^i, G \rangle = \langle f^i, G \rangle - \langle A^i H_g^i, G \rangle \quad \forall G \in \mathcal{U}, \quad i = 0, \dots, m. \quad (4.14)$$

A time discretization of (4.9)–(4.11) based on a backward Euler scheme reads as follows: find $H_u^i \in \mathcal{U}$ and $B^i \in \mathcal{U}'$, $i = 0, \dots, m$, satisfying

$$\bar{\partial} B^{i+1} + A^{i+1} H_u^{i+1} = F^{i+1} \quad \text{in } \mathcal{U}', \quad i = 0, \dots, m-1, \quad (4.15)$$

$$B^i = \tilde{\mathcal{B}}(H_u^i, t^i), \quad i = 0, \dots, m, \quad (4.16)$$

$$H_u^0 = H_0 - H_g^0 \quad \text{in } \Omega, \quad (4.17)$$

where $\bar{\partial} B^{i+1}$ denotes the difference quotient $\bar{\partial} B^{i+1} := (B^{i+1} - B^i) / \Delta t$.

The existence of a weak solution to the problem above at each time step is guaranteed by the following lemma.

Lemma 4.3.2 *There exists a unique solution of (4.15)–(4.17).*

Proof. First, for each $j = 0, \dots, m$, let us define $\tilde{\mathcal{B}}^j : L_r^2(\Omega) \rightarrow L_r^2(\Omega)$ as follows: given $G \in L_r^2(\Omega)$, $\tilde{\mathcal{B}}^j(G)(r, z) := \tilde{\mathcal{B}}(r, z, G(r, z), t^j)$, $(r, z) \in \Omega$. From (4.13) and the fact that $\tilde{\mathcal{B}}(\cdot, t)$ is a Carathéodory function for all $t \in [0, T]$, we have that $\tilde{\mathcal{B}}^j$ is continuous (see, for instance, [56, Lemma 16.1]).

Next, we notice that H_u^{i+1} is a solution of (4.15)–(4.16) if and only if it is a solution of the following non-linear problem:

$$Z(H_u^{i+1}) := \frac{\tilde{\mathcal{B}}^{i+1}(H_u^{i+1})}{\Delta t} + A^{i+1}H_u^{i+1} = F^{i+1} + \frac{\tilde{\mathcal{B}}^i(H_u^i)}{\Delta t} \quad \text{in } \mathcal{U}',$$

Since $\tilde{\mathcal{B}}^{i+1}$ is monotone (cf. (4.12)), continuous and $A^{i+1} : \mathcal{U} \rightarrow \mathcal{U}'$ is linear, bounded and elliptic, it is easy to check that $Z : \mathcal{U} \rightarrow \mathcal{U}'$ is strongly monotone, coercive and continuous. Thus, from the theory of monotone operators, it follows that the equation above has a unique solution (see, for instance, [78, Theorem 2.18]). \square

A priori estimates

The next goal is to prove an a priori estimate for the solution of (4.15)–(4.17). Notice that if \mathcal{B} were strongly monotone and Lipschitz continuous, then the results from [83, Lemma 3.1] could be applied with this purpose. Since this is not our case, the proof will follow an alternative path.

Here and thereafter C with or without subscripts will be used for positive constants not necessarily the same at each occurrence, but always independent of the time-step Δt and, in the following section, of the mesh-size h , too.

Lemma 4.3.3 *There exists $C > 0$ such that, for all $l = 0, \dots, m-1$,*

$$\left\| \bar{\partial} B^{l+1} \right\|_{\mathcal{U}'}^2 + \left\| H_u^{l+1} \right\|_{\tilde{H}_r^1(\Omega)}^2 \leq C.$$

Proof. We apply (4.15) to $(H_u^{i+1} - H_u^i) \in \mathcal{U}$. From the monotonicity property H.2, it is straightforward to obtain for $l = 0, \dots, m-1$,

$$\begin{aligned} & \sum_{i=0}^l \langle A^{i+1} H_u^{i+1}, H_u^{i+1} - H_u^i \rangle \\ & \leq \sum_{i=0}^l \langle F^{i+1}, H_u^{i+1} - H_u^i \rangle - \sum_{i=0}^l \int_{\Omega} \bar{\partial} B^{i+1} (H_g^{i+1} - H_g^i) r \, dr dz. \end{aligned} \quad (4.18)$$

To bound the term on the left-hand side of the above equation, first we use the classical identity $2(p-q)p = p^2 + (p-q)^2 - q^2$ to write

$$\begin{aligned} & 2 \langle A^{i+1} H_u^{i+1}, H_u^{i+1} - H_u^i \rangle \\ & \geq \langle A^{i+1} H_u^{i+1}, H_u^{i+1} \rangle - \langle A^{i+1} H_u^i, H_u^i \rangle \\ & = \langle A^{i+1} H_u^{i+1}, H_u^{i+1} \rangle - \langle A^i H_u^i, H_u^i \rangle + \langle (A^i - A^{i+1}) H_u^i, H_u^i \rangle. \end{aligned} \quad (4.19)$$

Now, for the last term on the right-hand side we have that

$$\begin{aligned} \left| \langle (A^i - A^{i+1}) H_u^i, H_u^i \rangle \right| & = \left| \int_{\Omega} \frac{\sigma^{i+1} - \sigma^i}{\sigma^{i+1} \sigma^i} \frac{1}{r} \left(|\partial_r(r H_u^i)|^2 + |\partial_z(r H_u^i)|^2 \right) dr dz \right| \\ & \leq \frac{1}{\sigma_*^2} \|\partial_t \sigma\|_{L^\infty(0,T;L^\infty(\Omega))} \Delta t \|H_u^i\|_{\tilde{H}_r^1(\Omega)}^2, \end{aligned} \quad (4.20)$$

where we have used that $\sigma^{i+1} - \sigma^i = \int_{t^i}^{t^{i+1}} \partial_t \sigma(s) ds$ and assumption H.4. Therefore, summing up (4.19) and using (4.20) and Lemma 4.3.1, it follows that

$$\begin{aligned} \sum_{i=0}^l \langle A^{i+1} H_u^{i+1}, H_u^{i+1} - H_u^i \rangle &\geq \frac{\gamma}{2} \|H_u^{l+1}\|_{\tilde{H}_r^1(\Omega)}^2 - \frac{1}{2\sigma_*} \|H_u^0\|_{\tilde{H}_r^1(\Omega)}^2 \\ &\quad - \frac{\|\partial_t \sigma\|_{L^\infty(0,T;L^\infty(\Omega))}}{2\sigma_*^2} \Delta t \sum_{i=0}^l \|H_u^i\|_{\tilde{H}_r^1(\Omega)}^2. \end{aligned} \quad (4.21)$$

On the other hand, for the first term on the right-hand side of (4.18), by summation by parts and using Young's inequality, we obtain for all $\eta > 0$

$$\begin{aligned} &\left| \sum_{i=0}^l \langle F^{i+1}, H_u^{i+1} - H_u^i \rangle \right| \\ &= \left| \langle F^{l+1}, H_u^{l+1} \rangle - \langle F^1, H_u^0 \rangle - \sum_{i=0}^{l-1} \langle F^{i+2} - F^{i+1}, H_u^{i+1} \rangle \right| \\ &\leq \frac{1}{2\eta} \|F^{l+1}\|_{\mathcal{U}'}^2 + \frac{\eta}{2} \|H_u^{l+1}\|_{\tilde{H}_r^1(\Omega)}^2 + \|F^1\|_{\mathcal{U}'} \|H_u^0\|_{\tilde{H}_r^1(\Omega)} \\ &\quad + \Delta t \sum_{i=0}^{l-1} \|H_u^{i+1}\|_{\tilde{H}_r^1(\Omega)}^2 + C \|\partial_t \sigma\|_{L^\infty(0,T;L^\infty(\Omega))}^2 \Delta t \sum_{i=0}^{l-1} \|H_g^{i+1}\|_{\tilde{H}_r^1(\Omega)}^2 \\ &\quad + C \Delta t \sum_{i=0}^{l-1} \|\bar{\partial} H_g^{i+2}\|_{\tilde{H}_r^1(\Omega)}^2 + C \Delta t \sum_{i=0}^{l-1} \|\bar{\partial} f^{i+2}\|_{\mathcal{U}'}^2, \end{aligned} \quad (4.22)$$

where the last three terms are derived by proceeding as in (4.20) from the following inequality (cf. (4.14)):

$$\|\bar{\partial} F^{i+2}\|_{\mathcal{U}'} \leq \|\bar{\partial} f^{i+2}\|_{\mathcal{U}'} + \|A^{i+2} \bar{\partial} H_g^{i+2}\|_{\mathcal{U}'} + \|\bar{\partial} A^{i+2} H_g^{i+1}\|_{\mathcal{U}'}.$$

Similarly, for the last term of (4.18), by summation by parts and using Young's inequality

and (4.13), it follows that for all $\eta > 0$

$$\begin{aligned}
& \left| \sum_{i=0}^l \int_{\Omega} \bar{\partial} B^{i+1} (H_g^{i+1} - H_g^i) r \, dr dz \right| \\
&= \left| \sum_{i=0}^l \int_{\Omega} (B^{i+1} - B^i) \bar{\partial} H_g^{i+1} r \, dr dz \right| \\
&\leq \int_{\Omega} |B^{l+1} \bar{\partial} H_g^{l+1}| r \, dr dz + \int_{\Omega} |B^0 \bar{\partial} H_g^1| r \, dr dz \\
&\quad + \sum_{i=0}^{l-1} \int_{\Omega} |B^{i+1} (\bar{\partial} H_g^{i+2} - \bar{\partial} H_g^{i+1})| r \, dr dz \\
&\leq \frac{\eta}{2} \|H_u^{l+1}\|_{L_r^2(\Omega)}^2 + C\eta \|H_g^{l+1}\|_{L_r^2(\Omega)}^2 + \frac{C}{\eta} \|\bar{\partial} H_g^{l+1}\|_{L_r^2(\Omega)}^2 \\
&\quad + \|B^0\|_{L_r^2(\Omega)} \|\bar{\partial} H_g^1\|_{L_r^2(\Omega)} + \Delta t \sum_{i=0}^{l-1} \|H_u^{i+1}\|_{L_r^2(\Omega)}^2 + C\Delta t \sum_{i=0}^{l-1} \|H_g^{i+1}\|_{L_r^2(\Omega)}^2 \\
&\quad + C + C\Delta t \sum_{i=0}^{l-1} \left\| \frac{\bar{\partial} H_g^{i+2} - \bar{\partial} H_g^{i+1}}{\Delta t} \right\|_{L_r^2(\Omega)}^2. \tag{4.23}
\end{aligned}$$

Whence, by replacing (4.21)–(4.23) into (4.18), choosing $\eta := \gamma/4$ and using that the last terms in (4.22) and (4.23) are respectively bounded by $\|f\|_{\tilde{H}^1(0,T;\mathcal{U}')}^2$ and $\|g\|_{\tilde{H}^2(0,T;\tilde{H}_r^{1/2}(\Gamma))}^2$ (cf. (4.8)), we obtain

$$\frac{\gamma}{4} \|H_u^{l+1}\|_{\tilde{H}_r^1(\Omega)}^2 \leq C + \Delta t \sum_{i=0}^{l-1} \|H_u^{i+1}\|_{L_r^2(\Omega)}^2.$$

Therefore, using a discrete Gronwall's lemma we arrive at

$$\|H_u^{l+1}\|_{\tilde{H}_r^1(\Omega)}^2 \leq C,$$

with a constant C depending on $\|H_0\|_{\tilde{H}_r^1(\Omega)}$, $\|f\|_{\tilde{H}^1(0,T;\mathcal{U}'')}$, $\|g\|_{\tilde{H}^2(0,T;\tilde{H}_r^{1/2}(\Gamma))}$ and $\|\sigma\|_{W^{1,\infty}(0,T;L^\infty(\Omega))}$.

Finally, to end the theorem, we bound $\|\bar{\partial} B^{l+1}\|_{\mathcal{U}''}^2$ by using (4.15) and the above inequality. \square

Convergence

The next step is to define approximate solutions to (4.9)–(4.11) and prove its weak convergence to an actual solution of this problem. With this aim, we introduce some notation. Let $B_{\Delta t} : [0, T] \rightarrow \mathcal{U}'$ be the piecewise linear continuous in time function given by

$$\begin{aligned}
B_{\Delta t}(t^0) &:= \tilde{\mathcal{B}}(H_u^0, t^0); \\
B_{\Delta t}(t) &:= \tilde{\mathcal{B}}(H_u^{i-1}, t^{i-1}) + (t - t^{i-1}) \bar{\partial} \tilde{\mathcal{B}}(H_u^i, t^i), \quad t \in (t^{i-1}, t^i], \quad i = 1, \dots, m.
\end{aligned}$$

Notice that, by virtue of (4.13), $B_{\Delta t}$ actually takes values in $L_r^2(\Omega)$. We also consider the step function $\bar{H}_{u\Delta t} : [0, T] \rightarrow \mathcal{U}$ defined as follows:

$$\bar{H}_{u\Delta t}(t^0) := H_u^0; \quad \bar{H}_{u\Delta t}(t) := H_u^i, \quad t \in (t^{i-1}, t^i], \quad i = 1, \dots, m.$$

Step functions $\bar{B}_{\Delta t}$, $\bar{H}_{g\Delta t}$, $\bar{A}_{\Delta t}$, $\bar{f}_{\Delta t}$ and $\bar{\sigma}_{\Delta t}$ are defined in a similar way.

Using the above notation and (4.14), we rewrite equation (4.15) as follows:

$$\partial_t B_{\Delta t} + \bar{A}_{\Delta t} \bar{H}_{u\Delta t} = \bar{f}_{\Delta t} - \bar{A}_{\Delta t} \bar{H}_{g\Delta t} \quad \text{in } \mathcal{U}', \quad \text{a.e. in } (0, T). \quad (4.24)$$

From Lemma 4.3.3, (4.13) and (4.8), we deduce that there exists $C > 0$ such that

$$\begin{aligned} \|\bar{B}_{\Delta t}\|_{L^\infty(0, T; L_r^2(\Omega))} + \|\partial_t B_{\Delta t}\|_{L^\infty(0, T; \mathcal{U}')} \\ + \|\bar{A}_{\Delta t} \bar{H}_{u\Delta t}\|_{L^\infty(0, T; \tilde{H}_r^1(\Omega)')} + \|\bar{H}_{u\Delta t}\|_{L^\infty(0, T; \tilde{H}_r^1(\Omega))} \leq C. \end{aligned} \quad (4.25)$$

This allows us to conclude that there exists H_u , B and X such that

$$\bar{H}_{u\Delta t} \rightarrow H_u \quad \text{in } L^\infty(0, T; \mathcal{U}) \text{ weakly star}, \quad (4.26)$$

$$B_{\Delta t} \rightarrow B \quad \text{in } L^\infty(0, T; L_r^2(\Omega)) \text{ weakly star}, \quad (4.27)$$

$$\partial_t B_{\Delta t} \rightarrow \partial_t B \quad \text{in } L^\infty(0, T; \mathcal{U}') \text{ weakly star}, \quad (4.28)$$

$$\bar{A}_{\Delta t}(\bar{H}_{u\Delta t} + \bar{H}_{g\Delta t}) \rightarrow X \quad \text{in } L^\infty(0, T; \mathcal{U}') \text{ weakly star}. \quad (4.29)$$

Hence, taking limit in (4.24), it follows that

$$\partial_t B + X = f \quad \text{in } \mathcal{U}', \quad \text{a.e. in } (0, T), \quad (4.30)$$

because $\bar{f}_{\Delta t} \rightarrow f$ in $L^2(0, T; \mathcal{U}')$, for $f \in H^1(0, T; \mathcal{U}')$. Next step is to derive that $B = \mathcal{B}(H_u + H_g)$ and $X = A(H_u + H_g)$. With this end, first we prove the following.

Lemma 4.3.4 $B_{\Delta t} \rightarrow B$ strongly in $\mathcal{C}([0, T]; \mathcal{U}')$.

Proof. As a consequence of Lemma 4.3.3, it is easy to check that the family of functions $\{B_{\Delta t} : [0, T] \rightarrow \mathcal{U}'\}_{\Delta t}$ is equicontinuous. Moreover, $\{B_{\Delta t}(t)\}_{\Delta t}$ is relatively compact in \mathcal{U}' for each $t \in [0, T]$. In fact, because of (4.25), $\{B_{\Delta t}(t)\}_{\Delta t}$ is a bounded set in $L_r^2(\Omega)$, which is compactly included in \mathcal{U}' (the latter because the inclusion $\tilde{H}_r^1(\Omega) \subset L_r^2(\Omega)$ is compact; see, for instance, [67]). Therefore, by applying the Ascoli's theorem (see, for instance, [58]), we obtain that $\{B_{\Delta t} : [0, T] \rightarrow \mathcal{U}'\}_{\Delta t}$ is relatively compact in $\mathcal{C}([0, T]; \mathcal{U}')$. This together with (4.27) allow us to conclude that the convergence $B_{\Delta t} \rightarrow B$ is strong in $\mathcal{C}([0, T]; \mathcal{U}')$. \square

Now we are in a position to prove the following two lemmas.

Lemma 4.3.5 Let H_u and B be the weak star limits defined in (4.26) and (4.27), respectively. Then,

$$B = \mathcal{B}(H_u + H_g) \quad \text{a.e. in } \Omega \times [0, T].$$

Proof. From Lemmas 4.3.3 and 4.3.4, we have that

$$\|\overline{B}_{\Delta t} - B\|_{L^\infty(0,T;\mathcal{U}')} \leq \|\overline{B}_{\Delta t} - B_{\Delta t}\|_{L^\infty(0,T;\mathcal{U}')} + \|B_{\Delta t} - B\|_{L^\infty(0,T;\mathcal{U}')} \rightarrow 0.$$

From the latter and the weak star convergence of $\overline{H}_{u\Delta t}$, it follows that

$$\int_0^T \langle \overline{B}_{\Delta t}, \overline{H}_{u\Delta t} \rangle dt \rightarrow \int_0^T \langle B, H_u \rangle dt.$$

On the other hand, from the monotonicity of \mathcal{B} and the fact that $\overline{B}_{\Delta t} = \mathcal{B}(\overline{H}_{u\Delta t} + \overline{H}_{g\Delta t})$, we have that

$$\int_0^T \langle \overline{B}_{\Delta t} - \mathcal{B}(G + \overline{H}_{g\Delta t}), \overline{H}_{u\Delta t} - G \rangle dt \geq 0 \quad \forall G \in L^2(0,T;L_r^2(\Omega)).$$

Since $\overline{H}_{g\Delta t}$ converges to H_g in $L^2(0,T;\tilde{H}_r^1(\Omega))$ and also a.e. in $\Omega \times [0,T]$, because of hypothesis H.1 we have that $\mathcal{B}(G + \overline{H}_{g\Delta t})$ converges to $\mathcal{B}(G + H_g)$ a.e. in $\Omega \times [0,T]$. Hence, this convergence also holds strongly in $L^2(0,T;L_r^2(\Omega))$ because of hypothesis H.3 and the Lebesgue dominated convergence theorem. Thus, we obtain

$$\int_0^T \int_\Omega (B - \mathcal{B}(G + H_g))(H_u - G) r dr dz dt \geq 0 \quad \forall G \in L^2(0,T;L_r^2(\Omega)).$$

Now, by taking $G := H_u + \epsilon U$, for any $U \in L^2(0,T;L_r^2(\Omega))$ and $\epsilon > 0$, we arrive at

$$\int_0^T \int_\Omega (B - \mathcal{B}(H_u + H_g - \epsilon U))U r dr dz dt \leq 0.$$

By taking $\epsilon \rightarrow 0$ and choosing $U := B - \mathcal{B}(H_u + H_g)$, it follows that $B = \mathcal{B}(H_u + H_g)$ a.e. in $\Omega \times [0,T]$ and we obtain the result. \square

Lemma 4.3.6 *Let H_u and X be the weak star limits defined in (4.26) and (4.29), respectively. Then,*

$$X = A(H_u + H_g) \quad \text{a.e. in } [0,T].$$

Proof. First notice that for all $G \in L^2(0,T;\tilde{H}_r^1(\Omega))$ and all $U \in \mathcal{U}$

$$\begin{aligned} \langle \overline{A}_{\Delta t}G - AG, U \rangle &= \int_\Omega \frac{\sigma - \overline{\sigma}_{\Delta t}}{\sigma \overline{\sigma}_{\Delta t}} \left(\partial_r(rG) \partial_r(rU) + \partial_z(rG) \partial_r(rU) \right) \frac{1}{r} dr dz \\ &\leq C_\sigma \|\sigma - \overline{\sigma}_{\Delta t}\|_{L^\infty(\Omega)} \|G\|_{\tilde{H}_r^1(\Omega)} \|U\|_{\tilde{H}_r^1(\Omega)}. \end{aligned}$$

Moreover, since $\sigma \in W^{1,\infty}(0,T;L^\infty(\Omega))$, it follows that

$$\|\sigma - \overline{\sigma}_{\Delta t}\|_{L^\infty(0,T;L^\infty(\Omega))} \leq \Delta t \|\partial_t \sigma\|_{L^\infty(0,T;L^\infty(\Omega))}$$

and, therefore,

$$\|\overline{A}_{\Delta t}G - AG\|_{L^2(0,T;\mathcal{U}')}^2 \leq C_\sigma \Delta t^2 \|\partial_t \sigma\|_{L^\infty(0,T;L^\infty(\Omega))}^2 \|G\|_{L^2(0,T;\tilde{H}_r^1(\Omega))}^2.$$

Finally, from the above result, Lemma 4.3.3, (4.26) and the fact that $\overline{H}_{g\Delta t} \rightarrow H_g$ in $L^2(0, T; \tilde{H}_r^1(\Omega))$, we obtain for all $V \in L^2(0, T; \mathcal{U})$

$$\begin{aligned} & \left| \int_0^T \langle \overline{A}_{\Delta t}(\overline{H}_{u\Delta t} + \overline{H}_{g\Delta t}) - A(H_u + H_g), V \rangle dt \right| \\ & \leq \|(\overline{A}_{\Delta t} - A)(\overline{H}_{u\Delta t} + \overline{H}_{g\Delta t})\|_{L^2(0, T; \mathcal{U}')} \|V\|_{L^2(0, T; \tilde{H}_r^1(\Omega))} \\ & \quad + \left| \int_0^T \langle A(\overline{H}_{u\Delta t} - H_u), V \rangle dt \right| + \left| \int_0^T \langle A(\overline{H}_{g\Delta t} - H_g), V \rangle dt \right| \rightarrow 0. \end{aligned}$$

Whence, from (4.29), $X = A(H_u + H_g)$ a.e. in $[0, T]$ and we end the proof. \square

Now we are in a position to conclude that Problem 4.3.1 has a solution.

Theorem 4.3.1 *Under assumptions H.1–H.6, Problem 4.3.1 has a solution.*

Proof. Let $H := H_u + H_g$. It follows from (4.30) and Lemma 4.3.6 that

$$\langle \partial_t B, G \rangle + a_t(H, G) = \langle f, G \rangle \quad \forall G \in \mathcal{U}, \quad \text{a.e. in } (0, T).$$

and, from Lemma 4.3.5, that $B = \mathcal{B}(H)$. On the other hand, since $H_u \in \mathcal{U}$, we have that $H|_\Gamma = g$. Finally, as a consequence of Lemma 4.3.4 we have that $B_{\Delta t}(0) \rightarrow B(0)$ in \mathcal{U}' . Hence, since $B_{\Delta t}(0) = \tilde{\mathcal{B}}(H_u^0, t^0) = \mathcal{B}(H_u^0 + H_g(0)) = \mathcal{B}(H_0) = B_0$, we conclude that $B(0) = B_0$. Therefore (H, B) is a solution to Problem 4.3.1. \square

In order to prove that Problem 4.3.1 has a unique solution, we will assume from now on the following strengthened forms of hypotheses H.2 and H.4:

H.2*: $\mathcal{B}(r, z, u)$ is strongly monotone with respect to u uniformly in Ω ; namely, there exists $\beta > 0$ such that

$$(\mathcal{B}(r, z, v) - \mathcal{B}(r, z, w))(v - w) \geq \beta |v - w|^2 \quad \forall v, w \in \mathbb{R}, \quad \text{a.e. } (r, z) \in \Omega.$$

H.4*: σ does not depend on time and there exist strictly positive constants σ_* and σ^* such that $\sigma_* \leq \sigma(r, z) \leq \sigma^*$ a.e. in Ω .

Hypothesis H.2* is a recurrent assumption in electromagnetism which covers a large number of models of physical interest (see [10, 80, 81, 82]). On the other hand, notice that from H.4* and the definition of $a_t(\cdot, \cdot)$, it follows that this bilinear form is also time independent. Thus, from now on, we will denote it $a(\cdot, \cdot)$.

As a first consequence of these hypotheses we can prove further regularity of the solution to Problem 4.3.1 and its uniqueness.

Theorem 4.3.2 *Under assumptions H.1, H.2*, H.3, H.4*, H.5 and H.6, Problem 4.3.1 has a unique solution (H, B) and there holds $H \in H^1(0, T; L_r^2(\Omega))$.*

Proof. The existence of solution follows from Theorem 4.3.1. The uniqueness is a consequence of [35, Theorem 4]. For the additional regularity, we notice that being \mathcal{B} strongly monotone (H.2*), by applying (4.15) to $(H_u^{i+1} - H_u^i)$ it is straightforward to prove that

$$\Delta t \sum_{i=0}^l \|\bar{\partial} H_u^{i+1}\|_{L_r^2(\Omega)}^2 \leq C, \quad l = 0, \dots, m-1. \quad (4.31)$$

The rest of the proof consists of adapting the previous arguments and using the a priori estimate above. Let us remark that this additional regularity result actually does not need of σ being time independent. \square

4.4 Numerical analysis. Time semi-discrete problem

The aim of this section is to derive error estimates for the semi-discrete in time scheme introduced in Section 4.3.3 to approximate Problem 4.3.1. With this end, we will use the following norm:

$$\left(\int_0^T \|G\|_{L_r^2(\Omega)}^2 dt + \left\| \int_0^T G dt \right\|_{\tilde{H}_r^1(\Omega)}^2 \right)^{1/2} \quad G \in L^2(0, T; \tilde{H}_r^1(\Omega)). \quad (4.32)$$

Let us remark that a similar norm appears in the analysis of other nonlinear problems in electromagnetism (see, for instance, [81]).

To obtain the estimates we will follow the techniques introduced in [82]. However, our approach is slightly different, mainly because of the presence of the non-homogeneous Dirichlet boundary condition. With this aim, we will further assume that the dependence of B on H is Lipschitz continuous. More precisely, from now on, we assume the following strengthened form of hypothesis H.1:

H.1*: The mapping $\mathcal{B} : \Omega \times \mathbb{R} \rightarrow \mathbb{R}$ is a Carathéodory function, uniformly Lipschitz continuous with respect to the third variable; namely:

- $\mathcal{B}(\cdot, u) : \Omega \rightarrow \mathbb{R}$ is measurable for each $u \in \mathbb{R}$;
- $\exists L > 0 : |\mathcal{B}(r, z, u) - \mathcal{B}(r, z, v)| \leq L |u - v| \quad \forall u, v \in \mathbb{R}, \quad \forall (r, z) \in \Omega.$

Remark 4.4.1 For \mathcal{B} satisfying hypotheses H.1* and H.2*, the a priori estimate (4.31) as well as that from Lemma 4.3.3 hold true even for $g \in \mathbf{H}^1(0, T; \tilde{\mathbf{H}}_r^{1/2}(\Gamma))$. Therefore, under assumptions H.1*, H.2*, H.3, H.4*, H.5 and a weaker form of H.6 with $g \in \mathbf{H}^1(0, T; \tilde{\mathbf{H}}_r^{1/2}(\Gamma))$ (instead of g in $\mathbf{H}^2(0, T; \tilde{\mathbf{H}}_r^{1/2}(\Gamma))$), Problem 4.3.1 also has a unique solution (H, B) and there holds $H \in \mathbf{H}^1(0, T; L_r^2(\Omega))$. Indeed, all the forthcoming results remain valid for $g \in \mathbf{H}^1(0, T; \tilde{\mathbf{H}}_r^{1/2}(\Gamma))$.

We consider the backward Euler time discretization of Problem 4.3.1 that we have introduced in Section 4.3.3. We keep the notation defined therein. The resulting discrete problem written now in terms of the main variable H^{i+1} , reads as follows:

Problem 4.4.1 For $i = 0, \dots, m-1$, find $H^{i+1} \in \tilde{H}_r^1(\Omega)$ satisfying

$$\begin{aligned} \int_{\Omega} \bar{\partial} \mathcal{B}(H^{i+1}) G r \, dr dz + a(H^{i+1}, G) &= \langle f^{i+1}, G \rangle & \forall G \in \mathcal{U}, \\ H^{i+1}|_{\Gamma} &= g^{i+1} & \text{on } \Gamma, \\ H^0 &= H_0 & \text{in } \Omega. \end{aligned}$$

The existence and the uniqueness of a weak solution at each time step follow from Lemma 4.3.2 by writing $H^i := H_u^i + H_g^i$, $i = 0, \dots, m$ (with H_g^i as defined in Section 4.3.3). The following result yields an a priori estimate for the solution of the above problem.

Lemma 4.4.1 There exists $C > 0$ such that, for all $l = 0, \dots, m-1$,

$$\left\| \bar{\partial} \mathcal{B}(H^{l+1}) \right\|_{\mathcal{U}'}^2 + \Delta t \sum_{i=0}^l \left\| \bar{\partial} H^{i+1} \right\|_{L_r^2(\Omega)}^2 + \left\| H^{l+1} \right\|_{\tilde{H}_r^1(\Omega)}^2 \leq C.$$

Proof. Since $H^i := H_u^i + H_g^i$, $i = 0, \dots, m$, the proof follows from Lemma 4.3.3, the a priori estimate (4.31) (established in the proof of Theorem 4.3.2) and the regularity of H_g (cf. (4.8)). \square

4.4.1 Error estimates for the time discretization

To derive an error estimate for the solution to Problem 4.4.1, first we notice that the piecewise linear function $B_{\Delta t}$ written in terms of H^i reads as follows:

$$\begin{aligned} B_{\Delta t}(t^0) &= \mathcal{B}(H_0); \\ B_{\Delta t}(t) &= \mathcal{B}(H^{i-1}) + (t - t^{i-1}) \bar{\partial} \mathcal{B}(H^i), \quad t \in (t^{i-1}, t^i], \quad i = 1, \dots, m. \end{aligned}$$

Also we define the step function $\bar{H}_{\Delta t} : [0, T] \rightarrow \tilde{H}_r^1(\Omega)$ as in Section 4.3.3:

$$\bar{H}_{\Delta t}(t^0) := H_0; \quad \bar{H}_{\Delta t}(t) := H^i, \quad t \in (t^{i-1}, t^i], \quad i = 1, \dots, m, \quad (4.33)$$

so that $\bar{H}_{\Delta t} = \bar{H}_{u\Delta t} + \bar{H}_{g\Delta t}$. Using this notation we rewrite the first equation from Problem 4.4.1 as follows:

$$\int_{\Omega} \partial_t B_{\Delta t} G r \, dr dz + a(\bar{H}_{\Delta t}, G) = \langle \bar{f}_{\Delta t}, G \rangle \quad \forall G \in \mathcal{U}, \quad \text{a.e. in } [0, T], \quad (4.34)$$

and we identify the solution of Problem 4.4.1 with its piecewise constant interpolant $\bar{H}_{\Delta t}$. Now, we are in a position to prove the following error estimate:

Theorem 4.4.1 Let H and $\bar{H}_{\Delta t}$ be the solutions to Problems 4.3.1 and 4.4.1, respectively. Under assumptions H.1*, H.2*, H.3, H.4*, H.5 and H.6, there holds

$$\begin{aligned} \int_0^T \|H - \bar{H}_{\Delta t}\|_{L_r^2(\Omega)}^2 dt + \left\| \int_0^T (H - \bar{H}_{\Delta t}) dt \right\|_{\tilde{H}_r^1(\Omega)}^2 \\ \leq C \Delta t^2 \left\{ 1 + \|g\|_{\mathbf{H}^1(0, T; \tilde{H}_r^{1/2}(\Gamma))}^2 + \|f\|_{\mathbf{H}^1(0, T; \mathcal{U}')}^2 \right\}. \end{aligned}$$

Proof. First, we subtract (4.34) from the first equation of Problem 4.3.1 and integrate with respect to time. Thus, we obtain for all $G \in \mathcal{U}$

$$\int_{\Omega} (B - B_{\Delta t})(t) G r \, dr dz + a \left(\int_0^t (H - \bar{H}_{\Delta t})(s) \, ds, G \right) = \left\langle \int_0^t (f - \bar{f}_{\Delta t})(s) \, ds, G \right\rangle.$$

Next, we take $G = (e - e_g)(t)$ in the above equation, with $e := H - \bar{H}_{\Delta t}$ and $e_g := H_g - \bar{H}_{g\Delta t}$, and integrate in time. Thus, we arrive at

$$\begin{aligned} & \int_0^T \int_{\Omega} (B - B_{\Delta t})(t) (e - e_g)(t) r \, dr dz \, dt + \int_0^T a \left(\int_0^t e(s) \, ds, (e - e_g)(t) \right) dt \\ &= \int_0^T \left\langle \int_0^t (f - \bar{f}_{\Delta t})(s) \, ds, (e - e_g)(t) \right\rangle dt \end{aligned}$$

or, equivalently,

$$\begin{aligned} & \int_0^T \int_{\Omega} (\mathcal{B}(H) - \mathcal{B}(\bar{H}_{\Delta t})) e r \, dr dz \, dt + \int_0^T a \left(\int_0^t (e - e_g)(s) \, ds, e - e_g \right) dt \\ &= \int_0^T \left\langle \int_0^t (f - \bar{f}_{\Delta t})(s) \, ds, e - e_g \right\rangle dt - \int_0^T a \left(\int_0^t e_g(s) \, ds, e - e_g \right) dt \\ &\quad + \int_0^T \int_{\Omega} (B_{\Delta t} - \mathcal{B}(\bar{H}_{\Delta t})) (e - e_g) r \, dr dz \, dt \\ &\quad + \int_0^T \int_{\Omega} (\mathcal{B}(H) - \mathcal{B}(\bar{H}_{\Delta t})) e_g r \, dr dz \, dt. \end{aligned}$$

We rewrite the second term on the left-hand side above as follows

$$\int_0^T a \left(\int_0^t (e - e_g)(s) \, ds, e - e_g \right) dt = \frac{1}{2} a \left(\int_0^T (e - e_g) \, dt, \int_0^T (e - e_g) \, dt \right).$$

Then, from the ellipticity of $a(\cdot, \cdot)$ (cf. Lemma 4.3.1) and the strong monotonicity of \mathcal{B} (cf. H.2*), we have that

$$\begin{aligned} & \beta \int_0^T \|e\|_{L_r^2(\Omega)}^2 \, dt + \frac{\gamma}{2} \left\| \int_0^T (e - e_g) \, dt \right\|_{\tilde{H}_r^1(\Omega)}^2 \\ & \leq \left| \int_0^T \left\langle \int_0^t (f - \bar{f}_{\Delta t})(s) \, ds, e - e_g \right\rangle dt \right| + \left| \int_0^T a \left(\int_0^t e_g(s) \, ds, e - e_g \right) dt \right| \\ & \quad + \left| \int_0^T \int_{\Omega} (B_{\Delta t} - \mathcal{B}(\bar{H}_{\Delta t})) (e - e_g) r \, dr dz \, dt \right| \\ & \quad + \left| \int_0^T \int_{\Omega} (\mathcal{B}(H) - \mathcal{B}(\bar{H}_{\Delta t})) e_g r \, dr dz \, dt \right|. \end{aligned} \tag{4.35}$$

The next step is to bound each term on the right-hand side of the above equation. First, from the Lipschitz continuity of \mathcal{B} (cf. H.1*) and Young's inequality, the last term is easily bounded as follows,

$$\left| \int_0^T \int_{\Omega} (\mathcal{B}(H) - \mathcal{B}(\bar{H}_{\Delta t})) e_g r \, dr dz \, dt \right| \leq \eta \int_0^T \|e\|_{L_r^2(\Omega)}^2 \, dt + \frac{C}{\eta} \int_0^T \|e_g\|_{L_r^2(\Omega)}^2 \, dt \tag{4.36}$$

for all $\eta > 0$. On the other hand, by using again the Lipschitz continuity of \mathcal{B} , we have that $|B_{\Delta t}(t) - \mathcal{B}(\bar{H}_{\Delta t}(t))| \leq \Delta t |\bar{\partial}\mathcal{B}(H^i)| \leq L\Delta t |\bar{\partial}H^i|$ for all $t \in (t^{i-1}, t^i]$. Then, from this and Lemma 4.4.1, it follows that also for all $\eta > 0$

$$\begin{aligned} & \left| \int_0^T \int_{\Omega} (B_{\Delta t} - \mathcal{B}(\bar{H}_{\Delta t})) (e - e_g) r \, dr dz \, dt \right| \\ & \leq L\Delta t \sum_{i=1}^m \int_{t^{i-1}}^{t^i} \|\bar{\partial}H^i\|_{L_r^2(\Omega)} \|e - e_g\|_{L_r^2(\Omega)} \, dt \\ & \leq \frac{C}{\eta} \Delta t^2 + \eta \int_0^T \|e\|_{L_r^2(\Omega)}^2 \, dt + \eta \int_0^T \|e_g\|_{L_r^2(\Omega)}^2 \, dt. \end{aligned} \quad (4.37)$$

Finally, for the two remaining terms on the right-hand side of (4.35), from integration by parts and Young's inequality we arrive at

$$\begin{aligned} & \left| \int_0^T \left\langle \int_0^t (f - \bar{f}_{\Delta t})(s) \, ds, e - e_g \right\rangle dt \right| \\ & = \left| \left\langle \int_0^T (f - \bar{f}_{\Delta t}) \, dt, \int_0^T (e - e_g) \, dt \right\rangle - \int_0^T \left\langle f - \bar{f}_{\Delta t}, \int_0^t (e - e_g)(s) \, ds \right\rangle dt \right| \\ & \leq \alpha \left\| \int_0^T (e - e_g) \, dt \right\|_{\tilde{H}_r^1(\Omega)}^2 + \int_0^T \left\| \int_0^t (e - e_g)(s) \, ds \right\|_{\tilde{H}_r^1(\Omega)}^2 \, dt \\ & \quad + C_{\alpha} \int_0^T \|f - \bar{f}_{\Delta t}\|_{\mathcal{U}'}^2 \, dt \end{aligned} \quad (4.38)$$

for all $\alpha > 0$ and, similarly,

$$\begin{aligned} & \int_0^T a \left(\int_0^t e_g(s) \, ds, e - e_g \right) dt \\ & \leq \alpha \left\| \int_0^T (e - e_g) \, dt \right\|_{\tilde{H}_r^1(\Omega)}^2 + \int_0^T \left\| \int_0^t (e - e_g)(s) \, ds \right\|_{\tilde{H}_r^1(\Omega)}^2 \, dt \\ & \quad + C_{\alpha} \int_0^T \|e_g\|_{\tilde{H}_r^1(\Omega)}^2 \, dt, \end{aligned} \quad (4.39)$$

for all $\alpha > 0$, too. Then, by replacing (4.36)–(4.39) into (4.35) with $\eta = \beta/4$ and $\alpha = \gamma/8$, we obtain that there exists $C > 0$ such that

$$\begin{aligned} & \frac{\beta}{2} \int_0^T \|e\|_{L_r^2(\Omega)}^2 \, dt + \frac{\gamma}{4} \left\| \int_0^T (e - e_g) \, dt \right\|_{\tilde{H}_r^1(\Omega)}^2 \\ & \leq C \left\{ \Delta t^2 + \|e_g\|_{L^2(0,T;\tilde{H}_r^1(\Omega))}^2 + \|f - \bar{f}_{\Delta t}\|_{L^2(0,T;\mathcal{U}')}^2 \right\} \\ & \quad + 2 \int_0^T \left\| \int_0^t (e - e_g)(s) \, ds \right\|_{\tilde{H}_r^1(\Omega)}^2 \, dt. \end{aligned}$$

Since this inequality actually holds with T substituted by τ for any $\tau \in (0, T]$, the result follows from Gronwall's lemma, classical interpolation results and (4.8). \square

Remark 4.4.2 Under the same assumptions as above, but with \mathcal{B} satisfying hypothesis H.2 instead of H.2* (namely, continuous instead of Lipschitz continuous), we have the following error estimate:

$$\int_0^T \|H - \bar{H}_{\Delta t}\|_{L_r^2(\Omega)}^2 dt + \left\| \int_0^T (H - \bar{H}_{\Delta t}) dt \right\|_{\tilde{\mathbf{H}}_r^1(\Omega)}^2 \leq C\Delta t.$$

(See Theorem 3.2 from [82] for a similar result in a 3D problem.) In fact, the Lipschitz continuity of \mathcal{B} was only used to prove (4.36) and (4.37). Then, it is enough to bound the corresponding left-hand sides without using the Lipschitz continuity. For that in (4.36), we notice that

$$\begin{aligned} & \left| \int_0^T \int_{\Omega} (B_{\Delta t} - \mathcal{B}(\bar{H}_{\Delta t})) (e - e_g) r dr dz dt \right| \\ & \leq \Delta t \left(\sum_{i=1}^{m-1} \Delta t \|\bar{\partial} \mathcal{B}(H^{i+1})\|_{\mathcal{U}'}^2 \right) \left(\int_0^T \|e - e_g\|_{\tilde{\mathbf{H}}_r^1(\Omega)}^2 dt \right)^{1/2}. \end{aligned}$$

Hence, from Lemma 4.4.1, the fact that $H \in L^\infty(0, T; \tilde{\mathbf{H}}_r^1(\Omega))$ and the regularity of H_g (cf. (4.8)), it follows that

$$\left| \int_0^T \int_{\Omega} (B_{\Delta t} - \mathcal{B}(\bar{H}_{\Delta t})) (e - e_g) r dr dz dt \right| \leq C\Delta t.$$

On the other hand, for the left-hand side in (4.37), we obtain from hypothesis H.3, Lemma 4.4.1, a classical interpolation result and (4.8)

$$\left| \int_0^T \int_{\Omega} (\mathcal{B}(H) - \mathcal{B}(\bar{H}_{\Delta t})) e_g r dr dz dt \right| \leq C\Delta t \|g\|_{\mathbf{H}^1(0, T; \tilde{\mathbf{H}}_r^{1/2}(\Gamma))},$$

which allows us to conclude the remark.

4.5 Numerical analysis. Fully discrete problem

In this section, we will introduce a space discretization of Problem 4.4.1 and obtain error estimates for the fully discrete approximation. First, we will estimate the error in the $L^2(0, T; L_r^2(\Omega))$ -norm without assuming any additional regularity of the solution. With this aim, we will derive an estimate for the difference between the fully and the semi-discrete problems and will use the results of the previous section (Lemma 4.4.1 and Theorem 4.4.1). Subsequently, by assuming further regularity of the solution H , we will also derive error estimates in a discrete version of the norm (4.32).

From now on, we assume that Ω is a polygonal domain. Let Γ_0 be the intersection between Γ and the symmetry axis ($r = 0$) and $\Gamma_1 := \Gamma \setminus \Gamma_0$. We consider a family of regular, quasi-uniform partitions $\{\mathcal{T}_h\}_{h>0}$ of Ω into triangles, where h denotes the mesh-size (i.e., the maximal length of the sides of the triangulation). Let \mathcal{L}_h be the space of piecewise linear continuous finite elements,

$$\mathcal{L}_h := \{G_h \in \mathcal{C}(\Omega) : G_h|_T \in \mathcal{P}_1 \ \forall T \in \mathcal{T}_h\},$$

and \mathcal{V}_h the subspace of functions vanishing on Γ_0 :

$$\mathcal{V}_h := \{G_h \in \mathcal{L}_h : G_h|_{\Gamma_0} = 0\}.$$

Notice that $\mathcal{V}_h \subset \tilde{H}_r^1(\Omega)$. We also consider the finite-dimensional subspace

$$\mathcal{U}_h := \mathcal{V}_h \cap \mathcal{U} = \{G_h \in \mathcal{L}_h : G_h|_{\Gamma} = 0\}.$$

Finally, we denote by $\mathcal{V}_h(\Gamma)$ the space of traces on Γ of functions in \mathcal{V}_h :

$$\mathcal{V}_h(\Gamma) := \{G_h|_{\Gamma} : G_h \in \mathcal{V}_h\}.$$

Notice too that for all $G_h \in \mathcal{V}_h(\Gamma)$, $G_h|_{\Gamma_0} = 0$.

In order to define a discrete approximation on Γ for the Dirichlet boundary data, we introduce the Sobolev space

$$L_r^2(\Gamma) := \left\{ v : \Gamma \rightarrow \mathbb{R} : \int_{\Gamma} v^2 r dS < \infty \right\}$$

and the orthogonal projector $\Pi_{\Gamma}^h : L_r^2(\Gamma) \rightarrow \mathcal{V}_h(\Gamma)$ defined for all $v \in L_r^2(\Gamma)$ by

$$\Pi_{\Gamma}^h v \in \mathcal{V}_h(\Gamma) : \quad \int_{\Gamma_1} \frac{1}{\sigma} \left(\Pi_{\Gamma}^h v - v \right) v_h r dS = 0 \quad \forall v_h \in \mathcal{V}_h(\Gamma).$$

We propose the following Galerkin discretization of Problem 4.4.1 as the fully discrete approximation of Problem 4.3.1:

Problem 4.5.1 For $i = 0, \dots, m-1$, find $H_h^{i+1} \in \mathcal{V}_h$ satisfying

$$\begin{aligned} \int_{\Omega} \bar{\partial} \mathcal{B}(H_h^{i+1}) G_h r dr dz + a(H_h^{i+1}, G_h) &= \langle f^{i+1}, G_h \rangle & \forall G_h \in \mathcal{U}_h, \\ H_h^{i+1}|_{\Gamma} &= \Pi_{\Gamma}^h g^{i+1}, \\ H_h^0 &= H_{0h}. \end{aligned}$$

In principle $H_{0h} \in \mathcal{V}_h$ is any arbitrary approximation of H_0 ; see Remarks 4.5.2 and 4.5.3 below for a discussion about a convenient choice. The existence and the uniqueness of solution follow by applying similar techniques as those in the proof of Lemma 4.3.2. The following lemma yields an a priori estimate for the solution of Problem 4.5.1.

Lemma 4.5.1 There exists $C > 0$ such that, for all $l = 0, \dots, m-1$,

$$\left\| \bar{\partial} \mathcal{B}(H_h^{l+1}) \right\|_{\mathcal{U}'}^2 + \Delta t \sum_{i=0}^l \left\| \bar{\partial} H_h^{i+1} \right\|_{L_r^2(\Omega)}^2 + \left\| H_h^{l+1} \right\|_{\tilde{H}_r^1(\Omega)}^2 \leq C.$$

Proof. It follows by applying the same techniques as in the proof of Lemma 4.4.1. \square

4.5.1 Finite element approximation properties

In order to derive error estimates for the proposed numerical scheme, first we will establish several approximation properties of the finite element spaces.

We consider the Clément-type operator $I_h : \tilde{\mathbf{H}}_r^1(\Omega) \rightarrow \mathcal{V}_h$ defined in [6, Eq. (36)]. In Theorem 2 from this reference it is proved that, for all $u \in \tilde{\mathbf{H}}_r^1(\Omega)$,

$$\|u - I_h u\|_{L_r^2(\Omega)} + h \|u - I_h u\|_{\tilde{\mathbf{H}}_r^1(\Omega)} \leq Ch \|u\|_{\tilde{\mathbf{H}}_r^1(\Omega)} \quad (4.40)$$

and, for all $u \in \mathbf{H}_r^2(\Omega) \cap \tilde{\mathbf{H}}_r^1(\Omega)$,

$$\|u - I_h u\|_{L_r^2(\Omega)} + h \|u - I_h u\|_{\tilde{\mathbf{H}}_r^1(\Omega)} \leq Ch^2 \|u\|_{\mathbf{H}_r^2(\Omega) \cap \tilde{\mathbf{H}}_r^1(\Omega)}. \quad (4.41)$$

Let \mathcal{N} be the set of all vertices of \mathcal{T}_h . For any $P \in \mathcal{N}$, ω_P denotes the union of all elements sharing P and $h_P := \sup_{T \subset \omega_P} h_T$, with h_T being the diameter of T . Let $\{\varphi_P : P \in \mathcal{N}\}$ be the standard nodal basis of \mathcal{L}_h .

Next, we establish a discrete lifting result that will be used in the sequel.

Lemma 4.5.2 *For all $u \in \tilde{\mathbf{H}}_r^1(\Omega)$, there exists $v_h \in \mathcal{V}_h$ which satisfies*

$$v_h = \Pi_\Gamma^h u - I_h u \quad \text{on } \Gamma$$

and

$$\|v_h\|_{\tilde{\mathbf{H}}_r^1(\Omega)} \leq C \|u\|_{\tilde{\mathbf{H}}_r^1(\Omega)}.$$

Moreover, if $u \in \mathbf{H}_r^2(\Omega) \cap \tilde{\mathbf{H}}_r^1(\Omega)$, then

$$\|v_h\|_{\tilde{\mathbf{H}}_r^1(\Omega)} \leq Ch \|u\|_{\mathbf{H}_r^2(\Omega) \cap \tilde{\mathbf{H}}_r^1(\Omega)}.$$

Proof. We define $v_h := \sum_{P \in \mathcal{N} \cap \Gamma_1} (\Pi_\Gamma^h u - I_h u)(P) \varphi_P$. Notice that $\text{supp } v_h \subset \bigcup \{T \in \mathcal{T}_h : T \cap \Gamma_1 \neq \emptyset\}$.

A straightforward computation allows us to show that $\|v_h\|_{L_r^2(\omega_P)}^2 \leq Ch_P \|\Pi_\Gamma^h u - I_h u\|_{L_r^2(\partial\omega_P \cap \Gamma_1)}^2$ for all $P \in \mathcal{N} \cap \Gamma_1$. Hence, using weighted inverse inequalities (see [6, Lemmas 3 & 4]), we obtain

$$\|v_h\|_{\tilde{\mathbf{H}}_r^1(\omega_P)}^2 \leq Ch_P^{-2} \|v_h\|_{L_r^2(\omega_P)}^2 \leq Ch_P^{-1} \|\Pi_\Gamma^h u - I_h u\|_{L_r^2(\partial\omega_P \cap \Gamma_1)}^2.$$

Summing for all $P \in \mathcal{N} \cap \Gamma_1$ and using the quasi-uniformity of the meshes lead to

$$\|v_h\|_{\tilde{\mathbf{H}}_r^1(\Omega)}^2 \leq Ch^{-1} \|\Pi_\Gamma^h u - I_h u\|_{L_r^2(\Gamma_1)}^2. \quad (4.42)$$

Moreover, since $\|\Pi_\Gamma^h u\|_{L_r^2(\Gamma_1)} \leq \frac{\sigma^*}{\sigma_*} \|u\|_{L_r^2(\Gamma_1)}$ and $\Pi_\Gamma^h I_h u = I_h u$ on Γ , we have

$$\|\Pi_\Gamma^h u - I_h u\|_{L_r^2(\Gamma_1)}^2 \leq \left(\frac{\sigma^*}{\sigma_*}\right)^2 \sum_{\ell \subset \Gamma_1} \|u - I_h u\|_{L_r^2(\ell)}^2. \quad (4.43)$$

Now, from [31, Lemma 4] it follows that

$$\|u - I_h u\|_{L_r^2(\ell)}^2 \leq C \left\{ h_T^{-1} \|u - I_h u\|_{L_r^2(T)}^2 + h_T \|u - I_h u\|_{\tilde{\mathbf{H}}_r^1(T)}^2 \right\}, \quad (4.44)$$

where $T \in \mathcal{T}_h$ is such that $\ell \subset \partial T$. If $u \in \tilde{\mathbf{H}}_r^1(\Omega)$, then, from the latter and (4.40), we obtain

$$\sum_{\ell \subset \Gamma_1} \|u - I_h u\|_{L_r^2(\ell)}^2 \leq Ch \|u\|_{\tilde{\mathbf{H}}_r^1(\Omega)}^2. \quad (4.45)$$

Therefore, the first inequality of the lemma follows from (4.42), (4.43) and (4.45). On the other hand, for $u \in \mathbf{H}_r^2(T) \cap \tilde{\mathbf{H}}_r^1(\Omega)$ we proceed analogously but applying (4.41) instead of (4.40) to bound (4.44). Thus, we conclude the proof. \square

Let us introduce the elliptic projector $P_h : \tilde{\mathbf{H}}_r^1(\Omega) \rightarrow \mathcal{V}_h$ defined for all $u \in \tilde{\mathbf{H}}_r^1(\Omega)$ as follows:

$$P_h u \in \mathcal{V}_h : \quad a(P_h u, w_h) = a(u, w_h) \quad \forall w_h \in \mathcal{U}_h, \quad (4.46)$$

$$P_h u = \Pi_\Gamma^h(u|_\Gamma) \quad \text{on } \Gamma. \quad (4.47)$$

To obtain an error estimate for this projector, first we prove the following lemma.

Lemma 4.5.3 *Let $\mathbf{p} := (p_r, p_z) \in \mathbf{H}_r^1(\Omega)^2$ be such that $p_z \in L_{1/r}^2(\Omega)$ and $\mathbf{p} \cdot \mathbf{t} = 0$ on Γ . Then, there exists $\mathbf{p}_h \in \mathcal{L}_h^2$ such that $\mathbf{p}_h \cdot \mathbf{t} = 0$ on Γ , $\mathbf{p}_h \cdot \mathbf{n}$ is continuous on Γ , and*

$$\|\mathbf{p} - \mathbf{p}_h\|_{L_r^2(\Omega)^2} + h \|\mathbf{p} - \mathbf{p}_h\|_{\mathbf{H}_r^1(\Omega)^2} \leq Ch \left\{ \|\mathbf{p}\|_{\mathbf{H}_r^1(\Omega)^2} + \|p_z\|_{L_{1/r}^2(\Omega)} \right\}. \quad (4.48)$$

Proof. We will use a Clément-type interpolant of \mathbf{p} . We define its values at each node $P \in \mathcal{N}$ differently according to its location:

- If $P \notin \Gamma$, then we set $\mathbf{p}_P := |\omega_P|^{-1} \int_{\omega_P} \mathbf{p} r \, dr dz$.
- If $P \in \Gamma$ is not a vertex of the polygon Ω , then the two edges ℓ_1 and ℓ_2 sharing P have the same tangent and normal vectors which we denote \mathbf{t}_P and \mathbf{n}_P , respectively. In this case, we set $\mathbf{p}_P := (\tilde{\mathbf{p}}_P \cdot \mathbf{n}_P) \mathbf{n}_P$, where $\tilde{\mathbf{p}}_P := |\omega_P|^{-1} \int_{\omega_P} \mathbf{p} r \, dr dz$.
- If P is a vertex of Ω , then we set $\mathbf{p}_P := \mathbf{0}$.

Finally, we define $\mathbf{p}_h := \sum_{P \in \mathcal{N}} \mathbf{p}_P \varphi_P$.

By construction $\mathbf{p}_h \in \mathcal{L}_h^2$ and $\mathbf{p}_h \cdot \mathbf{t} = 0$ on Γ . To prove (4.48), first we notice that, since $\sum_{P \in \mathcal{N}} \varphi_P = 1$, we have

$$\|\mathbf{p} - \mathbf{p}_h\|_{L_r^2(\Omega)^2}^2 = \int_{\Omega} (\mathbf{p} - \mathbf{p}_h) \sum_{P \in \mathcal{N}} \varphi_P (\mathbf{p} - \mathbf{p}_P) r \, dr dz.$$

Hence, by using Cauchy-Schwartz inequality, it is easy to check that

$$\|\mathbf{p} - \mathbf{p}_h\|_{L_r^2(\Omega)^2} \leq C \left(\sum_{P \in \mathcal{N}} \|\mathbf{p} - \mathbf{p}_P\|_{L_r^2(\omega_P)^2}^2 \right)^{1/2}. \quad (4.49)$$

Similar arguments allow us to write

$$\begin{aligned} \|\mathbf{p} - \mathbf{p}_h\|_{\mathbf{H}_r^1(\Omega)^2} &\leq C \left\{ \left\| \sum_{P \in \mathcal{N}} \nabla \varphi_P (\mathbf{p} - \mathbf{p}_P)^t \right\|_{L_r^2(\Omega)^{2 \times 2}} + \left\| \sum_{P \in \mathcal{N}} \varphi_P \nabla \mathbf{p} \right\|_{L_r^2(\Omega)^{2 \times 2}} \right\} \\ &\leq C \left\{ \|\mathbf{p}\|_{\mathbf{H}_r^1(\Omega)^2}^2 + \sum_{P \in \mathcal{N}} h_P^{-2} \|\mathbf{p} - \mathbf{p}_P\|_{L_r^2(\omega_P)^2}^2 \right\}^{1/2}, \end{aligned} \quad (4.50)$$

where we have also used that, for regular meshes, $\|\nabla\varphi_P\|_{L_r^2(\Omega)^2} \leq Ch_P^{-1}$.

Thus, there only remains to estimate $\|\mathbf{p} - \mathbf{p}_P\|_{L_r^2(\omega_P)^2}$ for all $P \in \mathcal{N}$. To do this, we distinguish again the same three cases as above:

- If $P \notin \Gamma$, since \mathbf{p}_P is the mean value of \mathbf{p} in $L_r^2(\omega_P)^2$, then, from [6, Lemma 6],

$$\|\mathbf{p} - \mathbf{p}_P\|_{L_r^2(\omega_P)^2} = \inf_{\mathbf{q} \in \mathbb{P}_0(\omega_P)^2} \|\mathbf{p} - \mathbf{q}\|_{L_r^2(\omega_P)^2} \leq Ch_P \|\mathbf{p}\|_{H_r^1(\omega_P)^2}. \quad (4.51)$$

- If $P \in \Gamma$ is not a vertex of Ω , since $\mathbf{p}_P \cdot \mathbf{t}_P = 0$, it follows that

$$\|\mathbf{p} - \mathbf{p}_P\|_{L_r^2(\omega_P)^2}^2 = \|\mathbf{p} \cdot \mathbf{t}_P\|_{L_r^2(\omega_P)}^2 + \|(\mathbf{p} - \mathbf{p}_P) \cdot \mathbf{n}_P\|_{L_r^2(\omega_P)}^2. \quad (4.52)$$

Now, since $\|(\mathbf{p} - \mathbf{p}_P) \cdot \mathbf{n}_P\|_{L_r^2(\omega_P)} = \|(\mathbf{p} - \tilde{\mathbf{p}}_P) \cdot \mathbf{n}_P\|_{L_r^2(\omega_P)}$, with $\tilde{\mathbf{p}}_P$ being the mean value of \mathbf{p} in $L_r^2(\omega_P)^2$, by proceeding as in (4.51) we obtain

$$\|(\mathbf{p} - \mathbf{p}_P) \cdot \mathbf{n}_P\|_{L_r^2(\omega_P)} \leq Ch_P \|\mathbf{p}\|_{H_r^1(\omega_P)^2}. \quad (4.53)$$

To bound the other term on the right-hand side of (4.52), we use that $\mathbf{p} \cdot \mathbf{t}_P$ vanishes on $\ell_1 \cup \ell_2 \subset \partial\omega_P$ and consider also three cases:

- If $P \in \Gamma_1$ and $\omega_P \cap \Gamma_0 = \emptyset$, then $\max_{\omega_P} r / \min_{\omega_P} r \leq C$, with C being a constant which only depends on the regularity of the mesh. In such a case, from the classical Poincaré inequality and a scaling argument we have

$$\begin{aligned} \|\mathbf{p} \cdot \mathbf{t}_P\|_{L_r^2(\omega_P)}^2 &\leq \max_{\omega_P} r \int_{\omega_P} |\mathbf{p} \cdot \mathbf{t}_P|^2 \, dr dz \\ &\leq Ch_P^2 \max_{\omega_P} r \int_{\omega_P} |\nabla(\mathbf{p} \cdot \mathbf{t}_P)|^2 \, dr dz \\ &\leq Ch_P^2 \frac{\max_{\omega_P} r}{\min_{\omega_P} r} \int_{\omega_P} |D\mathbf{p}|^2 r \, dr dz \leq Ch_P^2 \|\mathbf{p}\|_{H_r^1(\omega_P)^2}^2. \end{aligned} \quad (4.54)$$

- If $P \in \Gamma_1$ and $\omega_P \cap \Gamma_0 \neq \emptyset$, then let K_P be the smallest closed parallelogram such that $\omega_P \subset K_P \subset \bar{\Omega}$, with one edge on Γ_0 and other one on Γ_1 , as shown in Figure 4.1 (for the existence of such K_P , we may need to assume that the mesh is sufficiently fine).

We use the notation from Figure 4.1. In particular, the slope of the edge \overline{AB} is $m := L/R$ and the length of the edge \overline{AD} is M . Notice that $M \leq Ch_P$, with C a constant which only depends on the regularity of the mesh. For simplicity, we consider a coordinate system (r, z) centered at the vertex A .

Given $\mathbf{p} \in C^\infty(K_P)^2$, let $v := \mathbf{p} \cdot \mathbf{t}_P$. Then,

$$v(r, z) = \int_{mr}^z \partial_z v(r, s) \, ds, \quad mr \leq z \leq mr + M, \quad 0 \leq r \leq R.$$

- If P is a vertex of Ω , then $\mathbf{p}_P = \mathbf{0}$ and the unit vectors \mathbf{t}_1 and \mathbf{t}_2 , tangent to the respective edges ℓ_1 and ℓ_2 on Γ sharing P , form a basis of \mathbb{R}^2 . Therefore,

$$\|\mathbf{p} - \mathbf{p}_P\|_{L_r^2(\omega_P)}^2 = \|\mathbf{p}\|_{L_r^2(\omega_P)}^2 \leq C \left\{ \|\mathbf{p} \cdot \mathbf{t}_1\|_{L_r^2(\omega_P)}^2 + \|\mathbf{p} \cdot \mathbf{t}_2\|_{L_r^2(\omega_P)}^2 \right\}.$$

Since $\mathbf{p} \cdot \mathbf{t}_1|_{\ell_1} = 0$ and $\mathbf{p} \cdot \mathbf{t}_2|_{\ell_2} = 0$, a similar analysis to that leading to (4.55) and (4.56), yields

$$\|\mathbf{p} - \mathbf{p}_P\|_{L_r^2(\omega_P)}^2 \leq Ch_P \left\{ |\mathbf{p}|_{\mathbf{H}_r^1(\tilde{\omega}_P)}^2 + \|p_z\|_{L_{1/r}^2(\omega_P)}^2 \right\}. \quad (4.58)$$

Whence, by replacing (4.51), (4.57) and (4.58) into (4.49) and (4.50), we obtain (4.48). On the other hand, we notice that by construction \mathbf{p}_h vanishes at the vertices of Ω , so that $\mathbf{p}_h \cdot \mathbf{n}$ is continuous along the boundary Γ and we end the proof. \square

Now we are in a position to prove an error estimate for the projector P_h . This proof relies on a duality argument for which we will need additional regularity of the solution of the corresponding adjoint problem. This is the reason why, from now on, we also make the following assumption:

H.7: Given $w \in L_r^2(\Omega)$, the unique solution $\varphi \in \mathcal{U}$ of the elliptic problem

$$a(v, \varphi) = \int_{\Omega} v w r \, dr dz \quad \forall v \in \mathcal{U} \quad (4.59)$$

satisfies $\varphi \in \mathbf{H}_r^2(\Omega) \cap \tilde{\mathbf{H}}_r^2(\Omega)$ and

$$\|\varphi\|_{\mathbf{H}_r^2(\Omega)} + \|\varphi\|_{\tilde{\mathbf{H}}_r^2(\Omega)} \leq C \|w\|_{L_r^2(\Omega)}.$$

This assumption is fulfilled, for instance, when σ is constant and Ω is a rectangle (cf. [46, Theorem 4.1]).

Before proving an error estimate for the projector P_h , we establish the following auxiliary result which follows easily from assumption H.7.

Lemma 4.5.4 *Given $w \in L_r^2(\Omega)$, let $\varphi \in \mathcal{U}$ be the solution to (4.59). Then,*

$$a(v, \varphi) = - \int_{\Omega} \operatorname{div} \left(\frac{1}{\sigma r} \nabla(r\varphi) \right) v r \, dr dz + \int_{\Gamma_1} \frac{1}{\sigma r} \nabla(r\varphi) \cdot \mathbf{n} v r \, dS \quad \forall v \in \mathbf{H}_r^1(\Omega). \quad (4.60)$$

Proof. First notice that both integrals on the right-hand side above are well defined. In fact, on one hand, by testing (4.59) with $v \in \mathcal{D}(\Omega)$ it follows that $-\operatorname{div}(1/(\sigma r)\nabla(r\varphi)) = w \in L_r^2(\Omega)$. On the other hand, for the last integral we use that for $\varphi \in \tilde{\mathbf{H}}_r^2(\Omega)$, there holds $(1/r)\nabla(r\varphi) = ((1/r)\partial_r(r\varphi), \partial_z\varphi) \in \mathbf{H}_r^1(\Omega)^2$ and, hence, $(1/(\sigma r))\nabla(r\varphi) \cdot \mathbf{n} \in L_r^2(\Gamma_1)$, because of a trace result (see, for instance, [31, Lemma 4]) and the fact that σ is bounded below away from zero.

Therefore, to prove (4.60), it is enough to check it with $v \in \mathcal{C}^\infty(\bar{\Omega})$ vanishing in a neighborhood of Γ_0 , since the set of such functions is dense in $\mathbf{H}_r^1(\Omega)$ (see [67, Theorem 4.3(ii)]). For such

a function v , let $\varepsilon > 0$ be such that $\text{supp } v \subset \Omega_\varepsilon := \{(r, z) \in \bar{\Omega} : r > \varepsilon\}$. Then,

$$\begin{aligned} a(v, \varphi) &= \int_{\Omega_\varepsilon} \frac{1}{\sigma r} \nabla(r\varphi) \cdot \nabla(rv) \, dr dz \\ &= - \int_{\Omega_\varepsilon} \text{div} \left(\frac{1}{\sigma r} \nabla(r\varphi) \right) v r \, dr dz + \int_{\partial\Omega_\varepsilon} \frac{1}{\sigma r} \nabla(r\varphi) \cdot \mathbf{n} v r \, dS \\ &= - \int_{\Omega} \text{div} \left(\frac{1}{\sigma r} \nabla(r\varphi) \right) v r \, dr dz + \int_{\Gamma_1} \frac{1}{\sigma r} \nabla(r\varphi) \cdot \mathbf{n} v r \, dS. \end{aligned}$$

Thus, we conclude the proof. \square

The following lemma provides an optimal-order error estimate for $(u - P_h u)$.

Lemma 4.5.5 For all $u \in \mathbf{H}_r^2(\Omega) \cap \tilde{\mathbf{H}}_r^1(\Omega)$

$$\|u - P_h u\|_{\mathbf{L}_r^2(\Omega)} \leq Ch^2 \|u\|_{\mathbf{H}_r^2(\Omega) \cap \tilde{\mathbf{H}}_r^1(\Omega)}.$$

Proof. First, we prove an estimate in the norm induced by $a(\cdot, \cdot)$. From the definition of P_h we have that

$$a(u - P_h u, u - P_h u) \leq C \|u - P_h u - y_h\|_{\tilde{\mathbf{H}}_r^1(\Omega)}^2 \quad \forall y_h \in \mathcal{U}_h.$$

Then, taking $y_h := I_h u - P_h u + v_h$, with $v_h \in \mathcal{V}_h$ as in Lemma 4.5.2, it follows that

$$a(u - P_h u, u - P_h u) \leq C \left\{ \|u - I_h u\|_{\tilde{\mathbf{H}}_r^1(\Omega)}^2 + \|v_h\|_{\tilde{\mathbf{H}}_r^1(\Omega)}^2 \right\}.$$

Hence, from (4.41) and Lemma 4.5.2 we obtain

$$a(u - P_h u, u - P_h u) \leq Ch^2 \|u\|_{\mathbf{H}_r^2(\Omega) \cap \tilde{\mathbf{H}}_r^1(\Omega)}^2. \quad (4.61)$$

Next, we resort to a duality argument. Let $\varphi \in \mathcal{U}$ be the solution of

$$a(v, \varphi) = \int_{\Omega} v (u - P_h u) r \, dr dz \quad \forall v \in \mathcal{U}.$$

Hence, according to hypothesis H.7, $\varphi \in \mathbf{H}_r^2(\Omega) \cap \tilde{\mathbf{H}}_r^2(\Omega)$ and

$$\|\varphi\|_{\mathbf{H}_r^2(\Omega)} + \|\varphi\|_{\tilde{\mathbf{H}}_r^2(\Omega)} \leq C \|u - P_h u\|_{\mathbf{L}_r^2(\Omega)}. \quad (4.62)$$

Moreover, by taking $v \in \mathcal{D}(\Omega)$ in the equation above, we have that

$$-\text{div} \left(\frac{1}{\sigma r} \nabla(r\varphi) \right) = u - P_h u \quad \text{in } \Omega.$$

By multiplying this equation by $(u - P_h u)$ and using Lemma 4.5.4 and the definition of P_h (cf. (4.46)–(4.47)), we obtain for all $\varphi_h \in \mathcal{U}_h$,

$$\|u - P_h u\|_{\mathbf{L}_r^2(\Omega)}^2 = a(u - P_h u, \varphi - \varphi_h) - \int_{\Gamma_1} \frac{1}{\sigma r} \nabla(r\varphi) \cdot \mathbf{n} (u - \Pi_{\Gamma}^h u) r \, dS. \quad (4.63)$$

Next, we estimate the two terms on the right-hand side above. For the first one, we choose $\varphi_h = I_h^0 \varphi$, where $I_h^0 : \mathcal{U} \rightarrow \mathcal{U}_h$ is another Clément-type interpolant operator defined in [6, Eq. (37)]. Then, (4.61) and Theorem 2 from [6] lead to

$$a(u - P_h u, \varphi - \varphi_h) \leq Ch^2 \|u\|_{\mathbf{H}_r^2(\Omega) \cap \tilde{\mathbf{H}}_r^1(\Omega)} \|\varphi\|_{\mathbf{H}_r^2(\Omega) \cap \tilde{\mathbf{H}}_r^1(\Omega)}. \quad (4.64)$$

To estimate the other term, we define $\mathbf{p} = (p_r, p_z) := (1/r)\nabla(r\varphi)$. For $\varphi \in \tilde{\mathbf{H}}_r^2(\Omega)$, $\mathbf{p} \in \mathbf{H}_r^1(\Omega)^2$ and $p_z \in L_{1/r}^2(\Omega)$. Moreover, $\mathbf{p} \cdot \mathbf{t} = 0$ on Γ . In fact, since $\varphi \in \mathcal{U}$, we have $\mathbf{p} \cdot \mathbf{t}|_{\Gamma_0} = p_z|_{\Gamma_0} = (\partial_z \varphi)|_{\Gamma_0} = 0$, and $\mathbf{p} \cdot \mathbf{t}|_{\Gamma_1} = ((1/r)\varphi t_r)|_{\Gamma_1} + (\nabla \varphi \cdot \mathbf{t})|_{\Gamma_1} = 0$, too. Thus, \mathbf{p} satisfies the hypothesis of Lemma 4.5.3. Hence, let $\mathbf{p}_h \in \mathcal{L}_h^2$ be as in that lemma. Let w_h be defined on Γ by $w_h|_{\Gamma_1} := \mathbf{p}_h \cdot \mathbf{n}$ and $w_h|_{\Gamma_0} := 0$. Since $\mathbf{p}_h \cdot \mathbf{n}$ vanishes at the vertices of Ω (because $\mathbf{p}_h \cdot \mathbf{t} = 0$ on Γ and $\mathbf{p}_h \cdot \mathbf{n}$ is continuous on Γ), we have that $w_h \in \mathcal{V}_h(\Gamma)$. Whence, from the definition of Π_Γ^h we have that

$$\begin{aligned} \left| \int_{\Gamma_1} \frac{1}{\sigma r} \nabla(r\varphi) \cdot \mathbf{n} (u - \Pi_\Gamma^h u) r dS \right| &= \left| \int_{\Gamma_1} \frac{1}{\sigma} (\mathbf{p} \cdot \mathbf{n} - w_h) (u - \Pi_\Gamma^h u) r dS \right| \\ &\leq \frac{1}{\sigma_*} \|\mathbf{p} - \mathbf{p}_h\|_{L_r^2(\Gamma_1)^2} \|u - \Pi_\Gamma^h u\|_{L_r^2(\Gamma_1)}. \end{aligned} \quad (4.65)$$

Now, by proceeding as in Lemma 4.5.2 (cf. (4.43), (4.44)) and using (4.41), we obtain

$$\|u - \Pi_\Gamma^h u\|_{L_r^2(\Gamma_1)} \leq C \|u - I_h u\|_{L_r^2(\Gamma_1)} \leq Ch^{3/2} \|u\|_{\mathbf{H}_r^2(\Omega) \cap \tilde{\mathbf{H}}_r^1(\Omega)}. \quad (4.66)$$

On the other hand, using again [31, Lemma 4], we write for all edges $\ell \subset \Gamma_1$

$$\|\mathbf{p} - \mathbf{p}_h\|_{L_r^2(\ell)^2} \leq C \left\{ h_T^{-1} \|\mathbf{p} - \mathbf{p}_h\|_{L_r^2(T)^2} + h_T \|\mathbf{p} - \mathbf{p}_h\|_{\mathbf{H}_r^1(T)^2} \right\},$$

with $T \in \mathcal{T}_h$ such that $\ell \subset \partial T$. Therefore, from Lemma 4.5.3, we obtain

$$\|\mathbf{p} - \mathbf{p}_h\|_{L_r^2(\Gamma_1)^2} \leq Ch \left\{ \|\mathbf{p}\|_{\mathbf{H}_r^1(\Omega)^2}^2 + \|p_z\|_{L_{1/r}^2(\Omega)}^2 \right\} \leq Ch \|\varphi\|_{\tilde{\mathbf{H}}_r^2(\Omega)}^2. \quad (4.67)$$

Then, the result follows from (4.63)–(4.67) and (4.62). \square

Remark 4.5.1 *Using similar arguments, it is straightforward to prove that*

$$\|u - P_h u\|_{L_r^2(\Omega)} \leq Ch \|u\|_{\tilde{\mathbf{H}}_r^1(\Omega)} \quad \forall u \in \tilde{\mathbf{H}}_r^1(\Omega).$$

In fact, the only differences are that we use $a(u - P_h u, u - P_h u) \leq C \|u\|_{\tilde{\mathbf{H}}_r^1(\Omega)}^2$ instead of (4.61) and, instead of (4.66), we use $\|u - \Pi_\Gamma^h u\|_{L_r^2(\Gamma_1)} \leq Ch^{1/2} \|u\|_{\tilde{\mathbf{H}}_r^1(\Omega)}$ (which follows by the same arguments that (4.66), but using (4.40) instead of (4.41)).

4.5.2 Error estimates for the full discretization

The following auxiliary result yields an estimate for the difference between the fully and the semi-discrete problems.

Lemma 4.5.6 *Let H^{i+1} and H_h^{i+1} , $i = 0, \dots, m$, be the solutions to Problems 4.4.1 and 4.5.1, respectively. Then,*

$$\Delta t \sum_{i=1}^m \|H^{i+1} - H_h^{i+1}\|_{L_r^2(\Omega)}^2 \leq C \left(h^2 + \|H_0 - H_{0h}\|_{L_r^2(\Omega)}^2 \right).$$

Proof. We split the quantities to estimate into two terms:

$$H^{i+1} - H_h^{i+1} = (H^{i+1} - P_h H^{i+1}) + (P_h H^{i+1} - H_h^{i+1}) \quad (4.68)$$

The first one is a projection error that can be bounded by using the results from the previous section. The second one is a purely discrete term, which we denote

$$\rho_h^{i+1} := P_h H^{i+1} - H_h^{i+1}, \quad i = 0, \dots, m-1.$$

Notice that $\rho_h^{i+1} \in \mathcal{U}_h$, because $(P_h H^{i+1})|_\Gamma = \Pi_\Gamma^h(H^{i+1}|_\Gamma) = H_h^{i+1}|_\Gamma$ (cf. (4.47) and the second equation from Problem 4.5.1).

A calculation from the first equations of Problems 4.4.1 and 4.5.1 and (4.46) yields

$$\int_\Omega (\bar{\partial} \mathcal{B}(H^{i+1}) - \bar{\partial} \mathcal{B}(H_h^{i+1})) G_h r \, dr dz + a(\rho_h^{i+1}, G_h) = 0 \quad \forall G_h \in \mathcal{U}_h.$$

Summing up the above equations, we obtain

$$\begin{aligned} \int_\Omega \left(\mathcal{B}(H^{l+1}) - \mathcal{B}(H_h^{l+1}) \right) G_h r \, dr dz + \Delta t a \left(\sum_{i=0}^l \rho_h^{i+1}, G_h \right) \\ = \int_\Omega (\mathcal{B}(H_0) - \mathcal{B}(H_{0h})) G_h r \, dr dz \end{aligned}$$

for $l = 0, \dots, m-1$, or, equivalently,

$$\begin{aligned} \int_\Omega \left(\mathcal{B}(P_h H^{l+1}) - \mathcal{B}(H_h^{l+1}) \right) G_h r \, dr dz + \Delta t a \left(\sum_{i=0}^l \rho_h^{i+1}, G_h \right) \\ = \int_\Omega (\mathcal{B}(H_0) - \mathcal{B}(H_{0h})) G_h r \, dr dz + \int_\Omega \left(\mathcal{B}(P_h H^{l+1}) - \mathcal{B}(H^{l+1}) \right) G_h r \, dr dz. \end{aligned}$$

Hence, choosing $G_h = \rho_h^{l+1}$, using the strong monotonicity and Lipschitz continuity of \mathcal{B} (cf. H.2* and H.1*), Cauchy-Schwartz and Young's inequalities, we obtain

$$\begin{aligned} \frac{\beta}{2} \|\rho_h^{l+1}\|_{L_r^2(\Omega)}^2 + \Delta t a \left(\sum_{i=0}^l \rho_h^{i+1}, \rho_h^{l+1} \right) \\ \leq \frac{C}{\beta} \|H_0 - H_{0h}\|_{L_r^2(\Omega)}^2 + \frac{C}{\beta} \|P_h H^{l+1} - H^{l+1}\|_{L_r^2(\Omega)}^2. \end{aligned}$$

Now, summing up the above equations multiplied by Δt and using Remark 4.5.1,

$$\begin{aligned} & \frac{\beta}{2} \sum_{l=0}^{m-1} \Delta t \left\| \rho_h^{l+1} \right\|_{L_r^2(\Omega)}^2 + \Delta t^2 \sum_{l=0}^{m-1} a \left(\sum_{i=0}^l \rho_h^{i+1}, \rho_h^{l+1} \right) \\ & \leq \frac{CT}{\beta} \|H_0 - H_{0h}\|_{L_r^2(\Omega)}^2 + \frac{C\Delta t}{\beta} \sum_{l=0}^{m-1} h^2 \left\| H^{l+1} \right\|_{\tilde{H}_r^1(\Omega)}^2. \end{aligned}$$

On the other hand, writing $\rho_h^{l+1} = \sum_{i=0}^l \rho_h^{i+1} - \sum_{i=0}^{l-1} \rho_h^{i+1}$ and using the identity $2(p-q)p = p^2 + (p-q)^2 - q^2$ and the ellipticity of $a(\cdot, \cdot)$ (cf. Lemma 4.3.1), it is easy to obtain the following inequality:

$$\Delta t^2 \sum_{l=0}^{m-1} a \left(\sum_{i=0}^l \rho_h^{i+1}, \rho_h^{l+1} \right) \geq \frac{\gamma}{2} \left\| \Delta t \sum_{i=0}^{m-1} \rho_h^{i+1} \right\|_{\tilde{H}_r^1(\Omega)}^2. \quad (4.69)$$

Hence, substituting this inequality into the previous one, we have that

$$\begin{aligned} & \sum_{l=0}^{m-1} \Delta t \left\| \rho_h^{l+1} \right\|_{L_r^2(\Omega)}^2 + \left\| \Delta t \sum_{i=0}^{m-1} \rho_h^{i+1} \right\|_{\tilde{H}_r^1(\Omega)}^2 \\ & \leq C \left\{ \|H_0 - H_{0h}\|_{L_r^2(\Omega)}^2 + \Delta t \sum_{l=0}^{m-1} h^2 \left\| H^{l+1} \right\|_{\tilde{H}_r^1(\Omega)}^2 \right\}. \end{aligned}$$

Whence, from Lemma 4.4.1 we obtain

$$\sum_{l=0}^{m-1} \Delta t \left\| \rho_h^{l+1} \right\|_{L_r^2(\Omega)}^2 \leq C \left\{ \|H_0 - H_{0h}\|_{L_r^2(\Omega)}^2 + h^2 \right\}.$$

Thus, the result follows from the decomposition (4.68), the above inequality, Remark 4.5.1 and Lemma 4.4.1 again. \square

Remark 4.5.2 *If the initial data is taken as $H_{0h} := I_h H_0$, with I_h being the Clément-type interpolant operator used in the previous section, then, because of (4.40),*

$$\left(\Delta t \sum_{i=1}^m \left\| H^{i+1} - H_h^{i+1} \right\|_{L_r^2(\Omega)}^2 \right)^{1/2} \leq Ch \left\{ 1 + \|H_0\|_{\tilde{H}_r^1(\Omega)} \right\}.$$

The following result, whose proof follows immediately from Lemma 4.5.6 and Theorem 4.4.1, yields an error estimate for the fully discrete problem.

Theorem 4.5.1 *Let H and H_h^{i+1} , $i = 0, \dots, m$, be the solutions to Problems 4.3.1 and 4.5.1, respectively. Let $\bar{H}_{\Delta t}^h$ be the step function defined by*

$$\bar{H}_{\Delta t}^h(t^0) := H_h^0; \quad \bar{H}_{\Delta t}^h(t) := H_h^i, \quad t \in (t^{i-1}, t^i], \quad i = 1, \dots, m.$$

Then, under hypotheses H.1, H.2*, H.3, H.4*, H.5, H.6 and H.7,*

$$\left\| H - \bar{H}_{\Delta t}^h \right\|_{L^2(0,T;L_r^2(\Omega))} \leq C \left\{ h + \Delta t + \|H_0 - H_{0h}\|_{\tilde{H}_r^1(\Omega)} \right\}.$$

Notice that the above result does not require any additional regularity assumption on the solution of the continuous problem H . However, the order $\mathcal{O}(h)$ in the error estimate is not necessarily optimal for regular solutions. Our next goal is to show that this order can be improved when the solution to Problem 4.3.1 is assumed to be more regular.

Theorem 4.5.2 *Let H and H_h^{i+1} , $i = 0, \dots, m$, be the solutions to Problems 4.3.1 and 4.5.1, respectively. Under hypotheses H.1*, H.2*, H.3, H.4*, H.5, H.6 and H.7, if $H \in \mathbb{H}^1(0, T; \mathbb{H}_r^2(\Omega) \cap \tilde{\mathbb{H}}_r^1(\Omega))$, then*

$$\begin{aligned} & \left(\sum_{i=0}^{m-1} \Delta t \|H(t^{i+1}) - H_h^{i+1}\|_{\mathbb{L}_r^2(\Omega)}^2 \right)^{1/2} \\ & \leq C \left\{ (\Delta t + h^2) \|H\|_{\mathbb{H}^1(0, T; \mathbb{H}_r^2(\Omega) \cap \tilde{\mathbb{H}}_r^1(\Omega))} \right. \\ & \quad \left. + \|H_0 - H_{0h}\|_{\mathbb{L}_r^2(\Omega)} + \Delta t \|f\|_{\mathbb{H}^1(0, T; \mathcal{U}')} \right\}. \end{aligned}$$

Proof. Once more, we split the error into two terms,

$$H(t^{i+1}) - H_h^{i+1} = (H(t^{i+1}) - P_h H(t^{i+1})) + (P_h H(t^{i+1}) - H_h^{i+1}), \quad (4.70)$$

where the first one is a projection error that can be bounded by using Lemma 4.5.5 and the second one is a purely discrete term that we denote

$$\tilde{\rho}_h^{i+1} := P_h H(t^{i+1}) - H_h^{i+1}, \quad i = 0, \dots, m-1.$$

Notice that $\tilde{\rho}_h^{i+1} \in \mathcal{U}_h$, because $(P_h H(t^{i+1}))|_\Gamma = \Pi_\Gamma^h(g(t^{i+1})) = H_h^{i+1}|_\Gamma$ (cf. (4.47) and the second equations from Problems 4.3.1 and 4.5.1).

To estimate this term, we integrate from 0 to t^{l+1} the first equation of Problem 4.3.1 and use (4.46) to obtain for all $G_h \in \mathcal{U}_h$

$$\begin{aligned} & \int_\Omega \mathcal{B}(H(t^{l+1})) G_h r \, dr dz + \Delta t a \left(\sum_{i=0}^l P_h H(t^{i+1}), G_h \right) \\ & = a \left(\int_0^{t^{l+1}} (\widehat{H}_{\Delta t} - H) dt, G_h \right) + \left\langle \int_0^{t^{l+1}} f dt, G_h \right\rangle + \int_\Omega \mathcal{B}(H_0) G_h r \, dr dz, \end{aligned}$$

where $\widehat{H}_{\Delta t}$ denotes the step function defined by

$$\widehat{H}_{\Delta t}(t^0) := H(t^0), \quad \widehat{H}_{\Delta t}(t) := H(t^i), \quad t \in (t^{i-1}, t^i]. \quad i = 1, \dots, m.$$

(Notice that we have used a different notation this time, since $\overline{H}_{\Delta t}$ was already used in (4.33) for another step function.)

On the other hand, by summing up the first equation of Problem 4.5.1 for $i = 0, \dots, l$, it follows that for all $G_h \in \mathcal{U}_h$

$$\begin{aligned} & \int_\Omega \mathcal{B}(H_h^{l+1}) G_h r \, dr dz + \Delta t a \left(\sum_{i=0}^l H_h^{i+1}, G_h \right) \\ & = \left\langle \Delta t \sum_{i=0}^l f^{i+1}, G_h \right\rangle + \int_\Omega \mathcal{B}(H_{0h}) G_h r \, dr dz. \end{aligned}$$

Subtracting this equation from the previous one, we obtain for all $G_h \in \mathcal{U}_h$

$$\begin{aligned} & \int_{\Omega} \left(\mathcal{B}(P_h H(t^{l+1})) - \mathcal{B}(H_h^{l+1}) \right) G_h r \, dr dz + \Delta t a \left(\sum_{i=0}^l \tilde{\rho}_h^{i+1}, G_h \right) \\ &= \int_{\Omega} (\mathcal{B}(H_0) - \mathcal{B}(H_{0h})) G_h r \, dr dz \\ &+ \int_{\Omega} \left(\mathcal{B}(P_h H(t^{l+1})) - \mathcal{B}(H(t^{l+1})) \right) G_h r \, dr dz \\ &+ a \left(\int_0^{t^{l+1}} (\hat{H}_{\Delta t} - H) dt, G_h \right) + \left\langle \int_0^{t^{l+1}} (f - \bar{f}_{\Delta t}) dt, G_h \right\rangle. \end{aligned}$$

At this point we proceed as in the proof of Lemma 4.5.6. We choose $G_h = \hat{\rho}_h^{l+1}$ and use the strong monotonicity and Lipschitz continuity of \mathcal{B} (cf. H.2* and H.1*), Cauchy-Schwartz and Young's inequalities, to write

$$\begin{aligned} & \frac{\beta}{2} \left\| \hat{\rho}_h^{l+1} \right\|_{L_r^2(\Omega)}^2 + \Delta t a \left(\sum_{i=0}^l \tilde{\rho}_h^{i+1}, \hat{\rho}_h^{l+1} \right) \\ & \leq \frac{C}{\beta} \|H_0 - H_{0h}\|_{L_r^2(\Omega)}^2 + \frac{C}{\beta} \|P_h H(t^{l+1}) - H(t^{l+1})\|_{L_r^2(\Omega)}^2 \\ & + a \left(\int_0^{t^{l+1}} (\hat{H}_{\Delta t} - H) dt, \hat{\rho}_h^{l+1} \right) + \left\langle \int_0^{t^{l+1}} (f - \bar{f}_{\Delta t}) dt, \hat{\rho}_h^{l+1} \right\rangle. \end{aligned}$$

Then, we sum up the above equations multiplied by Δt and obtain

$$\begin{aligned} & \frac{\beta}{2} \sum_{l=0}^{m-1} \Delta t \left\| \hat{\rho}_h^{l+1} \right\|_{L_r^2(\Omega)}^2 + \Delta t^2 \sum_{l=0}^{m-1} a \left(\sum_{i=0}^l \tilde{\rho}_h^{i+1}, \hat{\rho}_h^{l+1} \right) \\ & \leq \frac{CT}{\beta} \|H_0 - H_{0h}\|_{L_r^2(\Omega)}^2 + \frac{C\Delta t}{\beta} \sum_{l=0}^{m-1} \|P_h H(t^{l+1}) - H(t^{l+1})\|_{L_r^2(\Omega)}^2 \\ & + \Delta t \sum_{l=0}^{m-1} a \left(\int_0^{t^{l+1}} (\hat{H}_{\Delta t} - H) dt, \hat{\rho}_h^{l+1} \right) + \Delta t \sum_{l=0}^{m-1} \left\langle \int_0^{t^{l+1}} (f - \bar{f}_{\Delta t}) dt, \hat{\rho}_h^{l+1} \right\rangle. \quad (4.71) \end{aligned}$$

We estimate the second term on the left-hand side above also as we did in the proof of Lemma 4.5.6 (cf. (4.69)):

$$\Delta t^2 \sum_{l=0}^{m-1} a \left(\sum_{i=0}^l \tilde{\rho}_h^{i+1}, \hat{\rho}_h^{l+1} \right) \geq \frac{\gamma}{2} \left\| \Delta t \sum_{i=0}^{m-1} \tilde{\rho}_h^{i+1} \right\|_{\tilde{H}_r^1(\Omega)}^2. \quad (4.72)$$

On the other hand, it is easy to prove by summation by parts that

$$\begin{aligned} & \Delta t \sum_{l=0}^{m-1} a \left(\int_0^{t^{l+1}} (\hat{H}_{\Delta t} - H) dt, \hat{\rho}_h^{l+1} \right) \\ &= a \left(\int_0^T (\hat{H}_{\Delta t} - H) dt, \Delta t \sum_{l=0}^{m-1} \hat{\rho}_h^{l+1} \right) - \sum_{l=0}^{m-2} a \left(\int_{t^{l+1}}^{t^{l+2}} (\hat{H}_{\Delta t} - H) dt, \Delta t \sum_{i=0}^l \tilde{\rho}_h^{i+1} \right) \end{aligned}$$

and

$$\begin{aligned} & \Delta t \sum_{l=0}^{m-1} \left\langle \int_0^{t^{l+1}} (f - \bar{f}_{\Delta t}) dt, \hat{\rho}_h^{l+1} \right\rangle \\ &= \left\langle \int_0^T (f - \bar{f}_{\Delta t}) dt, \Delta t \sum_{l=0}^l \hat{\rho}_h^{l+1} \right\rangle - \sum_{l=0}^{m-2} \left\langle \int_{t^{l+1}}^{t^{l+2}} (f - \bar{f}_{\Delta t}) dt, \Delta t \sum_{i=0}^l \hat{\rho}_h^{i+1} \right\rangle. \end{aligned}$$

Now, by replacing these two equations and (4.72) into (4.71) and using the continuity of $a(\cdot, \cdot)$ and Young's inequality, it follows that

$$\begin{aligned} & \sum_{l=0}^{m-1} \Delta t \left\| \hat{\rho}_h^{l+1} \right\|_{L_r^2(\Omega)}^2 + \left\| \Delta t \sum_{i=0}^{m-1} \hat{\rho}_h^{i+1} \right\|_{\tilde{H}_r^1(\Omega)}^2 \\ & \leq C \left\{ \|H_0 - H_{0h}\|_{L_r^2(\Omega)}^2 + \Delta t \sum_{l=0}^{m-1} \left\| P_h H(t^{l+1}) - H(t^{l+1}) \right\|_{L_r^2(\Omega)}^2 \right. \\ & \quad \left. + \|f - \bar{f}_{\Delta t}\|_{L^2(0,T;U')}^2 + \left\| \hat{H}_{\Delta t} - H \right\|_{L^2(0,T;\tilde{H}_r^1(\Omega))}^2 + \sum_{l=0}^{m-2} \left\| \Delta t \sum_{i=0}^l \hat{\rho}_h^{i+1} \right\|_{\tilde{H}_r^1(\Omega)}^2 \right\}. \end{aligned}$$

Hence, by using a discrete Gronwall's lemma, classical interpolation results and Lemma 4.5.5, we obtain

$$\begin{aligned} & \sum_{l=0}^{m-1} \Delta t \left\| \hat{\rho}_h^{l+1} \right\|_{L_r^2(\Omega)}^2 + \left\| \Delta t \sum_{i=0}^{m-1} \hat{\rho}_h^{i+1} \right\|_{\tilde{H}_r^1(\Omega)}^2 \\ & \leq C \left\{ \|H_0 - H_{0h}\|_{L_r^2(\Omega)}^2 + \Delta t^2 \|f\|_{H^1(0,T;L_r^2(\Omega))}^2 \right. \\ & \quad \left. + (\Delta t^2 + h^4) \|H\|_{H^1(0,T;H_r^2(\Omega) \cap \tilde{H}_r^1(\Omega))}^2 \right\}. \end{aligned} \quad (4.73)$$

Therefore, the result follows from (4.70), this estimate and Lemma 4.5.5. \square

Remark 4.5.3 When $H_0 \in H_r^2(\Omega) \cap \tilde{H}_r^1(\Omega)$, we can use, for instance, $H_{0h} := I_h H_0$, with I_h being again the Clément-type interpolant operator used in the previous section. In such a case, from (4.41) we have

$$\begin{aligned} & \left(\sum_{i=0}^{m-1} \Delta t \|H(t^{i+1}) - H_h^{i+1}\|_{L_r^2(\Omega)}^2 \right)^{1/2} \\ & \leq C \left\{ (\Delta t + h^2) \|H\|_{H^1(0,T;H_r^2(\Omega) \cap \tilde{H}_r^1(\Omega))} \right. \\ & \quad \left. + h^2 \|H_0\|_{H_r^2(\Omega) \cap \tilde{H}_r^1(\Omega)} + \Delta t \|f\|_{H^1(0,T;L_r^2(\Omega))} \right\}. \end{aligned}$$

Remark 4.5.4 *Let us further assume that Ω is a rectangle. In such a case, the following error estimate holds:*

$$\begin{aligned} & \max_{1 \leq l \leq m} \left\| \sum_{i=0}^{l-1} \Delta t (H(t^{i+1}) - H_h^{i+1}) \right\|_{\tilde{H}_r^1(\Omega)} \\ & \leq C \left\{ (\Delta t + h) \|H\|_{\mathbf{H}^1(0,T;\mathbf{H}_r^2(\Omega) \cap \tilde{\mathbf{H}}_r^1(\Omega))} \right. \\ & \quad \left. + \|H_0 - H_{0h}\|_{L_r^2(\Omega)} + \Delta t \|f\|_{\mathbf{H}^1(0,T;L_r^2(\Omega))} \right\}. \end{aligned}$$

In fact, a similar error estimate, but in the norm induced by $a(\cdot, \cdot)$ holds for any convex domain as a consequence of (4.61), (4.70) and (4.73). Hence, the estimate above follows from the equivalence between both norms in rectangles proved in [46, Proposition 3.1].

4.6 Numerical experiments

We have developed a Fortran code which implements the fully discrete numerical scheme analyzed in the previous section. To solve the non-linear systems we have used Newton's method.

In order to test the error estimate proved for the numerical scheme (cf. Theorem 4.5.2), we have used a problem with a known analytical solution. Let $\Omega := (0, 1) \times (-1, 1)$, $T = 1$ and the electrical conductivity $\sigma = 1$. We have considered a non-linear H-B curve given by

$$B(H) = H + \arctan(H).$$

Finally, we have chosen the right-hand side f , the boundary condition g and the initial data B_0 so that the solution is

$$H(r, z, t) = e^t \sin(\pi r/2) \sin(\pi z/2).$$

The method has been used on several successively refined meshes and time-steps, both chosen in a convenient way to analyze the convergence with respect to these discretization parameters. The numerical approximations have been compared with the analytical solution by computing the percentage error for H in a discrete $L^2(0, T; L_r^2(\Omega))$ -norm as follows:

$$E_h^{\Delta t}(H) := 100 \frac{\left(\sum_{i=0}^{m-1} \Delta t \|H(t^{i+1}) - H_h^{i+1}\|_{L_r^2(\Omega)}^2 \right)^{1/2}}{\left(\sum_{i=0}^{m-1} \Delta t \|H(t^{i+1})\|_{L_r^2(\Omega)}^2 \right)^{1/2}}.$$

We have also computed the percentage error for the eddy current $\mathbf{J} = \mathbf{curl} \mathbf{H}$ (cf. (4.3)) in the analogous discrete $L^2(0, T; L_r^2(\Omega)^2)$ -norm:

$$E_h^{\Delta t}(\mathbf{J}) := 100 \frac{\left(\sum_{i=0}^{m-1} \Delta t \|\mathbf{curl} \mathbf{H}(t^{i+1}) - \mathbf{curl} \mathbf{H}_h^{i+1}\|_{L_r^2(\Omega)^2}^2 \right)^{1/2}}{\left(\sum_{i=0}^{m-1} \Delta t \|\mathbf{curl} \mathbf{H}(t^{i+1})\|_{L_r^2(\Omega)^2}^2 \right)^{1/2}},$$

where $\mathbf{H}_h^{i+1} := H_h^{i+1} \mathbf{e}_\theta$.

Table 4.1 shows the percentage errors $E_h^{\Delta t}(H)$ for the magnetic field at different levels of discretization. Taking a small enough time-step Δt , one can observe the behavior of the error with respect to the space discretization (see, for instance, the last row of the table). On the other hand, by considering a small enough mesh-size h , one can inspect the order of convergence with respect to Δt (see, for instance, the last column). In this example, we observe an order of convergence $\mathcal{O}(h^2 + \Delta t)$, which coincides with that predicted by the theoretical analysis (cf. Remark 4.5.3).

Table 4.1: Percentage errors of the computed magnetic field: $E_h^{\Delta t}(H)$; $\Delta t_0 = 0.2$, $h_0 = \sqrt{2}/2$.

Δt	h_0	$h_0/2$	$h_0/4$	$h_0/8$	$h_0/16$	$h_0/32$
Δt_0	11.303186	2.776175	0.649365	0.244530	0.244530	0.257269
$\Delta t_0/2$	11.319166	2.813540	0.672449	0.169753	0.122235	0.131386
$\Delta t_0/4$	11.327962	2.834780	0.692873	0.161602	0.063345	0.065098
$\Delta t_0/8$	11.332618	2.846108	0.705389	0.167654	0.042866	0.031640
$\Delta t_0/16$	11.335037	2.852116	0.712470	0.173253	0.040402	0.016118
$\Delta t_0/32$	11.336268	2.855402	0.716551	0.177379	0.042634	0.010994
$\Delta t_0/64$	11.336871	2.858055	0.720272	0.181395	0.046589	0.013961

In Table 4.2 we report the percentage errors $E_h^{\Delta t}(\mathbf{J})$ for the current density. As in the previous table, one can observe the behavior of the error with respect to space and time discretization by taking small enough time-step Δt and mesh-size h , respectively. In this case we observe an order of convergence $\mathcal{O}(h + \Delta t)$. Although such behavior has not been proved, the reported numerical results agree with what can be expected from Remark 4.5.4.

Table 4.2: Percentage errors of the computed current density: $E_h^{\Delta t}(\mathbf{J})$; $\Delta t_0 = 0.5$, $h_0 = \sqrt{2}/16$.

Δt	h_0	$h_0/2$	$h_0/4$	$h_0/8$	$h_0/16$	$h_0/32$
Δt_0	2.295415	1.460797	1.164167	1.077472	1.054695	1.048924
$\Delta t_0/2$	2.115802	1.165048	0.763272	0.623870	0.583859	0.573421
$\Delta t_0/4$	2.055560	1.057179	0.588016	0.391297	0.323992	0.304855
$\Delta t_0/8$	2.037246	1.024542	0.528749	0.295576	0.198324	0.165304
$\Delta t_0/16$	2.031716	1.015408	0.511773	0.264467	0.148224	0.099893
$\Delta t_0/32$	2.029951	1.012872	0.507225	0.255804	0.132270	0.074239

Finally, we report simultaneous dependence on h and Δt for the errors in both quantities, the magnetic field and the current density: $E_h^{\Delta t}(H)$ and $E_h^{\Delta t}(\mathbf{J})$, respectively. With this aim, we proceed in the following way: first, in each case, we choose initial values of h and Δt so that

the time and the space discretization errors are both of approximately the same size; then, for each of the successively refined meshes, we take values of Δt proportional to h^2 in the first case and to h in the second one (see the values within boxes in Tables 4.1 and 4.2, respectively).

Figure 4.2 shows log-log plots of the corresponding percentage errors. The slopes of the curves show clear orders of convergence $\mathcal{O}(h^2) = \mathcal{O}(h^2 + \Delta t)$ for $E_h^{\Delta t}(H)$ and $\mathcal{O}(h) = \mathcal{O}(h + \Delta t)$ for $E_h^{\Delta t}(\mathbf{J})$.

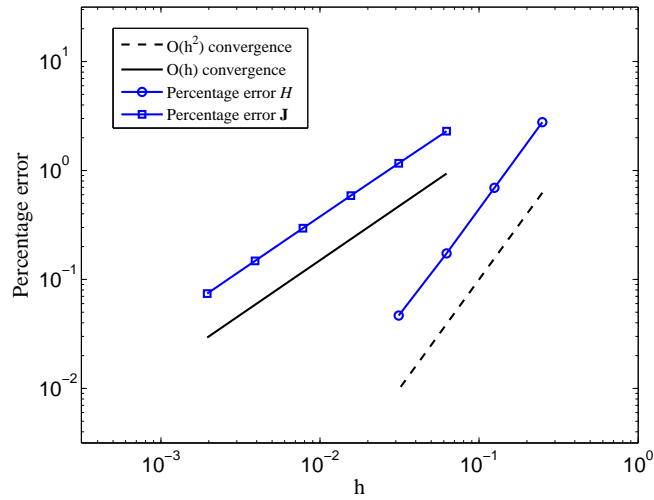


Figure 4.2: Percentage errors $E_h^{\Delta t}(H)$ and $E_h^{\Delta t}(\mathbf{J})$ versus the mesh-size h (log-log scale), with Δt proportional to h^2 for the former and to h for the latter.

Chapter 5

Numerical solution of transient non-linear axisymmetric eddy current models with hysteresis

5.1 Introduction

Electric machine is the generic name for devices that transform electric energy in mechanical energy or vice versa. They are very important in all sectors of the modern society: for infrastructure, industry, transport service and for domestic and commercial appliances. They are used, for instance, as large generators for producing the electric power we need. Most of them, however, are used as electric motors of different sizes and for all kind of applications: for driving pumps in water-supply plants, as traction motors for electrical trains, in electric cars, elevators and for many other infrastructure applications. The development has been fascinating and new applications and requirements still continue to push technology further.

It is widely known that the performance of electric machines depend strongly on the power losses. These losses are traditionally known as iron losses and are due to the fact that the magnetic field variations in the ferromagnetic materials composing the core of the machine produce energy dissipation.

The efficiency, the thermal behavior or the compactness are some of the design constraints which are strongly influenced by the losses. Then, it is very important to predict them accurately for an optimum design of the device.

The losses can be divided into three main components: eddy current (or classical) losses, due to the Joule effect, hysteresis losses and excess losses, which are related to the intrinsic nature of magnetic materials (see, for instance, [15]). In particular, unlike hysteresis, excess losses are function of how quickly the magnetization varies with time.

In the literature there are numerous publications devoted to obtain analytical simplified expressions to approximate the different components of these losses (see, for instance, [84, 15, 19]), which are only valid under certain assumptions that do not hold in many practical situations.

Numerical simulation is an interesting alternative in order to overcome these limitations and

thus, in the last years, we can find several works focused on the computation of iron losses (see [89, 38, 39, 75] and references therein). In this work we are only interested in computing the eddy current and the hysteresis losses.

As mentioned before, the eddy current losses are caused by the currents induced in the magnetic material by the time varying magnetic induction. These currents are dissipated as heat due to the Joule effect. As illustrated in Figure 5.1, the cores are usually laminated to reduce the eddy current losses. That is, the core consists of plates that are orthogonal to the direction of the currents in the coils. Thus, the effective electrical conductivity becomes small and hence the losses are highly reduced.

Hysteresis losses are heat losses caused by magnetic properties of the materials composing the core. When the core is in a magnetic field, the magnetic particles of the core tend to line up with the magnetic field. Then, if the applied magnetic field is variable along the time, the continuous movement of the magnetic particles, which are trying to align themselves with the magnetic field, produces a molecular friction, which, in its turn, produces heat. This heat is referred to as magnetic hysteresis losses.



Figure 5.1: Laminated core.

A first step in the computation of this kind of losses is the numerical solution of the underlying electromagnetic problem. This requires solving the quasi-static Maxwell's model, which is the aim of this chapter. In the framework of the non-linear eddy current model formulated in terms of the magnetic field, a common assumption is to consider that the relation between the magnetic field \mathbf{H} and the magnetic induction \mathbf{B} , the so-called B-H curve, is given by an univalued function (see, for instance, [80, 82, 60] in a 3D setting), so the hysteresis phenomenon is a priori neglected. In fact, this approach would only be valid for soft magnetic materials, i.e., those for which the hysteresis loop is very thin (see Figure 1.4 (left)). Once the magnetic field has been computed, the hysteresis losses are calculated a posteriori by using “analytical” approximated formulas.

Different models have been proposed to represent the magnetic hysteresis phenomenon. At the macroscopic level, the most popular is the Preisach model [76]. This model is based on

some hypotheses concerning the physical mechanisms of magnetization, and for this reason was primarily known in the area of magnetics. It was not until fifty years later when a group of Russian mathematicians developed the model into an abstract mathematical frame of *hysteresis operators* which can be applied to a wide variety of hysteresis phenomena [57].

In the context of parabolic equations with hysteresis there are several publications devoted to the mathematical analysis of the problem (see, [93, 94, 95, 49] and more recently [41, 44, 42]). In particular, [44] deals with an abstract parabolic equation motivated by a two-dimensional (2D) eddy current model with hysteresis but the numerical analysis and computer implementation of the problem are not considered. Numerical approximation of parabolic problems with hysteresis are considered, for instance, in [91, 92]. In the context of the computational methods for a 2D eddy current model with hysteresis we mention [89, 90]. However, to the best of the author's knowledge, the parabolic problem presented in [89] has not been mathematically analyzed

In this chapter, we also focus on the axisymmetric eddy current problem with hysteresis, namely, the B-H curve is given by a rather general hysteresis operator. Moreover, we also consider a time and space dependent electrical conductivity, an important issue because this quantity is typically a function of temperature which, in its turn, is a time dependent field. In view of applications we consider that the source inputs are current intensities or voltage drops. With this in mind, two source terms are considered: either the magnetic field on the boundary is given (Dirichlet condition) or, motivated by [89], the magnetic flux across a meridian section of the device (magnetic flux condition). These source terms are physically realistic in the sense that there exist industrial applications where it can be readily obtained from measurable quantities (see [40, 8, 9, 70, 62, 89]).

This work complements Chapter 3 and Chapter 4, where the mathematical and numerical analysis of a 2D nonlinear axisymmetric eddy current model was performed without considering hysteresis effects. These references deal with an eddy-current problem with different source data: non-homogeneous Dirichlet boundary condition in Chapter 4 and meridian magnetic flux in Chapter 3. In each case, existence of solution is shown and a full discretization is proposed, for which an optimal error estimate is obtained. Here, we are interested in the mathematical analysis and the numerical computation of a formulation including hysteresis effects.

By using classical weighted two-dimensional Sobolev spaces for axisymmetric problems, we prove the existence of solution to a weak formulation in terms of the magnetic field. The method used for this purpose consists of introducing an implicit time discretization, obtaining a priori estimates and then passing to the limit as the time-step goes to zero (see [77]). This approximation procedure is often used in the analysis of equations that include a memory operator (see, for instance, [42, 95]) because, at each time step we deal with a stationary problem where the memory operator is reduced to a nonlinear function. In particular, we base our proof on arguments given in [95] where existence of solution to a homogeneous Dirichlet problem is achieved. Let us remark that, to the best of the author's knowledge, the problems addressed in this chapter do not fit in this or other existing results because, on the one hand, in our case the coefficients depend on time and, on the other hand, different boundary conditions are considered.

For the mathematical modeling of hysteresis, we consider the Preisach model as hysteresis operator. For the numerical solution, a finite element discretization by piecewise linear functions

on triangular meshes, and the backward Euler time-discretization are used. We also propose a duality iterative algorithm to handle the nonlinearity at the discrete level which is based on some properties of the Yosida regularization of maximal monotone operators. This algorithm, introduced by Bermúdez and Moreno [12], has been extensively used for a wide range of applications with good numerical results.

The outline of the chapter is as follows: in Section 5.2 we introduce the concept of hysteresis operator needed for the mathematical analysis of the problem. In Section 5.3 we introduce the transient eddy current model with hysteresis to be analyzed. The axisymmetric case is considered and two alternative source terms are introduced. In Section 5.4, after recalling some analytic tools, weak formulations are obtained. Then existence of solution is proved for both formulations. Section 5.5 is devoted to the numerical implementation of the fully-discrete problem arising from a backward Euler time-discretization and a finite element method for space discretization. Then, we introduce the classical Preisach model for which we give a detailed description. In particular, we recall the method to identify, for a particular magnetic material, the function defining its associated Preisach operator. Finally, in Section 5.6, we report a numerical test in order to assess the order of convergence of the above numerical method.

The numerical results predict that we may expect a similar order of convergence as the one proved for the problem without hysteresis in Chapters 3 and 4.

5.2 Hysteresis operators

The hysteresis phenomenon is present in different areas of science such as electromagnetism (magnetic hysteresis, ferroelectric hysteresis) or mechanics, among others. Hysteresis early work date back to 1935 and was proposed by the physicist F. Preisach [74] in the context of ferromagnetism. From the mathematical point of view, we refer to the monograph of mathematicians M. Krasnoselkii and A. Pokrovskii [57] as well as to the books by Visintin [95] and Brokate [24] and, from a physical point of view, to Mayergoytz [63] and Bertotti [15].

In this section we recall some basic background material on hysteresis operators which is needed for the subsequent sections. The treatment of hysteresis operators is influenced by [95].

Most typical examples of hysteresis phenomena exhibit *hysteresis loops*, so we start by showing a classical example of such loops. Let us consider a simple setting, namely, a system whose state is characterized by two scalar variables, u and w , where w is determined by u and both of them depending on time t . Let us suppose that the evolution of w is determined by the one of u .

For instance, in Figure 5.2, if u increases from u_1 to u_2 , the pair (u, w) moves along monotone curve abc . Conversely, if u decreases from u_2 to u_1 , then (u, w) moves along a different monotone curve cda . Moreover, if u inverts its motion when $u_1 < u(t) < u_2$, then (u, w) moves in the interior of the hysteresis region, namely, the part of the (u, w) -plane that is bounded by the major loop $abcd$. Here we assume that the pair (u, w) moves along continuous curves so we speak of continuous hysteresis. Although most typical examples of hysteresis phenomena exhibit hysteresis loops, the occurrence of loops should not be regarded as an essential feature of hysteresis.

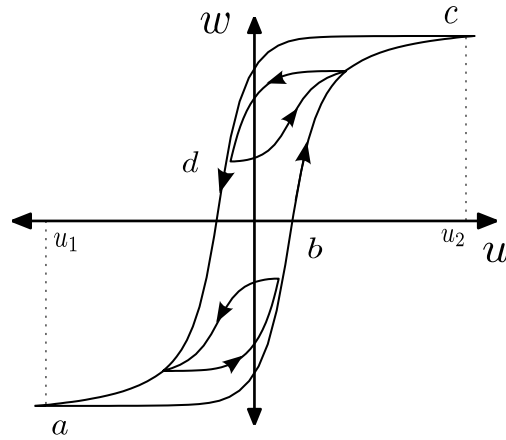


Figure 5.2: Hysteresis loop.

According to [95], we can distinguish two main characteristics of hysteresis phenomena: the *memory effect* and the *rate independence*.

To illustrate these concepts, we consider the (u, w) relation introduced above. The *memory effect* means that, at any instant t , the value of $w(t)$ depends on the previous evolution of u rather than on only $u(t)$. On the other hand, *rate independent* means that, at any instant t , $w(t)$ depends just on the range of function $u : [0, t] \rightarrow \mathbb{R}$ and on the order in which the values of u before t have been attained. In other words, w does not depend on the *velocity* of u .

We notice that, even in most typical hysteresis phenomena, like ferromagnetism, ferroelectricity or plasticity, memory effects are not purely rate independent, as hysteresis is coupled with viscous-type effects. However, in several cases the rate independent component prevails, provided that evolution is not too fast.

In order to introduce a functional setting for hysteresis operators, we first notice that, at any instant t , $w(t)$ will depend not only on the previous evolution of u (i.e., on $u|_{[0,t]}$) but also on the “initial state” of the system. Due to the memory dependence of hysteresis processes, additional information is needed to make up for the lack of history when the process begins. This initial information must represent the “history” of function u before $t = 0$. Hence, not only the standard initial value $(u(0), w(0))$ must be provided. In general, we consider a variable ξ containing all the information about the “initial state”. For instance, we express this as follows:

$$\tilde{\mathcal{F}} : C([0, T]) \times Y \rightarrow C([0, T]) \quad (5.1)$$

$$(u, \xi) \rightarrow w(t) = [\tilde{\mathcal{F}}(u, \xi)](t) \quad (5.2)$$

with Y a suitable metric space.

Here $\tilde{\mathcal{F}}(\cdot, \xi)$ represents an operator between suitable spaces of time-dependent functions, for any fixed ξ . We can now make explicit the assumptions of causality and rate independence.

$\tilde{\mathcal{F}}(\cdot, \xi)$ is *causal*: for any $t \in [0, T]$, the output $w(t)$ is independent of $u|_{[t, T]}$, i.e.,

$$\begin{aligned} & \forall (u_1, \xi), (u_2, \xi) \in \text{Dom}(\tilde{\mathcal{F}}), \\ & u_1|_{[0, t]} = u_2|_{[0, t]} \Rightarrow [\tilde{\mathcal{F}}(u_1, \xi)](t) = [\tilde{\mathcal{F}}(u_2, \xi)](t) \quad \forall t \in (0, T]. \end{aligned}$$

We require the path of the pair (u, w) to be invariant with respect to any increasing diffeomorphism $\varphi : [0, T] \rightarrow [0, T]$, i.e.,

$$\begin{aligned} & \forall (u, \xi) \in \text{Dom}(\tilde{\mathcal{F}}), \\ & [\tilde{\mathcal{F}}(u \circ \varphi, \xi)] = [\tilde{\mathcal{F}}(u, \xi)] \circ \varphi \quad \text{in } [0, T]. \end{aligned}$$

This means that at any instant t , $w(t)$ only depends on $u|_{[0, t]}$ and on the order in which the values of u have been attained before t (*rate independence*). We characterize a *hysteresis operator* as a causal and rate independent operator.

In what follows we shall deal with hysteresis operators that are continuous in the following sense:

$$\begin{aligned} & \forall \left\{ (u_n, \xi_n) \in \text{Dom}(\tilde{\mathcal{F}}) \right\}_{n \in \mathbb{N}}, \text{ if } u_n \rightarrow u \text{ uniformly in } [0, T] \text{ and } \xi_n \rightarrow \xi \text{ in } Y, \\ & \text{then } \tilde{\mathcal{F}}(u_n, \xi_n) \rightarrow \tilde{\mathcal{F}}(u, \xi) \text{ uniformly in } [0, T]. \end{aligned} \quad (5.3)$$

Also, another property which may be fulfilled by hysteresis operators is *order preservation*, that is

$$\begin{aligned} & \forall (u_1, \xi_1), (u_2, \xi_2) \in \text{Dom}(\tilde{\mathcal{F}}), \text{ if } u_1 \leq u_2 \text{ and } \xi_1 \leq \xi_2, \\ & \text{then } \|[\tilde{\mathcal{F}}(u_1, \xi_1)]\|(t) \leq \|[\tilde{\mathcal{F}}(u_2, \xi_2)]\|(t) \quad \forall t \in (0, T]. \end{aligned} \quad (5.4)$$

Moreover, for an operator $\tilde{\mathcal{F}}$ it is also natural to require the following property, usually named *piecewise monotonicity*:

$$\begin{aligned} & \forall (u, \xi) \in \text{Dom}(\tilde{\mathcal{F}}), \forall [t_1, t_2] \subset [0, T], \\ & \text{if } u \text{ is either nondecreasing or nonincreasing in } [t_1, t_2], \text{ then so is } \tilde{\mathcal{F}}(u, \xi). \end{aligned} \quad (5.5)$$

We notice that, the classical L^2 -monotonicity property

$$\int_0^T \left([\tilde{\mathcal{F}}(u_1, \xi)](t) - [\tilde{\mathcal{F}}(u_2, \xi)](t) \right) (u_1(t) - u_2(t)) dt \geq 0 \quad \forall u_1, u_2 \in \text{Dom}(\tilde{\mathcal{F}})$$

is a too strong requirement for hysteresis operators. Actually, a rate independent operator is monotone with respect to the usual scalar product of $L^2(0, T)$ only if it is of the form $\tilde{\mathcal{F}}(u, \xi) = \varphi \circ u$ for some function $\varphi : \mathbb{R} \rightarrow \mathbb{R}$ (see [16, Chapter I]).

5.2.1 Space and time dependence

The hysteresis operators introduced in the above section work between spaces of continuous functions, i.e.,

$$\tilde{\mathcal{F}} : C([0, T]) \times Y \rightarrow C([0, T]).$$

where Y is a suitable metric space containing all the information about the desired “initial state”. These operators are usually employed in problems in which time is the only independent variable, like in the case of ordinary differential equations (ODE). In the case of partial differential equations (PDE), these operators cannot be directly applied and it is necessary to extend $\tilde{\mathcal{F}}$ to some suitable operator \mathcal{F} acting between spaces involving the space variable.

To begin with, we first define appropriate Lebesgue spaces that will be used for the mathematical analysis of the problem (see [95, Section XII.2]). Let Q be a Banach space and $\widehat{\Omega}$ an open subset of \mathbb{R}^N ($N \geq 1$) with Lipschitz continuous boundary. We define $\mathcal{S}(\widehat{\Omega}; Q)$ the family of simple functions $\widehat{\Omega} \rightarrow Q$, namely, functions with finite range such that the inverse image of any element of Q is measurable. Then, we introduce the space of strongly measurable functions:

$$\mathcal{M}(\widehat{\Omega}; Q) := \left\{ v : \widehat{\Omega} \rightarrow Q : \exists \left\{ v_n \in \mathcal{S}(\widehat{\Omega}; Q) \right\}_{n \in \mathbb{N}} \text{ such that} \right. \\ \left. v_n \rightarrow v \text{ strongly in } Q \text{ a.e. in } \widehat{\Omega} \right\}.$$

Now, we are in a position to introduce a space-time hysteresis operator. Given a hysteresis operator $\tilde{\mathcal{F}}$, we introduce, for any $u : \widehat{\Omega} \times [0, T] \rightarrow \mathbb{R}$ and any $\xi : \widehat{\Omega} \rightarrow Y$, the corresponding space dependent operator $\mathcal{F} : \mathcal{M}(\widehat{\Omega}; C([0, T]) \times Y) \rightarrow \mathcal{M}(\widehat{\Omega}; C([0, T]))$ as follows

$$[\mathcal{F}(u, \xi)](x, t) := [\tilde{\mathcal{F}}(u(x, \cdot), \xi(x))](t) \quad \forall (x, t) \in \widehat{\Omega} \times [0, T].$$

We notice that operator $\tilde{\mathcal{F}}$ is here applied at each point $x \in \widehat{\Omega}$ independently, hence, the output $[\mathcal{F}(u, \xi)](x, t)$ depends on $u(x, \cdot)|_{[0, t]}$, but not on $u(y, \cdot)|_{[0, t]}$ for $y \neq x$.

Remark 5.2.1 Recall that the “initial state” ξ contains the “history” information needed to compute \mathcal{F} .

We conclude by summarizing some properties that will be useful in the following sections. In particular, given an “initial state” ξ , \mathcal{F} can be

Causal

$$\forall v_1, v_2 \in \mathcal{M}(\widehat{\Omega}; C([0, T])), \text{ if } v_1 = v_2 \text{ in } [0, t] \text{ a.e. in } \widehat{\Omega}, \\ \text{then } [\mathcal{F}(v_1, \xi)](\cdot, t) = [\mathcal{F}(v_2, \xi)](\cdot, t) \quad \forall t \in [0, T], \text{ a.e. in } \widehat{\Omega}. \quad (5.6)$$

Strongly continuous

$$\forall \left\{ v_n \in \mathcal{M}(\widehat{\Omega}; C([0, T])) \right\}_{n \in \mathbb{N}}, \text{ if } v_n \rightarrow v \text{ uniformly in } [0, T] \text{ a.e. in } \widehat{\Omega}, \\ \text{then } \mathcal{F}(v_n, \xi) \rightarrow \mathcal{F}(v, \xi) \text{ uniformly in } [0, T] \text{ a.e. in } \widehat{\Omega}. \quad (5.7)$$

Piecewise monotone

$$\forall v \in \mathcal{M}(\widehat{\Omega}; C([0, T])), \forall [t_1, t_2] \subset [0, T] \\ \text{if } v(x, \cdot) \text{ is affine in } [t_1, t_2] \text{ a.e. in } \widehat{\Omega} \text{ then} \\ ([\mathcal{F}(v, \xi)](x, t_2) - [\mathcal{F}(v, \xi)](x, t_1)) (v(x, t_2) - v(x, t_1)) \geq 0 \quad \text{a.e. in } \widehat{\Omega}. \quad (5.8)$$

5.2.2 Magnetic hysteresis

Ferromagnetic materials are very sensitive to be magnetized. This means that whenever magnetic flux passes through, they behave like a magnet. These materials are made up of small regions known as magnetic domains. Domains are very small regions in the material structure, where all the dipoles are paralleled in the same direction. In each domain, all of the atomic dipoles are coupled together in a preferential direction (see Figure 5.3 (left)). In other words, the domains are like small permanent magnets oriented randomly in the material.

Ferromagnetic materials become magnetized when the magnetic domains within the material are aligned (see Figure 5.3 (right)). This can be done by placing the material in a strong external magnetic field or by passing electrical current through the material. Some or all of the domains can become aligned. The more the aligned domains, the stronger the magnetic field in the material. When all of the domains are aligned, the material is said to be magnetically saturated. When a material is magnetically saturated, no additional amount of external magnetization force will cause an increase in its internal level of magnetization. After removing this external field, most of domains come again to random positions, but a few of them still remain in their changed position. Because of these unchanged domains the substance becomes slightly magnetized permanently. A similar process takes place if we consider a material magnetically saturated but in the opposite direction. The phenomenon which causes B to lag behind H , so that the magnetization curve for increasing and decreasing fields is not the same, is called hysteresis and the loop traced out by the magnetization curve is called a *hysteresis cycle* or *hysteresis loop*.

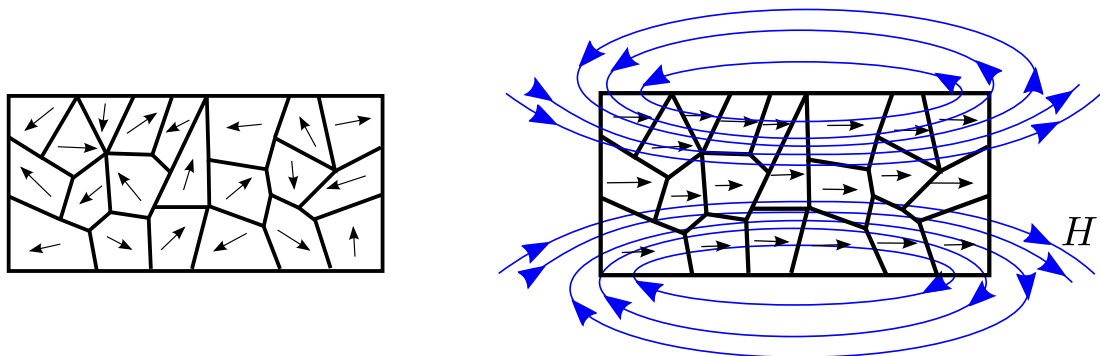


Figure 5.3: Randomly oriented domains (left) and aligned domains (right).

Figure 5.4 shows an example of a hysteresis loop. In this loop we represent the relationship between the induced magnetic flux density B and the magnetizing force H . It is often referred to as the B-H loop.

The loop is generated by measuring the magnetic flux of a ferromagnetic material while the magnetizing force is changed. We start at the *demagnetized* state, that is, when a ferromagnetic material has never been previously magnetized or has been thoroughly demagnetized. As H is increased the loop follows the dashed line. As this line shows, the greater the amount of magnetization, the stronger the magnetic induction. At point (H_m, B_m) almost all of the magnetic

domains are aligned and an additional increase in the magnetizing force will produce very little increase in the magnetic flux. The material has reached the point of magnetic saturation. At this point, when H decreases to zero, the curve will move from point (H_m, B_m) to point $(0, B_m)$. Here, it can be seen that some magnetic flux remains in the material even though the magnetizing force is zero. This point indicates the *remanence* or level of residual magnetism in the material (some of the magnetic domains remain aligned but some others have lost their alignment).

As the magnetizing force is increased in the negative direction, the material will again become magnetically saturated but in the opposite direction (point $(-H_m, -B_m)$). Reducing H to zero brings the curve to point $(0, -B_m)$. It will have a level of residual magnetism equal to that achieved in the other direction. Increasing H back in the positive direction the curve will take a different path from point $(0, -B_m)$ back to the saturation point where it complete the loop. Notice that, any (H, B) point is always inside the major hysteresis loop.

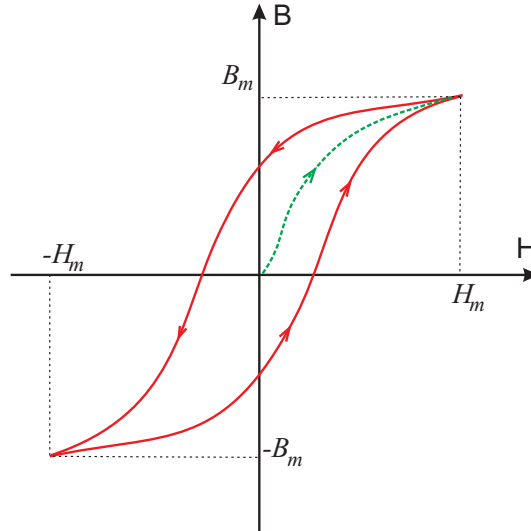


Figure 5.4: B-H cycle. Major hysteresis loop.

5.3 The transient eddy current model with hysteresis

Eddy currents are usually modeled by the so called low-frequency Maxwell equations:

$$\begin{aligned}\mathbf{curl} \mathbf{H} &= \mathbf{J}, \\ \frac{\partial \mathbf{B}}{\partial t} + \mathbf{curl} \mathbf{E} &= \mathbf{0}, \\ \mathbf{div} \mathbf{B} &= 0,\end{aligned}$$

where we have used standard notation in electromagnetism: \mathbf{E} is the electric field, \mathbf{B} is the magnetic induction, \mathbf{H} is the magnetic field and \mathbf{J} is the current density.

In order to get a closed system we need constitutive laws. We have the Ohm's law in conductors,

$$\mathbf{J} = \sigma \mathbf{E},$$

where σ is the electric conductivity and we consider the constitutive equation

$$\mathbf{B} = \mu_0 (\mathbf{H} + \mathbf{M}),$$

where \mathbf{M} is the magnetization and μ_0 is the magnetic permeability of the vacuum. In ferromagnetic and ferrimagnetic materials, where hysteresis phenomena may occur, the dependence between \mathbf{M} and \mathbf{H} exhibits a history-dependent behavior and must be represented by a suitable constitutive law accounting for hysteresis. We synthetically represent this dependence in the form

$$\mathbf{M} = \vec{\mathcal{F}}(\mathbf{H}),$$

where $\vec{\mathcal{F}}$ is a vector *hysteresis operator* (see [64, 63]). This dependence is nonlocal in time but pointwise in space. We notice that a real ferromagnetic material may exhibit rate dependent memory effects but they will not be considered in this analysis.

From the above equations we can easily obtain the following vector partial differential equation in conductors:

$$\frac{\partial \mathbf{B}}{\partial t} + \mathbf{curl} \left(\frac{1}{\sigma} \mathbf{curl} \mathbf{H} \right) = \mathbf{0}, \quad (5.9)$$

which has to be solved together with

$$\mathbf{div} \mathbf{B} = 0 \quad (5.10)$$

and the constitutive equation

$$\mathbf{B} = \mu_0 \left(\mathbf{H} + \vec{\mathcal{F}}(\mathbf{H}) \right). \quad (5.11)$$

5.3.1 Axisymmetric eddy current model

We restrict our attention to a case where source currents are axisymmetric and do not have azimuthal component so that the magnetic field is also axisymmetric with only non-null azimuthal component. Then, in order to reduce the dimension and thereby the computational effort, it is convenient to consider a cylindrical coordinate system (r, θ, z) . Let us denote \mathbf{e}_r , \mathbf{e}_θ and \mathbf{e}_z the corresponding unit vectors of the local orthonormal basis. We suppose that the computational three-dimensional (3D) domain $\tilde{\Omega}$ is cylindrical and that all fields are independent of the azimuth θ . Moreover, we assume that the magnetic field has only azimuthal component, i.e., it is of the form,

$$\mathbf{H}(r, z, t) = H(r, z, t) \mathbf{e}_\theta. \quad (5.12)$$

Then, for isotropic behavior, \mathbf{B} has only azimuthal component too:

$$\mathbf{B}(r, z, t) = B(r, z, t) \mathbf{e}_\theta. \quad (5.13)$$

Therefore a scalar hysteresis model may be used to describe the B-H relation (cf. (5.11)), that is,

$$B(r, z, t) = \mu_0 (H(r, z, t) + [\mathcal{F}(H)](r, z, t)), \quad (5.14)$$

where \mathcal{F} is a scalar hysteresis operator. Moreover, in order to get a well-posed problem (cf. Remark 5.2.1), we have to provide an appropriate “initial state” so that we can compute $[\mathcal{F}(H)]$ a.e. in $\Omega \times [0, T]$. Dependence of B on coordinates (r, z) permit us to deal with different materials in domain Ω . We notice that any field of the form (5.13) is divergence-free so (5.10) is automatically satisfied.

Accordingly, the current density is given by

$$\mathbf{J}(r, z, t) = \mathbf{curl} \mathbf{H}(r, z, t) = -\frac{\partial}{\partial z} H(r, z, t) \mathbf{e}_\theta + \frac{1}{r} \frac{\partial}{\partial r} (rH)(r, z, t) \mathbf{e}_z. \quad (5.15)$$

Then it is straightforward to see that equation (5.9) is equivalent to the following scalar PDE

$$\frac{\partial B}{\partial t} - \frac{\partial}{\partial r} \left(\frac{1}{\sigma r} \frac{\partial (rH)}{\partial r} \right) - \frac{\partial}{\partial z} \left(\frac{1}{\sigma} \frac{\partial H}{\partial z} \right) = 0.$$

This equation holds in a meridian section Ω of $\tilde{\Omega}$, for all time $t \in [0, T]$. In order to write a well-posed problem we add appropriate boundary conditions on the boundary $\Gamma := \partial\Omega$. In view of applications, throughout this chapter we consider alternatively the two following ones:

BC1 Dirichlet:

$$H(r, z, t) = g(r, z, t) \quad \text{on } \Gamma,$$

where g is a given function. For applications of this model, we refer for instance to [8, 9, 54], where a Dirichlet problem arises in the simulation of metallurgical electrodes. In this case, the Dirichlet boundary condition for the magnetic field can be obtained from the current intensity.

On the other hand, following [89] we consider the following non-local boundary condition

BC2 Magnetic flux:

$$\int_{\Omega} B(r, z, t) \, dr dz = b(t), \quad (5.16)$$

$$rH|_{\Gamma} = \psi(t) \quad \text{on } \Gamma, \quad (5.17)$$

where b is a given function but ψ is unknown. The above integral in (5.16) represents the magnetic flux $b(t)$ flowing through a meridian section Ω of the domain.

We notice that, in the problem of computing the eddy current losses in a toroidal laminated core surrounded by an infinitely thin coil, the boundary conditions are different depending on whether we know the current intensity or the voltage drop in the coil. For the former, a non-homogeneous Dirichlet condition naturally appears (see [62, 70]), whereas for the latter we have a magnetic flux condition (see [89]).

All together, the two resulting axisymmetric problems reads:

Problem 5.3.1 Find $H_D(r, z, t)$ and $B_D(r, z, t)$ such that

$$\frac{\partial B_D}{\partial t} - \frac{\partial}{\partial r} \left(\frac{1}{\sigma r} \frac{\partial(rH_D)}{\partial r} \right) - \frac{\partial}{\partial z} \left(\frac{1}{\sigma} \frac{\partial H_D}{\partial z} \right) = f \quad \text{in } \Omega \times (0, T), \quad (5.18)$$

$$B_D = \mu_0 (H_D + \mathcal{F}(H_D, \xi)) \quad \text{in } \Omega \times (0, T), \quad (5.19)$$

$$H_D = g \quad \text{on } \Gamma \times (0, T), \quad (5.20)$$

$$H_D|_{t=0} = H_{0D} \quad \text{in } \Omega. \quad (5.21)$$

Problem 5.3.2 Find $H_N(r, z, t)$, $B_N(r, z, t)$ and $\psi(t)$ such that

$$\frac{\partial B_N}{\partial t} - \frac{\partial}{\partial r} \left(\frac{1}{\sigma r} \frac{\partial(rH_N)}{\partial r} \right) - \frac{\partial}{\partial z} \left(\frac{1}{\sigma} \frac{\partial H_N}{\partial z} \right) = f \quad \text{in } \Omega \times (0, T), \quad (5.22)$$

$$B_N = \mu_0 (H_N + \mathcal{F}(H_N, \xi)) \quad \text{in } \Omega \times (0, T), \quad (5.23)$$

$$rH_N(r, z, t) = \psi(t) \quad \text{on } \Gamma \times (0, T), \quad (5.24)$$

$$\int_{\Omega} B_N(r, z, t) \, dr dz = b(t) \quad \text{in } (0, T), \quad (5.25)$$

$$H_N|_{t=0} = H_{0N} \quad \text{in } \Omega, \quad (5.26)$$

where $\sigma(r, z, t)$, $f(r, z, t)$, $g(r, z, t)$, $b(t)$, $\xi(r, z)$, $H_{0D}(r, z)$ and $H_{0N}(r, z)$ are given functions.

Remark 5.3.1 For the sake of generality, in (5.18) and (5.22) we have considered a general right-hand side f . Moreover, we consider a space and time dependent electrical conductivity σ because in practical applications it is a function of temperature which, in its turn, is a time dependent field.

Remark 5.3.2 From a practical point of view, a physically realistic initial condition (cf. (5.21) and (5.26)) is the so called demagnetized or virgin state of the material, namely, $(B, H)|_{t=0} = (0, 0)$. The demagnetized state can be achieved, for instance, by heating the material above its Curie temperature. Another method that returns the material to a nearly demagnetized state is to apply a magnetic field with a direction that changes back and forth while at the same time the field amplitude reduces to zero (see Figure 5.5).

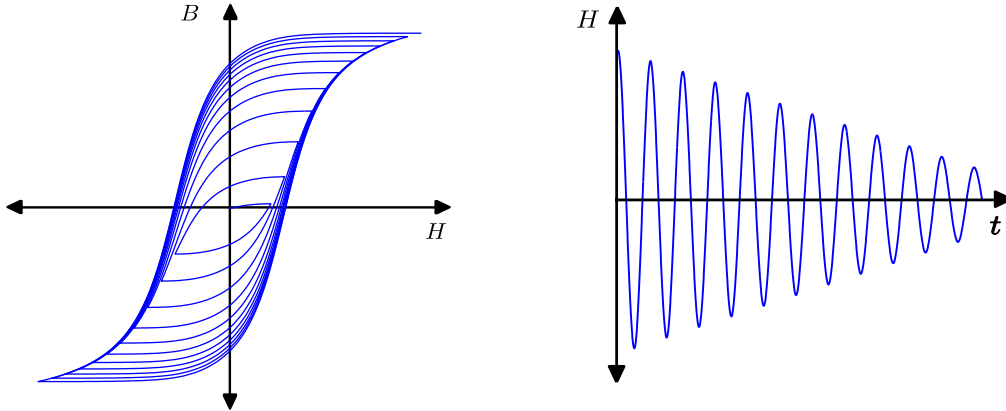


Figure 5.5: B-H curve (left) and magnetic field (right).

5.4 Mathematical analysis

In this section, we derive weak formulations for Problems 5.3.1 and 5.3.2, and prove that they are well posed. The techniques used for this purpose are based on [95, Chapter IX], where the existence of solution to a non-axisymmetric version of Problem 5.4.1 with homogeneous Dirichlet condition is proved (for a homogeneous Neumann condition we refer to [43]). The presence of time dependent coefficients, the different source terms (cf. (5.20) and (5.25)) and the symmetry assumption brings some technical complication to the analysis with respect to previous works on the subject. In particular, (5.24)-(5.25) yield a nonlinear parabolic term with a non-classical boundary condition. Such a condition and a time dependent conductivity (cf. Remark 5.3.1), lead us to deal with a time dependent bilinear form which, instead of being elliptic, satisfies a Gårding's inequality. On the other hand, in order to deal with condition (5.20), we have to introduce a *lifting* of the boundary data.

Firstly, we introduce some preliminary results to be used along the chapter.

5.4.1 Functional spaces and preliminary results

We define appropriate weighted Sobolev spaces that will be used for the mathematical analysis of the problem and recall some of their properties. For the sake of simplicity, in this paragraph the partial derivatives will be denoted by ∂_r and ∂_z .

Let $\Omega \subset \{(r, z) \in \mathbb{R}^2 : r \geq 0\}$ be a bounded connected two-dimensional open set with a connected Lipschitz boundary Γ . Let $L_r^2(\Omega)$ denote the weighted Lebesgue space of all measurable functions u defined in Ω for which

$$\|u\|_{L_r^2(\Omega)}^2 := \int_{\Omega} |u|^2 r \, dr dz < \infty.$$

The weighted Sobolev space $H_r^1(\Omega)$ consist of all functions in $L_r^2(\Omega)$ whose first derivatives are also in $L_r^2(\Omega)$. We define the norms and semi-norms in the standard way; in particular,

$$|u|_{H_r^1(\Omega)}^2 := \int_{\Omega} (|\partial_r u|^2 + |\partial_z u|^2) r \, dr dz.$$

Let $\tilde{H}_r^1(\Omega) := H_r^1(\Omega) \cap L_{1/r}^2(\Omega)$, where $L_{1/r}^2(\Omega)$ denotes the set of all measurable functions u defined in Ω for which

$$\|u\|_{L_{1/r}^2(\Omega)}^2 := \int_{\Omega} \frac{|u|^2}{r} \, dr dz < \infty.$$

$\tilde{H}_r^1(\Omega)$ is a Hilbert space with the norm

$$\|u\|_{\tilde{H}_r^1(\Omega)}^2 := \|u\|_{H_r^1(\Omega)}^2 + \|u\|_{L_{1/r}^2(\Omega)}^2.$$

We recall from [46, Section 3] that functions in $\tilde{H}_r^1(\Omega)$ have traces on Γ . We denote

$$\tilde{H}_r^{1/2}(\Gamma) := \left\{ v|_{\Gamma} : v \in \tilde{H}_r^1(\Omega) \right\}$$

endowed with the norm

$$\|g\|_{\tilde{\mathbf{H}}_r^{1/2}(\Gamma)} := \inf\{\|v\|_{\tilde{\mathbf{H}}_r^1(\Omega)} : v \in \tilde{\mathbf{H}}_r^1(\Omega), v|_\Gamma = g\}$$

which makes the trace operator $v \rightarrow v|_\Gamma$ continuous.

Also, let us introduce the function space $\hat{\mathbf{H}}_r^1(\Omega)$ defined by

$$\hat{\mathbf{H}}_r^1(\Omega) : \{u \in \mathbf{L}_r^2(\Omega) : \partial_r(ru) \in \mathbf{L}_{1/r}^2(\Omega), \partial_z u \in \mathbf{L}_r^2(\Omega)\}$$

which is a Hilbert space with the norm

$$\|u\|_{\hat{\mathbf{H}}_r^1(\Omega)}^2 := \left(\|u\|_{\mathbf{L}_r^2(\Omega)}^2 + \|\partial_r(ru)\|_{\mathbf{L}_{1/r}^2(\Omega)}^2 + \|\partial_z u\|_{\mathbf{L}_r^2(\Omega)}^2 \right)^{1/2}.$$

Clearly $\tilde{\mathbf{H}}_r^1(\Omega) \subset \hat{\mathbf{H}}_r^1(\Omega)$.

Finally, given a Banach space Q , we introduce $\mathbf{L}_r^2(\Omega; Q)$ the space of all function $u : \Omega \rightarrow Q$ such that

$$\|u\|_{\mathbf{L}_r^2(\Omega; Q)} := \left(\int_\Omega \|u(r, z)\|_Q^2 r \, dr dz \right)^{1/2} < \infty.$$

Remark 5.4.1 For Ω being a meridian section of a 3D axisymmetric domain $\tilde{\Omega}$, the space $\hat{\mathbf{H}}_r^1(\Omega)$ can be considered as an axisymmetric version of the 3D space $\mathbf{H}(\mathbf{curl}, \tilde{\Omega}) := \{\mathbf{u} \in \mathbf{L}^2(\tilde{\Omega}) : \mathbf{curl} \mathbf{u} \in \mathbf{L}^2(\tilde{\Omega})\}$, with $\mathbf{L}^2(\tilde{\Omega}) := \mathbf{L}^2(\tilde{\Omega})^3$. That is to say, it is easy to see that $G(r, z) \in \hat{\mathbf{H}}_r^1(\Omega)$ if and only if $\mathbf{G}(r, z, \theta) = G(r, z)\mathbf{e}_\theta(\theta) \in \mathbf{H}(\mathbf{curl}, \tilde{\Omega})$. Similarly, we deduce that $G(r, z) \in \tilde{\mathbf{H}}_r^1(\Omega)$ if and only if $\mathbf{G}(r, z, \theta) = G(r, z)\mathbf{e}_\theta(\theta) \in \mathbf{H}^1(\tilde{\Omega}) := \mathbf{H}^1(\tilde{\Omega})^3$.

Moreover, given \mathbf{G} of the form $\mathbf{G}(r, z, \theta) = G(r, z)\mathbf{e}_\theta$, then $\text{div} \mathbf{G} = 0$ and $\mathbf{G} \cdot \mathbf{n} = 0$ on $\partial\tilde{\Omega}$, i.e., \mathbf{G} belong to $\mathbf{H}_0(\text{div}^0; \tilde{\Omega}) := \{\mathbf{u} \in \mathbf{L}^2(\tilde{\Omega}) : \text{div} \mathbf{u} = 0, \mathbf{u} \cdot \mathbf{n} = 0\}$. Thus $\hat{\mathbf{H}}_r^1(\Omega)$ can be identified with a closed subspace of $\mathbf{H}(\mathbf{curl}, \tilde{\Omega}) \cap \mathbf{H}_0(\text{div}^0; \tilde{\Omega})$ continuously included in $\mathbf{H}^s(\tilde{\Omega})$ for $s > 1/2$, which, in its turn, is compactly included in $\mathbf{L}^2(\tilde{\Omega})$ (see [45, Theorem I.1.3]). Then,

$$\hat{\mathbf{H}}_r^1(\Omega) \subset \mathbf{L}_r^2(\Omega)$$

with compact inclusion and we deduce that $\tilde{\mathbf{H}}_r^1(\Omega)$ is also compactly included in $\mathbf{L}_r^2(\Omega)$.

5.4.2 Weak formulation

In order to build a weak formulation of the above problems, let us define the closed subspaces of $\tilde{\mathbf{H}}_r^1(\Omega)$ and $\hat{\mathbf{H}}_r^1(\Omega)$:

$$\mathcal{U} := \left\{ G \in \tilde{\mathbf{H}}_r^1(\Omega) : G|_\Gamma = 0 \right\},$$

$$\mathcal{W} := \left\{ G \in \hat{\mathbf{H}}_r^1(\Omega) : rG|_\Gamma \text{ is constant} \right\}.$$

Hence, for each $t \in [0, T]$ a weak formulation of Problem 5.3.1 is given by:

Problem 5.4.1 Given $g \in \mathbf{H}^2(0, T; \widetilde{\mathbf{H}}_r^{1/2}(\Gamma))$, $f \in \mathbf{H}^1(0, T; \mathcal{U}')$, $H_{0D} \in \mathbf{L}_r^2(\Omega)$, and $\xi \in Y$ a.e. in Ω , find $H_D \in \mathbf{L}^2(0, T; \widetilde{\mathbf{H}}_r^1(\Omega)) \cap \mathbf{L}^\infty(0, T; \mathbf{L}_r^2(\Omega))$ and $B_D \in \mathbf{L}^2(0, T; \mathbf{L}_r^2(\Omega))$ with $\partial_t B_D \in \mathbf{L}^2(0, T; \mathcal{U}')$, such that

$$\begin{aligned} \left\langle \frac{\partial B_D}{\partial t}, G \right\rangle_{\mathcal{U}, \mathcal{U}'} + \int_{\Omega} \frac{1}{\sigma r} \left(\frac{\partial(rH_D)}{\partial r} \frac{\partial(rG)}{\partial r} + \frac{\partial(rH_D)}{\partial z} \frac{\partial(rG)}{\partial z} \right) dr dz &= \langle f, G \rangle_{\mathcal{U}, \mathcal{U}'} \\ \forall G \in \mathcal{U}, \quad \text{a.e. in } [0, T], \\ B_D &= \mu_0 (H_D + \mathcal{F}(H_D, \xi)) \quad \text{in } \Omega \times (0, T), \\ H_D &= g \quad \text{on } \Gamma \times (0, T), \\ H_D|_{t=0} &= H_{0D} \quad \text{in } \Omega. \end{aligned}$$

We use the classical notation of the duality product $\langle \cdot, \cdot \rangle_{\mathcal{U}, \mathcal{U}'}$ between \mathcal{U} and its dual space \mathcal{U}' .

Before stating a weak formulation of Problem 5.3.2, we notice that if the boundary of Ω intersect the symmetry axis ($r = 0$), then $\psi(t)$ should be identically zero because r vanishes there. In that case, (5.24) would become a homogeneous Dirichlet boundary condition and Problem 5.3.2 without condition (5.25) would be exactly Problem 5.3.1 with $g = 0$, so there is no reason for (5.25) to hold for a given $b(t)$. However, this does not happen in the application that motivates this problem in which the domain is well separated from the symmetry axis (see [89]). This is the reason why, from now on, we will assume that

$$\inf\{r > 0 : (r, z) \in \Omega\} > 0 \quad (5.27)$$

and, hence, $\mathbf{L}_r^2(\Omega)$ and $\mathbf{L}_{1/r}^2(\Omega)$ are both identical to $\mathbf{L}^2(\Omega)$. Similarly, $\widetilde{\mathbf{H}}_r^1(\Omega)$ is identical to $\mathbf{H}^1(\Omega)$.

Straightforward computations lead to the following weak formulation for Problem 5.3.2 (see Chapter 3):

Problem 5.4.2 Given $b \in \mathbf{H}^2(0, T)$, $f \in \mathbf{H}^1(0, T; \mathcal{W}')$, $H_{0N} \in \mathbf{L}_r^2(\Omega)$ and $\xi \in Y$ a.e. in Ω , find $H_N \in \mathbf{H}^1(0, T; \mathbf{L}_r^2(\Omega)) \cap \mathbf{L}^\infty(0, T; \mathcal{W})$ and $B_N \in \mathbf{L}^2(0, T; \mathbf{L}_r^2(\Omega))$ with $\partial_t B_N \in \mathbf{L}^2(0, T; \mathcal{W}')$, such that

$$\begin{aligned} \left\langle \frac{\partial B_N}{\partial t}, G \right\rangle_{\mathcal{W}, \mathcal{W}'} + \int_{\Omega} \frac{1}{\sigma r} \left(\frac{\partial(rH_N)}{\partial r} \frac{\partial(rG)}{\partial r} + \frac{\partial(rH_N)}{\partial z} \frac{\partial(rG)}{\partial r} \right) dr dz &= \langle f, G \rangle_{\mathcal{W}, \mathcal{W}'} \\ + (b'(t) - \langle f, r^{-1} \rangle_{\mathcal{W}, \mathcal{W}'}) (rG)|_{\Gamma} \quad \forall G \in \mathcal{W}, \quad \text{a.e. in } [0, T], \\ B_N &= \mu_0 (H_N + \mathcal{F}(H_N, \xi)) \quad \text{in } \Omega \times (0, T), \\ H_N|_{t=0} &= H_{0N} \quad \text{in } \Omega. \end{aligned}$$

We introduce the following assumptions that will be used to prove the existence of a solution to problem 5.4.1 and problem 5.4.2:

H.1 $\mathcal{F} : \mathbf{L}_r^2(\Omega; C([0, T]) \times Y) \rightarrow \mathbf{L}_r^2(\Omega; C([0, T]))$ is causal, strongly continuous and piecewise monotone (cf. (5.6)–(5.8)). Also we assume that \mathcal{F} is affinely bounded, namely,

$$\begin{aligned} \exists L_{\mathcal{F}} > 0, \exists \tau \in \mathbf{L}_r^2(\Omega) : \forall v \in \mathbf{L}_r^2(\Omega; C([0, T])), \\ \|\mathcal{F}(v, \xi)\|(r, z, \cdot)_{C([0, T])} \leq L_{\mathcal{F}} \|v(r, z, \cdot)\|_{C([0, T])} + \tau(r, z) \quad \text{a.e. in } \Omega. \end{aligned} \quad (5.28)$$

H.2 $\sigma : (0, T) \times \Omega \rightarrow \mathbb{R}$ belongs to $W^{1,\infty}(0, T; L^\infty(\Omega))$ and there exists non-negative constants σ_* and σ^* such that

$$\sigma_* \leq \sigma(r, z, t) \leq \sigma^* \quad \text{a.e. in } (0, T) \times \Omega.$$

H.3 The initial functions H_{0N} and H_{0D} belong to \mathcal{W} and $\tilde{\mathbf{H}}_r^1(\Omega)$, respectively.

We define the initial conditions of the hysteresis operator given by $W_{0N} := \mathcal{F}(H_N, \xi)(0)$ and $W_{0D} := \mathcal{F}(H_D, \xi)(0)$. Clearly, because of H.1 and H.3 it follows that $W_{0N}, W_{0D} \in L_r^2(\Omega)$.

Also, for each $t \in [0, T]$, let us denote by $a_t(\cdot, \cdot)$ the bilinear form defined by

$$a_t(G_1, G_2) := \int_{\Omega} \frac{1}{\sigma(\cdot, t)} \left(\frac{1}{r} \frac{\partial(rG_1)}{\partial r} \frac{1}{r} \frac{\partial(rG_2)}{\partial r} + \frac{\partial G_1}{\partial z} \frac{\partial G_2}{\partial z} \right) r \, dr dz \quad G_1, G_2 \in \hat{\mathbf{H}}_r^1(\Omega). \quad (5.29)$$

From H.2 we obtain the following result.

Lemma 5.4.1 *The bilinear forms $a_t : \hat{\mathbf{H}}_r^1(\Omega) \times \hat{\mathbf{H}}_r^1(\Omega) \rightarrow \mathbb{R}$, $t \in [0, T]$, are continuous uniformly in t and they satisfy the Gårding's inequality*

$$a_t(G, G) + \lambda \|G\|_{L_r^2(\Omega)}^2 \geq \gamma \|G\|_{\hat{\mathbf{H}}_r^1(\Omega)}^2 \quad \forall G \in \hat{\mathbf{H}}_r^1(\Omega), \quad (5.30)$$

with $\lambda = \gamma = 1/\sigma^*$. Moreover, there exists $\gamma_u > 0$ such that

$$a_t(G, G) \geq \gamma_u \|G\|_{\hat{\mathbf{H}}_r^1(\Omega)}^2 \quad \forall G \in \mathcal{U}. \quad (5.31)$$

Proof. The continuity and (5.30) follow directly from the definition of $a_t(\cdot, \cdot)$ and the $\hat{\mathbf{H}}_r^1(\Omega)$ -norm, and from the boundedness assumption on σ (cf. H.2), whereas, (5.31) follows by easy calculations (see Lemma 4.3.1, Chapter 4). \square

Finally, we introduce the linear operator $A(t) : \hat{\mathbf{H}}_r^1(\Omega) \rightarrow \hat{\mathbf{H}}_r^1(\Omega)'$ induced by $a_t(\cdot, \cdot)$. Clearly $A(t)$ is linear and continuous, namely, it belongs to $\mathcal{L}(\hat{\mathbf{H}}_r^1(\Omega), \hat{\mathbf{H}}_r^1(\Omega)')$ for all $t \in [0, T]$.

Remark 5.4.2 *From the definition of $a_t(\cdot, \cdot)$, it follows that $a_t : \tilde{\mathbf{H}}_r^1(\Omega) \times \tilde{\mathbf{H}}_r^1(\Omega) \rightarrow \mathbb{R}$, $t \in [0, T]$, are continuous uniformly in t , and therefore, the linear operator $A(t) : \tilde{\mathbf{H}}_r^1(\Omega) \rightarrow \tilde{\mathbf{H}}_r^1(\Omega)'$ belongs to $\mathcal{L}(\tilde{\mathbf{H}}_r^1(\Omega), \tilde{\mathbf{H}}_r^1(\Omega)')$ for all $t \in [0, T]$.*

The next two sections are devote to study the existence of solution to Problems 5.4.1 and 5.4.2. The analysis is based on an implicit time discretization scheme. This approximation procedure is often used in the analysis of equations that include a memory operator as at any time-step we solve a stationary problem in which this operator is reduced to a nonlinear mapping. We apply this technique to \mathcal{F} . Then, the proof of an existence result is carried out through three different steps: existence of solution to the time discretization scheme, a priori estimates and passage to the limit by using compactness. From now on, when there is no possibility of confusion we will omit to write the dependence on the “initial state”. Thus, we will write $\mathcal{F}(u)$ instead of $\mathcal{F}(u, \xi)$ and so on.

5.4.3 Existence of solution. Magnetic flux problem

In this section we will prove that, under certain assumptions, there exist (H_N, B_N) solution of Problem 5.4.2.

Time discretization

Let us fix $m \in \mathbb{N}$ and set $\Delta t := T/m$. Now, for $n = 1, \dots, m$, we define $t^n := n\Delta t$, $b^n := b(t^n)$, $\sigma^n(r, z) := \sigma(r, z, t^n)$, $f^n := f(t^n)$ and $A(t^n) := A^n$. Notation $\bar{\partial}z^n$ refers to the difference quotient

$$\bar{\partial}z^n := \frac{z^n - z^{n-1}}{\Delta t}.$$

A time discretization of Problem 5.4.2 based on backward Euler's scheme reads as follows:

For $n = 1, \dots, m$, find $H_N^n \in \mathcal{W}$ and $W_N^n \in L_r^2(\Omega)$ satisfying

$$\mu_0 \bar{\partial}H_N^n + \mu_0 \bar{\partial}W_N^n + A^n H_N^n = R_N^n \quad \text{in } \mathcal{W}', \quad n = 1, \dots, m, \quad (5.32)$$

$$W_N^n = [\mathcal{F}(H_{N\Delta t^n}, \xi)](t^n), \quad n = 1, \dots, m, \quad (5.33)$$

$$H_N^0 = H_{0N}, \quad W_N^0 = W_{0N} \quad \text{in } \Omega, \quad (5.34)$$

where $H_{N\Delta t^n} : [0, t^n] \rightarrow \mathcal{W}$ is the piecewise linear in time interpolant of $\{H_N^i\}_{i=0}^n$ given by

$$H_{N\Delta t^n}(t^0) := H_{0N}; \quad (5.35)$$

$$H_{N\Delta t^n}(t) := H_N^{i-1} + (t - t^{i-1}) \bar{\partial}H_N^i, \quad t \in (t^{i-1}, t^i], \quad i = 1, \dots, n, \quad (5.36)$$

and

$$\langle R_N^n, G \rangle_{\mathcal{W}, \mathcal{W}'} := \langle f^n, G \rangle_{\mathcal{W}, \mathcal{W}'} + (\bar{\partial}b^n - \langle f^n, r^{-1} \rangle_{\mathcal{W}, \mathcal{W}'}) (rG) |_{\Gamma}.$$

We notice that, since for $n \in \{1, \dots, m\}$ we already know H_N^1, \dots, H_N^{n-1} , then $W_N^n(\cdot) = [\mathcal{F}(H_{N\Delta t^n}, \xi)](\cdot, t^n)$ depends only on $H_{N\Delta t^n}(\cdot, t)|_{[0, t^{n-1}]}$, which is known, and on H_N^n , which must be determined.

In order to analyze the discrete problem, we define $F^n : \Omega \times \mathbb{R} \rightarrow \mathbb{R}$ as follows: given $s \in \mathbb{R}$

$$F^n(r, z, s) := [\mathcal{F}(U_{\Delta t}^s, \xi)](r, z, t^n) \quad \text{a.e. in } \Omega,$$

with $U_{\Delta t}^s$ the piecewise linear in time function such that $U_{\Delta t}^s(r, z, t^l) = H_N^l(r, z)$, $l = 0, \dots, n-1$ and $U_{\Delta t}^s(r, z, t^n) = s$. This allows us to introduce an operator $\mathbb{F}^n : L_r^2(\Omega) \rightarrow L_r^2(\Omega)$ by $\mathbb{F}^n(G)(\cdot) := F^n(\cdot, G(\cdot))$ for all $G \in L_r^2(\Omega)$. The following lemma gives us properties of \mathbb{F}^n that will be used in the sequel.

Lemma 5.4.2 For all $n = 1, \dots, m$, $\mathbb{F}^n : L_r^2(\Omega) \rightarrow L_r^2(\Omega)$ is a continuous and non-decreasing operator. Moreover,

$$\int_{\Omega} \mathbb{F}^n(G) G r \, dr dz \geq -C_1 \|G\|_{L_r^2(\Omega)} - C_2 \quad \forall G \in L_r^2(\Omega), \quad (5.37)$$

where $C_1, C_2 > 0$ depend on $\{H_N^l\}_{l=0}^{n-1}$ but are independent of G .

Proof. The continuity of \mathbb{F}^n follows from H.1 (cf. (5.7) and (5.28)) and the Lebesgue dominated convergence theorem. Indeed, let $\{v_n\}_{n \in \mathbb{N}} \in L_r^2(\Omega)$ and $v \in L_r^2(\Omega)$ be such that $v_n \rightarrow v$ in $L_r^2(\Omega)$. From the strongly continuous property of \mathcal{F} it follows that $\mathbb{F}^n(v) \rightarrow \mathbb{F}^n(v)$ a.e. in Ω , then the

convergence in $L_r^2(\Omega)$ follows from the affinely bounded assumption (5.28) and the Lebesgue dominated convergence theorem. To prove the non-decreasing property, we consider that \mathcal{F} is piecewise monotone (cf. (5.8)). Let $u, v \in L_r^2(\Omega)$. We define the piecewise linear functions $U_{\Delta t} : [0, t^n] \rightarrow L_r^2(\Omega)$ and $V_{\Delta t} : [0, t^n] \rightarrow L_r^2(\Omega)$ satisfying

$$U_{\Delta t}(r, z, t^i) = V_{\Delta t}(r, z, t^i) = H_N^i(r, z) \quad \text{for } i = 0, \dots, n-1$$

and

$$U_{\Delta t}(r, z, t^n) = u(r, z), \quad V_{\Delta t}(r, z, t^n) = v(r, z),$$

a.e. $(r, z) \in \Omega$. From the definition of \mathbb{F}^n we have:

$$\mathbb{F}^n(u)(r, z) = [\mathcal{F}(U_{\Delta t}, \xi)](r, z, t^n) \quad \text{and} \quad \mathbb{F}^n(v)(r, z) = [\mathcal{F}(V_{\Delta t}, \xi)](r, z, t^n).$$

Now, let $(r, z) \in \Omega$ and suppose that

$$H_N^{n-1}(r, z) \leq v(r, z) \leq u(r, z),$$

then, there exist $t^* \in [t^{n-1}, t^n]$ such that $U_{\Delta t}(r, z, t^*) = v(r, z)$ and since \mathcal{F} is rate independent we have that $\mathbb{F}^n(v)(r, z) = [\mathcal{F}(V_{\Delta t})](r, z, t^n) = [\mathcal{F}(U_{\Delta t})](r, z, t^*)$. Therefore

$$\begin{aligned} & (\mathbb{F}^n(u)(r, z) - \mathbb{F}^n(v)(r, z)) (u(r, z) - v(r, z)) \\ &= ([\mathcal{F}(U_{\Delta t})](r, z, t^n) - [\mathcal{F}(U_{\Delta t})](r, z, t^*)) ((U_{\Delta t}(r, z, t^n) - U_{\Delta t}(r, z, t^*))) > 0. \end{aligned}$$

The same inequality holds if $v(r, z) \leq u(r, z) \leq H_N^{n-1}(r, z)$.

Otherwise, if we suppose

$$v(r, z) \leq H_N^{n-1}(r, z) \leq u(r, z), \tag{5.38}$$

then

$$\begin{aligned} & (\mathbb{F}^n(u)(r, z) - \mathbb{F}^n(v)(r, z)) (u(r, z) - v(r, z)) \\ &= ([\mathcal{F}(U_{\Delta t})](r, z, t^n) - [\mathcal{F}(U_{\Delta t})](r, z, t^{n-1})) (U_{\Delta t}(r, z, t^n) - V_{\Delta t}(r, z, t^n)) \\ &\quad + ([\mathcal{F}(V_{\Delta t})](r, z, t^{n-1}) - [\mathcal{F}(V_{\Delta t})](r, z, t^n)) (U_{\Delta t}(r, z, t^n) - V_{\Delta t}(r, z, t^n)). \end{aligned}$$

Then, since \mathcal{F} is piecewise monotone, from (5.38) we have

$$([\mathcal{F}(U_{\Delta t})](r, z, t^n) - [\mathcal{F}(U_{\Delta t})](r, z, t^{n-1})) > 0$$

and also $([\mathcal{F}(V_{\Delta t})](r, z, t^{n-1}) - [\mathcal{F}(V_{\Delta t})](r, z, t^n)) > 0$. Then,

$$(\mathbb{F}^n(u)(r, z) - \mathbb{F}^n(v)(r, z)) (u(r, z) - v(r, z)) > 0,$$

and we conclude the non-decreasing property of \mathbb{F}^n . On the other hand, to prove (5.37) we first notice that from (5.28) it follows that

$$|\mathbb{F}^n(G)(r, z)| \leq L_{\mathcal{F}} \max\{|H_N^0(r, z)|, |H_N^1(r, z)|, \dots, |H_N^{n-1}(r, z)|, |G(r, z)|\} + \tau(r, z) \quad \text{a.e. in } \Omega. \tag{5.39}$$

Moreover, from (5.8) and (5.33) we have

$$(\mathbb{F}^n(G)(r, z) - W_N^{n-1}(r, z)) (G(r, z) - H_N^{n-1}(r, z)) \geq 0 \quad \text{a.e. in } \Omega. \quad (5.40)$$

Therefore, (5.37) follows from (5.39), (5.40) and the Cauchy-Schwartz inequality. \square

The existence and uniqueness of a weak solution at each time step is guaranteed by the following lemma.

Lemma 5.4.3 *There exists a uniquely determined (H_N^n, W_N^n) solving (5.32)–(5.34) for any $n = 1, \dots, m$.*

Proof. First, we rewrite (5.32)–(5.34) as follows:

Find $H_N^n \in \mathcal{W}$ for $n = 1, \dots, m$ such that

$$\begin{aligned} Z(H_N^n) &:= \mu_0 H_N^n + \mu_0 \mathbb{F}^n(H_N^n) + \Delta t A^n H_N^n = \widehat{R}_N^n && \text{in } \mathcal{W}', \\ \widehat{F}^0(H_N^0) &= W_{0N} && \text{in } \Omega, \end{aligned}$$

where $\widehat{R}_N^n := \Delta t R_N^n + \mu_0 H_N^{n-1} + \mu_0 \mathbb{F}^{n-1}(H_N^{n-1})$. From Lemmas 5.4.1 (cf. (5.30)) and 5.4.2 we have that $Z : \mathcal{W} \rightarrow \mathcal{W}'$ is strongly monotone and continuous. Moreover, from (5.30) and (5.37) it follows that Z is coercive, more precisely,

$$\lim_{\|G\|_{\widehat{H}_T^1(\Omega)} \rightarrow \infty} \frac{\langle Z(G), G \rangle_{\mathcal{W}, \mathcal{W}'}}{\|G\|_{\widehat{H}_T^1(\Omega)}} = +\infty.$$

Hence, equation $Z(H_N^n) = \widehat{R}_N^n$ has a unique solution for $n = 1, \dots, m$ (see, for instance, [78, Theorem 2.18]). \square

A priori estimates

The aim of this section is to prove an a priori estimate for the solution of (5.32)–(5.34).

Here and thereafter C and c , with or without subscripts, will be used for positive constants not necessarily the same at each occurrence, but always independent of the time-step Δt .

Lemma 5.4.4 *There exists $C > 0$ such that, for all $l = 1, \dots, m$*

$$\Delta t \sum_{n=1}^l \|\bar{\partial} W_N^n\|_{\mathcal{W}'}^2 + \|H_N^l\|_{\widehat{H}_T^1(\Omega)}^2 + \Delta t \sum_{n=1}^l \|\bar{\partial} H_N^n\|_{L_T^2(\Omega)}^2 \leq C.$$

Proof. Let us multiply (5.32) by $(H_N^n - H_N^{n-1})$. For $n = 1, \dots, m$, we obtain

$$\begin{aligned} \mu_0 \Delta t \left\| \frac{H_N^n - H_N^{n-1}}{\Delta t} \right\|_{L_T^2(\Omega)}^2 &+ \int_{\Omega} \frac{\mu_0}{\Delta t} (W_N^n - W_N^{n-1})(H_N^n - H_N^{n-1}) + \langle A^n H_N^n, H_N^n - H_N^{n-1} \rangle_{\mathcal{W}, \mathcal{W}'} \\ &= \langle f^n, H_N^n - H_N^{n-1} \rangle_{\mathcal{W}, \mathcal{W}'} + (\bar{\partial} b^n - \langle f^n, r^{-1} \rangle_{\mathcal{W}, \mathcal{W}'}) (r H_N^n - r H_N^{n-1})|_{\Gamma}. \end{aligned} \quad (5.41)$$

First, we estimate the terms on the left hand side. From the piecewise monotonicity of \mathcal{F} (cf. (5.8)) we have that

$$\int_{\Omega} \frac{1}{\Delta t} (W_N^n - W_N^{n-1})(H_N^n - H_N^{n-1}) \, dr dz \geq 0. \quad (5.42)$$

On the other hand, in order to estimate the last term on the left-hand side of (5.41) we use the identity $2(p-q)p = p^2 + (p-q)^2 - q^2$ to obtain that

$$\begin{aligned} 2\langle A^n H_N^n, H_N^n - H_N^{n-1} \rangle_{\mathcal{W}, \mathcal{W}'} &\geq \langle A^n H_N^n, H_N^n \rangle_{\mathcal{W}, \mathcal{W}'} - \langle A^n H_N^{n-1}, H_N^{n-1} \rangle_{\mathcal{W}, \mathcal{W}'} \\ &= \langle A^n H_N^n, H_N^n \rangle_{\mathcal{W}, \mathcal{W}'} - \langle A^{n-1} H_N^{n-1}, H_N^{n-1} \rangle_{\mathcal{W}, \mathcal{W}'} + \langle (A^{n-1} - A^n) H_N^{n-1}, H_N^{n-1} \rangle_{\mathcal{W}, \mathcal{W}'} \end{aligned} \quad (5.43)$$

where

$$|\langle (A^{n-1} - A^n) H_N^{n-1}, H_N^{n-1} \rangle_{\mathcal{W}, \mathcal{W}'}| \leq C_{\sigma} \|\partial_t \sigma\|_{L^{\infty}(0, T; L^{\infty}(\Omega))} \Delta t \|H_N^{n-1}\|_{\hat{H}_r^1(\Omega)}^2. \quad (5.44)$$

Summing up (5.41) for $n = 1, \dots, l$ with $l \in \{1, \dots, m\}$, from (5.42)–(5.44) we obtain

$$\begin{aligned} &\sum_{n=1}^l \mu_0 \Delta t \|\bar{\partial} H_N^n\|_{L_r^2(\Omega)}^2 + \frac{1}{2} \langle A^l H_N^l, H_N^l \rangle_{\mathcal{W}, \mathcal{W}'} \\ &\leq \frac{1}{2} \langle A^0 H_{0N}, H_{0N} \rangle_{\mathcal{W}, \mathcal{W}'} + \sum_{n=1}^l C_{\sigma} \|\partial_t \sigma\|_{L^{\infty}(0, T; L^{\infty}(\Omega))} \Delta t \|H_N^{n-1}\|_{\hat{H}_r^1(\Omega)}^2 \\ &\quad + \sum_{n=1}^l \langle f^n, H_N^n - H_N^{n-1} \rangle_{\mathcal{W}, \mathcal{W}'} + \sum_{n=1}^l (\bar{\partial} b^n - \langle f^n, r^{-1} \rangle_{\mathcal{W}, \mathcal{W}'}) (r H_N^n - r H_N^{n-1})|_{\Gamma}. \end{aligned} \quad (5.45)$$

Next, we estimate the last two terms on the right-hand side of (5.45). By summation by parts, Young's inequality and inequality $(rG)|_{\Gamma} \leq C \|G\|_{\hat{H}_r^1(\Omega)}$, $\forall G \in \mathcal{W}$, we have that

$$\begin{aligned} &\left| \sum_{n=1}^l (\bar{\partial} b^n - \langle f^n, r^{-1} \rangle_{\mathcal{W}, \mathcal{W}'}) (r H_N^n - r H_N^{n-1})|_{\Gamma} \right| \\ &= \left| (\bar{\partial} b^l - \langle f^l, r^{-1} \rangle_{\mathcal{W}, \mathcal{W}'}) (r H_N^l)|_{\Gamma} - (\bar{\partial} b^1 - \langle f^1, r^{-1} \rangle_{\mathcal{W}, \mathcal{W}'}) (r H_{0N})|_{\Gamma} \right. \\ &\quad \left. - \sum_{n=1}^{l-1} (\bar{\partial} b^{n+1} - \bar{\partial} b^n - \langle f^{n+1} - f^n, r^{-1} \rangle_{\mathcal{W}, \mathcal{W}'}) (r H_N^n)|_{\Gamma} \right| \\ &\leq C_{\varepsilon} \left\{ \|b\|_{\mathbb{H}^2(0, T)}^2 + \|f\|_{\mathbb{H}^1(0, T; \mathcal{W}')}^2 + \Delta t \sum_{n=1}^{l-1} \left| \frac{\bar{\partial} b^{n+1} - \bar{\partial} b^n}{\Delta t} \right|^2 + \Delta t \sum_{n=1}^{l-1} \|\bar{\partial} f^{n+1}\|_{\mathcal{W}'}^2 \right\} \\ &\quad + \varepsilon \|H_N^l\|_{\hat{H}_r^1(\Omega)}^2 + \Delta t \sum_{n=1}^{l-1} \|H_N^n\|_{\hat{H}_r^1(\Omega)}^2 + \|H_{0N}\|_{\hat{H}_r^1(\Omega)}^2. \end{aligned} \quad (5.46)$$

In a similar way,

$$\left| \sum_{n=1}^l \langle f^n, H_N^n - H_N^{n-1} \rangle_{\mathcal{W}, \mathcal{W}'} \right| \leq C_\varepsilon \|f\|_{\mathbb{H}^1(0, T; \mathcal{W}')}^2 + \varepsilon \|H_N^l\|_{\widehat{\mathbb{H}}_r^1(\Omega)}^2 + \Delta t \sum_{n=1}^{l-1} \|H_N^n\|_{\widehat{\mathbb{H}}_r^1(\Omega)}^2 + \|H_{0N}\|_{\widehat{\mathbb{H}}_r^1(\Omega)}^2, \quad (5.47)$$

for all $\varepsilon > 0$. On the other hand, in order to deal with the second term on the left-hand side of (5.45), we first notice that $H_N^l = H_{0N} + \Delta t \sum_{n=1}^l \bar{\partial} H_N^n$ and then

$$\Delta t \sum_{n=1}^l \|\bar{\partial} H_N^n\|_{L_r^2(\Omega)}^2 \geq \frac{1}{T} \left\{ \frac{\|H_N^l\|_{L_r^2(\Omega)}^2}{2} - \|H_{0N}\|_{L_r^2(\Omega)}^2 \right\}.$$

Therefore, from the latter and Lemma 5.4.1 (cf. (5.30)) we obtain that there exists $\widehat{\gamma} := \min \left\{ \frac{\mu_0}{4T}, \frac{1}{2} \right\} \gamma$, such that

$$\begin{aligned} \mu_0 \Delta t \sum_{n=1}^l \|\bar{\partial} H_N^n\|_{L_r^2(\Omega)}^2 + \frac{1}{2} \langle A^l H_N^l, H_N^l \rangle_{\mathcal{W}, \mathcal{W}'} \\ \geq \frac{\Delta t \mu_0}{2} \sum_{n=1}^l \|\bar{\partial} H_N^n\|_{L_r^2(\Omega)}^2 + \widehat{\gamma} \|H_N^l\|_{\widehat{\mathbb{H}}_r^1(\Omega)}^2 - \mu_0 \frac{\|H_{0N}\|_{L_r^2(\Omega)}^2}{2T}. \end{aligned} \quad (5.48)$$

Then, by replacing (5.46)–(5.48) into (5.45) and choosing $\varepsilon = \frac{\widehat{\gamma}}{4}$ we get

$$\begin{aligned} & \frac{\mu_0 \Delta t}{2} \sum_{n=1}^l \|\bar{\partial} H_N^n\|_{L_r^2(\Omega)}^2 + \frac{\widehat{\gamma}}{2} \|H_{\Delta t}^l\|_{\widehat{\mathbb{H}}_r^1(\Omega)}^2 \\ & \leq C \left\{ \|b\|_{\mathbb{H}^2(0, T)}^2 + \|f\|_{\mathbb{H}^1(0, T; \mathcal{W}')}^2 + \Delta t \sum_{n=1}^l \left| \frac{\bar{\partial} b^n - \bar{\partial} b^{n-1}}{\Delta t} \right|^2 + \Delta t \sum_{n=1}^l \|\bar{\partial} f^n\|_{\mathcal{W}'}^2 \right\} \\ & \quad + C \Delta t \sum_{n=1}^l \|H_N^{n-1}\|_{\widehat{\mathbb{H}}_r^1(\Omega)}^2 + \frac{(\sigma_* \mu_0 + T)}{2T \sigma_*} \|H_{0N}\|_{\widehat{\mathbb{H}}_r^1(\Omega)}^2. \end{aligned}$$

Hence, by using the discrete Gronwall's lemma we obtain

$$\Delta t \sum_{n=1}^l \|\bar{\partial} H_N^n\|_{L_r^2(\Omega)}^2 + \|H_{\Delta t}^l\|_{\widehat{\mathbb{H}}_r^1(\Omega)}^2 \leq C \quad l = 1, \dots, m,$$

with $C > 0$ depending on $\|b\|_{\mathbb{H}^2(0, T)}$, $\|H_{0N}\|_{\widehat{\mathbb{H}}_r^1(\Omega)}$, $\|f\|_{\mathbb{H}^1(0, T; \mathcal{W}')}$ and $\|\sigma\|_{W^{1, \infty}(0, T; L^\infty(\Omega))}$. Finally, we estimate $\sum_{n=1}^l \|\bar{\partial} W_N^n\|_{\mathcal{W}'}^2$ by using (5.32) and the latter inequality. \square

Convergence

Now, we will define a family of approximate solutions to Problem 5.4.2 and prove its weak convergence to a solution. With this aim, we introduce some notation: let $W_{N\Delta t} : [0, T] \rightarrow L_r^2(\Omega)$

be the piecewise linear in time interpolant of $\{W_N^n\}_{n=0}^m$ (cf. (5.35)–(5.36)). We also introduce the step function $\bar{H}_{N\Delta t} : [0, T] \rightarrow \mathcal{W}$ by:

$$\bar{H}_{N\Delta t}(t^0) := H_{0N}; \quad \bar{H}_{N\Delta t}(t) := H_N^n, \quad t \in (t^{n-1}, t^n], \quad i = n, \dots, m, \quad (5.49)$$

and define the step functions $\bar{A}_{\Delta t}$ and $\bar{R}_{N\Delta t}$ in a similar way.

Using the above notation we rewrite equation (5.32) as follows:

$$\mu_0 \frac{\partial H_{N\Delta t}}{\partial t} + \mu_0 \frac{\partial W_{N\Delta t}}{\partial t} + \bar{A}_{\Delta t} \bar{H}_{N\Delta t} = \bar{R}_{N\Delta t} \quad \text{in } \mathcal{W}', \quad \text{a.e. in } (0, T). \quad (5.50)$$

From Lemma 5.4.4 we deduce that there exists $C > 0$ such that

$$\begin{aligned} \left\| \frac{\partial W_{N\Delta t}}{\partial t} \right\|_{L^2(0, T; \mathcal{W}')} + \|\bar{A}_{\Delta t} \bar{H}_{N\Delta t}\|_{L^\infty(0, T; \mathcal{W}')} \\ + \|H_{N\Delta t}\|_{H^1(0, T; L_r^2(\Omega)) \cap L^\infty(0, T; \hat{H}_r^1(\Omega))} + \|\bar{H}_{N\Delta t}\|_{L^\infty(0, T; \hat{H}_r^1(\Omega))} \leq C. \end{aligned} \quad (5.51)$$

Moreover, since $H^1(0, T; L_r^2(\Omega)) = L_r^2(\Omega; H^1(0, T)) \hookrightarrow L_r^2(\Omega; C([0, T]))$ with continuous injection, by using the affinely bounded assumption and (5.51) it follows that

$$\|W_{N\Delta t}\|_{L_r^2(\Omega \times [0, T])} \leq \sqrt{T} \|W_{N\Delta t}\|_{L_r^2(\Omega; C([0, T]))} \leq \sqrt{T} \|H_{N\Delta t}\|_{L_r^2(\Omega; C([0, T]))} + \sqrt{T} \|\tau\|_{L_r^2(\Omega)} \leq C.$$

This allows us to conclude that there exists H_N , W_N and X such that,

$$H_{N\Delta t} \rightharpoonup H_N \quad \text{in } H^1(0, T; L_r^2(\Omega)) \cap L^\infty(0, T; \hat{H}_r^1(\Omega)) \text{ weakly star}, \quad (5.52)$$

$$\bar{H}_{N\Delta t} \rightharpoonup H_N \quad \text{in } L^\infty(0, T; \hat{H}_r^1(\Omega)) \text{ weakly star}, \quad (5.53)$$

$$W_{N\Delta t} \rightharpoonup W_N \quad \text{in } L_r^2(\Omega \times [0, T]) \text{ weakly}, \quad (5.54)$$

$$\frac{\partial}{\partial t} H_{N\Delta t} \rightharpoonup \frac{\partial}{\partial t} H_N \quad \text{in } L^2(0, T; \mathcal{W}') \text{ weakly}, \quad (5.55)$$

$$\frac{\partial}{\partial t} W_{N\Delta t} \rightharpoonup \frac{\partial}{\partial t} W_N \quad \text{in } L^2(0, T; \mathcal{W}') \text{ weakly}, \quad (5.56)$$

$$\bar{A}_{\Delta t} \bar{H}_{N\Delta t} \rightharpoonup X \quad \text{in } L^\infty(0, T; \mathcal{W}') \text{ weakly star}. \quad (5.57)$$

Let $R_N \in H^1(0, T; \mathcal{W}')$ be such that

$$\langle R_N, G \rangle_{\mathcal{W}, \mathcal{W}'} = \langle f, G \rangle_{\mathcal{W}, \mathcal{W}'} + (b'(t) - \langle f, r^{-1} \rangle_{\mathcal{W}, \mathcal{W}'}) (rG) |_\Gamma \quad \forall G \in \mathcal{W}, \quad \text{a.e. in } [0, T].$$

By passing to the limit in (5.50) we obtain

$$\mu_0 \frac{\partial H_N}{\partial t} + \mu_0 \frac{\partial W_N}{\partial t} + X = R_N \quad \text{in } \mathcal{W}', \quad \text{a.e. in } (0, T), \quad (5.58)$$

because $\bar{R}_{N\Delta t} \rightarrow R_N$ in $L^2(0, T; \mathcal{W}')$, for $f \in H^1(0, T; \mathcal{W}')$ and $b \in H^2(0, T)$. The next step is to prove that $X = AH_N$ and $W_N = \mathcal{F}(H_N, \xi)$. The first equality, follows from (5.53), (5.57) and H.2 (see, for instance, Lemma 4.3.6, Chapter 4). To prove the remaining one, we proceed by using a compactness result and the strong continuity of \mathcal{F} (cf. (5.7)). First, we recall that, given the assumption on the domain (cf. (5.27)) $L_r^2(\Omega)$ and $\hat{H}_r^1(\Omega)$ are both identical to $L^2(\Omega)$ and $H^1(\Omega)$, respectively.

Lemma 5.4.5 *Let H_N and W_N be the limits defined in (5.52) and (5.54), respectively. We have*

$$W_N = \mathcal{F}(H_N, \xi) \quad \text{a.e. in } [0, T] \times \Omega.$$

Proof. From (5.51) we have that $H_{N\Delta t}$ is bounded in $H^1(0, T; L_r^2(\Omega)) \cap L^2(0, T; \widehat{H}_r^1(\Omega))$. On the other hand, by using an interpolation result (see [61, Chapter 1, Theorem 5.1 and Remark 9.5]) we obtain, for $s \in (0, 1/2)$.

$$H^1(0, T; L_r^2(\Omega)) \cap L^2(0, T; \widehat{H}_r^1(\Omega)) \subset H^s(\Omega; H^{1-s}(0, T)) \subset L_r^2(\Omega; C([0, T]))$$

with continuous injection and compact inclusion, respectively. Hence, we have

$$H_{N\Delta t} \longrightarrow H_N \quad \text{in } L_r^2(\Omega; C([0, T])) \text{ strongly} \quad (5.59)$$

and therefore

$$H_{N\Delta t} \longrightarrow H_N \quad \text{uniformly in } [0, T], \text{ a.e. in } \Omega.$$

Using the strong continuity of \mathcal{F} we obtain

$$\mathcal{F}(H_{N\Delta t}, \xi) \longrightarrow \mathcal{F}(H_N, \xi) \quad \text{uniformly in } [0, T], \text{ a.e. in } \Omega. \quad (5.60)$$

On the other hand, since $[\mathcal{F}(H_{N\Delta t}, \xi)](r, z, \cdot)$ is uniformly continuous in $[0, T]$ a.e. in Ω and $W_{N\Delta t}(r, z, \cdot)$ is the linear in time interpolant of

$$W_{N\Delta t}(r, z, t^n) = [\mathcal{F}(H_{N\Delta t}, \xi)](r, z, t^n) \quad n = 1, \dots, m,$$

it is straightforward to obtain that

$$\|W_{N\Delta t} - \mathcal{F}(H_N, \xi)\|_{C([0, T])} \leq \|W_{\Delta t} - \mathcal{F}(H_{N\Delta t}, \xi)\|_{C([0, T])} + \|\mathcal{F}(H_{N\Delta t}, \xi) - \mathcal{F}(H_N, \xi)\|_{C([0, T])} \rightarrow 0,$$

by using (5.60). Therefore, we have

$$W_{N\Delta t} \longrightarrow \mathcal{F}(H_N, \xi) \quad \text{uniformly in } [0, T], \text{ a.e. in } \Omega$$

Moreover, because the affinely bounded assumption (cf. (5.28)), $W_{N\Delta t}$ converges strongly in $L_r^2(\Omega; C(0, T))$. Then, from (5.54) we obtain the result. \square

From the latter, we are in a position to obtain the following result.

Theorem 5.4.1 *Let us assume hypotheses H.1, H.2 and H.3. Then Problem 5.4.2 has a solution.*

Proof. From (5.58) and Lemma 5.4.5 it follows that

$$\begin{aligned} \left\langle \frac{\partial B_N}{\partial t}, G \right\rangle_{\mathcal{W}, \mathcal{W}'} + a_t(H_N, G) &= \langle f, G \rangle_{\mathcal{W}, \mathcal{W}'} \\ &+ (b'(t) - \langle f, r^{-1} \rangle_{\mathcal{W}, \mathcal{W}'}) (rG) |_{\Gamma} \quad \forall G \in \mathcal{W}, \quad \text{a.e. in } [0, T], \\ B_N &= \mu_0 (H_N + \mathcal{F}(H_N, \xi)) \quad \text{in } \Omega \times (0, T). \end{aligned}$$

Moreover, as a consequence of (5.59), (5.60) and Lebesgue dominated convergence theorem it follows that $H_{N\Delta t}(0) \rightarrow H_N(0)$ in $L_r^2(\Omega)$ and $W_{N\Delta t}(0) \rightarrow \mathcal{F}(H_N, \xi)(0)$ in $L_r^2(\Omega)$. Hence

$$H_N(0) = H_{0N} \quad \text{and} \quad \mathcal{F}(H_N, \xi)(0) = W_{0N} \quad \text{in } \Omega.$$

Therefore (H_N, B_N) is solution to Problem 5.4.2. \square

5.4.4 Existence of solution. Dirichlet problem

We prove the existence of solution to Problem 5.4.1 by using the same techniques as in the previous section, namely, we approximate the continuous problem by using a time discretization, prove error estimates for this discrete solution and then pass to the limit as the time step goes to zero.

To prove that Problem 5.4.1 has a solution, we first consider a lifting of the boundary data. We notice that, from the regularity of g , there exist $H_g \in \mathbf{H}^2(0, T; \tilde{\mathbf{H}}_r^1(\Omega))$ such that $H_g|_\Gamma = g$ with

$$\|H_g\|_{\mathbf{H}^k(0, T; \tilde{\mathbf{H}}_r^1(\Omega))} \leq C \|g\|_{\mathbf{H}^k(0, T; \tilde{\mathbf{H}}_r^{1/2}(\Gamma))}, \quad k = 1, 2, \quad (5.61)$$

being C a constant independent of g (cf. Section 4.3.2, Chapter 4). Next, we write $H_D = H_u + H_g$ and clearly $H_u \in \mathcal{U}$. Hence, from the above, we rewrite Problem 5.4.1 as follows:

$$\begin{aligned} & \text{Find } H_u \in \mathbf{H}^1(0, T; \mathbf{L}_r^2(\Omega)) \cap \mathbf{L}^\infty(0, T; \mathcal{U}), \text{ such that} \\ & \mu_0 \int_{\Omega} \frac{\partial H_u}{\partial t} Gr \, dr dz + \mu_0 \left\langle \frac{\partial \mathcal{F}(H_u + H_g, \xi)}{\partial t}, G \right\rangle_{\mathcal{U}, \mathcal{U}'} + a_t(H_u, G) = \langle R_D, G \rangle_{\mathcal{U}, \mathcal{U}'} \quad \forall G \in \mathcal{U}, \end{aligned} \quad (5.62)$$

$$H_u|_{t=0} = H_{0D} - H_g(0) \quad \text{in } \Omega, \quad (5.63)$$

with $R_D \in \mathbf{H}^1(0, T; \mathcal{U}')$ such that

$$\langle R_D, G \rangle_{\mathcal{U}, \mathcal{U}'} := \langle f, G \rangle_{\mathcal{U}, \mathcal{U}'} - a_t(H_g, G) - \mu_0 \int_{\Omega} \frac{\partial H_g}{\partial t} Gr \, dr dz \quad \forall G \in \mathcal{U}, \text{ a.e. in } [0, T].$$

Time discretization

We consider the definitions and notations introduced in Section 5.4.3 and define $H_g^n(r, z) := H_g(r, z, t^n)$, $n = 0, \dots, m$, a.e. in Ω . We approximate (5.62)-(5.63) by an implicit time discretization scheme and obtain the following problem:

For $n = 1, \dots, m$, find $H_u^n \in \mathcal{U}$ and $W_D^n \in \mathbf{L}_r^2(\Omega)$ satisfying

$$\mu_0 \bar{\partial} H_u^n + \mu_0 \bar{\partial} W_D^n + A^n H_u^n = R_D^n \quad \text{in } \mathcal{U}, \quad n = 1, \dots, m, \quad (5.64)$$

$$W_D^n = [\mathcal{F}(H_{u\Delta t^n} + H_{g\Delta t^n}, \xi)](t^n) \quad \text{in } \Omega, \quad n = 1, \dots, m, \quad (5.65)$$

$$H_u^0 = H_{0D} - H_g^0, \quad W_D^0 = W_{0D} \quad \text{in } \Omega, \quad (5.66)$$

where $H_{u\Delta t^n}$ and $H_{g\Delta t^n}$ are the linear in time interpolants of $\{H_u^i\}_{i=0}^n$ and $\{H_g^i\}_{i=0}^n$, respectively (cf. (5.35)–(5.36)), and $R_D^n \in \mathcal{U}'$, $n = 1, \dots, m$, defined by

$$\langle R_D^n, G \rangle_{\mathcal{U}, \mathcal{U}'} := \langle f^n, G \rangle_{\mathcal{U}, \mathcal{U}'} - \langle A^n H_g^n, G \rangle_{\mathcal{U}, \mathcal{U}'} - \mu_0 \int_{\Omega} \bar{\partial} H_g^n Gr \, dr dz \quad \forall G \in \mathcal{U}.$$

We notice that W_D^n depends on the known functions $\{H_u^l\}_{l=0}^{n-1}$, $\{H_g^l\}_{l=0}^n$ and the unknown function H_u^n .

The existence and uniqueness of solution of the discrete problem is guaranteed by the following lemma.

Lemma 5.4.6 *For any $n = 1, \dots, m$, there exists a unique solution $H_u^n \in \mathcal{U}$ and $W_D^n \in L_r^2(\Omega)$ to (5.64)–(5.66).*

Proof. First, we define $\mathbb{F}_g^n : L_r^2(\Omega) \rightarrow L_r^2(\Omega)$ by $\mathbb{F}_g^n(G)(r, z) = F_g^n(G(r, z), r, z)$ a.e. in Ω , with $F_g^n : \mathbb{R} \times \Omega \rightarrow \mathbb{R}$, such that

$$F_g^n(r, z, s) := [\mathcal{F}(U_{\Delta t}^s, \xi)](r, z, t^n) \quad \text{a.e. in } \Omega,$$

with $U_{\Delta t}^s$ the piecewise linear in time function such that $U_{\Delta t}^s(r, z, t^l) = H_u^l(r, z) + H_g^l(r, z)$, $l = 0, \dots, n-1$ and $U_{\Delta t}^s(r, z, t^n) = s + H_g^n(r, z)$. As in Lemma 5.4.2, it follows that \mathbb{F}_g^n is monotone and continuous and there exist constants $C_1, C_2 > 0$ depending on $\{H_u^l\}_{l=0}^{n-1}$ and $\{H_g^l\}_{l=0}^n$ such that

$$\int_{\Omega} \mathbb{F}_g^n(G) G r \, dr dz \geq -C_1 \|G\|_{L_r^2(\Omega)} - C_2 \quad \forall G \in L_r^2(\Omega).$$

Hence, from Lemma 5.4.1 (cf. (5.31)), the result follows by using the theory of monotone operators (cf. Lemma 5.4.3). \square

A priori estimates

The following lemma gives us a priori estimates for the solution to (5.64)–(5.66).

Lemma 5.4.7 *There exists $C > 0$ such that, for all $l = 1, \dots, m$*

$$\Delta t \sum_{n=1}^l \|\bar{\partial} W_D^n\|_{\mathcal{U}'}^2 + \|H_u^l\|_{\tilde{H}_r^1(\Omega)}^2 + \Delta t \sum_{n=1}^l \|\bar{\partial} H_u^n\|_{L_r^2(\Omega)}^2 \leq C.$$

Proof. We multiply (5.64) by $(H_u^n - H_u^{n-1})$ to obtain

$$\begin{aligned} \mu_0 \Delta t \left\| \frac{H_u^n - H_u^{n-1}}{\Delta t} \right\|_{L_r^2(\Omega)}^2 + \frac{\mu_0}{\Delta t} \int_{\Omega} (W_D^n - W_D^{n-1})(H_u^n - H_u^{n-1}) r \, dr dz \\ + \langle A^n H_u^n, H_u^n - H_u^{n-1} \rangle_{\mathcal{U}, \mathcal{U}'} = \langle R_D^n, H_u^n - H_u^{n-1} \rangle_{\mathcal{U}, \mathcal{U}'}. \end{aligned} \quad (5.67)$$

Now, we estimate each term of the above equation. First, we focus on the left-hand side. For the second term on the left-hand side, by using the piecewise monotonicity property of \mathcal{F} (cf. (5.8)), we arrive at

$$\frac{1}{\Delta t} \int_{\Omega} (W_D^n - W_D^{n-1})(H_u^n - H_u^{n-1}) r \, dr dz \geq \int_{\Omega} -(W_D^n - W_D^{n-1})(\bar{\partial} H_g^n) r \, dr dz. \quad (5.68)$$

On the other hand, from the analysis of the previous section (cf. (5.43) and (5.44)), we estimate the last term on the left-hand side of (5.67) as follows

$$\begin{aligned} \langle A^n H_u^n, H_u^n - H_u^{n-1} \rangle_{\mathcal{U}, \mathcal{U}'} \geq \frac{1}{2} \langle A^n H_u^n, H_u^n \rangle_{\mathcal{U}, \mathcal{U}'} - \frac{1}{2} \langle A^{n-1} H_u^{n-1}, H_u^{n-1} \rangle_{\mathcal{U}, \mathcal{U}'} \\ - C_{\sigma} \|\partial_t \sigma\|_{L^{\infty}(0, T; L^{\infty}(\Omega))} \Delta t \|H_u^{n-1}\|_{\tilde{H}_r^1(\Omega)}^2. \end{aligned} \quad (5.69)$$

Then, summing up (5.67) for $n = 1, \dots, l$, with $l \in \{1, \dots, m\}$, by replacing (5.68) and (5.69) into (5.67) and using Lemma 5.4.1 (cf. (5.31)) we obtain that

$$\begin{aligned} & \mu_0 \Delta t \sum_{n=1}^l \|\bar{\partial} H_u^n\|_{L_r^2(\Omega)}^2 + \frac{\gamma_u}{2} \|H_u^l\|_{\tilde{H}_r^1(\Omega)}^2 \\ & \leq C \|H_u^0\|_{\tilde{H}_r^1(\Omega)}^2 + C \|\partial_t \sigma\|_{L^\infty(0,T;L_r^\infty(\Omega))} \Delta t \sum_{n=1}^l \|H_u^{n-1}\|_{\tilde{H}_r^1(\Omega)}^2 \\ & \quad + \left| \sum_{n=1}^l \langle R_D^n, H_u^n - H_u^{n-1} \rangle_{\mathcal{U}, \mathcal{U}'} \right| + \mu_0 \left| \sum_{n=1}^l \int_{\Omega} (W_D^n - W_D^{n-1})(\bar{\partial} H_g^n) r \, dr dz \right|. \end{aligned} \quad (5.70)$$

Finally, we estimate the last two terms on the right-hand side of (5.70) by Young's inequality and summation by parts. First, by proceeding like in (5.46) and (5.47) we obtain

$$\begin{aligned} & \left| \sum_{n=1}^l \langle R_D^n, H_u^n - H_u^{n-1} \rangle_{\mathcal{U}, \mathcal{U}'} \right| \\ & \leq \left| \sum_{n=1}^l \langle f^n, H_u^n - H_u^{n-1} \rangle_{\mathcal{U}, \mathcal{U}'} \right| + \left| \sum_{n=1}^l \langle A^n H_g^n, H_u^n - H_u^{n-1} \rangle_{\mathcal{U}, \mathcal{U}'} \right| \\ & \quad + \frac{\mu_0 \Delta t}{4} \sum_{n=1}^l \|\bar{\partial} H_u^n\|_{L_r^2(\Omega)}^2 + \mu_0 \Delta t \sum_{n=1}^l \|\bar{\partial} H_g^n\|_{L_r^2(\Omega)}^2 \\ & \leq \varepsilon \|H_u^l\|_{\tilde{H}_r^1(\Omega)}^2 + \Delta t \sum_{n=1}^{l-1} \|H_u^n\|_{\tilde{H}_r^1(\Omega)}^2 + \frac{\mu_0 \Delta t}{4} \sum_{n=1}^l \|\bar{\partial} H_u^n\|_{L_r^2(\Omega)}^2 \\ & \quad + C_\varepsilon \left\{ \|f\|_{\mathbb{H}^1(0,T;\mathcal{U}')}^2 + \|H_g\|_{\mathbb{H}^2(0,T;\tilde{H}_r^1(\Omega))}^2 + \|H_u^0\|_{\tilde{H}_r^1(\Omega)}^2 \right\}, \end{aligned} \quad (5.71)$$

for all $\varepsilon > 0$. For the last term, by summation by parts we obtain that

$$\begin{aligned} & \left| \sum_{n=1}^l \int_{\Omega} (W_D^n - W_D^{n-1})(\bar{\partial} H_g^n) r \, dr dz \right| \\ & \leq \int_{\Omega} |W_D^l \bar{\partial} H_g^l r \, dr dz| + \int_{\Omega} |W_{0D} \bar{\partial} H_g^1 r \, dr dz| \\ & \quad + \Delta t \sum_{n=1}^{l-1} \int_{\Omega} \left| W_D^n \left(\frac{\bar{\partial} H_g^{n+1} - \bar{\partial} H_g^n}{\Delta t} \right) r \, dr dz \right| \\ & \leq \eta \|W_D^l\|_{L_r^2(\Omega)}^2 + \Delta t \sum_{n=1}^{l-1} \|W_D^n\|_{L_r^2(\Omega)}^2 + C \|W_{0D}\|_{L_r^2(\Omega)}^2 \\ & \quad + C_\eta \|H_g\|_{\mathbb{H}^2(0,T;L_r^2(\Omega))}^2 + C \Delta t \sum_{n=1}^{l-1} \left\| \frac{\bar{\partial} H_g^{n+1} - \bar{\partial} H_g^n}{\Delta t} \right\|_{L_r^2(\Omega)}^2, \end{aligned} \quad (5.72)$$

for all $\eta > 0$. In order to deal with the first two terms on the right-hand side of the above equation, which depend on $\{W_D^i\}_{i=1}^l$, we consider the following inequalities

$$\begin{aligned} \|W_D^l\|_{L_r^2(\Omega)}^2 &\leq 2L_{\mathcal{F}}^2 \int_{\Omega} \left(\max_{i=0,\dots,l} \{|H_u^i + H_g^i|\} \right)^2 r \, dr dz + 2 \|\tau\|_{L_r^2(\Omega)}^2, \\ &\leq 4L_{\mathcal{F}}^2 \int_{\Omega} \left(\max_{i=0,\dots,l} \{|H_u^i|\} \right)^2 r \, dr dz + 4L_{\mathcal{F}}^2 \|H_g\|_{L_r^2(\Omega; C([0,T]))}^2 + 2 \|\tau\|_{L_r^2(\Omega)}^2, \end{aligned} \quad (5.73)$$

and, for $i = 0, \dots, l$

$$|H_u^i| \leq |H_u^0| + \Delta t \sqrt{i} \left(\sum_{n=1}^i |\bar{\partial} H_u^n|^2 \right)^{1/2} \quad \text{a.e. in } \Omega, \quad (5.74)$$

where the first one follows from (5.28). Then, from (5.73)–(5.74) and the continuous inclusion $H^1(0, T; L_r^2(\Omega)) = L_r^2(\Omega; H^1(0, T)) \subset L_r^2(\Omega; C([0, T]))$, we arrive at

$$\|W_D^l\|_{L_r^2(\Omega)}^2 \leq 8L_{\mathcal{F}}^2 \|H_{0N}\|_{L_r^2(\Omega)}^2 + 8TL_{\mathcal{F}}^2 \Delta t \sum_{n=1}^l \|\bar{\partial} H_u^n\|_{L_r^2(\Omega)}^2 + C \|H_g\|_{H^1(0,T;L_r^2(\Omega))}^2 + 2 \|\tau\|_{L_r^2(\Omega)}^2, \quad (5.75)$$

$$\begin{aligned} \Delta t \sum_{n=1}^{l-1} \|W_D^n\|_{L_r^2(\Omega)}^2 &\leq 8TL_{\mathcal{F}}^2 \Delta t \sum_{n=1}^{l-1} \left(\Delta t \sum_{i=1}^n \|\bar{\partial} H_u^i\|_{L_r^2(\Omega)}^2 \right) \\ &\quad + C \left(\|H_{0N}\|_{L_r^2(\Omega)}^2 + \|H_g\|_{H^1(0,T;L_r^2(\Omega))}^2 + \|\tau\|_{L_r^2(\Omega)}^2 \right). \end{aligned} \quad (5.76)$$

Therefore, by replacing (5.75)–(5.76) into (5.72), and then (5.72)–(5.71) into (5.70), choosing $\eta = \frac{1}{32L_{\mathcal{F}}^2 T}$ and $\varepsilon = \frac{\gamma_u}{4}$, from the regularity of the data (cf. H.3 and (5.61)) it follows that

$$\frac{\mu_0 \Delta t}{2} \sum_{n=1}^l \|\bar{\partial} H_u^n\|_{L_r^2(\Omega)}^2 + \frac{\gamma_u}{4} \|H_u^l\|_{\tilde{H}_r^1(\Omega)}^2 \leq C \Delta t \sum_{n=1}^{l-1} \left(\|H_u^n\|_{\tilde{H}_r^1(\Omega)}^2 + \Delta t \sum_{i=1}^n \|\bar{\partial} H_u^i\|_{L_r^2(\Omega)}^2 \right) + C.$$

Hence, by applying a discrete Gronwall's lemma to $\{y^j\}_{j=1}^l$, with $y^j := \sum_{n=1}^j \|\bar{\partial} H_u^n\|_{L_r^2(\Omega)}^2 + \|H_u^j\|_{\tilde{H}_r^1(\Omega)}^2$ we arrive at

$$\Delta t \sum_{n=1}^l \|\bar{\partial} H_u^n\|_{L_r^2(\Omega)}^2 + \|H_u^l\|_{\tilde{H}_r^1(\Omega)}^2 \leq C \quad l = 1, \dots, m,$$

with a constant C depending on $\|H_{0D}\|_{\tilde{H}_r^1(\Omega)}$, $\|f\|_{H^1(0,T;\mathcal{U})}$, $\|g\|_{H^2(0,T;\tilde{H}_r^{1/2}(\Gamma))}$, $\|\tau\|_{L_r^2(\Omega)}$ and $\|\sigma\|_{W^{1,\infty}(0,T;L^\infty(\Omega))}$. Finally, we estimate $\sum_{n=1}^l \|\bar{\partial} W_D^n\|_{\mathcal{U}'}^2$ by using the latter inequality and (5.64). \square

Convergence

At this point we introduce some further notation. Let $H_{u\Delta t}$ and $\bar{H}_{u\Delta t}$ be the linear and piecewise constant in time interpolants of $\{H_u^n\}_{n=0}^m$ (cf. (5.35)–(5.36) and (5.49), respectively). Similarly, we introduce the linear and the piecewise constant interpolant of $\{H_g^n\}_{n=0}^m$ defined by $H_{g\Delta t}$ and $\bar{H}_{g\Delta t}$, respectively. The step function $\bar{f}_{\Delta t}$ is defined in a similar way.

From the above definitions, we rewrite (5.64) as follows:

$$\mu_0 \frac{\partial H_{u\Delta t}}{\partial t} + \mu_0 \frac{\partial H_{g\Delta t}}{\partial t} + \mu_0 \frac{\partial W_{D\Delta t}}{\partial t} + \bar{A}_{\Delta t}(\bar{H}_{u\Delta t} + \bar{H}_{g\Delta t}) = \bar{f}_{\Delta t} \quad \text{in } \mathcal{U}' \quad \text{a.e. in } (0, T). \quad (5.77)$$

From Lemma 5.4.7, the regularity assumption on the data and the properties of \mathcal{F} (cf. (5.28)), we obtain,

$$\begin{aligned} \left\| \frac{\partial W_{D\Delta t}}{\partial t} \right\|_{L^2(0, T; \mathcal{U}')} + \|W_{D\Delta t}\|_{L^2_r(\Omega \times [0, T])} + \|\bar{A}_{\Delta t} \bar{H}_{u\Delta t}\|_{L^\infty(0, T; \mathcal{U}')} \\ + \|H_{u\Delta t}\|_{H^1(0, T; L^2_r(\Omega)) \cap L^\infty(0, T; \mathcal{U})} + \|\bar{H}_{u\Delta t}\|_{L^\infty(0, T; \mathcal{U})} \leq C. \end{aligned} \quad (5.78)$$

Therefore, we conclude that there exists H_u and W_D such that,

$$H_{u\Delta t} \rightharpoonup H_u \quad \text{in } H^1(0, T; L^2_r(\Omega)) \cap L^\infty(0, T; \mathcal{U}) \text{ weakly star}, \quad (5.79)$$

$$\bar{H}_{u\Delta t} \rightharpoonup H_u \quad \text{in } L^\infty(0, T; \mathcal{U}) \text{ weakly star}, \quad (5.80)$$

$$W_{D\Delta t} \rightharpoonup W_D \quad \text{in } L^2(0, T; L^2_r(\Omega)) \text{ weakly}, \quad (5.81)$$

$$\frac{\partial W_{D\Delta t}}{\partial t} \rightharpoonup \frac{\partial W_D}{\partial t} \quad \text{in } L^2(0, T; \mathcal{U}') \text{ weakly star}. \quad (5.82)$$

From the latter convergences, the regularity of H_g (cf. (5.61)) and H.2 we obtain

$$\bar{A}_{\Delta t}(\bar{H}_{u\Delta t} + \bar{H}_{g\Delta t}) \rightharpoonup A(H_u + H_g) \quad \text{in } L^2(0, T; \mathcal{U}') \text{ weakly}. \quad (5.83)$$

Taking the limit in (5.77) and since $f \in H^1(0, T; \mathcal{U}')$, it follows that

$$\mu_0 \frac{\partial (H_u + H_g)}{\partial t} + \mu_0 \frac{\partial W_D}{\partial t} + A(H_u + H_g) = f \quad \text{in } \mathcal{U}', \text{ a.e. in } (0, T). \quad (5.84)$$

To prove that $W_D = \mathcal{F}(H_u + H_g, \xi)$ a.e. on $[0, T]$, we consider the following lemma based on a compactness result. Unlike Problem 5.4.2, here we are dealing with weighted Sobolev spaces with singular weight. Thus, we obtain the compactness result by identifying the axisymmetric spaces with their respective 3D versions.

Lemma 5.4.8 *Let H_u and W_D be the limits defined in (5.79) and (5.81), respectively. Then*

$$W_D = \mathcal{F}(H_u + H_g, \xi) \quad \text{a.e. in } [0, T] \times \Omega.$$

Proof. From Remark 5.4.1, the space $H^1(0, T; L^2_r(\Omega)) \cap L^\infty(0, T; \tilde{H}^1_r(\Omega))$ can be identified to $H^1(0, T; \mathbf{L}^2(\tilde{\Omega})) \cap L^\infty(0, T; \mathbf{H}^1(\tilde{\Omega}))$. Moreover by using an interpolation result we have

$$H^1(0, T; \mathbf{L}^2(\tilde{\Omega})) \cap L^\infty(0, T; \mathbf{H}^1(\tilde{\Omega})) \subset \mathbf{L}^2(\tilde{\Omega}; C([0, T])),$$

with compact inclusion. From this inclusion and the identification of the axisymmetric Sobolev spaces, we obtain the compact inclusion: $H^1(0, T; L_r^2(\Omega)) \cap L^\infty(0, T; \tilde{H}_r^1(\Omega)) \subset L_r^2(\Omega; C([0, T]))$. By proceeding as in Section 5.4.3 with $H_{N\Delta t} := H_{u\Delta t} + H_{g\Delta t}$ we get the result. \square

Now we are in a position to prove that Problem 5.4.1 has a solution.

Theorem 5.4.2 *Let us assume hypotheses H.1, H.2 and H.3. Then Problem 5.4.1 has a solution.*

Proof. Let $H_D := H_u + H_g$ and $B_D := \mu_0(H_D + \mathcal{F}(H_D, \xi))$. Then from (5.84) and Lemma 5.4.8 we get

$$\left\langle \frac{\partial B_D}{\partial t}, G \right\rangle_{\mathcal{U}, \mathcal{U}'} + a_t(H_D, G) = \langle f, G \rangle_{\mathcal{U}, \mathcal{U}'} \quad \forall G \in \mathcal{U} \quad \text{a.e. in } (0, T).$$

Clearly $H_D|_\Gamma = g$. Moreover, from the compact inclusion $H^1(0, T; L_r^2(\Omega)) \cap L^\infty(0, T; \tilde{H}_r^1(\Omega)) \subset L_r^2(\Omega; C([0, T]))$ and the strongly continuous assumption (cf. (5.7)) we have $H_{u\Delta t}(0) \rightarrow H_u(0)$ and $W_{D\Delta t}(0) \rightarrow \mathcal{F}(H_u + H_g, \xi)(0)$ in $L_r^2(\Omega)$. From the definition of $H_{u\Delta t}$ and $W_{D\Delta t}$, (5.66) and H.3 it follows that

$$H_D(0) = H_{0D} \quad \text{and} \quad W_{D\Delta t}(0) = \mathcal{F}(H_D, \xi)(0) \quad \text{in } \Omega.$$

Hence, from the latter we conclude that (H_D, B_D) is a solution of Problem 5.4.1. \square

Remark 5.4.3 *There is not a uniqueness result for a generic hysteresis operator satisfying (5.6)–(5.8), even though it is possible to prove a uniqueness result by choosing a particular operator, for instance, the Prandtl-Ishlinskii operator of play type (see, for instance, [49] and more recently [42, Theorem 5.1]).*

5.5 Numerical implementation

In this section we present a numerical implementation to solve a fully discretization of Problem 5.4.1. It is straightforward to extend the same procedure to solve Problem 5.4.2. In what follows we drop subscript D for the sake of simplicity in notation.

From now on we assume Ω is a convex polygon. We associate a family of partitions $\{\mathcal{T}_h\}_{h>0}$ of Ω into triangles, where h denotes the mesh size (i.e., the maximal length of the sides of the triangulation). Let \mathcal{V}_h be the space of continuous piecewise linear finite elements vanishing on the symmetry axis ($r = 0$), so that $\mathcal{V}_h \subset \tilde{H}_r^1(\Omega)$. We also consider the finite-dimensional space $\mathcal{U}_h := \mathcal{V}_h \cap \mathcal{U}$ and denote by $\mathcal{V}_h(\Gamma)$ the space of traces on Γ of functions in \mathcal{V}_h .

In order to analyze the fully-discrete problem, we define $\mathcal{B}^n : L_r^2(\Omega) \rightarrow L_r^2(\Omega)$, $n = 1, \dots, m$, such that, given $u \in L_r^2(\Omega)$

$$\mathcal{B}^n(u)(r, z) := \mu_0(u(r, z) + [\mathcal{F}(U_{h\Delta t^n}, \xi)](r, z, t^n)) \quad \text{a.e. in } \Omega, \quad (5.85)$$

with $U_{h\Delta t^n}$ being the piecewise linear in time function such that $U_{h\Delta t^n}(r, z, t^l) = H_h^l(r, z)$, $l = 0, \dots, n - 1$ and $U_{h\Delta t^n}(r, z, t^n) = u(r, z)$. Under assumption H.1 and Lebesgue dominated

convergence theorem it follows that \mathcal{B}^n , $n = 1, \dots, m$ is continuous and strongly monotone (cf. Lemma 5.4.2), i.e.,

$$\int_{\Omega} (\mathcal{B}^n(u) - \mathcal{B}^n(v))(u - v)r \, dr dz \geq \mu_0 \|u - v\|_{L_r^2(\Omega)}^2.$$

By using the above finite element space for the space discretization and the backward Euler scheme for time discretization, we are led to the following Galerkin approximation of Problem 5.4.1:

Problem 5.5.1 Find $H_h^n \in \mathcal{V}_h$ and $B_h^n \in L_r^2(\Omega)$, $n = 1, \dots, m$, such that

$$\begin{aligned} \frac{1}{\Delta t} \int_{\Omega} B_h^n G_{hr} \, dr dz + \int_{\Omega} \frac{1}{\sigma^n r} \left(\frac{\partial(rH_h^n)}{\partial r} \frac{\partial(rG_h)}{\partial r} + \frac{\partial(rH_h^n)}{\partial z} \frac{\partial(rG_h)}{\partial r} \right) \, dr dz \\ = \langle f^n, G_h \rangle_{\mathcal{U}, \mathcal{U}'} + \frac{1}{\Delta t} \int_{\Omega} B_h^{n-1} G_{hr} \, dr dz \quad \forall G_h \in \mathcal{U}_h, \\ B_h^n(r, z) = \mathcal{B}^n(H_h^n)(r, z) \quad \text{a.e. in } \Omega, \\ H_h^n = g_h^n \quad \text{on } \Gamma, \\ B_h^0 = \mu_0 (H_h^0 + W_0) \quad \text{in } \Omega, \end{aligned}$$

where $H_h^0 \in \mathcal{V}_h$ and $g_h^n \in \mathcal{V}_h(\Gamma)$ are convenient approximations of $H_0 \in \widetilde{H}_r^1(\Omega)$ (cf. H.3) and $g(t^n)$, for $n = 1, \dots, m$, respectively.

Since \mathcal{B}^n is a maximal monotone operator, then, in order to solve the discretized problem we can use the iterative algorithm proposed in [12]. This algorithm, based on the properties of maximal monotone operators and their Yosida regularization, has been extensively used for a wide range of applications with good numerical performance.

Before introducing the algorithm, let us first consider the following definitions. Let V be a Hilbert space and $\mathcal{G} : V \rightarrow V$ a maximal monotone operator. For β a positive number, we define

$$\mathcal{G}^\beta(v) = \mathcal{G}(v) - \beta v \quad \forall v \in V. \quad (5.86)$$

Then we recall that the Yosida regularization of \mathcal{G}^β is defined by

$$\mathcal{G}_\lambda^\beta(v) := \frac{v - J_\lambda^\beta(v)}{\lambda} \quad (5.87)$$

where J_λ^β is the resolvent operator of \mathcal{G}^β , i.e.,

$$J_\lambda^\beta := \left(I + \lambda \mathcal{G}^\beta \right)^{-1}, \quad (5.88)$$

with $\lambda > 0$ being a real parameter such that $\lambda\beta \leq 1$.

A simple way to transform the nonlinearities is to use the following lemma, which is the basis for the algorithm given below.

Lemma 5.5.1 Let V be a Hilbert space and $\mathcal{G} : V \rightarrow V$ a maximal monotone operator (possibly multivalued). If $\lambda\beta \leq 1$, then the following statements are equivalent:

$$i) v \in \mathcal{G}^\beta(u),$$

$$ii) v = \mathcal{G}_\lambda^\beta(u + \lambda v), \quad u, v \in V, \beta \in \mathbb{R}, \lambda > 0.$$

By using this lemma, Problem 5.5.1 can be reformulated as follows:

Find $H_h^n \in \mathcal{V}_h$ and $q_h^n \in L_r^2(\Omega)$, $n = 1, \dots, m$, such that

$$\begin{aligned} & \frac{1}{\Delta t} \int_{\Omega} \beta H_h^n G_h r \, dr dz + \int_{\Omega} \frac{1}{\sigma^n r} \left(\frac{\partial(rH_h^n)}{\partial r} \frac{\partial(rG_h)}{\partial r} + \frac{\partial(rH_h^n)}{\partial z} \frac{\partial(rG_h)}{\partial r} \right) \, dr dz \\ & + \frac{1}{\Delta t} \int_{\Omega} q_h^n G_h r \, dr dz = \langle f^n, G_h \rangle_{\mathcal{U}, \mathcal{U}'} + \frac{1}{\Delta t} \int_{\Omega} B_h^{n-1} G_h r \, dr dz \quad \forall G_h \in \mathcal{U}_h, \\ & q_h^n = \mathcal{B}_\lambda^{n,\beta}(H_h^n + \lambda q_h^n) \quad \text{in } \Omega, \\ & B_h^{n-1} = \beta H_h^{n-1} + q_h^{n-1} \quad \text{in } \Omega, \\ & H_h^n = g_h^n \quad \text{on } \Gamma, \\ & B_h^0 = \mu_0 (H_h^0 + W_0) \quad \text{in } \Omega, \end{aligned}$$

where $\mathcal{B}_\lambda^{n,\beta}$ is the Yoshida regularization of $\mathcal{B}^{n,\beta} := \mathcal{B}^n - \beta I$.

The algorithm consists in a fixed-point iteration using this formulation of the problem. Field H_h^n is computed as the limit of the sequence $\{H_{h,[s]}^n\}_{s \in \mathbb{N}}$ which is obtained as follows:

- At the beginning, function $q_{h,[0]}^n$ is given arbitrarily in \mathcal{V}_h .
- Step s : $q_{h,[s-1]}^n$ is known
 - Compute $H_{h,[s]}^n$ as the unique solution of the following linear problem:

$$\begin{aligned} & \frac{1}{\Delta t} \int_{\Omega} \beta H_{h,[s]}^n G_h r \, dr dz + \int_{\Omega} \frac{1}{\sigma^n r} \left(\frac{\partial(rH_{h,[s]}^n)}{\partial r} \frac{\partial(rG_h)}{\partial r} + \frac{\partial(rH_{h,[s]}^n)}{\partial z} \frac{\partial(rG_h)}{\partial r} \right) \, dr dz \\ & = \langle f^n, G_h \rangle_{\mathcal{U}, \mathcal{U}'} + \frac{1}{\Delta t} \int_{\Omega} B_h^{n-1} G_h r \, dr dz - \frac{1}{\Delta t} \int_{\Omega} q_{h,[s-1]}^n G_h r \, dr dz \quad \forall G_h \in \mathcal{U}_h, \end{aligned} \tag{5.89}$$

$$B_h^{n-1} = \beta H_h^{n-1} + q_h^{n-1} \quad \text{in } \Omega, \tag{5.90}$$

$$H_{h,[s]}^n = g_h^n \quad \text{on } \Gamma, \tag{5.91}$$

$$B_h^0 = \mu_0 (H_h^0 + W_0) \quad \text{in } \Omega, \tag{5.92}$$

where q_h^{n-1} is the limit of the sequence $\{q_{h,[s]}^{n-1}\}_{s \in \mathbb{N}}$.

- Update $q_{h,[s]}^n$ by computing its values at the mesh nodes from the formula,

$$q_{h,[s]}^n(r, z) = \mathcal{B}_\lambda^{n,\beta}(H_{h,[s]}^n + \lambda q_{h,[s-1]}^n)(r, z) \quad \text{a.e. in } \Omega. \tag{5.93}$$

Convergence of this algorithm is proved in [12] in an abstract general setting when $\lambda\beta \leq 1/2$.

Remark 5.5.1 *Given that at each time step $n \in \{1, \dots, m\}$ \mathcal{B}^n is a nonlinear mapping, then from (5.93) it follows that $q_{h,[s]}^n \notin \mathcal{V}_h$. Hence, the last integral of (5.89) can not be computed exactly, so we need to use numerical integration. Then, it is enough to compute (5.93) only in a few points as the vertices or barycenters of the triangles in the mesh.*

Remark 5.5.2 *An interesting feature of the algorithm is that, in cases where the domain and σ are time independent, the matrix associated to the linear problem (5.89) is independent of n and s , and then it can be assembled and factorized only once before the loop in time steps.*

5.5.1 The Preisach model

The Preisach model was first suggested to describe ferromagnetism (see [76]). Nowadays it is recognized as a fundamental tool for describing a wide range of hysteresis phenomena in different subjects as physics, mechanics or superconductivity, among others. Here we briefly recall the classical definition and some properties of this operator following the works of Visintin and Mayergoyz (see [63, 95]).

The classical Preisach model is constructed from an infinite set of hysteresis operators called *relay operators*. A relay operator is represented by elementary rectangular loops with “up” and “down” switching values. Given any couple $\rho = (\rho_1, \rho_2) \in \mathbb{R}^2$, with $\rho_1 < \rho_2$, the corresponding relay operator h_ρ , depicted in Figure 5.6, is defined as follows: for any $u \in C([0, T])$ and $\xi \in \{1, -1\}$, $h_\rho(u, \xi)$ is a function from $[0, T]$ to \mathbb{R} such that,

$$h_\rho(u, \xi)(0) := \begin{cases} -1 & \text{if } u(0) \leq \rho_1, \\ \xi & \text{if } \rho_1 < u(0) < \rho_2, \\ 1 & \text{if } u(0) \geq \rho_2. \end{cases}$$

Then, for any $t \in (0, T]$, let us set $X_u(t) := \{\tau \in (0, t] : u(\tau) = \rho_1 \text{ or } \rho_2\}$ and define

$$h_\rho(u, \xi)(t) := \begin{cases} h_\rho(u, \xi)(0) & \text{if } X_u(t) = \emptyset, \\ -1 & \text{if } X_u(t) \neq \emptyset \text{ and } u(\max X_u(t)) = \rho_1, \\ 1 & \text{if } X_u(t) \neq \emptyset \text{ and } u(\max X_u(t)) = \rho_2. \end{cases}$$

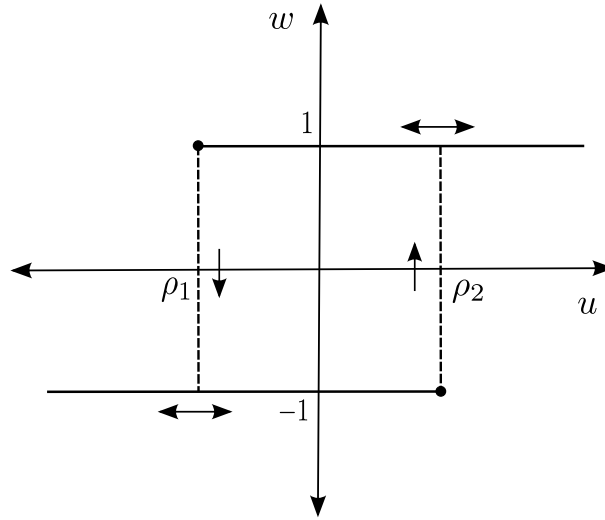


Figure 5.6: Scalar relay.

We notice that $h_\rho = \pm 1$ with up-switch at ρ_2 and down-switch at ρ_1 . The value of the relay operator remains at the last value (± 1) until u takes the value of one opposite switch, that is, switch to value $+1$ when u attains the value ρ_2 from below, and to -1 when it attains ρ_1 from above. This operator is the most simple model of discontinuous hysteresis.

Let us now introduce the half-plane $\mathcal{P} := \{\rho = (\rho_1, \rho_2) \in \mathbb{R}^2 : \rho_1 < \rho_2\}$ called the *Preisach plane*. Let us denote by Y the family of Borel measurable functions $\mathcal{P} \rightarrow \{-1, 1\}$, and by ξ , a generic element of Y . For any finite Borel measure μ over \mathcal{P} , let us then define the Preisach operator

$$\begin{aligned} \tilde{\mathcal{F}} : C([0, T]) \times Y &\longrightarrow L^\infty(0, T), \\ (u, \xi) &\longmapsto [\tilde{\mathcal{F}}(u, \xi)](t) = \int_{\mathcal{P}} [h_\rho(u, \xi(\rho))](t) d\mu(\rho). \end{aligned} \quad (5.94)$$

The Preisach model can be interpreted as the sum of a family of relays, distributed with a certain density μ .

Let us recall the following results (see [95] Chapter IV, Theorems 1.2 and 3.2, respectively).

Proposition 5.5.1 *For any finite Borel measure μ over \mathcal{P} , the operator $\tilde{\mathcal{F}}$ is causal and rate independent, so it is a hysteresis operator. Moreover, if $\mu \geq 0$ then $\tilde{\mathcal{F}}$ is piecewise monotone and order preserving.*

Proposition 5.5.2 *Let μ be a finite Borel measure over \mathcal{P} such that*

$$|\mu|(\mathbb{R} \times \{r\}) = |\mu|(\{r\} \times \mathbb{R}) = 0 \quad \forall r \in \mathbb{R}.$$

Then, for any $\xi \in \bar{\mathcal{S}}$ the operator $\tilde{\mathcal{F}}(\cdot, \xi) : C([0, T]) \rightarrow C([0, T])$ is strongly continuous, where $\bar{\mathcal{S}}$ is the family of relay configurations which can be attained by applying a continuous input to a

system initially in the so-called virgin state, namely, a system which has never experienced any hysteresis process:

$$\xi^\nu(\rho) := \begin{cases} 1 & \text{if } \rho_1 + \rho_2 < 0, \\ -1 & \text{if } \rho_1 + \rho_2 > 0. \end{cases} \quad (5.95)$$

Remark 5.5.3 ξ^ν represents an “initial state” from which it is possible to obtain the information needed to compute the Preisach operator. Notice that the mathematical analysis of the operator is valid for any choice of ξ^ν .

Geometric Interpretation

The understanding of the Preisach operator is considerably facilitated by its geometric interpretation. This interpretation is based on the fact that there is a one-to-one correspondence between relay operators h_ρ and points (ρ_1, ρ_2) of the half plane \mathcal{P} .

We notice that, given $u \in C([0, T])$ and ξ , each relay $h_\rho(u, \xi(\rho))$ is such that, for any $t \in [0, T]$

$$\begin{cases} \text{if } u(t) \leq \rho_1, & \text{then } [h_\rho(u, \xi(\rho))](t) = -1 \\ \text{if } u(t) \geq \rho_2, & \text{then } [h_\rho(u, \xi(\rho))](t) = 1 \\ \text{if } \rho_1 < u(t) < \rho_2, & \text{then } [h_\rho(u, \xi(\rho))](t) \text{ depends on } u|_{[0,t]} \text{ and } \xi(\rho). \end{cases} \quad (5.96)$$

That is, for a given $u(t)$, all the relays h_ρ such that $\rho_1 \geq u(t)$ are “switched down”. Similarly the relays h_ρ such that $\rho_2 \leq u(t)$ are “switched up” (see Figure 5.7).

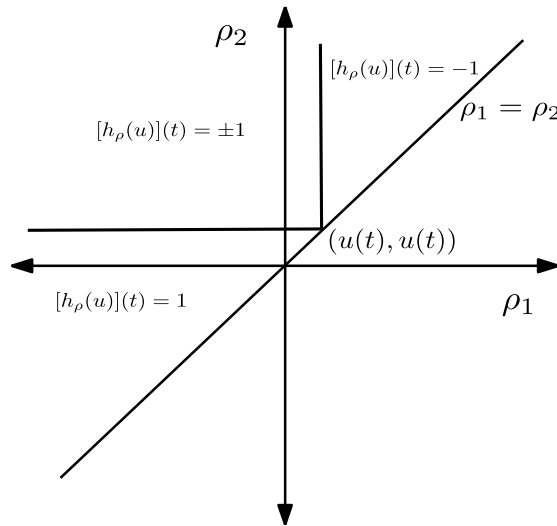


Figure 5.7: Preisach domain. $h_\rho(u) := h_\rho(u, \xi(\rho))$.

In order to study the Preisach operator, we will make the following assumptions:

H.4 We choose the measure μ having a density, i.e.

$$d\mu(\rho) = p(\rho) d\rho, \quad (5.97)$$

with $0 < p \in L^1(\mathcal{P})$, usually known as *Preisach function*.

H.5 Let $\mathcal{T} \subset \mathcal{P}$ be the right-angled triangle such that its hypotenuse is part of the line $\rho_1 = \rho_2$, while the remaining vertex has coordinates $(-\rho_0, \rho_0)$. From now on, we consider that p has support in \mathcal{T} , i.e., p vanishes outside the triangle $\mathcal{T} \subset \mathcal{P}$ (see Figure 5.8).

Both assumptions are reasonable with regard to physical systems in magnetism; the former states that it is possible to consider a statistical distribution of the points in the Preisach plane (see [15]), and the latter is consistent with the occurrence of negative and positive “saturation”.

From the latter assumptions and Propositions 5.5.1 and 5.5.2 we have the following result.

Lemma 5.5.2 *Given ξ , under assumption H.4 it follows that the Preisach operator $\tilde{\mathcal{F}}(\cdot, \xi) : C([0, T]) \rightarrow C([0, T])$, is a hysteresis operator, strongly continuous, piecewise monotone and order preserving. If we further assume H.5, it follows that*

$$|[\tilde{\mathcal{F}}(u, \xi)](t)| \leq \int_{\mathcal{T}} p(\rho) d\rho \quad \forall u \in C(0, T).$$

As in Section 5.2.1 it is possible to define the operator $\mathcal{F} : \mathcal{M}(\Omega; C([0, T]) \times Y) \rightarrow \mathcal{M}(\Omega; C([0, T]))$ as follows

$$[\mathcal{F}(u, \xi)](r, z, t) := [\tilde{\mathcal{F}}(u(r, z), \xi(r, z))](t) \quad \text{a.e. in } \Omega \times [0, T]. \quad (5.98)$$

Then, by using similar results as those stated in Propositions 3.1 and 3.2 in [95, Section XII.3], but for the case of weighted Sobolev spaces, we can prove the following one:

Lemma 5.5.3 *Let $\xi : \Omega \rightarrow Y$ be an “initial state” and assume that H.4 and H.5 holds. Then, the operator $\mathcal{F}(\cdot, \xi) : L_r^2(\Omega; C(0, T)) \rightarrow L_r^2(\Omega; C(0, T))$ is causal, strongly continuous, piecewise monotone and affinely bounded (cf. (5.6), (5.7), (5.8) and (5.28), respectively).*

From the latter we obtain the following existence result.

Lemma 5.5.4 *Let us assume H.2, H.3, H.4 and H.5. Then, by choosing as hysteresis operator the classical Preisach operator \mathcal{F} (cf. (5.98)) in the constitutive equations (5.19) and (5.23) it follows that there exist (H_D, B_D) and (H_N, B_N) solution to Problems 5.4.1 and 5.4.2, respectively.*

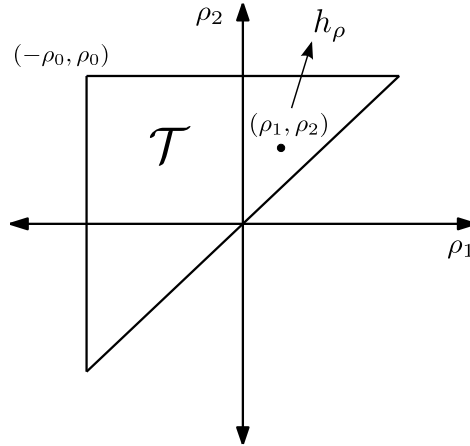


Figure 5.8: Preisach triangle.

Now, to understand the geometrical interpretation of the Preisach operator, we consider a simple setting. First we assume that $u(t)$ at some instant of time t^0 has a value less than $-\rho_0$. Notice that, from the particular choice of u , all the relays are well defined in \mathcal{T} without the need of giving an “initial state” ξ , for $t > t^0$. Given that, $u(t^0) \leq -\rho_0 \leq \rho_1$ for all $(\rho_1, \rho_2) \in \mathcal{T}$, then from (5.96) it follows that all the relay operators $[h_\rho(u)](t) := [h_\rho(u, \xi)](t^0) = -1$ in \mathcal{T} . Now, we consider that u increases monotonically. From the definition of the relay operator, the relays will only change to a positive state. Thus, triangle \mathcal{T} is subdivided into two sets (one possibly empty):

$$S_u^-(t) = \{(\rho_1, \rho_2) \in \mathcal{T} : [h_\rho(u)](t) = -1\} \quad \text{and} \quad S_u^+(t) = \{(\rho_1, \rho_2) \in \mathcal{T} : [h_\rho(u)](t) = 1\}. \quad (5.99)$$

Since the change to a positive state of the relay h_ρ depends only on the value of ρ_2 , we obtain that $L_u(t) := \partial S_u^-(t) \cap \partial S_u^+(t)$ is orthogonal to ρ_2 axis and moves up. This subdivision is made by the line $\rho_2 = u(t)$ (see Figure 5.9 (left)). Function u increases until it reaches some maximum value $-\rho_0 < u_1 < \rho_0$ at time t^1 (see Figure 5.9 (right)).

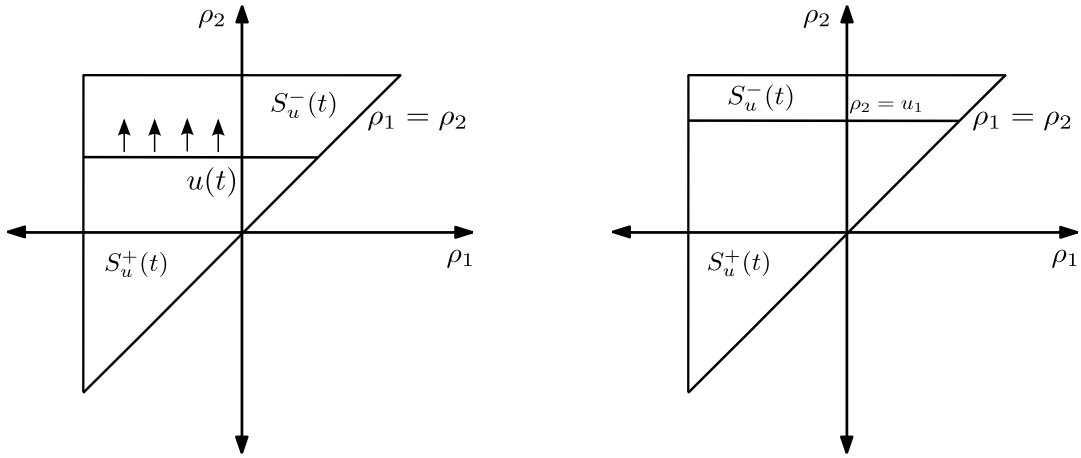


Figure 5.9: $L_u(t)$: $u(t)$ is increasing (left) and attains a maximum at u_1 (right).

Now, we assume that $u(t)$ decrease monotonically. Then, the relays will only change to a negative state. Since the change to a negative state of the relay h_ρ depends only on the value of ρ_1 , we obtain that the line $\rho_1 = u(t)$ moves from right to left (see Figure 5.10 (left)). Function u decreases until it reaches at time t^2 some value $- \rho_0 < u_2$. At this point, the interface $L_u(t)$ between $S_u^+(t)$ and $S_u^-(t)$ has now two segments, the horizontal and vertical ones depicted in Figure 5.10 (right).

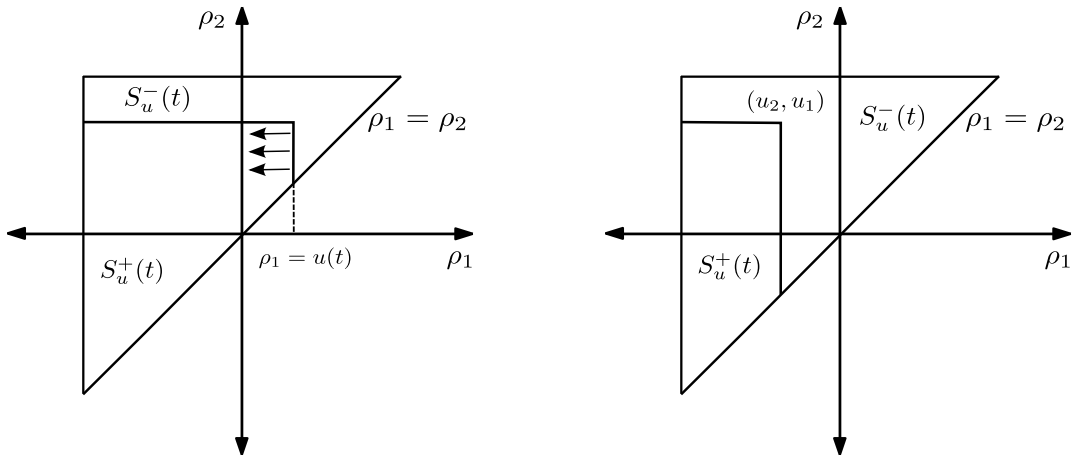


Figure 5.10: $L_u(t)$: $u(t)$ is decreasing from u_1 (left) and attains a minimum at u_2 (right).

Now, we assume that $u(t)$ increases again until it reaches at time t^3 some maximum value u_3 that is less than u_1 . Geometrically, this increment produce a new horizontal segment in $L_u(t)$ which moves up. This motion is terminated when the maximum u_3 is reached. This is shown

in Figure 5.11 (left). Finally we assume that $u(t)$ decreases until it reaches at time t^4 some minimum value $u_4 > u_2$. This variation results in the formation of a new vertical line in $L_u(t)$ that moves from right to left as it is shown in Figure 5.11 (right). At this point, $L_u(t)$ has two vertices (u_2, u_1) and (u_4, u_3) (see Figure 5.12).

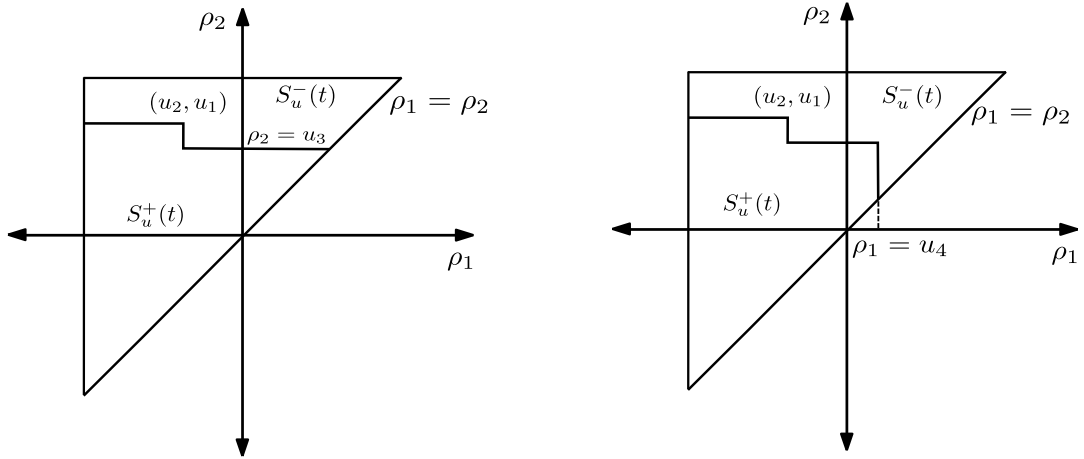


Figure 5.11: $L_u(t)$: $u(t)$ attains a maximum at u_3 (left) and attains a minimum at u_4 (right).

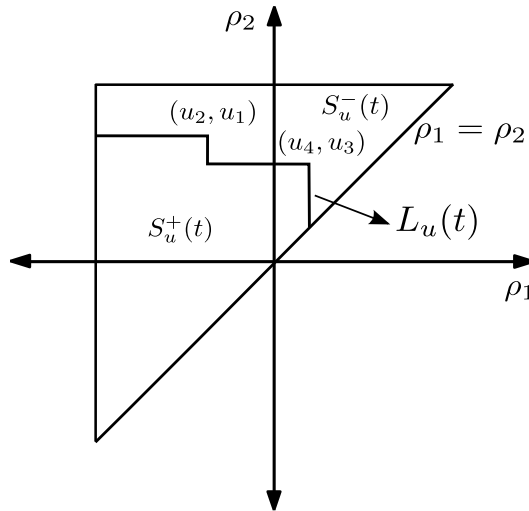


Figure 5.12: Staircase line L_u at $t = t^4$.

A similar figure can be obtained if we consider a function $v \in C([0, T])$ such that, unlike $u(t)$,

at some instant of time t^0 has a value that is greater than ρ_0 . We assume that $v(t)$ decreases to $v_1 > -\rho_0$, then increases to $v_2 \leq \rho_0$, next decreases to v_3 and finally increases to v_4 as is depicted Figure 5.13 (right). $L_v(t)$ is illustrated in Figure 5.13 (left); we notice that the first line of $L_v(t)$ is a vertical line, because $v(t)$ decreases from a value greater than ρ_0 .

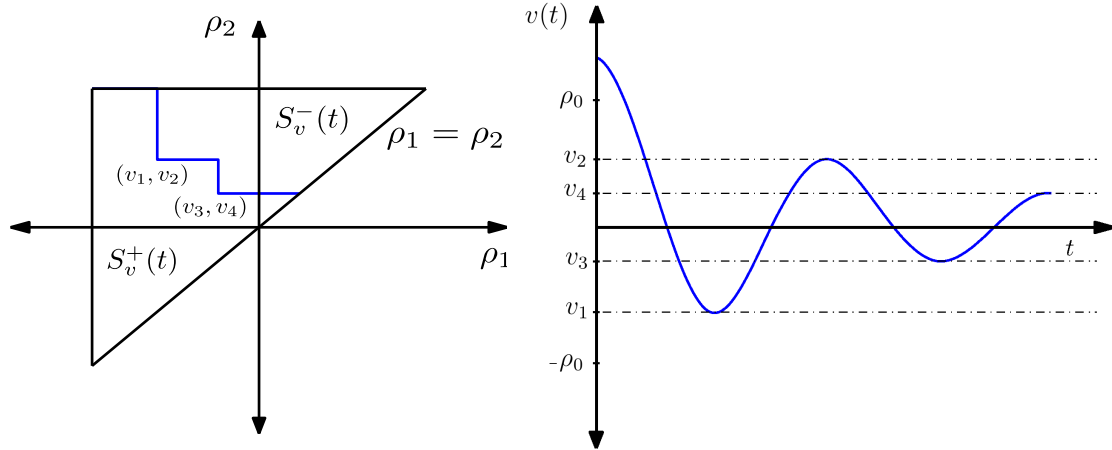


Figure 5.13: Staircase line $L_v(t)$ (left) and input $v(t)$ (right).

We can summarize the above analysis as follows; for a given $u \in C([0, T])$, and any instant t of time, the triangle \mathcal{T} is subdivided into two sets: $S_u^+(t)$ consisting of points (ρ_1, ρ_2) for which the corresponding relay operators $h_\rho(u)$ are positive (in the “up” position), and $S_u^-(t)$ consisting of points (ρ_1, ρ_2) for which the corresponding relay operators $h_\rho(u)$ take negative values (in the “down” position). The interface $L_u(t)$ between $S_u^+(t)$ and $S_u^-(t)$ is a staircase line whose vertices have coordinates (ρ_1, ρ_2) coinciding respectively with the local minimum and maximum values of u at previous instants of time. At time t , the staircase line $L_u(t)$ is attached to the line $\rho_1 = \rho_2$ in the current value of u , namely, $L_u(t)$ intersect the line $\rho_1 = \rho_2$ in $(u(t), u(t))$. $L_u(t)$ moves when $u(t)$ changes, intersects the line $\rho_1 = \rho_2$ horizontally and it moves up as $u(t)$ increases. Otherwise, $L_u(t)$ intersects the line $\rho_1 = \rho_2$ vertically and it moves from right to left as $u(t)$ decreases (see Figure 5.14).

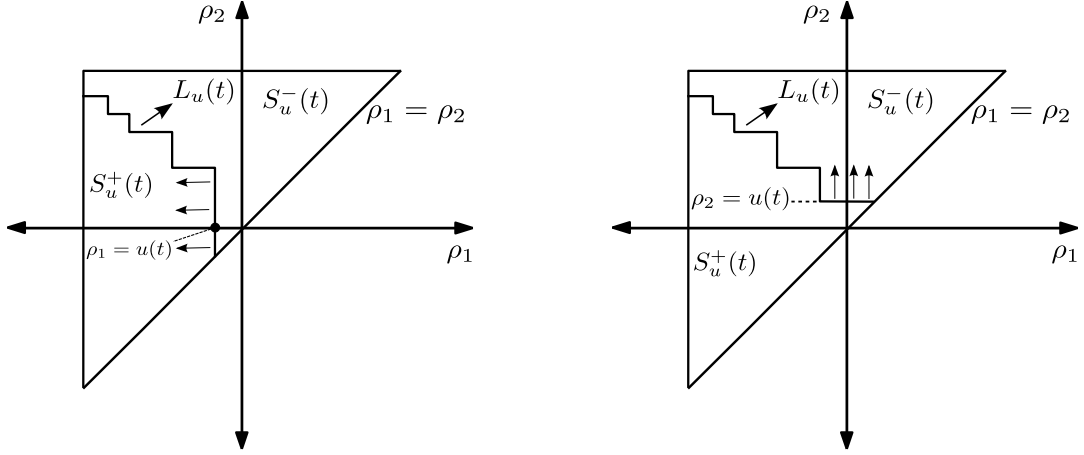


Figure 5.14: Staircase line $L_u(t)$ moving right to left (left) and moving up (right).

Hence, from the latter and the assumption on μ we notice that, at any instant of time t the integral in (5.94) can be subdivided into two integrals, over $S_u^+(t)$ and $S_u^-(t)$, respectively:

$$\begin{aligned} w_u(t) &:= [\tilde{\mathcal{F}}(u)](t) = \int_{\mathcal{P}} [h_\rho(u)](t) p(\rho) d\rho = \int_{\mathcal{T}} [h_\rho(u)](t) p(\rho) d\rho \\ &= \int_{S_u^+(t)} [h_\rho(u)](t) p(\rho) d\rho + \int_{S_u^-(t)} [h_\rho(u)](t) p(\rho) d\rho. \end{aligned}$$

We recall that, because of the particular choice of the values of u we do not need an “initial state” ξ . Moreover, because of (5.99) and the latter equation we obtain that

$$w_u(t) = \int_{S_u^+(t)} p(\rho) d\rho - \int_{S_u^-(t)} p(\rho) d\rho. \quad (5.100)$$

Remark 5.5.4 *To compute the Preisach model in $(0, T]$, in general it is enough to know $u(0)$, the Preisach function p and the history of u represented by $S_u^+(t)$ and $S_u^-(t)$, which contain the minimum information to compute (5.100). Notice that for $t = 0$ the above sets are deduced from the “initial state” ξ .*

From expression (5.100), it follows that $[\tilde{\mathcal{F}}(u)](t)$ depends on the particular subdivision of the limiting triangle, \mathcal{T} , into $S_u^+(t)$ and $S_u^-(t)$. Therefore, it depends on the shape of the interface $L_u(t)$, which in its turn is determined by the extremum values of $u(t)$ at previous instants of time. It turns out that not all extremum input values are accumulated by the model, in fact, given the dependence of the staircase line $L_u(t)$ we can see that the Preisach operator has a wiping-out property. This property states that each time the input reaches a local maximum $u(t)$, $L_u(t)$ erases, or “wipes out” the previous vertices whose ρ_2 value is lower than the current value $u(t)$. As a result, all previous dominate maxima values recorded in $L_u(t)$ which have a value lower than the current maxima are taken out. Similarly, each time an input reaches a local minimum $u(t)$,

the memory curve erases all previous vertices whose ρ_1 value was higher than the current $u(t)$ value. To illustrate this property, we consider a simple setting. Let $u \in C([0, T])$ characterized by a finite decreasing sequence $\{u_1, u_3, u_5, u_7\}$ of local maxima and an increasing sequence $\{u_2, u_4, u_6, u_8\}$ of local minima, with $-\rho_0 < u_i < \rho_0$, $i = 1, \dots, 8$ (see Figure 5.15). Now, let us assume that $u(t)$ is monotonically increasing until it reaches u_9 , such that $u_3 < u_9 < u_1$. This increase of $u(t)$ results in the formation of a new line in $L_u(t)$ which intersects the line $\rho_1 = \rho_2$ horizontally and moves up until the maximum value u_9 is reached. Then we obtain a modified staircase line $L_u(t)$ where all vertices whose ρ_2 -coordinates were below u_9 have been wiped out (see Figure 5.16).

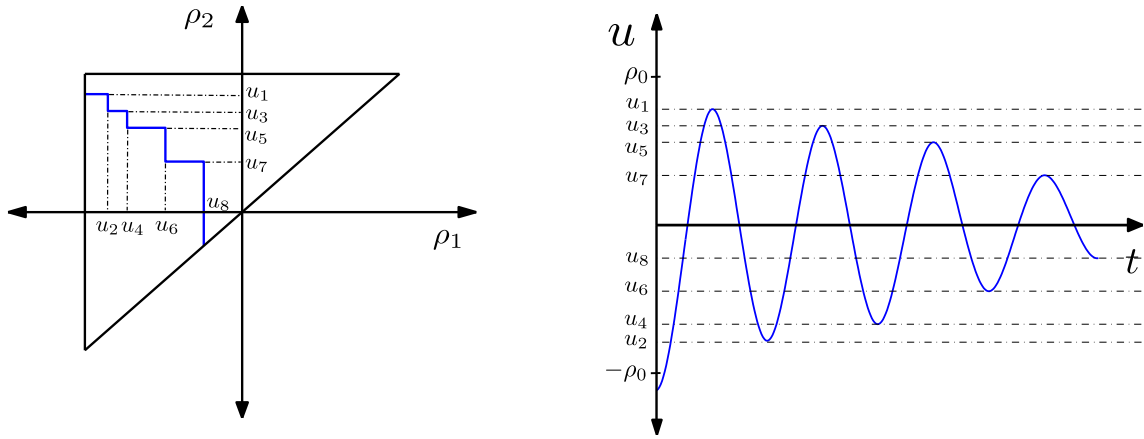


Figure 5.15: Initial staircase line L_u (left) and function u (right).

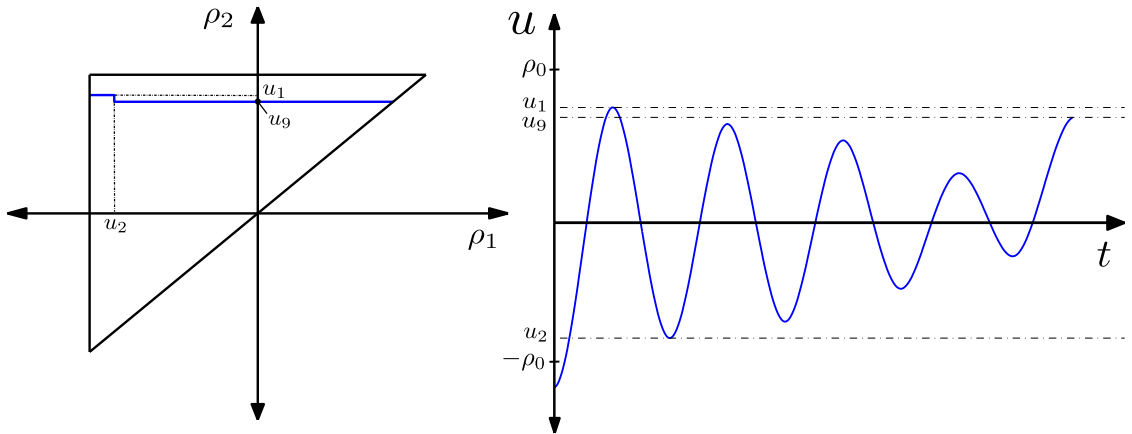


Figure 5.16: L_u for increasing u until u_9 (left) and function u (right).

Similarly, instead of assuming that $u(t)$ is monotonically increasing, let us suppose that it decreases until it reaches u_9 , such that $u_2 < u_9 < u_4$. Function u and the corresponding staircase line $L_u(t)$ are depicted in Figure 5.17.

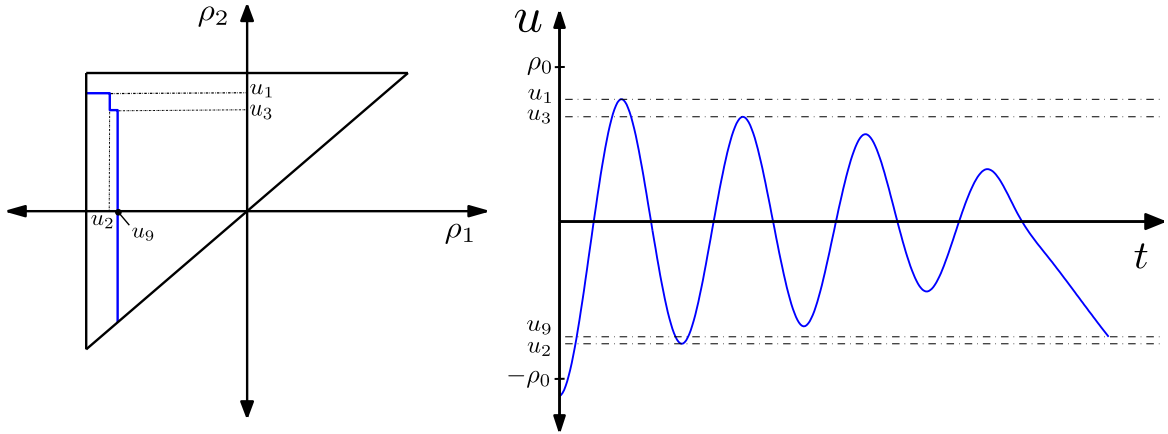


Figure 5.17: L_u for decreasing u until u_9 (left) and function u (right).

Another important property of the Preisach operator is referred to as the *congruency property*. This property states that as the input is cycled between two extremum values, the minor loop traced will have the same shape, independently of history (see Figure 5.18). However, the position of the minor loop along the output axis will be determined by the history of past input variations (for further details, see [63]).

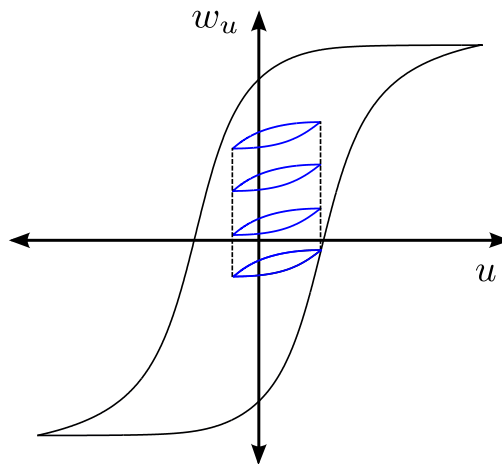


Figure 5.18: Congruency property.

Identification Problem

When using the Preisach operator to model a physical system it is necessary to find the density function p , that characterizes the phenomenon. Therefore, the identification of the measure p is an important step for the effective use of this model in real applications.

There are many different analytical expressions to represent the Preisach distribution, e.g., Factorized-Lorentzian or Gauss-Gauss distribution functions (see [15]).

The Factorized-Lorentzian distribution function is

$$p(\rho_1, \rho_2) := N \left(\left(1 + \left(\frac{\rho_2 - \omega}{\gamma\omega} \right)^2 \right) \left(1 + \left(\frac{\rho_1 + \omega}{\gamma\omega} \right)^2 \right) \right)^{-1}.$$

The Gauss-Gauss distribution function is defined as follows:

$$p(\rho_1, \rho_2) := N \exp \left(- \frac{(\frac{\rho_2 - \rho_1}{2} - \omega)^2 - (\frac{\rho_2 + \rho_1}{2})^2}{2\gamma^2\omega^2} \right),$$

Parameter N is the so-called normalization factor, and ω and γ are unknowns which can be determined with only a few measurements. Examples of the distribution functions are shown in Figures 5.19 and 5.20. The parameters are considered as in [48] to approximate the mayor hysteresis loop of Co-coated Fe_2O_3 .

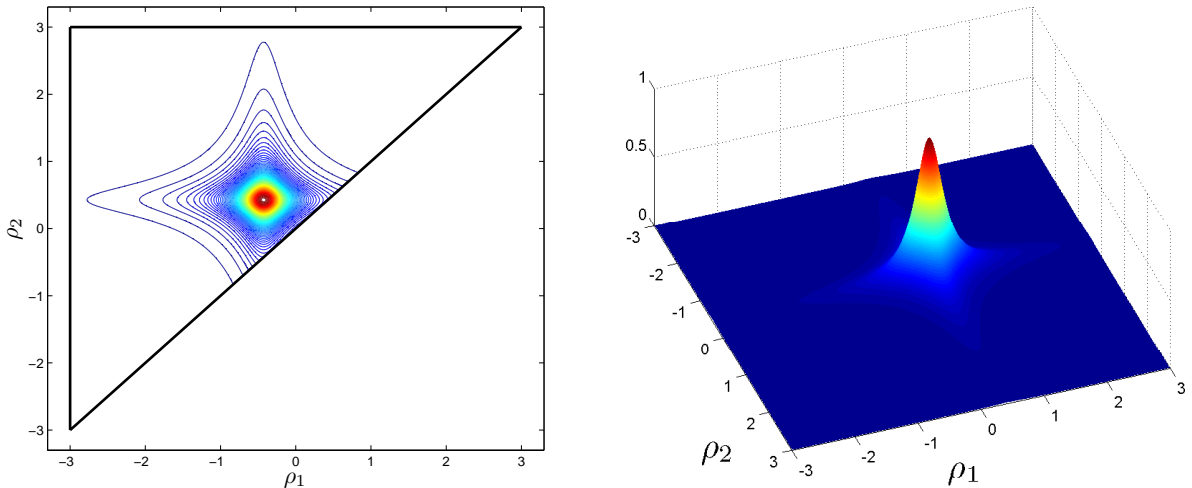


Figure 5.19: Factorized-Lorentzian distribution function with $\gamma = 0.614152$ and $\omega = 0.427471$.

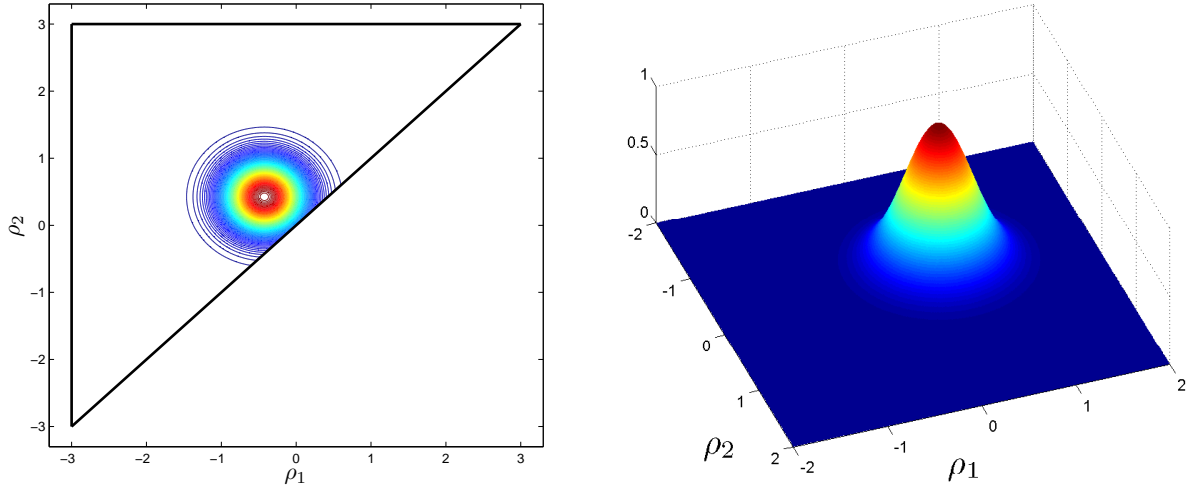


Figure 5.20: Gauss-Gauss distribution function with $\gamma = 0.582933$ and $\omega = 0.425094$.

On the other hand, there are several methods to approximate the Preisach function based on experimental data; for details see, for instance [17, 51, 71, 32].

Preisach implementation issues

Once we have the distribution function and an “initial state”, given $u \in C([0, T])$ we can compute $w_u(t) := [\tilde{\mathcal{F}}(u)](t)$ by means of (5.94). Based on this feature, Mayergoyz [63] developed another approach for the numerical implementation of the Preisach model that not require the Preisach function p , but a function E called *Everett function* which describes the effect of p on the hysteresis operator. To obtain the Everett function, first order transition curves are required. To define a first order transition curve, we consider a function $u \in C([0, T])$, such that at time t^0 , $u(t^0) \leq -\rho_0$. Then, u is monotonically increased until it reaches some value ρ'_2 at time t^1 . We denote by $w_{\rho'_2} = w_u(t^1)$. A first order transition curve is formed as the above monotonic increase of u is followed by a subsequent monotonic decrease, namely, from ρ'_2 , u decreases monotonically until it reaches some value ρ'_1 at time t^2 and we denote by $w_{\rho'_2, \rho'_1} = w_u(t^2)$ (see Figures 5.21 and 5.22).

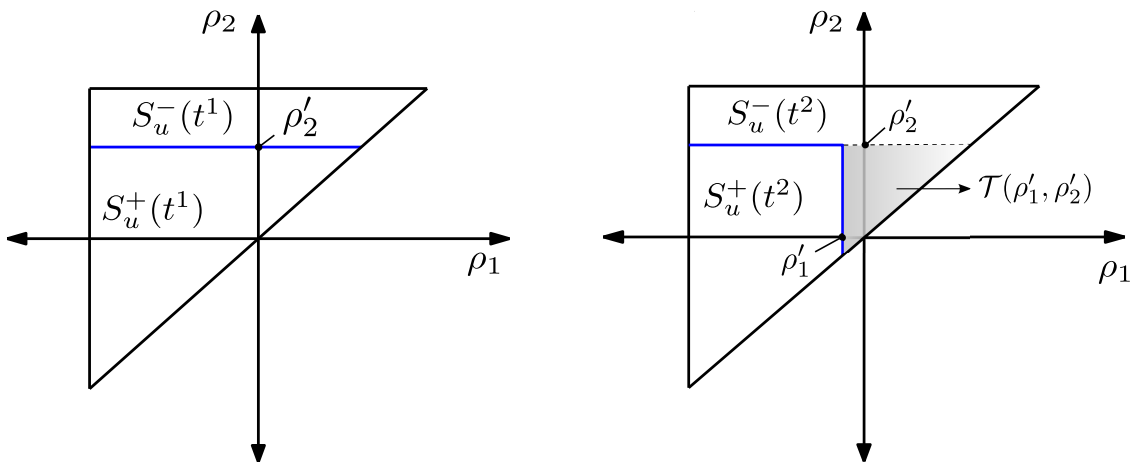


Figure 5.21: Staircase line $L_u(t)$ at time t^1 (left) and at time t^2 (right).

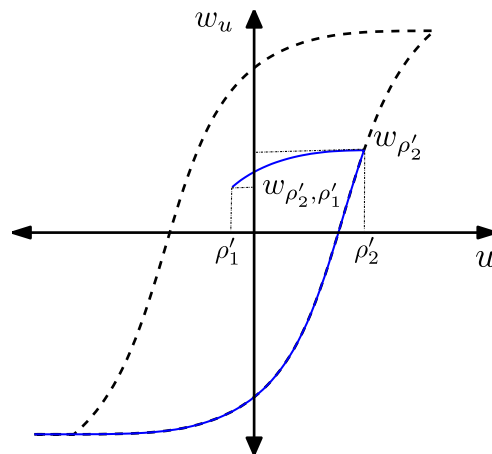


Figure 5.22: First order transition curve.

We define the Everett function $E : \mathcal{T} \rightarrow \mathbb{R}$ by

$$E(\rho'_1, \rho'_2) = \frac{w_{\rho'_2} - w_{\rho'_2, \rho'_1}}{2}. \tag{5.101}$$

From (5.100), we notice that

$$\begin{aligned} w_{\rho'_2, \rho'_1} - w_{\rho'_2} &= \left(\int_{S_u^+(t^2)} p(\rho) d\rho - \int_{S_u^-(t^2)} p(\rho) d\rho \right) - \left(\int_{S_u^+(t^1)} p(\rho) d\rho - \int_{S_u^-(t^1)} p(\rho) d\rho \right) \\ &= -2 \int_{\mathcal{T}(\rho'_1, \rho'_2)} p(\rho) d\rho, \end{aligned}$$

with $\mathcal{T}(\rho'_1, \rho'_2)$ the triangle such that its hypotenuse is part of the line $\rho_1 = \rho_2$, while the remaining vertex has the coordinate (ρ'_1, ρ'_2) . This is so because $S_u^+(t^2) = S_u^+(t^1) \setminus \mathcal{T}(\rho'_1, \rho'_2)$ and $S_u^-(t^2) = S_u^-(t^1) \cup \mathcal{T}(\rho'_1, \rho'_2)$ (see Figure 5.21 (right)). Therefore, we obtain the following relation between the Preisach function p and the Everett function

$$E(\rho_1, \rho_2) = \int_{\mathcal{T}(\rho_1, \rho_2)} p(\rho) d\rho \quad \forall (\rho_1, \rho_2) \in \mathcal{T}. \quad (5.102)$$

To take into account this relation in the computation of the Preisach operator, first we rewrite (5.100). By adding and subtracting the integral of p over $S_u^+(t)$, the expression (5.100) can be represented in the form:

$$w_u(t) = 2 \int_{S_u^+(t)} p(\rho) d\rho - \int_{\mathcal{T}} p(\rho) d\rho,$$

where \mathcal{T} is the limiting triangle. Moreover, from (5.102) and the definition of the limiting triangle, namely, $\mathcal{T} = \mathcal{T}(-\rho_0, \rho_0)$ it follows that,

$$w_u(t) = 2 \int_{S_u^+(t)} p(\rho) d\rho - E(-\rho_0, \rho_0). \quad (5.103)$$

By assuming that the Preisach function p is known, then to obtain $w_u(t)$ we can compute the first term on the right-hand side of (5.103). For this purpose we consider two cases: increasing and decreasing arguments. For decreasing arguments, we subdivide $S_u^+(t)$ into n trapezoids $Q_k(t)$ (see Figure 5.23 (left)). We can perform this subdivision because, for decreasing arguments, the staircase line $L_u(t)$ intersects the line $\rho_1 = \rho_2$ vertically. Then we have

$$\int_{S_u^+(t)} p(\rho) d\rho = \sum_{k=1}^{n(t)} \int_{Q_k(t)} p(\rho) d\rho, \quad (5.104)$$

where $n(t)$ is the number of local maxima of u up to time t , by taking into account the wiped-out property.

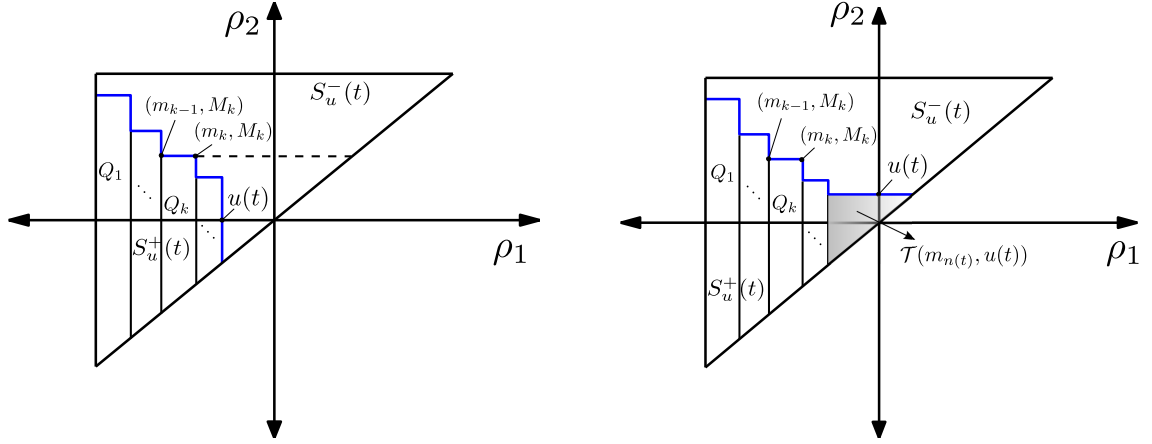


Figure 5.23: Staircase line for a decreasing input (left) and a increasing input (right).

Each trapezoid $Q_k(t)$ depends on the local maximum M_k and on the local minima m_k and m_{k-1} . Notice that, for $k = 1$, m_0 is equal to $-\rho_0$. Moreover, each trapezoid can be represented as the difference of two triangles $\mathcal{T}(m_{k-1}, M_k)$ and $\mathcal{T}(m_k, M_k)$:

$$\int_{Q_k(t)} p(\rho) d\rho = \int_{\mathcal{T}(m_{k-1}, M_k)} p(\rho) d\rho - \int_{\mathcal{T}(m_k, M_k)} p(\rho) d\rho. \quad (5.105)$$

Now, from (5.102), it follows that

$$E(m_{k-1}, M_k) = \int_{\mathcal{T}(m_{k-1}, M_k)} p(\rho) d\rho \quad \text{and} \quad E(m_k, M_k) = \int_{\mathcal{T}(m_k, M_k)} p(\rho) d\rho.$$

Then, from the latter and (5.105), we rewrite (5.104) in terms of the Everett function as follows

$$\int_{S_u^+(t)} p(\rho) d\rho = \sum_{k=1}^{n(t)} (E(m_{k-1}, M_k) - E(m_k, M_k)). \quad (5.106)$$

Finally, from (5.106) and (5.103), we obtain

$$w_u(t) = 2 \sum_{k=1}^{n(t)} (E(m_{k-1}, M_k) - E(m_k, M_k)) - E(-\rho_0, \rho_0).$$

Since we consider u monotonically decreasing, we obtain that the last minimum value $m_{n(t)}$ is equal to the current value of u , namely, $m_{n(t)} = u(t)$. Then

$$w_u(t) = -E(-\rho_0, \rho_0) + 2 \sum_{k=1}^{n(t)-1} (E(m_{k-1}, M_k) - E(m_k, M_k)) \quad (5.107)$$

$$+ 2 (E(m_{n(t)-1}, M_{n(t)}) - E(u(t), M_{n(t)})). \quad (5.108)$$

Because of the decomposition of S_u^+ into trapezoids (see Figure 5.23), this expression is valid only for u being monotonically decreasing. If $u(t)$ is monotonically increasing, then staircase line

$L_u(t)$ intersects the line $\rho_1 = \rho_2$ horizontally. Hence, we may decompose S_u^+ into trapezoids and a triangle (see Figure 5.23 (right)). It follows that

$$\int_{S_u^+(t)} p(\rho) d\rho = \sum_{k=1}^{n(t)-1} (E(m_{k-1}, M_k) - E(m_k, M_k)) + E(m_{n(t)-1}, M_{n(t)}). \quad (5.109)$$

In this case, the last maximum value $M_{n(t)}$ is equal to the current value of u , namely, $M_{n(t)} = u(t)$. Hence, from (5.109) we write (5.103) for a monotonically increasing u as follows:

$$w_u(t) = -E(-\rho_0, \rho_0) + 2 \sum_{k=1}^{n(t)-1} (E(m_{k-1}, M_k) - E(m_k, M_k)) + 2E(m_{n(t)-1}, u(t)). \quad (5.110)$$

From (5.107) and (5.110) we obtain the following expression to compute the Preisach operator in term of the Everett function

$$w_u(t) := \begin{cases} -E(-\rho_0, \rho_0) + 2 \sum_{k=1}^{n(t)-1} (E(m_{k-1}, M_k) - E(m_k, M_k)) \\ + 2(E(m_{n(t)-1}, M_{n(t)}) - E(u(t), M_{n(t)})) & \text{for } u \text{ decreasing,} \\ -E(-\rho_0, \rho_0) + 2 \sum_{k=1}^{n(t)-1} (E(m_{k-1}, M_k) - E(m_k, M_k)) \\ + 2E(m_{n(t)-1}, u(t)) & \text{for } u \text{ increasing.} \end{cases}$$

As an example, we compute $w_u(t)$ by using the Preisach function p given by the Factorized-Lorentzian distribution with parameters $N = 1, \omega = 0.8$ and $\sigma = 0.6$ (see Figure 5.24). Also, the Preisach triangle \mathcal{T} is characterized by $\rho_0 = 5$. Figures 5.25 to 5.27 show the $w_u - u$ loop, the final staircase line $L_u(t)$ and the input $u(t)$.

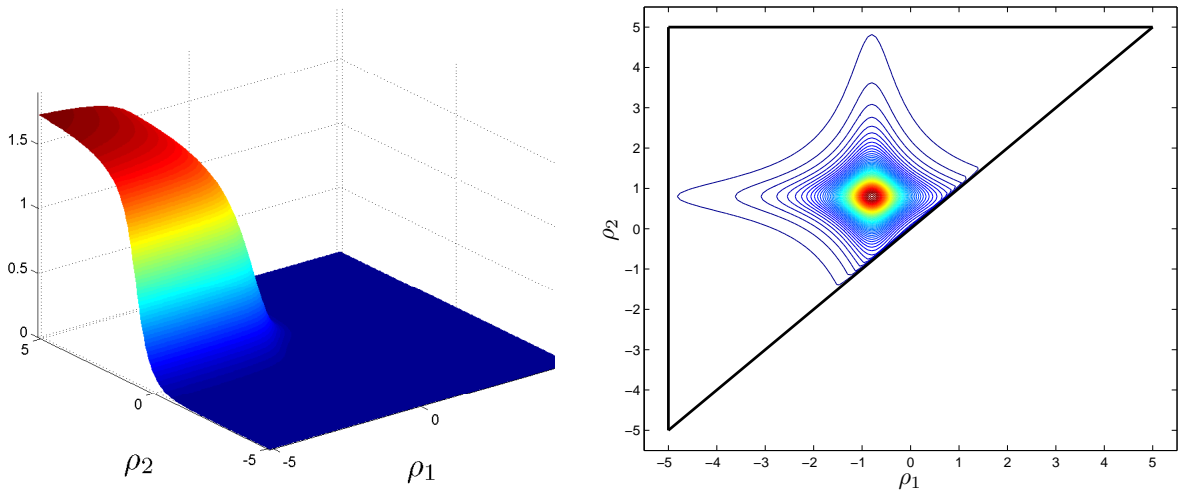
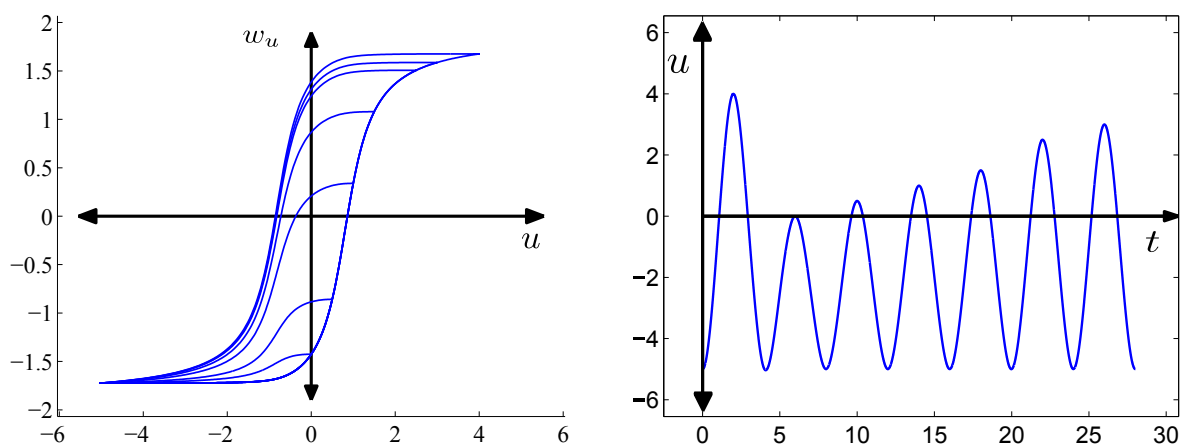
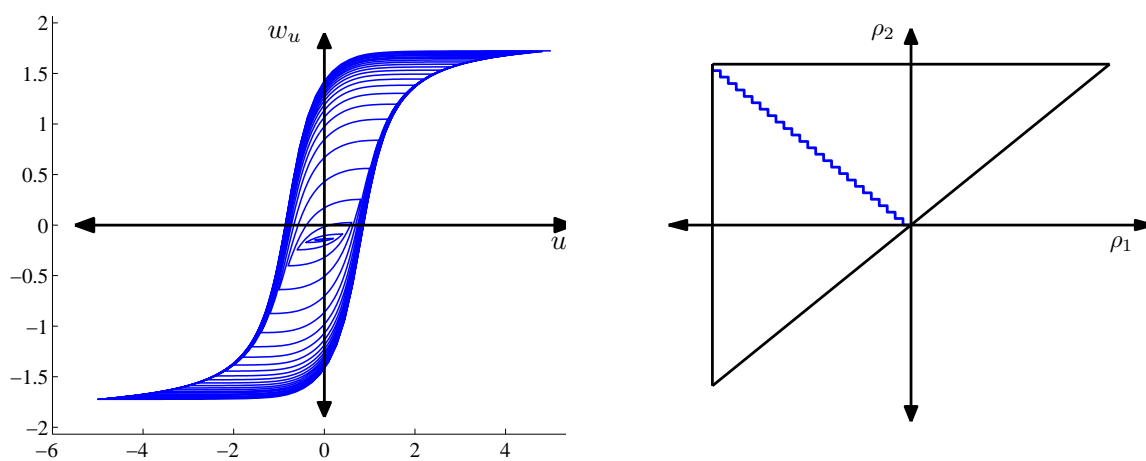


Figure 5.24: Everett function (left) and Factorized-Lorentzian distribution function (right).

Figure 5.25: $w_u - u$ curve (left) and function u (right).Figure 5.26: $w_u - u$ curve (left) and staircase function (right).

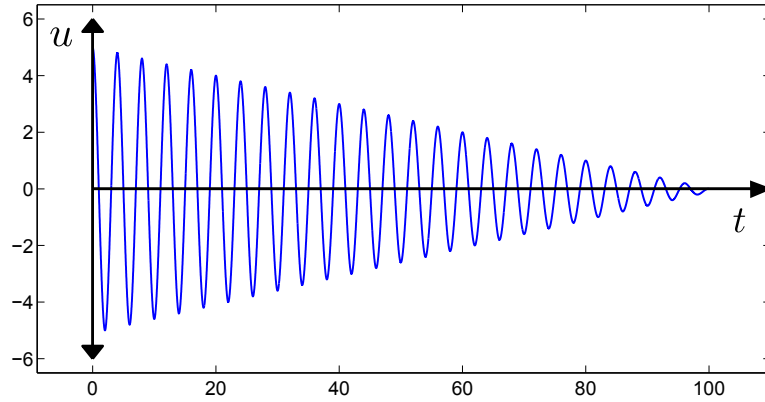


Figure 5.27: Function u .

Remark 5.5.5 *In the previous examples we consider different inputs u , such that $u(0) \geq \rho_0$ or $u(0) \leq -\rho_0$. Clearly, in both cases $S_u^+(0)$ and $S_u^-(0)$ are determined and because of that, there is not need to consider additional information to compute $w_u(t)$, $t \geq 0$. In particular, we have $w_u(0) = E(-\rho_0, \rho_0)$ if $u(0) \geq \rho_0$, and $-E(-\rho_0, \rho_0)$ if $u(0) \leq -\rho_0$. In the case of $-\rho_0 < u(0) < \rho_0$ then, to compute $w_u(0)$ we must have an “initial state”. Depending on this state we obtain different values of $w_u(0)$. For instance, if we consider the “initial states” given by the staircase lines $L_u^1(0)$, $L_u^2(0)$ and $L_u^3(0)$ depicted on Figure 5.28 (left) to compute $w_u(0)$, then we obtain different values w_u^1 , w_u^2 and w_u^3 , respectively (Figure 5.28 (right)).*

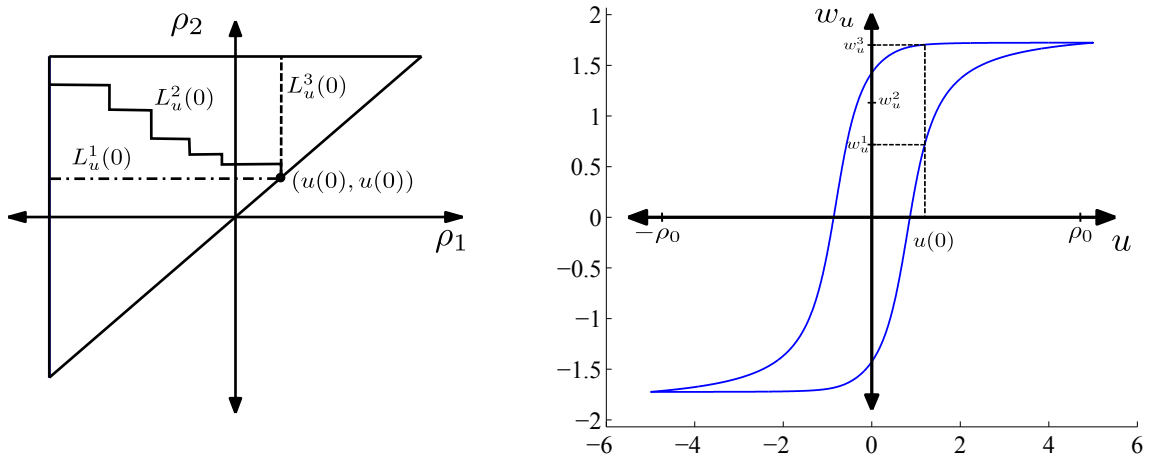


Figure 5.28: Staircase function (left) $w_u - u$ curve (right).

From a practical point of view, the Everett function is given at various points throughout the limiting Preisach triangle \mathcal{T} as depicted in Figure 5.29. The value of the Everett function at each point can be obtained experimentally from the first order transition curves (cf. (5.101)). Using

this discretization, the values of the Everett function on \mathcal{T} are calculated by interpolation.

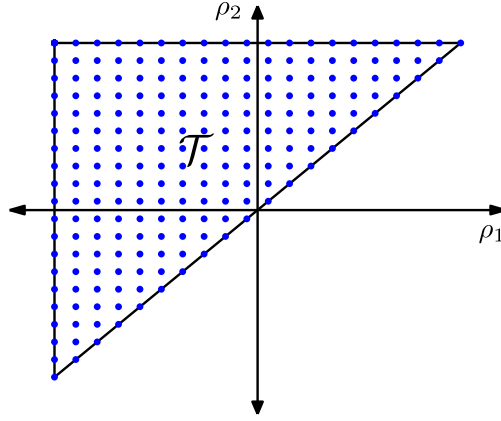


Figure 5.29: Discretization of the Preisach triangle.

Updating procedure $q_{h,[s-1]}^n$

If the hysteresis phenomenon is not considered, that is, if the value of B at time t is determined by the value of H at the same time, the magnetic behaviour is characterized by a monotone function, may be nonlinear. In this case, the computation of the Yosida regularization (cf. (5.87)) involves simple algebraic operations. For instance, if we consider the B-H anhysteretic curve given by $B = \mathcal{G}(H) = \arctan(H)$, then, in order to compute the Yosida regularization we need first to obtain J_λ^β . Since

$$J_\lambda^\beta(s) = \left(I + \lambda \mathcal{G}^\beta \right)^{-1} (s),$$

for a given s we have to solve the following equation to compute $y = J_\lambda^\beta(s)$ (cf (5.86) and (5.88))

$$y + \lambda (\arctan(y) - \beta y) = s.$$

Therefore, given s , $y = J_\lambda^\beta(s)$ is obtained by solving the nonlinear equation $f(y) = 0$, where

$$f(y) := y(1 - \lambda\beta) + \lambda \arctan(y) - s.$$

This equation can be solved, for instance, by the Newton-Raphson method.

In practical applications the B-H curve is obtained by means of physical experiments, then, instead of an analytical representation of the B-H curve, a standard table of the anhysteretic curve of the material is available. To compute the Yosida regularization, we interpolate the curve and proceed as above.

Usually these curves may depend on the space variable but not on time. This is the case, for instance, when we are dealing with heterogeneous media. In this case, each material has its own

curve. However, presence of hysteresis implies that, at each time step n , due to the definition of the hysteresis operator (cf. (5.85) and (5.98)) we have to deal with a nonlinear function \mathcal{B}^n which also depends on the position in space.

Then, given $n \in \{1, \dots, m\}$, to update $q_{h,[s-1]}^n$ in (5.93), because of Remark 5.5.1 it is enough to compute a table for the B-H relation for each vertex or barycenter of the mesh, depending on the quadrature formula that we use to compute the “mass matrix”. Notice that these tables are different at each point and time step $n \in \{1, \dots, m\}$. By using these tables, we compute the Yosida regularization $\mathcal{B}_\lambda^{n,\beta}$ and solve (5.93) pointwise.

Now, let us compute such a table at a specific point $P := (r, z) \in \Omega$ and $n \in \{1, \dots, m\}$. From the iterative algorithm, it follows that there exists $\{u_0, \dots, u_{n-1}\} \subset \mathbb{R}$ which represent the history of the fully-discrete problem at point P , namely, $u_i := H_h^i(P)$, $i = 0, \dots, n-1$. We assume that the B-H relation (cf. (5.19)) is given by a Preisach operator with Preisach function p and “initial state” ξ . Because of the latter, we may define $\mathcal{B}_P^n : \mathbb{R} \rightarrow \mathbb{R}$ (cf. (5.85)) by

$$\mathcal{B}_P^n(s) := [\tilde{\mathcal{F}}(U_{\Delta t^n}^s, \xi)](t^n), \quad (5.111)$$

with $U_{\Delta t^n}^s$ the piecewise linear in time function such that $U_{\Delta t^n}^s(t^l) = u_l$, $l = 0, \dots, n-1$ and $U_{\Delta t^n}^s(t^n) = s$. Finally, the B-H table $(H, \mathcal{B}_P^n(H))$, is computed by discretizing the interval $[-\rho_0, \rho_0]$ defined by the Preisach distribution. Figures 5.30 and 5.31 show the B-H curves for different sequences $\{u_i\}_{i=0}^l$, $l \in \{1, \dots, m\}$ by computing (5.111) with a Preisach function p defined by a Factorized-Lorentian distribution with parameters $N = 1$, $\omega = 0.8$ and $\gamma = 0.6$ (see Figure 5.24). We consider “initial conditions” given by a Staircase function (see Figure 5.30 (left)) or a set of values (see Figure 5.31 (left)). Notice that, from the previous analysis it is clear that we can associate a staircase function to the history data given in Figure 5.31 (left).

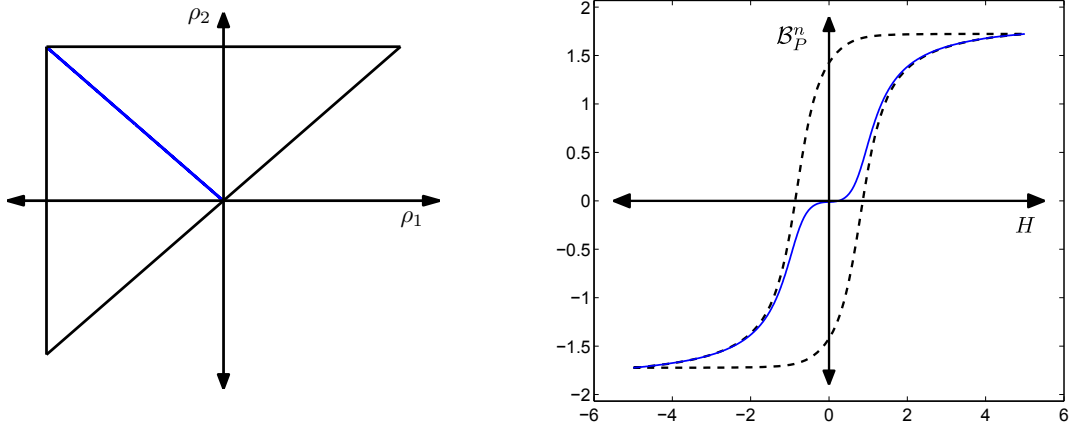


Figure 5.30: History data $L_u(t)$ (left) and B-H curve (right).

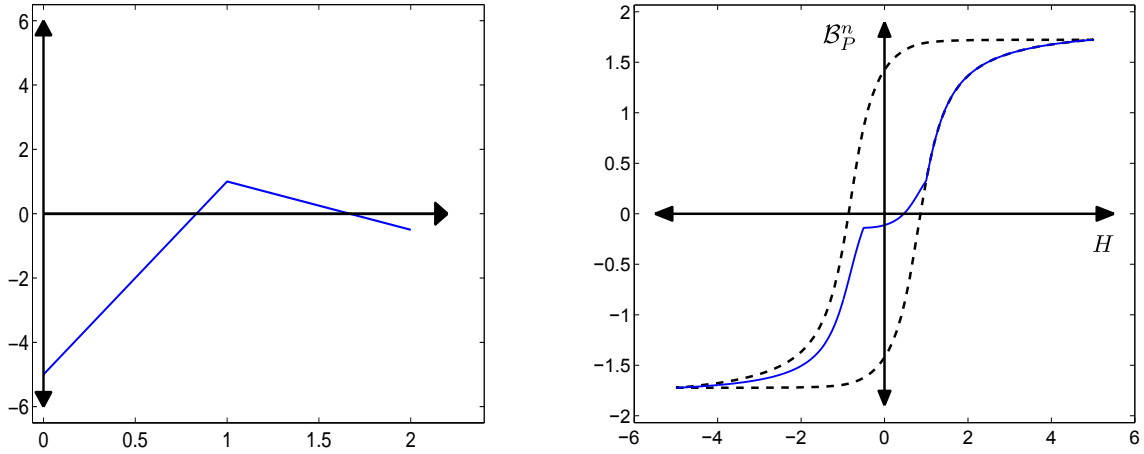


Figure 5.31: History data for H (left) and B-H curve (right).

5.6 Numerical example

In this section we report a numerical result obtained with a Fortran code which implements the numerical method described in Section 5.5 to approximate the solution to Problem 5.4.1.

We describe the problem of computing the eddy current model in a toroidal laminated core surrounded by an infinitely thin coil. We will see that the eddy current model fits within the axisymmetric setting described in the previous sections so we can apply the numerical method proposed above. First, we will describe the problem to be solved in each sheet and deduce the boundary conditions which are different depending on whether we know the current intensity or the voltage drop in the coil.

To the best of the author's knowledge there is not an analytical solution to Problem 5.4.1, so we will assess the order of the method by comparing the computed results with those obtained by computing the numerical solution on a very fine mesh and with a very small time step, which will be taken as "exact" solution.

5.6.1 The eddy current model in a toroidal laminated core

Let us consider a toroidal laminated core consisting of N sheets of rectangular section and thickness d (see Figure 5.32). Let us denote by R_1 and R_2 the internal and external radius, respectively, of the core.

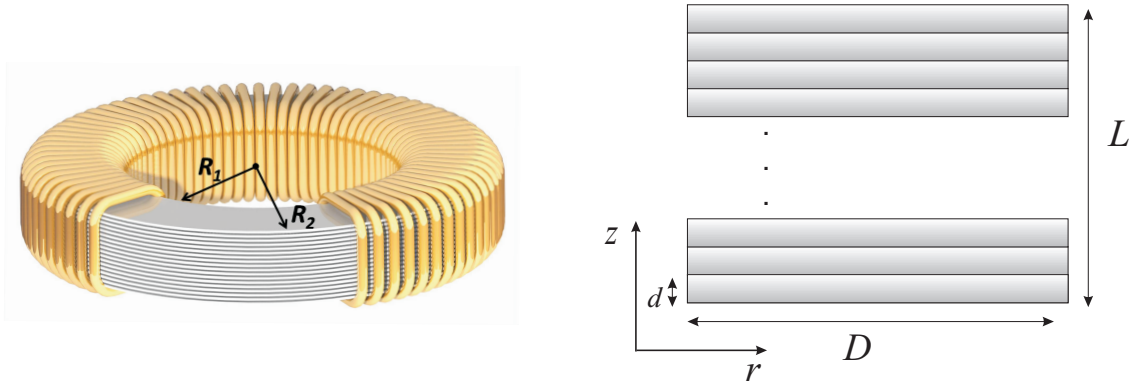


Figure 5.32: Toroidal domain (left) and meridian section (right).

Let n_e be the number of turns of the coil and $I(t)$ the current intensity at time t . The coil will be considered as infinitely thin so it will be modelled as a surface current of surface density (A/m) given by

$$\mathbf{J}_S(R_1, z, t) = \frac{n_e I(t)}{2\pi R_1} \mathbf{e}_z, \quad (5.112)$$

$$\mathbf{J}_S(r, L, t) = \frac{n_e I(t)}{2\pi r} \mathbf{e}_r, \quad (5.113)$$

$$\mathbf{J}_S(R_2, z, t) = -\frac{n_e I(t)}{2\pi R_2} \mathbf{e}_z, \quad (5.114)$$

$$\mathbf{J}_S(r, 0, t) = -\frac{n_e I(t)}{2\pi r} \mathbf{e}_r, \quad (5.115)$$

on the interior, upper, exterior and lower surfaces, respectively. We neglect the thickness of the dielectric between each two sheets so that $L = Nd$. Moreover, we use cylindrical coordinates in order to exploit the cylindrical symmetry of the problem. In particular, the magnetic field only has azimuthal component, namely,

$$\mathbf{H}(r, z, t) = H_\theta(r, z, t)\mathbf{e}_\theta,$$

and the current density in the sheets has the form given in (5.15).

By using Ampère's law and the axisymmetry of the problem it is easy to see that the magnetic field is null outside the core. Hence, since the jump through the boundary of its tangential component is equal to the surface current density, we easily get the following Dirichlet boundary condition for the magnetic intensity (we drop subscript θ for simplicity):

$$H(r, z, t) = \frac{n_e I(t)}{2\pi r}. \quad (5.116)$$

In particular, H is independent of the z -coordinate on the boundary of the core. Moreover, on the internal surfaces between sheets, the normal component of the current density has to be null because they are isolated. Then, according to (5.15),

$$rH(r, z, t) = C(t)$$

where $C(t)$ depends, in principle, on the internal surface. However, since for $r = R_2$

$$R_2 H(R_2, z, t) = n_e I(t),$$

then $C(t) = n_e I(t)$ and therefore the magnetic field is also given by (5.116) on these internal surfaces. Hence, we can compute the magnetic field in one single sheet because we know the Dirichlet boundary conditions on the whole surface of each sheet. This is extremely important from the computational point of view.

Hence, if the current intensity in the coil is given, we arrive at a problem which is a particular case of Problem 5.4.1 with $\Omega := [R_1, R_2] \times [0, d]$, $f \equiv 0$ and

$$g(r, z, t) := \frac{n_e I(t)}{2\pi r}.$$

However, sometimes the data is the potential drop at the ends of the coil along the time, $V(t)$. By applying Faraday's law in the radial section Ω we immediately deduce

$$\frac{\partial}{\partial t} \left(\int_{\Omega} B \, dr dz \right) = \frac{V(t)}{n_e N}, \quad (5.117)$$

because $V(t)/n_e$ is the potential drop along one turn of the coil.

At this point it is interesting to write an energy conservation principle for the whole core. For this purpose we choose in Problem 5.4.1 the test function

$$G(r, z) = H(r, z, t) - \frac{n_e I(t)}{2\pi r},$$

and multiply the resulting equality by $2\pi N$. We get

$$\begin{aligned} 2\pi N \int_{\Omega} \frac{\partial B}{\partial t} H r \, dr dz + \frac{2\pi N}{\sigma} \int_{\Omega} \frac{1}{r} \left[\left| \frac{\partial(rH)}{\partial r} \right|^2 + \left| \frac{\partial(rH)}{\partial z} \right|^2 \right] dr dz = \\ 2\pi N \int_{\Omega} \frac{\partial B}{\partial t} \frac{n_e I(t)}{2\pi r} r \, dr dz = I(t) n_e N \frac{\partial}{\partial t} \left(\int_{\Omega} B \, dr dz \right) = I(t) V(t). \end{aligned} \quad (5.118)$$

The right-hand side represents the power supplied to the system at time t . The first term on the left-hand side is the rate of energy stored by the magnetic field while the second one is the dissipated power by the Joule effect in the laminate (the so-called "classical" eddy current losses).

Then, if the data is the potential drop $V(t)$ instead of the current intensity, the problem to be solved is a particular case of Problem 5.4.2 for $f \equiv 0$ and

$$b'(t) := \frac{V(t)}{n_e N}. \quad (5.119)$$

5.6.2 Numerical solution

Let us consider the eddy current Problem 5.4.1 in a toroidal laminated core consisting of N sheets of rectangular section, thickness d and width $D = R_2 - R_1$. We compute (H, B) in

Table 5.1: Geometrical and physical data for the test

Internal radius of the core, R_1 :	0.0825 m
External radius of the core, R_2 :	0.0925 m
Thickness of the laminate, d :	0.00065 m
Number of turns of the coil, n_e :	1
Electrical conductivity, σ :	4×10^6 (Ohm/m) $^{-1}$
Frequency, f :	50 Hz

the radial section $\Omega = [R_1, R_2] \times [0, d]$, with the non-homogeneous Dirichlet condition given by $g = n_e I(t)/(2\pi r)$. The geometrical and physical data have been summarized in Table 5.1.

Given that in practical applications the measurable data is the B-H curve, usually represented by the Everett function, we assume that the B-H relation (cf. (5.19)) is given by the Preisach operator characterized by the Everett function depicted in Figure 5.33 (left). With this Everett function and the definition of the Preisach operator (cf. (5.94)), the major loop of the B-H curve is illustrated in Figure 5.33 (right).

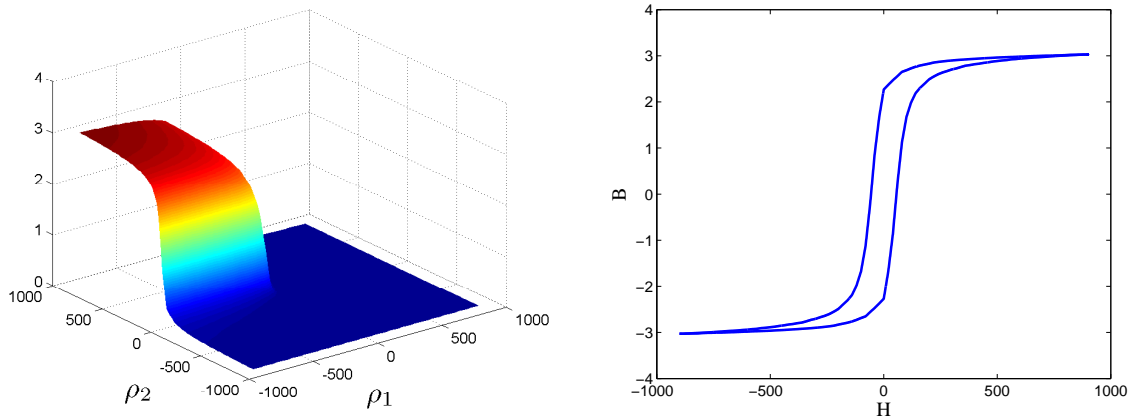


Figure 5.33: Everett function (left) and the corresponding B-H curve (right).

To obtain the Dirichlet boundary condition (5.20), we solve Problem 5.4.2 without hysteresis (see Chapter 3). We consider an anhysteretic B-H curve (see Figure 5.34 (left)) and input data given by the voltage drop $V(t) := dB_m(R_2 - R_1) \cos(2\pi f_V t) 2\pi f_V$ with $f_V = 50$ Hz and $B_m = 1.5$ T, and obtain rH (cf. (5.24)) depicted on Figure 5.34 (right).

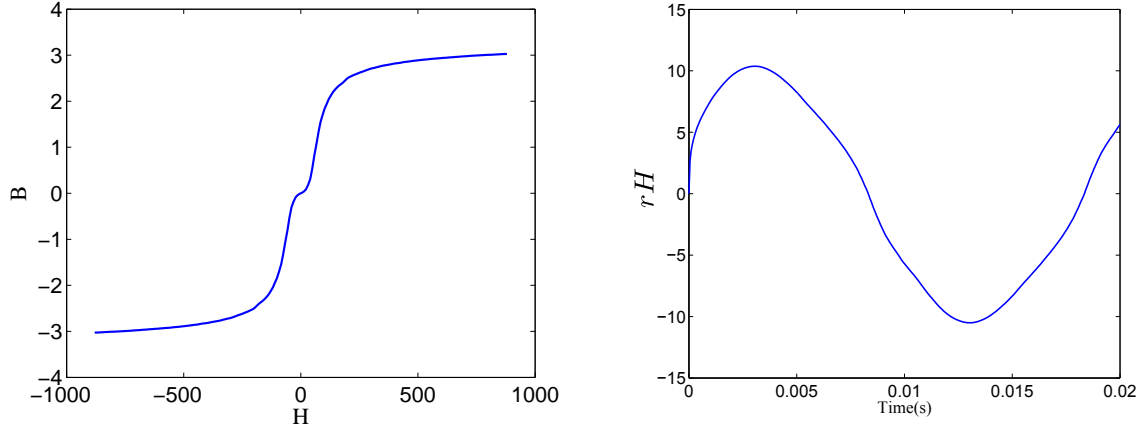


Figure 5.34: Anhysteretic B-H curve (left) and rH on the boundary (right).

We solve the fully discrete Problem 5.5.1 with the above data, $H_0 = f = 0$ and “initial state” given by the a staircase line as depicted on Figure 5.30 (left). Given that there is no analytical solution to this problem we asses the behavior of the method by comparing the computed results with those obtained by computing the numerical solution on a very fine uniform mesh of size $h_0/128$ and time step $\Delta t_0/64$, where $\Delta t_0 = 0.004$ and $h_0 = 1.67 \times 10^{-4}$. The solution to this problem will be taken as the “exact” solution H .

The method has been used on several successively refined meshes and time-steps, both chosen in a convenient way in order to analyze the convergence with respect to these discretization parameters. The numerical approximations have been compared with the “exact” solution by computing the percentage error for H in a discrete $L^2(0, T; L_r^2(\Omega))$ -norm as follows:

$$E_h^{\Delta t}(H) := 100 \frac{\left(\sum_{i=0}^{m-1} \Delta t \|H(t^{i+1}) - H_h^{i+1}\|_{L_r^2(\Omega)}^2 \right)^{1/2}}{\left(\sum_{i=0}^{m-1} \Delta t \|H(t^{i+1})\|_{L_r^2(\Omega)}^2 \right)^{1/2}}.$$

We have also computed the percentage error for the eddy current $\mathbf{J} = \mathbf{curl} \mathbf{H}$ (cf. (5.15)) in the analogous discrete $L^2(0, T; L_r^2(\Omega)^2)$ -norm:

$$E_h^{\Delta t}(\mathbf{J}) := 100 \frac{\left(\sum_{i=0}^{m-1} \Delta t \|\mathbf{curl} \mathbf{H}(t^{i+1}) - \mathbf{curl} \mathbf{H}_h^{i+1}\|_{L_r^2(\Omega)^2}^2 \right)^{1/2}}{\left(\sum_{i=0}^{m-1} \Delta t \|\mathbf{curl} \mathbf{H}(t^{i+1})\|_{L_r^2(\Omega)^2}^2 \right)^{1/2}},$$

with $\mathbf{H}_h^{i+1} := H_h^{i+1} \mathbf{e}_\theta$.

Table 5.2 shows the percentage errors for the magnetic field, $E_h^{\Delta t}(H)$, at different levels of discretization. Taking a small enough time-step Δt , one can observe the behavior of the error with respect to the space discretization (see, for instance, the last row of the table). On the other hand, by considering a small enough mesh-size h , one can inspect the order of convergence with respect to Δt (see, for instance, the last column). In this example, we observe an order of convergence $\mathcal{O}(\Delta t)$ in time and an order a little greater than $\mathcal{O}(h)$ in space (see Figure 5.35), but not quadratic which is the expected order in the case without hysteresis (see Chapter 4).

Table 5.2: Percentage errors of the computed magnetic field: $E_h^{\Delta t}(H)$.

Δt	h_0	$h_0/2$	$h_0/4$	$h_0/8$	$h_0/16$
Δt_0	18.910304	18.358260	18.377855	18.401430	18.408941
$\Delta t_0/2$	11.127365	9.562454	9.534205	9.573410	9.583821
$\Delta t_0/4$	8.670993	5.300164	5.186250	5.233997	5.252391
$\Delta t_0/8$	9.267023	3.195960	2.466612	2.479539	2.500379
$\Delta t_0/16$	9.914650	2.764764	1.256052	1.147084	1.159387
$\Delta t_0/32$	10.372782	2.800711	0.828586	0.475372	0.461344
$\Delta t_0/64$	10.629753	2.891255	0.791227	0.254920	0.153066

In Table 5.3 we report the percentage errors for the current density, $E_h^{\Delta t}(\mathbf{J})$. As in the previous table, one can observe the behavior of the error with respect to space and time discretization by taking small enough time-step Δt and mesh-size h , respectively. In this case we observe an order of convergence $\mathcal{O}(h + \Delta t)$.

Table 5.3: Percentage errors of the computed current density: $E_h^{\Delta t}(\mathbf{J})$.

Δt	h_0	$h_0/2$	$h_0/4$	$h_0/8$	$h_0/16$
Δt_0	43.229227	34.719852	32.327732	31.710448	31.560407
$\Delta t_0/2$	38.705228	24.263115	18.982495	17.438602	17.036104
$\Delta t_0/4$	39.071419	21.515507	13.634777	10.679927	9.814513
$\Delta t_0/8$	40.087750	20.849198	11.243344	6.860906	5.225194
$\Delta t_0/16$	40.806282	21.000062	10.750589	5.635523	3.278034
$\Delta t_0/32$	41.251761	21.199471	10.720544	5.327327	2.567221
$\Delta t_0/64$	41.488977	21.320158	10.764578	5.287913	2.387532

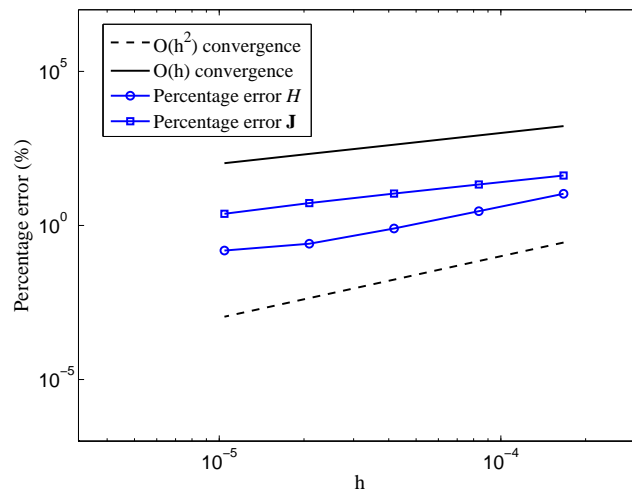


Figure 5.35: Percentage errors $E_h^{\Delta t}(H)$ and $E_h^{\Delta t}(J)$ versus the mesh-size h (log-log scale).

Finally we present the evolution of the solution. Figures 5.37 and 5.38 show the magnetic field and magnetic induction, respectively, at different times on a single sheet of the laminated meridian section, whereas Figure 5.36 (left) shows the evolution of the B-H curve in a fixed point of the mesh and Figure 5.36 (right) the waveforms in the middle and at the surface of the laminate. In Figures 5.38 and 5.36 (right), we can see the presence of skin effect.

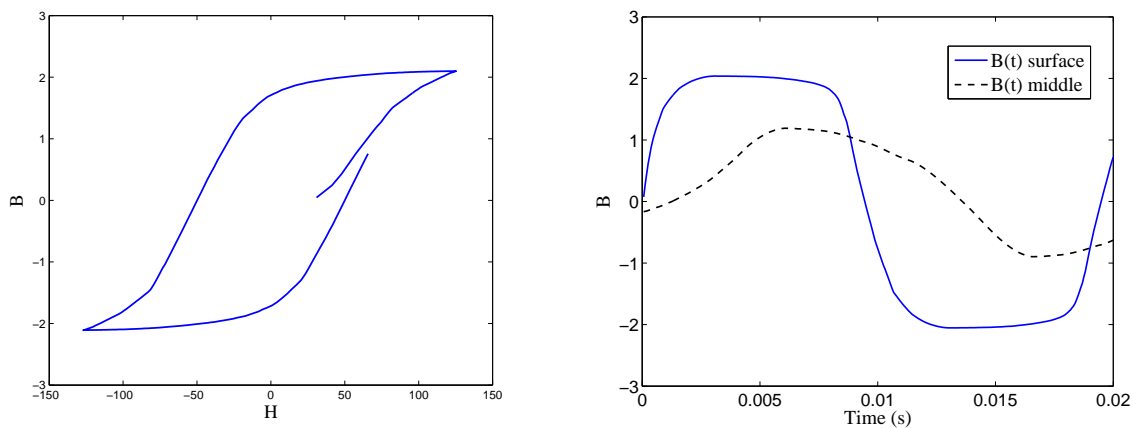


Figure 5.36: B-H curve at the surface of the sheet (left) and B vs. time in the middle and at the surface of the sheet (right).

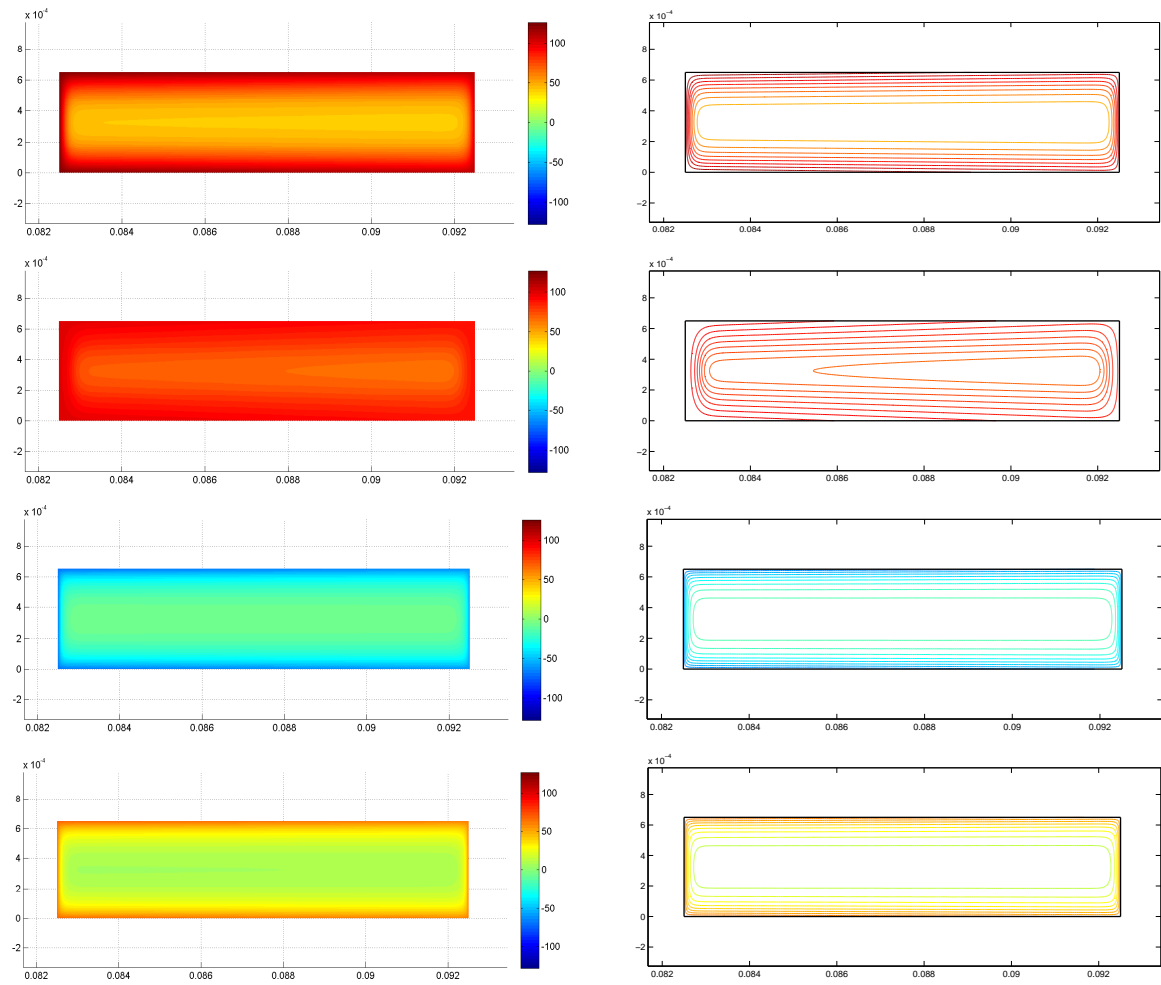


Figure 5.37: Magnetic field H (left) and level set (right) at times $t = 0.0025, 0.0050, 0.0100, 0.0200$ s.

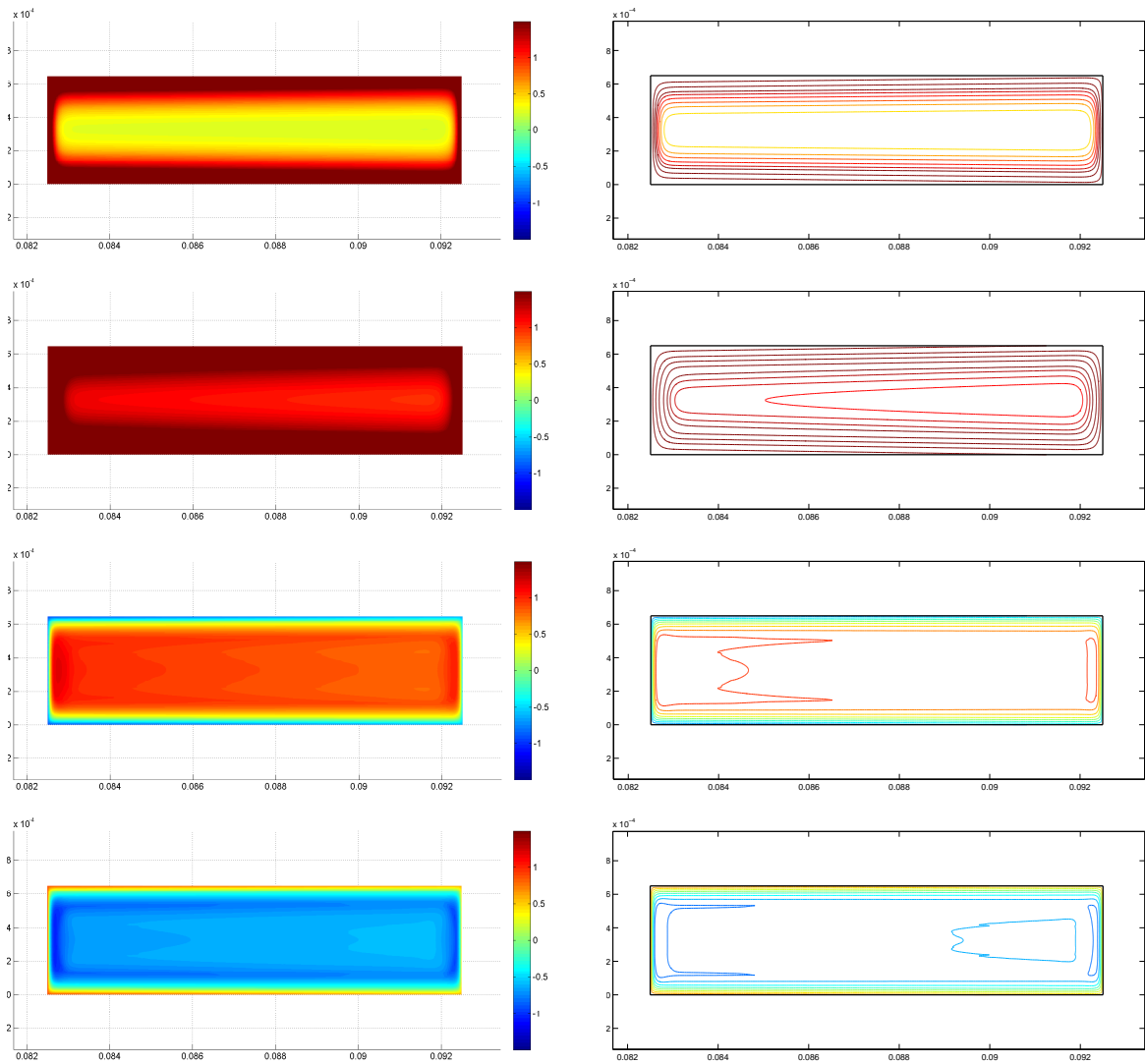


Figure 5.38: Magnetic induction B (left) and level set (right) at times $t = 0.0025, 0.0050, 0.0100, 0.0200$ s.

Chapter 6

Conclusiones y trabajo futuro

En este capítulo se presenta un resumen de los principales aportes de esta tesis y una descripción del trabajo futuro a desarrollar.

6.1 Conclusiones

La tesis recoge el análisis matemático y numérico de dos problemas motivados por aplicaciones en electromagnetismo: el cálculo de autovalores del operador rotacional y el problema de corrientes inducidas en régimen transitorio en dominios axisimétricos, considerando materiales no lineales con y sin histéresis.

A continuación se enumeran los resultados más importantes alcanzados en cada uno de estos problemas.

1. En el Capítulo 2 se caracterizó el espectro del operador rotacional mediante la equivalencia del problema de autovalores y un problema mixto. Se propusieron dos formulaciones para aproximar numéricamente el problema de autovalores, las cuales fueron analizadas matemática y numéricamente. Para ambas formulaciones se obtuvieron estimaciones de error. Se desarrollaron códigos escritos en MATLAB que permiten resolver los esquemas numéricos propuestos previamente. La convergencia de uno de los métodos numéricos ha sido validada mediante un ejemplo académico con solución analítica conocida.
2. Se estudió el problema evolutivo no lineal de corrientes inducidas en dominios axisimétricos en términos del campo magnético. En el Capítulo 3 se abordó el problema considerando como dato una condición de flujo magnético. Para la formulación obtenida se demostró existencia y unicidad de solución utilizando un resultado abstracto. En el Capítulo 4 se resolvió un problema análogo pero considerando como dato el campo magnético en la frontera del dominio (condición de Dirichlet). Se demostró la existencia de solución de la formulación obtenida utilizando el método de Rothe. Para ambas formulaciones se propusieron esquemas numéricos basados en elementos finitos para la discretización espacial y el método de Euler implícito para la discretización temporal. En ambos casos se demostró

que el esquema completamente discreto resultante está bien planteado y que genera aproximaciones de orden óptimo, las cuales fueron validadas numéricamente.

3. En el Capítulo 5 se estudió el problema evolutivo de corrientes inducidas en dominios axisimétricos con presencia de histéresis. La diferencia con los problemas abordados en los capítulos 3 y 4 reside en que la relación no lineal entre el campo magnético y la inducción magnética viene dada por un operador de histéresis. Se consideraron dos tipos de datos fuente: condición de flujo magnético en la sección meridional del dominio y condición de Dirichlet no homogénea. Para las formulaciones obtenidas con cada uno de estos datos, se demostró existencia de solución. Para la modelización de la histéresis magnética se utilizó el operador de Preisach clásico, y se describieron sus principales características, así como su implementación numérica. Utilizando este operador para describir la relación B-H, se propone un esquema numérico que utiliza un método de elementos finitos para la discretización en espacio y el método de Euler implícito para la discretización en tiempo. Para resolver el problema no lineal en tiempo se utilizó el algoritmo de Bermúdez-Moreno.
4. Se elaboraron diversos códigos FORTRAN que permiten resolver los esquema numéricos de los problemas analizados en los Capítulos 3, 4 y 5.

6.2 Trabajo futuro

1. Estudiar el problema de autovalores en dominios múltiplemente conexos. En este caso, y como se menciona en el Capítulo 2, será necesario modificar convenientemente las condiciones de contorno.
2. Estudiar la unicidad de solución y analizar la convergencia del esquema numérico propuesto en el problema de corrientes inducidas con histéresis, considerando los dos tipos de datos.
3. Calcular las pérdidas por corrientes inducidas y por histéresis, y validar los resultados obtenidos con fórmulas analíticas y resultados experimentales. En este sentido, se contará con la colaboración del Prof. Luc Dupré del Department of Electrical Energy, Systems and Automation de la Universidad de Gant (Bélgica) para la realización de medidas experimentales sobre materiales ferromagnéticos.
4. Considerar el campo de densidades de potencia de las pérdidas por histéresis y corrientes inducidas como fuente en un modelo de transmisión de calor con objeto de determinar la temperatura del dispositivo.
5. Realizar el análisis matemático y numérico del problema de corrientes inducidas utilizando un operador de histéresis de tipo "Preisach dinámico". Esto permitirá tener en cuenta las "pérdidas por exceso" en el modelo.

Bibliography

- [1] A. Alonso Rodríguez and A. Valli, *Eddy current approximation of Maxwell equations*, Springer Verlag, 2010.
- [2] C. Amrouche, C. Bernardi, M. Dauge, and V. Girault, *Vector potentials in three-dimensional non-smooth domains*, Math. Methods Appl. Sci. **21** (1998), 823–864.
- [3] V. Barbu, *Nonlinear differential equations of monotone type in Banach spaces*, Springer Verlag, 2010.
- [4] V. Barbu and Th. Precupanu, *Convexity and optimization in Banach spaces*, Sÿthoff & Noordhoff International Publishers, 1978.
- [5] S. Bartels, C. Carstensen, and G. Dolzmann, *Inhomogeneous Dirichlet conditions in a priori and a posteriori finite element error analysis*, Numer. Math. **99** (2004), 1–24.
- [6] Z. Belhachmi, C. Bernardi, and S. Deparis, *Weighted Clément operator and application to the finite element discretization of the axisymmetric Stokes problem*, Numer. Math. **105** (2006), 217–247.
- [7] E. Beltrami, *Considerazioni idrodinamiche*, Rend. Inst. Lombardo Acad. Sci. Let. **22** (1889), 122–131, (English translation: *Considerations on hydrodynamics*, Int. J. Fusion Energy, **3** (1985) 53–57.).
- [8] A. Bermúdez, J. Bullón, and F. Pena, *A finite element method for the thermoelectrical modelling of electrodes*, Commun. Numer. Meth. Eng. **14** (1998), 581–593.
- [9] A. Bermúdez, J. Bullón, F. Pena, and P. Salgado, *A numerical method for transient simulation of metallurgical compound electrodes*, Finite Elem. Anal. Des. **39** (2003), 283–299.
- [10] A. Bermúdez, D. Gómez, R. Rodríguez, P. Salgado, and P. Venegas, *Numerical solution of a transient non-linear axisymmetric eddy current model with non-local boundary conditions*, Math. Models Methods Appl. Sci. (2013), DOI: 10.1142/S0218202513500383.
- [11] A. Bermúdez, D. Gómez, and P. Salgado, *Eddy-current losses in laminated cores and the computation of an equivalent conductivity*, IEEE Trans. Magn. **44** (2008), 4730–4738.
- [12] A. Bermúdez and C. Moreno, *Duality methods for solving variational inequalities*, Comput. Math. Appl. **7** (1981), 43–58.

-
- [13] A. Bermúdez, R. Rodríguez, and P. Salgado, *Numerical analysis of electric field formulations of the eddy current model*, Numer. Math. **102** (2005), 181–201.
- [14] C. Bernardi, M. Dauge, and Y. Maday, *Spectral methods for axisymmetric problems*, Gauthier-Villars, 1999.
- [15] G. Bertotti, *Hysteresis in magnetism*, Academic Press, 1998.
- [16] G. Bertotti and I. D. Mayergoyz (eds.), *The science of hysteresis. Vol. I*, Elsevier/Academic Press, Amsterdam, 2006.
- [17] G. Biorci and D. Pescetti, *Analytical theory of the behaviour of ferromagnetic materials*, II Nuovo Cimento **7** (1958), 829–842.
- [18] D. Boffi, *Finite element approximation of eigenvalue problems*, Acta Numer. **19** (2010), 1–120.
- [19] A. Boglietti, A. Cavagnino, M. Lazzari, and M. Pastorelli, *Predicting iron losses in soft magnetic materials with arbitrary voltage supply: An engineering approach*, IEEE Trans. Magn. **39** (2003), 981–989.
- [20] A. Bossavit, *Computational electromagnetism. Variational formulations, complementarity, edge elements*, Academic Press, 1998.
- [21] T.Z. Boulmezaud and T. Amari, *Approximation of linear force-free fields in bounded 3-D domains*, Math. Comp. Model. **31** (2000), 109–129.
- [22] ———, *A finite-element method for computing nonlinear force-free fields*, Math. Comput. Model. **34** (2001), 903–920.
- [23] T.Z. Boulmezaud, Y. Maday, and T. Amari, *On the linear force-free fields in bounded and unbounded three-dimensional domains*, M²AN Math. Model. Numer. Anal. **33** (1999), 359–393.
- [24] M. Brokate and J. Sprekels, *Hysteresis and phase transitions*, Springer, Berlin, 1996.
- [25] A. Buffa, M. Costabel, and D. Sheen, *On traces for $H(\mathbf{curl}; \Omega)$ in Lipschitz domains*, J. Math. Anal. Appl. **276** (2002), 845–867.
- [26] J. Cantarella, D. De Turck, H. Gluck, and M. Teytel, *The spectrum of the curl operator on spherically symmetric domains*, Phys. Plasmas **7** (2000), 2766–2775.
- [27] S. Chandrasekhar and P.C. Kendall, *On force-free magnetic fields*, Astrophys. J. **126** (1957), 457–460.
- [28] S. Chandrasekhar and L. Woltjer, *On force-free magnetic fields*, Proc. Nat. Acad. Sci. USA **44** (1958), 842–847.

-
- [29] S. Clain, J. Rappaz, M. Swierkosz, and R. Touzani, *Numerical modeling of induction heating for two-dimensional geometries*, Math. Models Methods Appl. Sci. **3** (1993), 805–822.
- [30] E.A. Coddington, *An introduction to ordinary differential equations*, Prentice-Hall, 1961.
- [31] D. M. Copeland and J. E. Pasciak, *A least-squares method for axisymmetric div-curl systems*, Numer. Linear Algebra Appl. **13** (2006), 733–752.
- [32] E. Della Torre, J. Oti, and G. Kadar, *Preisach modeling and reversible magnetization*, IEEE Trans. Magn. **26** (1990), 3052–3058.
- [33] J. Descloux, N. Nassif, and J. Rappaz, *On spectral approximation. I. The problem of convergence*, RAIRO Anal. Numér. **12** (1978), 97–112.
- [34] ———, *On spectral approximation. II. Error estimates for the Galerkin method*, RAIRO Anal. Numér. **12** (1978), 113–119.
- [35] E. Di Benedetto and R. E. Showalter, *Implicit degenerate evolution equations and applications*, SIAM J. Math. Anal. **12** (1981), 731–751.
- [36] P. Dular, J. Gyselinck, and L. Kräenbühl, *A time-domain finite element homogenization technique for laminated stacks using skin effect sub-basis functions*, COMPEL **25** (2006), 6–16.
- [37] L. Dupré, M. De Wulf, D. Makaveev, V. Permiakov, A. Pulnikov, and J. A. A. Melkebeek, *Modeling of electromagnetic losses in asynchronous machines*, COMPEL **22** (2003), 1051–1065.
- [38] L. Dupré, J. A. A. Melkebeek, and R. Van Keer, *On a numerical method for the evaluation of electromagnetic losses in electric machinery*, Int. J. Numer. Methods Eng. **39** (1996), 1535–1553.
- [39] ———, *Modelling and identification of iron losses in nonoriented steel laminations using Preisach theory*, IEE Proc. - Electric Power Appl. **144** (1997), 227–234.
- [40] L.R. Egan and E.P. Furlani, *A computer simulation of an induction heating system*, IEEE Trans. Magn. **27** (1991), 4343 – 4354.
- [41] M. Eleuteri, *An existence result for a P.D.E. with hysteresis, convection and a nonlinear boundary condition*, Discrete Contin. Dyn. Syst. (2007), 344–353.
- [42] ———, *Wellposedness results for a class of parabolic partial differential equations with hysteresis*, NoDEA Nonlinear Differential Equations Appl. **15** (2008), 557–580.
- [43] M. Eleuteri and P. Krejčí, *Asymptotic behavior of a Neumann parabolic problem with hysteresis*, ZAMM Z. Angew. Math. Mech. **87** (2007), 261–277.
- [44] ———, *An asymptotic convergence result for a system of partial differential equations with hysteresis*, Commun. Pure Appl. Anal. **6** (2007), 1131–1143.

-
- [45] V. Girault and P.-A. Raviart, *Finite element approximations of the Navier-Stokes equations, theory and algorithms*, Springer, Berlin, 1986.
- [46] J. Gopalakrishnan and J. E. Pasciak, *The convergence of V-cycle multigrid algorithms for axisymmetric Laplace and Maxwell equations*, *Math. Comp.* **75** (2006), 1697–1719.
- [47] P. Hahne, R. Dietz, and T. Weiland, *Determination of anisotropic equivalent conductivity of laminated cores for numerical computation*, *IEEE Trans. Magn.* **32** (1996), 1184–1187.
- [48] O. Henze and W. M. Rucker, *Application of Preisach model on a real existent material*, Proc. 9th Int. IGTE Symp. Numerical Field Calculation in Electrical Engineering, 2000, pp. 380–384.
- [49] M. Hilpert, *On uniqueness for evolution problems with hysteresis*, Mathematical models for phase change problems, *Internat. Ser. Numer. Math.*, vol. 88, Birkhäuser, Basel, 1989, pp. 377–388.
- [50] R. Hiptmair, *Finite elements in computational electromagnetism*, *Acta Numer.* **11** (2002), 237–339.
- [51] K.-H. Hoffmann, J. Sprekels, and A. Visintin, *Identification of hysteresis loops*, *J. Comp. Phys.* **78** (1988), 215 – 230.
- [52] V.-M. Hokkanen, *An implicit nonlinear time dependent equation has a solution*, *J. Math. Anal. Appl.* **161** (1991), 117–141.
- [53] K. Hollaus and O. Biro, *A FEM formulation to treat 3D eddy currents in laminations*, *IEEE Trans. Magn.* **36** (2000), 1289–1292.
- [54] R. Innvær and L. Olsen, *Practical use of mathematical models for Söderberg electrodes*, Elkem Carbon Technical Paper presented at the A.I.M.E. Conference (1980).
- [55] J. Jerome and M.E. Rose, *Error estimates for the multidimensional two-phase Stefan problem*, *Math. Comp.* **39** (1982), 377–414.
- [56] O. Kavian, *Introduction à la théorie des points critiques et applications aux problèmes elliptiques*, Springer-Verlag, Paris, 1994.
- [57] M.A. Krasnosel'skiĭ and A.V. Pokrovskiĭ, *System with hysteresis*, Springer, Berlin, 1989, (Russian edition, Nauka, Moscow (1983)).
- [58] A. Kufner, O. John, and S. Fučík, *Function spaces*, Noordhoff International Publishing, Leyden, 1977.
- [59] A. Lakhtakia, *Victor Trkal, Beltrami fields and Trkalian flows*, *Czech J. Phys.* **44** (1994), 89–96.
- [60] P. Li and W. Zheng, *An $\mathbf{H} - \psi$ formulation for the three-dimensional eddy current problem in laminated structures*, *J. Differential Equations* **254** (2013), 3476–3500.

- [61] J.-L. Lions and E. Magenes, *Problèmes aux limites non homogènes et applications. Vol. 1*, Dunod, Paris, 1968.
- [62] M. Markovic and Y. Perriard, *Eddy current power losses in a toroidal laminated core with rectangular cross section*, 2009 International Conference on Electrical Machines and Systems (ICEMS) (New York), IEEE, 2009, pp. 1249–1252.
- [63] I.D. Mayergoyz, *Mathematical models of hysteresis*, Springer, New York, 1991.
- [64] I.D. Mayergoyz and G. Friedman, *Isotropic vector Preisach model of hysteresis*, J. Appl. Phys **61** (1987), 4022–4024.
- [65] S. Meddahi and V. Selgas, *A mixed-FEM and BEM coupling for a three-dimensional eddy current problem*, M²AN Math. Model. Numer. Anal. **37** (2003), 291–318.
- [66] B. Mercier, J. Osborn, J. Rappaz, and P.-A. Raviart, *Eigenvalue approximation by mixed and hybrid methods*, Math. Comp. **36** (1981), 427–453.
- [67] B. Mercier and G. Raugel, *Resolution d'un problème aux limites dans un ouvert axisymétrique par éléments finis en r , z et séries de fourier en θ* , RAIRO, Anal. Numér. **16** (1982), 405–461.
- [68] P. Monk, *Finite element methods for Maxwell's equations*, Oxford University Press, New York, 2003.
- [69] E.C. Morse, *Eigenfunctions of the curl in cylindrical geometry*, J. Math. Phys. **46** (2005), 113511.
- [70] K.V. Namjoshi, J.D. Lavers, and P.P. Biringer, *Eddy-current power loss in toroidal cores with rectangular cross section*, IEEE Trans. Magn. **34** (1998), 636–641.
- [71] C. Natale, F. Velardi, and C. Visone, *Identification and compensation of Preisach hysteresis models for magnetostrictive actuators*, Physica B **306** (2001), 161–165.
- [72] J.C. Nédélec, *Mixed finite elements in \mathbb{R}^3* , Numer. Math. **35** (1980), 315–341.
- [73] R.H. Nochetto, *Error estimates for two-phase Stefan problems in several space variables. I. Linear boundary conditions*, Calcolo. **22** (1985), 457–499.
- [74] K. Preis, *A contribution to eddy current calculations in plane and axisymmetric multiconductor systems*, IEEE Trans. Magn. **19** (1983), 2397–2400.
- [75] K. Preis, O. Biro, and I. Tigar, *FEM analysis of eddy current losses in nonlinear laminated iron cores*, IEEE Trans. Magn. **41** (2005), 1412–1415.
- [76] F. Preisach, *Über die magnetische nachwirkung*, Zeitschrift für Physik, **94** (1935), 277–302.
- [77] E. Rothe, *Zweidimensionale parabolische Randwertaufgaben als Grenzfall eindimensionaler Randwertaufgaben*, Math. Ann. **102** (1930), 650–670.

- [78] T. Roubíček, *Non linear partial differential equations with applications*, Birkhäuser, 2005.
- [79] L.R. Scott and S. Zhang, *Finite element interpolation of nonsmooth functions satisfying boundary conditions*, Math. Comp. **54** (1990), 483–493.
- [80] M. Slodička, *A time discretization scheme for a nonlinear degenerate eddy current model for ferromagnetic materials*, IMA J. Numer. Anal. **26** (2006), 173–187.
- [81] ———, *Nonlinear diffusion in type-II superconductors*, J. Comput. Appl. Math. **215** (2008), 568–576.
- [82] M. Slodička and J. Busa, *Error estimates for the time discretization for nonlinear Maxwell's equations*, J. Comput. Math. **26** (2008), 677–688.
- [83] M. Slodička and S. Dehilis, *A nonlinear parabolic equation with a nonlocal boundary term*, J. Comput. Appl. Math. **233** (2010), 3130–3138.
- [84] C.P. Steinmetz, *On the law of hysteresis*, Trans. Ame. Inst. Elect. Engrs. **9** (1892), 3–51, (reprinted in Proc. of the IEEE. **72** (1984), 197–221).
- [85] J. B. Taylor, *Relaxation of toroidal plasma and generation of reverse magnetic fields*, Phys. Rev. Lett. **33** (1974), 1139–1141.
- [86] V. Thomée, *Galerkin finite element methods for parabolic problems*, Springer-Verlag, 2006.
- [87] V. Trkal, *Poznámka k hydrodynamice viskózních tekutin*, Časopis pro Pěstování Matematiky a Fysiky **48** (1919), 302–311, (English translation: *A note on the hydrodynamics of viscous fluids*, Czech J. Phys., **44** (1994) 97–106.).
- [88] S. Tumanski, *Handbook of magnetic measurements*, CRC Press, 2011.
- [89] R. Van Keer, L. Dupré, and J. A. A. Melkebeek, *On a numerical method for 2D magnetic field computations in a lamination with enforced total flux*, J. Comput. Appl. Math. **72** (1996), 179–191.
- [90] ———, *Computational methods for the evaluation of the electromagnetic losses in electrical machinery*, Arch. Comput. Methods Engrg. **5** (1998), 385–443.
- [91] C. Verdi and A. Visintin, *Numerical approximation of hysteresis problems*, IMA J. Numer. Anal. **5** (1985), 447–463.
- [92] ———, *Numerical approximation of the Preisach model for hysteresis*, RAIRO Modél. Math. Anal. Numér. **23** (1989), 335–356.
- [93] A. Visintin, *A model for hysteresis of distributed systems*, Ann. Mat. Pura Appl. **131** (1982), 203–231.
- [94] ———, *On the Preisach model for hysteresis*, Nonlinear Anal-Theor. **8** (1984), 977–996.

-
- [95] ———, *Differential models of hysteresis*, Springer, Berlin, 1994.
- [96] L. Woltjer, *The crab nebula*, Bull. Astron. Inst. Neth. **14** (1958), 39–80.
- [97] ———, *A theorem on force-free magnetic fields*, Proc. Nat. Acad. Sci. U.S.A. **44** (1958), 489–491.
- [98] Z. Yoshida and Y. Giga, *Remarks on spectra of operator rot*, Math. Z. **204** (1990), 235–245.